UAB
Universitat Autònoma de Barcelona

Doctoral Thesis

PhD in Electrochemistry. Science and Technology

Smart Materials for Bacterial Detection Based on Electrochromic Molecules

Amparo Ferrer Vilanova

Directors:

Dr. Xavier Muñoz Berbel

Dr. Gonzalo Guirado López

Department of Chemistry

Faculty of Science

2023

The present doctoral thesis entitled **'Smart materials for bacterial detection based on electrochromic molecules'** is presented by Amparo Ferrer Vilanova as a partial fulfilment of the requirements to obtain the degree of Doctor of Philosophy in Electrochemistry.

This thesis was carried out at the Institute of Microelectronics of Barcelona (IMB-CNM, CSIC) in the Chemical Transducers Group (GTQ), under the supervision of Dr. Xavier Muñoz Berbel and Dr. Gonzalo Guirado López.

With the approval of:

Dr. Xavier Muñoz Berbel   Dr. Gonzalo Guirado López.

(Director)   (Director and Tutor)

Amparo Ferrer Vilanova

(Author)

Contents

List of Abbreviations, Units and Symbols

Abbreviations

4-VP	4-vinylpyridine
A.U.	Arbitrary units
AFM	Atomic Force Microscopy
AMPs	Antimicrobial peptides
ATCC	American Type Culture Collection
ATP	Adenosine 5'-triphosphate
BC	Benzalkonium chloride
CAGR	Compound Annual Growth Rate
CE	Counter electrode
CFU	Colony forming units
CLAESS	Core Level Absorption and Emission Spectroscopies
CMC	Sodium carboxymethylcellulose
CNC	5-cyano-2,3-ditolyl tetrazolium chloride
CNTs	Carbon nanotubes
CPC	Cetylpyridin chloride
CV	Cyclic voltammetry
DMEM	Dulbecco's Modified Eagle's Medium
DNA	Deoxyribonucleic acid

DST	Defined substrate technology
E. coli	*Escherichia coli*
ECDC	European Centre for Disease Prevention
EDX	Energy Dispersive X-Ray Analysis
EGCG	Epigallocatechin-3-gallate
EIPAs	Eu^{3+}-induced polyelectrolyte nano-aggregates
ELISA	Enzyme-linked immunosorbent assay
EMB	Eosin Methlylene blue
EPS	Extracellular polymeric substances
ETC	Electron transport chain
EXAFS	Extended X-ray absorption fine structure
FADH	Flavin adenine dinucleotide
FE-SEM	Field Emission Scanning Electron Microscopy
FMNH	Flavin mononucleotide
GO	Graphene oxide
HAI	Hospital acquired infection
HPMC	Hydroxypropyl methylcellulose
ICP-OES	Inductively-Coupled Plasma - Optical Emission Spectrometry
IMS	Intermatrix synthesis
INT	2-(4-iodophenyl)-3-(4-nitrophenyl)-5-phenyl tetrazolium chloride
ISO	International Standards Organization

ITO	Indium tin oxide
IUPAC	International Union of Pure and Applied Chemistry
LB	Luria-Bertani
MB	Methylene blue
MCE	Mixed cellulose ester
MES	2-(N-morpholino)ethane-sulfonic acid
MH	Mueller-Hinton
MQ	Menaquinone
MTT	3-[4,5-dimethylthiazol-2-yl]-2,5 diphenyl tetrazolium bromide
NADH	Nicotinamide adenine dinucleotide
NADPH	Nicotinamide adenine dinucleotide phosphate
NC	Nitrocellulose
NHE	Normal hydrogen electrode
NPs	Nanoparticles
ONPG	Ortho-nitrophenyl-β-galactoside
P. putida	*Pseudomonas putida*
PANI	Polyaniline
PB	Prussian blue
PB$_{Ins}$	Insoluble Prussian blue
PBS	Phosphate buffer saline
PB$_{Sol}$	Soluble Prussian blue

PCR	Polymerase chain reaction
PEG	Polyethylene glycol
PET	Poly(ethylene terephthalate)
PHGH	Polyhexamethylene guanidine hydrochloride
PHMB	Poly(hexamethylene biguanide)
PMMA	Poly(methyl methacrylate)
PPE	Poly(3,4-propylenedioxythiophenalt-3,4-ethylenedioxythuophene)
PVA	Polyvinyl alcohol
PVP	Polyvinyl pyrrolidone
PW	Prussian white
QACs	Quaternary ammonium compounds
QQ	Quorum quenching
RE	Reference electrode
RNA	Ribonucleic acid
S. aureus	*Staphylococcus aureus*
SCDLP	Soya Casein Digest Lecithin Polysorbate
STAC	Stearyl trimethyl ammonium chloride
TCFH	Tricyanofuran hydrazine
UV	Ultraviolet
WE	Working electrode
WHO	World Health Organization

WST-1	2-[4-iodophenyl]-3-[4-nitro-phenyl]-5-[2,4-disulfophenyl]-2H-tetrazolium monosodium salt
XANES	X-ray absorption near edge structure
XAS	X-ray absorption

Units

A	Ampere
Å	Angstrom
C	Coulomb
°C	Celsius degree
eV	Electronvolt
g	Gram
Hz	Hertz
L	Liter
m	Meter
min	Minute
s	Second
V	Volt
W	Watt
Ω	Ohm

Symbols

M	Molar (mol L^{-1})
λ	Wavelength (nm)
R	Bond distance (Å)
σ^2	Debye-Waller factor (10^{-3} Å^2)
Deg	Degeneracy of the scattering path
S_0^2	Many body amplitude reduction factor
h	Plank's constant (6,62 kg m^2 s^{-1})
A	Absorbance
ε	Extinction molar coefficient (M^{-1} cm^{-1})
c	Molar concentration (M)
l	Optical path length (cm)
σ	Standard deviation
n	Number of moles
Q	Electric charge (C)
z	Number of electrons
F	Faraday constant (96485 C mol^{-1})
ν	Frequency (Hz)

Summary

Nosocomial or hospital acquired infections are those acquired by hospital patients due to contaminated equipment, bed linens, or humidity in the environment, among others. In order to minimize the number of HAIs, antibacterial fabrics have been developed by incorporating bactericidal nanoparticles into them. However, these materials lose their activity over time increasing the risk of contamination and infection. Therefore, bacterial detection in situ is required. As a strategy to detect bacteria, metabolic indicators are molecules that only change in direct contact with live bacteria due to bacterial metabolism, producing a change in conductivity, pH or color. Electrochromic metabolic indicators have shown the ability to act as electron acceptors in the bacterial respiration process, such as Prussian blue, which has a different color for both its oxidized and reduced forms. The current PhD thesis is focused on the study of the bacterial-sensing response of Prussian blue, its application to the development of smart materials and their implementation in antimicrobial textiles and water filter membranes for the prevention of bacterial infections. The incorporation of bacterial sensing molecules in the smart materials will allow the in situ determination of the life-time of the bactericide materials and their effectiveness in the control of bacterial infections. This technology, initially conceived to prevent HAI in hospital settings, has been of interest in other application sectors including schools, elderly homes, public transport or public furniture, among others.

Resumen

Las infecciones nosocomiales o infecciones asociadas a la atención médica (IAAS) son aquellas adquiridas por pacientes hospitalizados debido a equipos contaminados, ropa de cama o humedad en el ambiente, entre otras fuentes de infección. Con el fin de minimizar el número de IAAS, se han desarrollado tejidos antibacterianos incorporando en ellos nanopartículas bactericidas. Sin embargo, estos materiales pierden su actividad con el tiempo aumentando el riesgo de contaminación e infección. Por lo tanto, la detección de bacterias in situ es requerida. Como estrategia para detectar bacterias, los indicadores metabólicos son moléculas que solo cambian en contacto directo con bacterias vivas debido al metabolismo bacteriano, produciendo un cambio en la conductividad, el pH o el color. Los indicadores metabólicos electrocrómicos han demostrado la capacidad de actuar como aceptores de electrones en el proceso de respiración bacteriana, como el azul de Prusia, que tiene un color diferente tanto para su forma oxidada como reducida. Esta tesis doctoral se centra en el estudio de la respuesta de detección bacteriana del azul de Prusia, su aplicación en el desarrollo de materiales inteligentes y su implementación en tejidos antimicrobianos y membranas de filtros de agua para la prevención de infecciones producidas por bacterias. La incorporación de moléculas detectoras de bacterias en los materiales inteligentes permitirá determinar in situ el tiempo de vida de los materiales bactericidas y su eficacia en el control de infecciones bacterianas. Esta tecnología, inicialmente concebida para prevenir las IAAS en entornos hospitalarios, ha sido de interés en otros sectores de aplicación como colegios, residencias de ancianos, transporte público o mobiliario público, entre otros.

1
Introduction

1.1 Bacterial Infections: Impact, Risks, Treatments and Prevention

Bacteria are microorganisms commonly associated with several healthcare and safety problems, including infectious diseases, food poisoning and water pollution. The World Health Organization (WHO) positions two infectious diseases, i.e., lower respiratory infections and diarrheal disease, in the top ten causes of death worldwide.[1] Besides, the same institution estimates a total of 600 million foodborne illnesses and 420,000 deaths per year associated with the ingestion of contaminated food and water.[2] Antibiotics, the first barrier to bacterial infections, are now losing effectiveness due to their overuse in healthcare and farming.[3] This fact results in the emergence of a number of multidrug-resistant pathogens worldwide, which are not sensitive to antibacterial compounds and thus, very difficult to treat and control. For this reason, the prevention of bacterial infections from contaminated sources is now considered a priority, and particular attention has been paid to environments with individuals highly susceptible or more often adversely affected by infections such as hospitals, schools or nursing homes. In the case of

One day in Europe:

Hospitals

1/15
Hospital patients have at least one HAI

98 000
Patients have at least one HAI

long-term care facilities

1/24
Long-term care facilities residents have at least one HAI

124 000
Residents have at least one HAI

8.8 million HAIs occur each year

4.4 million — Hospitals
4.4 million — Long-term care facilities

More than half of certain HAIs are considered preventable.

HAIs are frequently treated without taking microbiological samples or samples remain negative

The responsable microorganism was identifiedin 53% of HAIs in hospitals and only in 19% os HAIs in long-term care facilities.

1 in 3 bacteria associated with HAIs was resistant to antibiotics

Figure 1.1. HAIs infographic. ECDC healthcare associated infections infographic adapted from ref 10.

hospitals, the incidence of "nosocomial" or "hospital-acquired infections" (HAIs), this term referring to those infections that the patient acquires under medical care, is very high both in developing and in developed countries.[4–9] The European Centre for Disease Prevention and Control (ECDC) has estimated HAI incidence in more than 8.8 million infections and 37.000 direct deaths per year only in Europe, contributing indirectly to 110.000 additional deaths. [10] Apart from that, the ECDC also relates HAIs with more than 16 million extra days of hospital stays every year, economic losses of approximately € 7 billion/year, considering direct costs only,[11] and other socio-economic adverse effects summarized in Figure 1.1.

In order to estimate the impact of HAI in society, it is fundamental to determine bacterial infection prevalence. This parameter contributes to evaluate the population's health and provides clear indications of the dynamics of the disease, which is strongly correlated with infection risk factors. Infection prevalence is generally estimated as either the proportion of infected individuals ("individual-based estimation") or the proportion of samples ("anonymous estimation") in which evidence of infection is detected.[12] Considering that, HAIs prevalence has been estimated to be around 7 % in high-income countries (7 affected patients per 100 patients; see Figure 1.2),[11] while

Figure 1.2. Prevalence of HAIs in high-income countries (1995-2010).

3

reaching values above 10 % in low-/middle-income countries, e.g., 33 % in India[13] and 13 % in Ethiopia.[14]

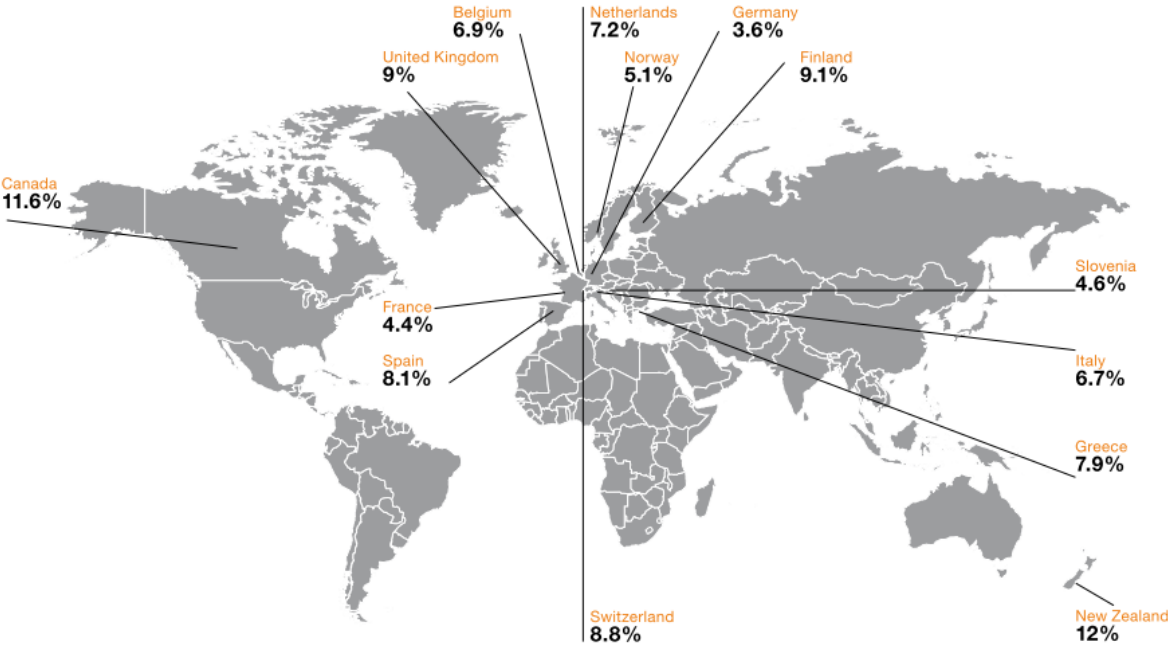In both high- and low-income countries, most of HAIs are caused by one of the following five bacterial species, i.e., *Staphylococcus aureus*, *Enterococcus* species, *Candida* species, *Escherichia coli* and *Pseudomonas aeruginosa*, and result in pneumonia, surgical site infections, bloodstream infections, respiratory infections, urinary tract infections or skin and soft tissue infections.[15,16] HAIs are associated with the presence of contaminated air, surfaces/materials or water, and the most common means of transmission are (Figure 1.3):[17]

- **Translocation**, caused when the own microbiota of the affected patient moves to a new site of infection.
- **Patient-to-patient transmission**, which can be produced by direct physical contact or through indirect way.
- **Healthcare workers** as a source of infection.
- **Infections from the environment**, produced by aerosols, contaminated water used for drinking or washing, and contaminated food.
- **Medical devices or facilities** as a source of infection, such as shared instruments, furniture or hospital fabrics.

From the previous ones, airborne spread in aerosols, respiratory droplets from body fluids and contact transmission from unclean surfaces containing bacteria are the most common ways of transmission, the latter representing the majority of the transmissions in healthcare settings. The WHO and other institutions such as the ECDC, are well aware of this situation and have proposed a roadmap with several interventions to minimize bacterial spreading in healthcare facilities.

Core strategies consist of a competency-based training and monitoring of adherence with feedback of results for good practices, which require the participation, complicity and adherence of the hospital staff. These good practices include precaution in the manipulation of medical devices and the establishment of good hygiene and disinfection protocols such as hand hygiene, environmental cleaning and disinfection, and the use of personal protective equipment, among

others.[18,19] Additionally, complementary actions are now being considered, which are less dependent on human intervention and, thus, less susceptible to human errors. These involve the systematic replacement of medical devices, which implies patient discomfort and increases treatment costs,[20] and surface modification/coating of medical devices, fabrics, air/water filters and furniture with antimicrobial/antifouling compounds.
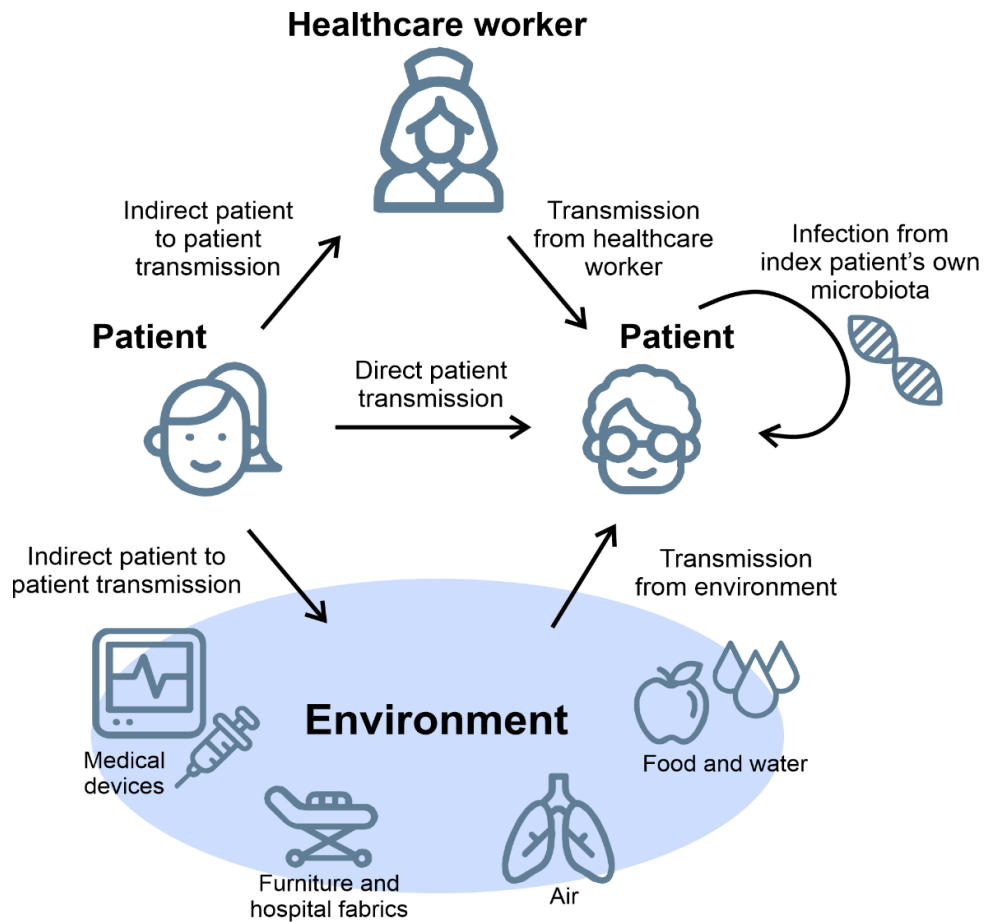
Figure 1.3. Main routes of HAIs transmission.

This strategy is being explored at both research and industrial level, and companies like Dupond, Akzo Nobel N.V. or The Sherwin-Williams Company are now providing antimicrobial/antifouling coating technologies for the production of biocide surfaces. Based on that need, a new market on antimicrobial coatings has emerged, which is calculated to be USD 4.2 billion in 2022 and projected to reach USD 7.36 billion by 2025, at a CAGR of 8.2 %. This significant

increase in the antimicrobial coating market is calculated considering the increasing demand from the medical and healthcare sector associated with a more stringent government regulations and changes in the norms and standards in the healthcare sector.[21] The modification of hospital fabrics, including pajamas, curtains, feathers, pillows, comforters or any other textile implemented in the room furniture, as well as water and air filters, or medical devices such as catheters, is considered one of the most promising strategies to prevent bacterial infection and spreading. Recent trends in antimicrobial coatings and smart materials to prevent bacterial infections and transmissions in healthcare settings will be discussed in the following sections.

1.2 Antimicrobial Coating Agents and Technologies

In this section, the most recent advances in surface modification for the production of materials with antibacterial and antifouling activity are presented and discussed, with special focus on cotton/cotton-polyester textiles and nitrocellulose filters due to their wide use in healthcare facilities and their relationship with bacterial transmissions associated to HAIs.

1.2.1 Antimicrobial textiles

Among fabric products, polyester and cotton are the most common materials employed for apparel and textile goods, being responsible for over 70 % of the global fiber market in 2019.[22] They are also the first choice hospital fabrics, particularly in the case of material in direct physical contact with the human skin (e.g., bedclothes, underclothes, socks, non-implantable medical textile materials like bandages, plasters, gauze dressing, wadding, etc. and hygiene products such as gowns, caps, and uniforms). Since this kind of materials are the most susceptible of bacterial transmissions by contact with contaminated surfaces, the production of antimicrobial textiles based on cotton and polyester is gaining attention over the last few years, being one of the fastest growing sectors of the textiles industry.[23]

Two main aspects should be considered in the production of textiles with biocide activity, namely (i) the type of biocide molecule, which determines the antimicrobial mechanism of the

material and its effectiveness; and (ii) the coating technology, which determines the stability and performance of the antimicrobial molecule, and should be adapted to the physic-chemical properties of the materials and the production costs.

1.2.1.1 Type of biocide molecule and antimicrobial mechanisms

Regarding the biocide molecules, several antimicrobial compounds have been implemented into textiles, including quaternary ammonium compounds (QACs),[24–26] halogenated phenols (such as pentachlorophenol, chlorocresol or triclosan, among others),[27–29] polybiguanides,[30,31] chitosan,[32–34] N-halamines,[35–37] metal/metal-oxide based NPs (e.g. Ag, Cu, CuO, TiO$_2$, ZnO, etc.)[38–41] and antimicrobial peptides (AMPs),[42] among others. Each antimicrobial molecule presents different mechanisms, which may influence their antimicrobial activity and the final effectiveness and performance of the material. The main possible antimicrobial mechanisms are summarized in Figure 1.4[43] and the antimicrobial mechanisms performed by each type of biocide molecule are explained below.
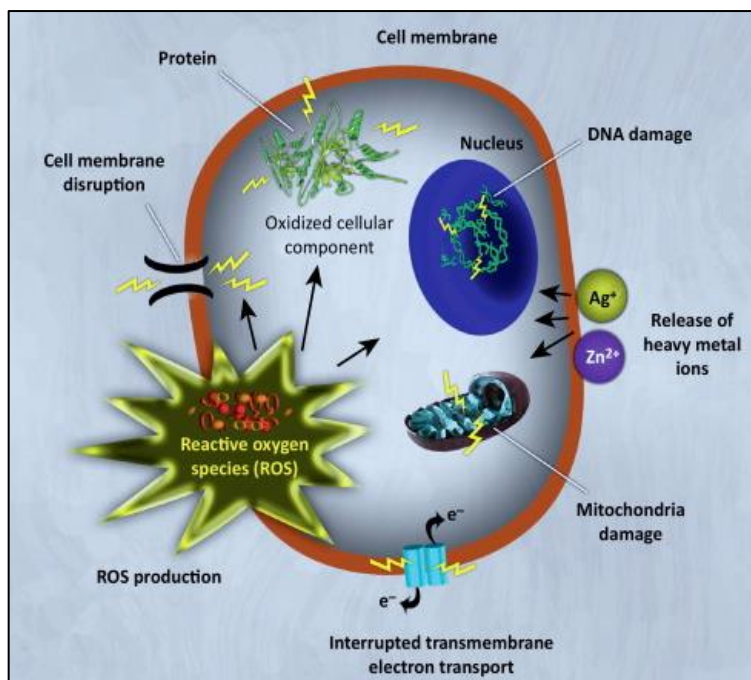

Figure 1.4. Antibacterial NPs toxicity mechanisms. Possible toxicity mechanisms of NPs against bacteria. Copyright 2012. Reproduced from ref 43 with permission from Elsevier Ltd.

7

In the case of **QACs**, a positive charge is located at the N atom in solution, which allows their attachment to the anionic fiber of the textile by ionic interaction. This positive charge is also responsibly of their antibacterial activity, forming attractive interactions with the negatively charged cell membrane of the microorganism. This phenomenon produces the inactivation of bacterial cells by damaging the cell membranes, denaturing structural proteins and disrupting the cell structure.[44,45] QACs also produces the loss of multiplication ability in the bacterial DNA.[46] Their antimicrobial activity remains active as long as the compound is attached to the textile.

Among the halogenated phenols, **triclosan** (5-chloro-2-(2,4-dichlorophenoxy) phenol) is the most used biocide. Triclosan essentially produces the inhibition of fatty acid biosynthesis by blocking the lipid biosynthesis (e.g. phospholipids, lipopolysaccharides and lipoproteins), as well as by interacting with amino acid residues of the enzyme-active site in the membrane, causing the instability of cell membranes.[23,30]

Polybiguanides are polycationic amines made of cationic biguanide repeat units separated by aliphatic chains. The antimicrobial activity of these compounds is based on the electrostatic attractions occurring between the positively charged biguanide groups and the negative charges present on the bacterial cell surface. Besides, their hydrophobic properties also contribute to this antibacterial activity, which produce the cell membrane disruption and the lethal leakage of cytoplasmic materials.[47]

Chitosan is a cationic polymer derived from chitin. Their antimicrobial mechanism is not clear, but it is generally accepted that the positively charged primary amine groups in the structure can interact with the negatively charged bacterial surface, resulting in extensive changes in the cell surface and cell permeability, leading to the release of intracellular substances. Chitosan may also interact with the bacterial DNA avoiding the protein synthesis.[34]

Other biocide compounds are the **N-halamines**, which are heterocyclic organic molecules that may contain one or two covalent bonds between nitrogen and a halogen, being usually chlorine, but it can also be bromine or iodine. They are effective antibacterial compounds since the electrophilic substitution of Cl by H in the presence of water results in the production of free Cl cations that bind to the microorganisms, interfering their metabolic pathways and leading to

their destruction. The resulting N-H bond can be restored by reacting it with Cl or Br donor compounds (such as sodium hypochlorite or sodium hypobromite, among others), regenerating the antimicrobial system.[48]

Metal and metal oxides NPs have been widely produced and used as antibacterial coatings, being Ag, TiO_2, ZnO and CuO the most exploited ones.[48] Their nano-size and charge confer them with antimicrobial activity. In fact, the antimicrobial effect of the metal NPs decreases with the particle size, since small particles have larger specific surfaces for interacting with microorganisms. The main toxic mechanism of NPs is performed by oxidative stress, producing reactive particles able to damage lipids, proteins and bacterial DNA.[49] However, the antibacterial mechanism may vary between NP type. In the case of Ag-NPs, their antibacterial mechanism is not fully elucidated and there are different proposed hypothesis. One of them is based on the penetration of these NPs on the bacterial cells by endocytosis.[50] Other authors support that their antibacterial capacity depends on the Ag-NPs aggregation, having more antibacterial effect in a dispersed NPs solution than when forming agglomerates.[51] Contrarily, some works support the formation of clusters and their anchorage to the bacterial cell surface as the main mechanisms.[52] Although the mechanism is fully elucidated, it is widely accepted that their main antibacterial effect is based on Ag partial oxidation and release of Ag^+ ions, producing disruption of ATP production and DNA replication, disruption protein synthesis and/or causing cell lysis.[53]

On the other hand, the antimicrobial properties of TiO_2, and most of the metal oxides, arise from their photocatalytic activity to kill microorganisms by the production of reactive oxygen species generation. These species are able to oxidize the lipid molecules on the cell membrane, producing its disruption.[54,55]

Finally, **AMPs** are natural compounds made up of a large number of small proteins and presenting high antimicrobial activity against several microorganisms. Antibacterial mechanisms of AMPs are based on the interruption of internal cellular processes from macromolecular synthesis (e.g., RNA, DNA synthesis) to the loss of ATP from actively respiring cells.[56]

Due to their different mechanisms, stability and effectiveness, each molecule type presents advantages and disadvantages, which are summarized in Table 1.1.

Table 1.1. Summary of the main advantages and disadvantages of antimicrobial agents implemented in textiles.

Antimicrobial agent	Examples	Advantages	Disadvantages
QACs	- benzalkonium chloride (BC) - stearalkonium chloride - cetrimonium chloride/bromide (cetrimide) - cetylpyridin chloride (CPC)	- active against a wide range of microorganisms	- easy detachment from the textile fibers - poor washing durability - poor biodegradability - low efficiency against biofilms
Halogenated phenols	- triclosan - pentachlorophenol - chlorocresol	- control on the action mechanism - high antimicrobial action	- generate bacterial resistances - specific to some bacterial types - toxicity
Polybiguanides	- poly(hexamethylene biguanide) (PHMB) - bisbiguanide chlorhexidine	- potent and broad spectrum bactericidal agent - water soluble - low toxicity	- large amount needed - potential bacterial resistance
Chitosan	Derivatives of Chitosan: - Quaternized Chitosan derivatives - Carboxyalkylated Chitosan derivatives - Chitosan-Amino Acid conjugates	- non-toxicity -biodegradability -biocompatibility	- finishing not durable - high dependence on the molecular weight, pH and temperature
N-halamines	- amine N-halamines - amide N-halamines - imide N-halamines	- recyclable antimicrobial effect - efficient against a broad spectrum of bacteria - long-term stability and low cost	- poor UV stability - adsorbed Cl after treatment, producing unpleasant odor and discolor of the fabric
Metal NPs and Metal/oxide NPs	- Ag, Cu, Au, Se - Ag_2O, CuO, TiO_2, ZnO, SiO_2, MgO	- wide antimicrobial actions against different bacterial types - effective at low concentrations - high stability and antimicrobial action	- nanotoxicity - Ag^+ release
AMPs	- pexiganan - L-cysteine - daptomycin	- broad spectrum of antimicrobial activity -environmentally friendly -low antimicrobial resistance	- usually presents problems of release from the substrate

QACs are the most commonly used antimicrobial agents in textiles because of their proved efficiency after implementation in fabrics of different structure and composition. However, their stability into the textiles fibers through ionic interactions is very low, and QACs are quickly released to the medium during washing.[23,57] Besides, their antimicrobial effectiveness decreases at high microbial densities (e.g. biofilm formation) and they also present poor biodegradability.[45]

Triclosan, the most common member of the halogenated phenols family, is a strong antimicrobial agent, very effective against a wide range of microorganisms including antibiotic-resistant bacteria. Its mechanism have been widely studied, established and accepted. Nevertheless, the widespread use of triclosan as antimicrobial agent has resulted in the emergence of bacterial resistances.[30]

N-halamines, on the other hand, present the particularity of being able to restore their antimicrobial activity through a chemical process after used. These low-cost agents present strong biocide activity against a broad spectrum of bacteria, and are stable for long-time periods.[36] The main problem of these compounds is that after treatment, some residual halogens can be trapped on the fibers, conferring to the fabrics an unpleasant odor and discoloration. This fact makes their application in the textile industry complicate.[44]

Compared to the last group, polybiguanides present higher antibacterial capacity, being more effective against Gram-positive than for Gram-negative bacteria. Besides, they present low toxicity and water solubility.[30] However, biguanides also present some drawbacks like the demand of large amount of product to accomplish an effective antimicrobial activity or the bacterial resistance developed by some types of polybiguanides.[58]

Due to its wide antimicrobial spectrum and high antimicrobial activity at lower concentrations, textiles coating with antimicrobial-metal and metal oxide NPs are gaining attention in the last years. Among them, silver is the most common NPs currently used for antimicrobial textiles production.[59] However, textile modification methods involving NPs may present cytotoxicity, and Ag in particular has demonstrated preliminary indications of bacterial resistance development.[60,61]

On the other hand, many peptides are already used in medicine, such as daptomycin, pexiganan or psoriazyna. Some others are under development, such as plectasin NZ2114 or L-cysteine, which are promising as durable antimicrobial agents. They present a broad antimicrobial spectrum against several microorganisms including Gram-positive and Gram-negative bacteria.[62] Furthermore, their natural origin prevents the antimicrobial resistance and make them environmentally friendly. However, their easy release form some substrates can become a drawback.[63]

Apart from the biocide agent used in the coating of the textile, the technology applied for that purpose has a huge influence in the final product. The main coating technologies employed in textiles industry are exposed and compared below, as well as their advantages and drawbacks.

1.2.1.2 Coating Technologies

The coating technology used to implement the biocide agent is fundamental since it determines the properties of the final antimicrobial textile. An ideal antimicrobial textile should keep the original properties of the non-modified material, while presenting a broad spectrum antimicrobial activity, durability of the antimicrobial activity throughout the life of the textile and low toxicity to human beings. Among these goals, antimicrobial durability may be the greatest challenge for researchers, because textiles are subjected to multiple actions, such as wear, washing, drying, ironing etc., during their life.

Based on the latter, two coating technologies are commercially available nowadays, mostly focused on the production of silver-based antimicrobial textiles:

- **incorporation into polymer melts** before fiber formation using e.g. in situ polymerization,[64,65] sol-gel technique[66] and laser ablation;[67]
- **impregnation** onto the fibers.

In general terms, the incorporation of the antimicrobial molecules into the polymer melts before fiber formation allows the production of the antibacterial textile fibers before textile production. It provides high stability to the antimicrobial compounds in the textile and a huge versatility in the manufacturing process, ensuring both the stability and durability of the

antimicrobial activity and the complementarity with industrial textile production lines. However, this technology also presents important drawbacks. First, the exposure to a melt-processing stage causes significant morphological changes to the antimicrobial molecules, this compromising their structure and antibacterial activity. This is critical in the case of organic molecules such as enzymes, QACs and antibiotics, which may lose their antimicrobial activity when implemented in the textile fibers through this technology. Even the antibacterial activity of inorganic NPs can be compromised with this technology, being necessary to use large amounts reagents (>3 % in the case of silver) to achieve adequate antimicrobial effects. Additional drawbacks of the technology include problematic spinning and yarn breakage, the use of toxic reagents and the impossibility to prepare micro/nano fibers.

In the case of impregnation, this process is much simpler and requires softer experimental conditions, being able to impregnate antimicrobial compounds of any nature, including organic and inorganic ones. After impregnation, the material remains on the textile surface, but it is not incorporated inside the fibers. For this reason, the antimicrobial compound is superficial and may be released to the medium with facility, compromising the durability of the antimicrobial activity in the textile. This low stability of the antimicrobial coating is one of the main drawbacks of impregnation, when compared to the previous one. Apart from that, inorganic molecules impregnated on the fabric from a coating solution produce deposits on the textile surface, which may produce negative effects on the user. For example, silver NPs impregnated with Smith&Nephew's ActicoatTM solution produce large amount of the nano-crystalline particles that tend to release into the wound, causing irritation.

Attempts to create fiber-based products having effective antimicrobial properties with minimum agent release have been unsuccessfully produced so far. For this reason, other technologies are now being explored, mostly applied to metallic NPs, metal oxides and metal salts. These methods are conventionally divided into two:

- **"Sol"-methods**, involving the direct deposition of colloidal suspensions of the antimicrobial agent, e.g., sonochemical coating[68] or plasma deposition[69].

13

- **Solution methods**, employing precursor solutions to synthetize in situ the antimicrobial molecule on the textile surfaces, e.g., intermatrix synthesis[70].

In **sonochemical coating**, the antimicrobial molecule is incorporated in the textile after application of high intensity ultrasounds in water medium. The ultrasonic waves (at frequency rates of 20 KHz - 1 MHz) generates the so-called cavitation phenomenon, which corresponds to the formation, growth and collapse of bubbles in the solution.[71] Thus, microjects and shock waves produced by the acoustic cavitation project the NPs towards the textile fibers, forming stable and homogeneous coatings. High-intensity ultrasound is a highly scalable, simple, fast, efficient and environmentally friendly approach for surface functionalization. In addition, this process has been upvoted by IUPAC as a top-ten emerging technology in 2021, highlighting the durability of antibacterial textile coating.[72] However, the use of high power intensities and the erosion of the tips may represent some drawbacks in the reproducibility of samples.[73]

Plasma deposition involves the deposition of organic-metal complexes with antimicrobial activity on the surface of the textile. This method allows the formation of very thin layers (few microns) in a fast and simple process involving the evaporation of the complex at low temperature to avoid textile damage, the generation of the room-temperature plasma (i.e. oxygen plasma with the volatile antimicrobial complex) and the deposition on the textile. The material is quite stable after deposition, providing high antibacterial effectiveness for long times. Main disadvantages are: (i) plasma coating requires low-volatility metallic/metal oxide complexes, which not easy to synthetize; and (ii) the technology is quite energy demanding and thus, more expensive than others.

Intermatrix synthesis refers to a chemical process where the ions in the precursor solution are retained by ionic interactions with the charged groups in the polymeric support matrix and reduced in situ to form metallic or metal oxide NPs.[74,75] The process can be repeated several times with the same precursor solution, thus increasing the NPs size, or with other solutions, resulting in the production of core-shell NPs with synergistic effects.[76] The NPs in the material matrix are stable for long time periods and provide high antimicrobial activities. However, the procedure is restricted to matrices with reactive functional groups, such as cotton or cellulose, and metal/metal

oxide NPs based on ionic precursors. Additionally, the formation in situ of these compounds requires the use of large amounts of reagents in the synthesis and aggressive reducing agents that may compromise textile integrity and properties.

Finally, other antimicrobial finishes based on resin binders with silver-ions overcoat,[77] binder systems or transfer methods from a donor fabric to a target textile in the presence of moisture and upon exposure to heat,[78] the use of inorganic metal salts[79] or zeolites[80] has also been described. In general, most of these coating technologies are currently under development and often require time-consuming or harsh fabric pre-treatments such as chemical activation. In addition, the stability of the antimicrobial agent after coating with these technologies is relatively low, and they require subsequent coating stabilization using different cross-linking techniques.[81] Without cross-linking, the release of the active agents during fabric exploitation remains a major concern, which compromises the durability of the antibacterial effect and the safety at use, increasing the risk of contamination and infection.

1.2.2 Antimicrobial and anti-biofilm water treatment membranes

Biofouling is generally defined as the deleterious attachment of bacterial cells and extracellular polymeric substances (EPS) to a solid surface, finally resulting in the formation of a biological structure known as biofilm. EPS are constituted of lipids, proteins, polysaccharides and nucleic acid released from bacteria and it helps in biofilm formation. Once the biofilm is mature, it present some dynamism recruiting bacteria from the medium but also releasing fragments containing high bacterial concentrations to the medium. Thus, biofilms are important bacterial contamination and infection sources and should be controlled. Additionally, biofilms are the main obstacle in membrane filtration systems, owing to the decreased permeates flux and therefore increased operation and maintenance costs.[82]

Traditional techniques for water contaminants treatment include adsorption, coagulation-flocculation, precipitation, electro dialysis or ion exchange, among others. However, these methods come along with several drawbacks and their efficiency for membrane biofouling mitigation is questioned. For example, adsorption processes are tedious to develop with long

protocol times and produce the agglomeration of NPs. Precipitation method is considered ineffective when high concentrations of heavy metals are present and produces high amounts of toxic sludge. With coagulation-flocculation methods, the sludge produced has better settling and dewatering characteristics, however, the volume of sludge generated is much higher. Electrodialysis implies high operational costs due to energy consumption and membrane fouling. Finally, ion exchange has high treatment capacity and removal efficiency, but the cost is also high due to synthetic resins generation.[83]

For this reason, nowadays physicochemical approaches based on chemical compounds are currently used to control membrane biofouling, e.g. chlorine, which eliminate bacteria and thus any risk of contamination. The continuous injection of chemicals in the water networks is costly, time-consuming and results in the formation of toxic and carcinogenic by-products. Other techniques are ozonation and ultraviolet radiation, but their implementation is expensive and ozone can also create mutagenic and carcinogenic by-products.

Due to the important limitation of current technologies, new approaches are now being explored to prevent biofilm formation, which are based on surface modification of the membranes by coating or grafting them with antifouling and/or antimicrobial agents.

1.2.2.1 Membrane modification with antifouling agents

The use of materials on which bacteria adhere less, e.g. silicone,[84] is considered as first choice to prevent bacterial colonization and spreading. Silicone is hydrophobic and initially prevents bacterial attachment. However, this effect is not lasting since this material favors nonspecific protein adsorption, resulting in the formation of protein layers on the material surface that promote bacterial recruitment and attachment, and thus biofilm formation after some time. Other molecules with higher anti-adhesion properties[85] such as surface PEGylation[86] significantly minimize bacterial attachment and colonization, but require hazardous polymerization reactions[87] that compromise the material properties and its biocompatibility.

Other strategies rely on the enhancement of the hydrophilicity of the membranes. In hydrophilic membranes, hydrogen bonds can be formed with the adjacent water molecules,

16

creating a thin water boundary between the membrane and bulk solution. This layer minimizes hydrophobic foulants adhesion to the membrane, preventing the biofilm formation.[88] Polymeric membranes are hydrophobic, so more susceptible to biofouling. Thus, to enhance their hydrophilicity, membranes can be modified with different materials. One of the most effective methods to avoid biofilm adhesion is polymeric blending. With this process, two or more organic and/or inorganic materials are mixed to endow the membranes with the desired properties.[89] In this context, different hydrophilic organic polymers have been used, such as polyvinyl pyrrolidone (PVP), chitosan or polyethylene glycol (PEG), among others. However, this strategy presents some drawbacks, like the poor compatibility of these polymers with polymer matrix.

Another approach to minimize membrane biofouling is based on the quorum quenching (QQ). Quorum sensing is the cell-to-cell communication used by microorganisms to coordinate their behaviors including biofilm formation or detachment. This process requires the production and release of autoinducers, which are inactivated by QQ enzymes. Thus, these type of processes may produce the decrease of bulk viscosity, hydrophobicity and the amount of EPS released.[90] However, the QQ enzyme presents some drawbacks as high cost, the need for purification steps and the low enzyme stability.[91]

Some hydrophilic metal oxides have been used to reduce fouling by increasing membrane hydrophilicity. This is the case of Al_2O_3,[92] silica,[93] zeolites[94] or TiO_2,[95] among others. Apart from the antifouling properties, all these compounds also exhibit antibacterial properties, and the combination of both hydrophilic and antibacterial activity enhances their effectivity in preventing biofilm formation. For these reasons, most recent surface modification protocols for preventing bacterial colonization have been based on the use of nanomaterials as antimicrobial agents.

1.2.2.2 Membrane modification with antimicrobial agents

Several antimicrobial agents have been already coated into polymer membranes and used for water disinfection and microbial control. The most relevant are antimicrobial chitosan NPs, metal and metal/oxide nanomaterials (e.g., Ag, Cu, Au, ZnO, TiO_2, CuO, ZrO_2, SiO_2 and Al_2O_3), enzymes and carbon nanomaterials (e.g., fullerenes, carbon nanotubes and graphene-based nanomaterials).[96] Advantages and disadvantages of these materials are shown in Table 1.2.

Table 1.2. Summary of the main advantages and disadvantages of antimicrobial agents implemented in water filters.

Antimicrobial agent		Advantages	Disadvantages
Chitosan		- high hydrophobicity - easy fabrication - good antibacterial activity and low organic fouling propensity[97]	- can only dissolve in acidic solution[98]
Metal and metal/oxide nanomaterials	TiO$_2$	- antibacterial and antifouling properties - presents photoactivity - nontoxic	- photocatalytic membranes lack stability - the overall cost of the enhanced membranes[99]
	Ag, AgO	- enhanced mechanical strength and antifouling properties - thermal and chemical stability	- NPs release to water; prone to biofouling for continuous processes[100] - toxic at acid conditions[101]
	Al$_2$O$_3$	- enhanced mechanical strength and antifouling properties	- membranes highly sensitive to NPs concentration
	ZrO$_2$	- enhanced water retention - very stable at high temperatures and humidity	- susceptible to fouling - expensive raw material
	SiO$_2$	- resistant to oil bearing water - high chemical and thermal stability - high permeability	- susceptible to fouling - higher NPs concentration deteriorate performance
	Cu, CuO	- resistant to microbes - enhanced mechanical properties - modifications may improve antifouling - lower price than Ag NPs[98]	- low quality NPs by physical synthesis - toxic NPs by chemical synthesis - their leaching from the membranes can be harmful to the human being[91]
	ZnO	- antibacterial and antifouling properties - selectivity	- physical and chemical synthesis costly and harmful to the living beings[91] - poor chemical stability in acidic conditions[102]
Enzymes		- high activity - selectivity and specificity - non-toxic products[97]	- difficult development and scalability of an enzymatically antimicrobial membrane[97]
Carbon nanomaterials	Fullerenes	- non-toxic -biocompatible -may adsorb organic compounds	- expensive[103] - low solubility and poor dispersibility[104]
	G/GO	- high antimicrobial and antifouling activities - enhance mechanical strength - enhance permeability	- difficult to scale-up for economic reasons[105]
	CNTs	- high antimicrobial and antifouling activities - cheaper than other carbon nanomaterials	- use restricted by their poor solubility in most solvents[106] - lack of control in the nanotubes alignment[107]

- **Chitosan** has been widely used in water and wastewater treatment systems as a coagulant/flocculant.[108,109] It has been implemented by coating in storage tanks, sponges and polymeric membranes.[110–112] Some advantages of this antimicrobial agent include hydrophilicity, which contribute to the biofouling mitigation, high antimicrobial activity and easy synthesis. As a main drawback, chitosan can only be dissolved in acidic media. Despite all its advantages, only a few studies have investigated chitosan as the single component of antimicrobial membranes.

- **Metal and metal/oxide materials** have been used in water or wastewater treatment for decades because of their numerous advantages such as their low cost, easy synthesis, ability to kill bacteria, UV stability and high hydrophilicity.[91] Their incorporation into polymeric membranes produces the improvement of the physicochemical properties and performance of the membranes in terms of porosity, hydrophilicity, charge density, chemical, thermal and mechanical stability. Furthermore, they endow the membranes with antibacterial activity. That is, some of the metal/oxide NPs generate superoxide radical anions or hydroxyl radicals through a photocatalytic process. These radicals are strong oxidizing agents and decompose organic matter. In other NPs, the antimicrobial mechanism relies on electrostatic interactions between the metal/metal oxide and bacterial components, which disrupt their cellular membrane structure. Finally, they can also produce free radicals without the need for photocatalysis, thus creating oxidative stress and reactive oxygen species against bacteria and causing cell damage.[113] However, depending on the metal or metal/oxide used, they may present some advantages or drawbacks, which are specified in Table 1.2.

There are also several types of **enzymes** present in nature with antimicrobial characteristics, such as proteolytic enzymes, polysaccharide degrading enzymes, oxidative enzymes and antiquorum sensing enzymes. These proteins with biocatalytic activity have been used as anti-adhesion and antimicrobial agents on the modification of membranes due to their high activity, specificity and selectivity. Additionally, the processes carried out by enzymes to eliminate biofilms and bacteria are mostly non-toxic and effective even under soft conditions.[114] In terms of activity, they present a multi-functional antibacterial mechanism at different levels, including: i) the biofilm destabilization, ii) biofilm degradation; and iii) bacterial cell lysis.[115] In this context, several types of enzymes have been used for decreasing biofouling formation in membranes, such as lysozyme,

savinase, dispersion B, alginate lyase, proteinase K and serratiopeptidase,[63,116,117] among others. When immobilized in polymeric membranes, they are usually coupled with other antimicrobial components such as TiO$_2$,[118] organic molecules[119] or graphene,[120] to enhance the antibacterial and antifouling properties of the membrane. Despite their advantages, the development of an enzymatically antimicrobial membrane is quite complicated and not easily scalable.[97]

- **Carbon nanomaterials**, such as fullerenes, graphene/graphene oxide and carbon nanotubes, are considered an emerging class of novel materials with antibacterial properties and their incorporation into polymeric membranes has been already achieved. In general, the use of carbon nanomaterials provide a great spectrum of advantages, such as electrical conductivity, mechanical resistance, thermal conductivity, photo-luminescence, transparency, constructional durability and antimicrobial activity against microorganisms.[121] Their antimicrobial activity relies on their composition, surface modification, target microorganism and reaction environment.[122] Below, the specific antibacterial mechanisms for each type of carbon nanomaterial, as well as their advantages and drawbacks are exposed.

Fullerenes are carbon atoms disposed in the form of a large spheroidal molecule. These compounds have proved antibacterial activity against both, Gram-positive and Gram-negative bacteria. However, often Gram-positive bacteria are more susceptible to fullerenes due to their interaction with the bacterial cell wall, producing cell wall destruction, alterations in the phospholipid structure, and increasing the permeability of the cell membrane.[123] Fullerenes reduce the proportion of unsaturated fatty acids and increase the proportion of cyclopropane fatty acids in the bacterial cell wall of Gram-negative bacteria.[123] Other theories support that fullerenes may inhibit the bacterial respiratory chain[124] or can produce the induction of cell membrane disruption.[125] Fullerenes have been used in wastewater treatment because of their high affinity and surface-volume ratios, making them ideal to capture contaminants from aqueous solutions (e.g. heavy metals).[126] However, since fullerenes are expensive, normally they are embedded with other composites in antibacterial membranes, increasing the sorption structures. Fullerenes can be incorporated into different polymers by formation of donor-acceptor or covalent bonds, like poly(phenylene-isophthalamide) membranes,[127] or tri-diethyl malonate membrane.[128] Despite their numerous advantages, the use of fullerenes in membranes in

challenging because of their low solubility and poor dispersibility.[104] For these reasons, their use is mainly produced in suspension.

Graphene and graphene oxides (GO) are potential antimicrobial agents due to their extensive surface areas, thermal, electrical and physicochemical characteristics.[129,130] The synthesis of GO is simple, fast and cheap and only presents minimal toxicity for mammalian cells at low concentrations.[131] Their antimicrobial mechanism is based on the production of reactive oxygen species, which affect the cell membrane and cell wall of microorganisms by physical demolition and chemical oxidation, resulting in bacteria death and furthermore, a decrease in microbial resistance.[132,133] Furthermore, GO has been combined with a great variety of NPs due to the increment in their antibacterial activity against a wider range of microorganisms, for example with gold NPs,[134] titanium NPs,[135] iron NPs[136] or silver NPs,[137] among others. Graphene and GO have been used for the development of membranes for water filtration. In fact, a singer-layer graphene has been used as a membrane itself in several works,[138,139] due to its low hydrodynamic resistance produced by the thin monoatomic thickness and the formation of subnanometer pores on the graphene sheet.[107] However, membrane surface modification is technically easier to achieve and to scale-up. Thus, the modification of polymer membranes with graphene and GO has been developed in many studies with high antibacterial and antifouling efficiency, increasing permeability and mechanical strength.[140–143] However, there are economic obstacles that make their implementation in a scale-up process difficult.[105]

Carbon nanotubes (CNTs) can be formed by single, double or multiple layers of graphene cylinders. CNTs studies are gaining interest in the recent years for a wide range of applications. However, their use is restricted because these materials are insoluble in most of solvents[106] and surface modification is needed in many cases to improve their implementation. CNTs exhibit excellent antimicrobial activity probably due to the nano-size of these compounds. It is widely accepted that these compounds, which no toxic in their bulk form, increase their antibacterial activity when their size diminishes. It may be associated to an increase in the surface-to-volume ratio, which produces a strong bond with the cell wall or plasma membrane, thus enhancing their efficiency as antimicrobial agent. Antimicrobial mechanism of CNTs relies in their interaction with bacteria, producing the disruption of their cellular membrane, metabolic procedures and

morphology.[144] These interactions are performed by direct contact with microorganisms, resulting in bacterial cell death and morphological changes that produce the loss of cellular integrity. Besides, after exposure to small CNTs, a more than fivefold increase of plasmid DNA, a twofold increase of RNA and efflux of cytoplasmic materials has been observed in solution.[145] Regarding the membranes based on the use of CNTs, monolayer membranes formed by CNTs with antibacterial and antifouling properties have been reported for water treatment showing high performance in terms of permeability and decrease of biofilm formation.[146,147] Nevertheless, the fabrication of CNTs monolayer implies vertically aligned CNT-based membranes, which is a great challenge and requires arduous multi-step processes, analogous to the graphene membranes fabrication. Their scale-up production can be more easily achieved by embedding CNTs into polymeric membranes taking into account that the use of CNTs is cheaper than other types of carbon nanomaterials. Nevertheless, the lack of control in the alignment of the nanotubes is still a drawback in this context and their chemical functionalization is required in most of the cases for ensuring compatibility of the hydrophobic nanomaterial with the fabrication process.[148]

It is important to remark that all these antimicrobial agents are often combined in the polymeric membranes, which allows to the enhancement of their properties.

A growing number of antimicrobial agents implemented in antibacterial surfaces are based on the use of organic molecules, such as QACs,[149] polyhexamethylene guanidine hydrochloride (PHGH),[150] 4-vinylpyridine (4-VP),[151] N-halamine compounds[152] and capsaicin.[153] Despite of being potential antimicrobial agents for biofouling reduction, the number of studies to fabricate antibacterial membranes is limited, especially for water treatment processes.

Finally, new eco-friendly approaches relying on biological control of membrane biofouling have been also developed at laboratory level.[154] However, limitations, primarily concerning the stability of the nanomaterials on the membranes, and thus the durability of the antimicrobial effect, exist. As in the case of cotton textiles, there is a need to reduce nanomaterial loss and to prevent the impact of the nano-coatings on humans and environment.

1.2.2.3 Antibacterial membrane preparation methods

The selection of the appropriate methodology for functionalizing polymeric membranes with biocide agents is of crucial significance since determines the control of biofouling and antimicrobial properties of the membrane. Surface functionalization should not alter or impair the original properties of the polymeric membrane, such as separation performance, permeability or selectivity. Choosing the most convenient method depends on the demands of each case, however some features on the membrane are intended to accomplish, such as high loading of antibacterial agents with good exposure, low aggregation and controlled release of antibacterial particles. Thus, there exist several approaches for membrane modification with biocide agents, being the most outstanding blending, surface grafting, surface coating, interfacial polymerization and layer-by-layer assembly. Their main features and drawbacks are exposed below.

- **Blending** antibacterial nanofiller with polymer matrix. The incorporation of NPs into polymer matrix by physical blending is a wide used method for antibacterial membrane preparation because of its several advantages, such as having an extensive spectrum of antibacterial activity, easy fabrication and the preservation of the membrane structure, maintaining the separation properties.[155,156] Normally, the blending process of the nanomaterials to polymeric membranes consists of dispersing NPs in the polymer solution and subsequent either, phase inversion (controlled polymer transformation from a liquid phase to a solid phase) or solvent evaporation. However, this method presents some important drawbacks such as a limited direct contact between bacteria and the NPs embedded in the membrane, which diminishes the biofouling resistance. Besides, it exits a leaching of the NPs after long-term use, which reduces the antibacterial activity and also causes secondary pollution by the flow of this NPs.[157] To solve this last problem, some approaches have been developed based on the reinforcement of the interactions between the NPs and the polymeric membranes, mostly based on the addition of polymers electrostatically charged[158] or the use of organically modified NPs with improved affinity to the polymer membranes.[159]

- **Coating** antibacterial agents on polymer membrane surface. This method provides enhanced antibacterial properties to the modified membranes. For coating membrane surfaces

both, chemical and physical treatments have been used. These include dip coating,[160] spin coating[161] and direct filtration techniques.[162] Dip coating is based on the immersion of the membrane into a solution with either, sol-gel precursor or a NPs suspension, followed by thermal treatment or simply sensing with water. This process is simple and the coatings' surface can be adapted to optimize antibacterial and antibiofouling properties. Spin coating is developed by either, casting the solution on a spinning substrate or casting it on a static one and then applying the centrifugal force with the spinner. This method provides smoother, thinner and more uniform coatings than dip the coating method, although the assembly of multilayers in non-flat surfaces still remains a challenge. Finally, direct filtration of a suspension with antibacterial agents through polymeric membranes assisted by vacuum or hydraulic pressure is an effective antimicrobial coating method. Nevertheless, prior membrane functionalization is usually required since the final coatings have very low stability.

- **Interfacial polymerization** of antibacterial agents is a rapid and effective method to produce thin film composite membranes at the interface between two phases, normally used in water desalination. The polymerization is a polycondensation reaction between two highly reactive monomers dissolved in two immiscible liquids. Generally, an aqueous solution containing diamine monomers is placed in contact with a porous substrate and the residual solution is removed. Then, organic solution containing monomers is deposited on the substrate, which is saturated with the aqueous solution, producing the physically attachment to the membrane substrate. The typical interfacial polymerization process is found in water/oil interface. Recently, this process has been used for the production of thin film membranes with antimicrobial activity, by co-depositing antimicrobial agents with aqueous monomers and then, attaching these compounds with the organic monomer in oil phase.[163] These processes showed good solubility, permeability and antibacterial properties. However, depending on the composition of the membrane, this process requires a post-treatment to improve the stability of the obtained layer.[164]

- **Layer-by-layer** self-assembly is an effective technique to produce functionalized multilayers on a membrane surface by assembling alternatively opposite charged species like polyelectrolytes.[165,166] This technique allows a high control of the function and thickness of the

24

obtained multilayers. Nevertheless, conventional layer-by-layer assembly is based on dip coating, which relies in long protocols and may result in non-homogenous coatings.

Finally, other membrane modification methods are based on *electrostatic interactions* between metal ions coordinated with positively charged polyelectrolytes and polymer membranes negatively charged,[158] or *surface grafting* consisting in the in situ reduction of metal ions on the membrane surface.[167] However, these processes are restricted to some specific metal ions and reducing agents, and are strongly limited by the physicochemical properties of the membrane. Since most polymers are chemically inert, these procedures normally require pre-treatments to introduce active functional groups into the membrane surface, which make the protocols to be longer and tedious to develop.

In summary, both antimicrobial textile fabrics and filters suffer from important stability problems, resulting in the loss of antimicrobial activity over time. Once the antimicrobial activity of the material is lost, it becomes again susceptible of colonization, and new living and infective bacteria can be found in the material surface. To prevent risk infection, the presence of these microorganisms should be detected as soon as possible with fast, simple and sensitive technologies, which will additionally serve as shelf life indicators. Considering this, traditional and most advanced bacterial detection technologies are presented in the following sections, paying particular attention to those susceptible of implementation in textile fabrics and water treatment membranes.

1.3 Bacterial Detection Techniques

Although fast and sensitive bacterial detection is crucial for the control and prevention of infectious diseases, most of the technologies available nowadays still rely on laboratory techniques and instruments, mainly based on cell culturing, imaging[168,169] or sequencing.[170,171] As a step forward, standard microbial detection methods based on cell culturing and colony counting[172] are now being replaced by simpler and less tedious technologies. Among them, two methods, namely the polymerase chain reaction (PCR),[173] based on the identification of specific oligonucleotide

sequences (e.g., genes), and the enzyme-linked immunosorbent assay (ELISA),[174] consisting of the recognition of specific external proteins (e.g., receptors) with selective antibodies, are now being implemented as routine technologies in a number of central laboratories in hospitals. Unfortunately, these techniques still require sample collection and transport to the central laboratory for analysis, which delays time-to-result and decision-making.

With the aim to tackle the challenge of microbial detection out of the laboratory, portable and miniaturized versions of these techniques have been developed,[175] also in the format of biosensors, where bacteria are detected and identified through selective DNA strains (DNAsensors)[176] or antigens/antibodies (immune sensors).[177] These portable systems allow to transport bacterial detection at the place of patient care (point-of-care),[178,179] but in most of the cases they still rely on the processing of the sample, e.g. concentration and/or amplification, before analysis. Furthermore, they cannot differentiate between live and dead bacteria, which particularly relevant in the case of DNA-based technologies for the high stability of oligonucleotide strains. Although some strategies to distinguish live/dead bacteria have been already developed,[180] only living organisms are infective and these systems are highly susceptible of false positives.

Alternative test kits able to distinguish between live and dead bacteria are now commercially available and gaining popularity for their simplicity, easy detection, rapid response and high sensitivity. Most popular test kits are based on the detection of adenosine triphosphate (ATP)[181] or the use of either defined substrate technology (DST)[182] or metabolic indicators.[3,183] DST, e.g., Colilert Test or Colipat Test, are based on the use of nutrient-indicators, which are selectively metabolized by specific bacterial strains. In the case of the Colilert Test, two nutrient-indicators are incorporated in the substrate formulation for the selective detection of: (i) coliforms, which selectively metabolize ortho-nitrophenyl-β-galactoside (ONPG) molecules by their β-galactosidase activity, producing a brownish color by the release of O-nitrophenol; and (ii) *Escherichia coli* (*E. coli*), which is detected fluorescently after metabolizing MUG and releasing fluorescent 4-methyl-umbelliferone molecules thanks to the activity of the *E. coli* enzyme β-glucuronidase. Although simple, the number of DST is very small since requiring specie-specific enzymatic activities not available for all bacteria. Additionally, these tests need bacterial proliferation in controlled

environmental conditions to provide reliable results. Finally, the detection of low bacterial concentrations is possible, but only after long incubation times at the previous conditions. For all these reasons, the implementation of this technology out of the laboratory is very challenging.

Fluorescent determination of ATP is simpler, only requiring dispensing the detection solution on the surface under study. It is also much more sensitive than the previous one, enabling close to single bacterium detection after revealing the reaction with ATP by irradiation with UV-light. The detection mechanism is based on the fact that ATP is the main energy molecule in bacteria, and its presence is associated to bacterial contamination. This method is currently widely used in the identification of contaminated surfaces in the food industry.[184] Its main limitation is on the need for spreading the reagent on the surface under study, thus being tedious and restricted to the small areas.

Metabolic indicator refers to those molecules capable to change their properties in response to bacterial metabolism. This definition includes different types of chemical molecules, which can be classified according to their sensing strategy in:

- **pH-sensitive molecules**, since bacterial metabolism reduces pH;[185,186]
- **conductivity-sensitive molecules**, since bacterial metabolism tends to increase medium conductivity;[187,188]
- **redox molecules susceptible of reduction** (i.e. accept electrons) by the proteins and/or mediators present in the bacterial electron transport chain (ETC).[189,190]

In general, all these metabolic indicators respond to bacterial presence by changing their colour (chromic response). Main difference between them is that pH- and conductivity-sensitive molecules respond indirectly to bacterial metabolism, while redox metabolic indicators directly interact with the molecules responsible of bacterial metabolism in the plasma membrane. For this reason, redox metabolic indicators are more accurate, more sensitive and less prone to false positive than the other two.

1.3.1 Electrochromic metabolic indicators

Redox metabolic indicators report on bacterial presence by changing of color after accepting electrons from protein/mediators involved in bacterial metabolism. These proteins/mediators responsible of the color change comprise the ETC. The ETC consists of a series of protein complexes, and other molecules, located in the plasma membrane. These molecules sequentially oxidize nutrients transferring the electrons from the initial electron donor, i.e. a carbon hydrate such as glucose, to the final electron acceptor, the latter generally being either oxygen for aerobic bacteria or sulfate, nitrate or fumarate for anaerobic ones.[191] Hence, the electron donor transfers electrons to the first complex in the ETC. Electrons are then passed along a chain of redox centers in the adjacent proteins. The electron transference between centers occurs when the bottom redox center has higher affinity to electrons than the top one, or when the distance between adjacent redox centers permits an electron jump. Each electron transference process in the ETC produces small amounts of energy, which used to pump protons (obtained from the oxidation of organic molecules) through the plasma membrane. The proton unbalance is finally used to produce ATP thanks to the rotation of the protein subunits of the ATP synthase. A scheme of the ETC of *E. coli* is illustrated in Figure 1.5, which includes their principal components: NADPH (E^0 = 320 mV), FADH (E^0 = 220 mV), FMNH (E^0 = 210 mV), NADH (E^0 = 320 mV) and cytochromes (E^0 = 290 mV to + 80 mV).[192]

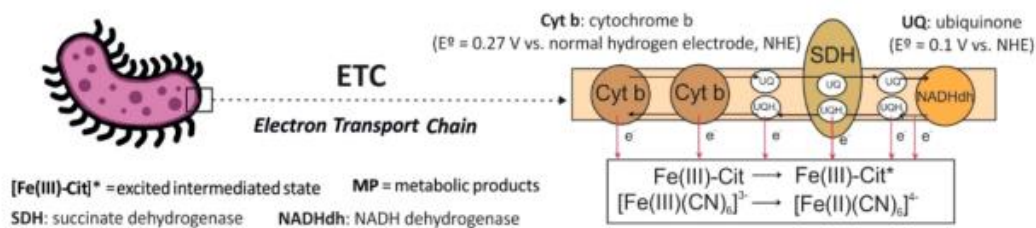**Figure 1.5. Main components of the E.coli ETC**, presented with the corresponding redox potentials (referred to NHE).

Considering the previous description of the ETC, metabolic indicators are molecules capable to accept electrons from one or several proteins/mediators in the ETC. Some of them can even act as final electron acceptors. As already commented, many of these metabolic indicators change of

color after accepting electrons. The property of changing of color when oxidized or reduced is known as electrochromism and thus, most of redox metabolic indicators are also electrochromic molecules. Different electrochromic metabolic indicators capable of accepting electrons from bacterial ETC have been reported, mainly electrochromic organic dyes, metal oxides, conducting polymers or iron derivatives. Representative examples of each family are included in Table 1.3 as well as their properties, advantaged and drawbacks.

Transition metal oxides (such as tungsten trioxide or polyoxometalates) have been widely used as inorganic electrochromic materials for bacterial detection.[213–215] However, due to their redox potential, the application of these indicators is restricted to exoelectrogenic bacteria growing in anaerobic conditions. Furthermore, the synthesis of tungsten trioxide nanoclusters is still complex, affecting the cost of both compound production and the final test kit.

Organic redox-active dyes, including azo dyes (e.g.tetrazolium salts) such as 5-cyano-2,3-ditolyl tetrazolium chloride (CNC), 2-(4-iodophenyl)-3-(4-nitrophenyl)-5-phenyl tetrazolium chloride (INT) or 2-[4-iodophenyl]-3-[4-nitro- phenyl]-5-[2,4-disulfophenyl]-2H-tetrazolium monosodium salt (WST-1) have been extensively used as bacterial electron acceptors, being reduced mostly by plasma or/and membrane dehydrogenase enzymes.[216–218] This type of salts are suitable for end-point cell viability assay, but are not very convenient for monitoring cell activity[219] since most of them are highly toxic and potentially mutagenic.[199,220] Additionally, some of them present low-intensity color changes difficult to be detected with the bare eye. Alternatively, the organic dye resazurin, also known commercially as Alamar Blue,[221,222] improve the chromatic change by providing more intense color changes. However, this compound is still difficult to detect visually since the color change involves is a small wavelength shift from blue to purple, which difficult to observe with the naked eye. In fact, fluorescence measurements are recommended by the supplier, particularly when assessing the detection of low bacterial concentrations.

Table 1.3. Different features of some electrochromic species that can behave as metabolic indicators.

Electrochromes	Standard redox Potential (E°/mV) (vs. NHE)	Molar extinction coefficient (M^{-1} cm^{-1})	Toxicity	Stability	Advantages	Disadvantages
WO$_3$	+500 [193]	31300 M-1cm-1 (In dye molecule D35) [194]	Low toxicity [195]	Stable at pH 6 [196]	Strong absorption in the visible spectrum range and low cost	Only work under anaerobic conditions and its synthesis remains complex [197]
CTC	-200 (at pH 7) [198]	16240 M-1cm-1 (in 95% ethanol) (at 450 nm) [198]	High toxicity [199]	(Low efficiency at pH ≠ 6.5) [200] (Insoluble in water) [198]	Produce suitable color changes and has been widely used	Stable at determinate conditions
Resazurin or Alamar blue	+380 (at pH 7) [192]	47000 M^{-1} cm^{-1} (at 602 nm) and 56000 M^{-1} cm^{-1} (at 572 nm) [201]	Toxic to several cell lines [202]	Stable in culture medium (pH between 7.0 and 7.4) [192]	Produces changes in color and fluorescence and the assay is simple [203]	Can produce false positives for its toxicity [204]
PANI	Depends directly on the proton activity in the solution [205]	Data not available	Low cytotoxicity [207]	High stability in acidic and alkaline solutions [208]	Facile preparation, low cost and environmental stability [209]	Low solubility, infusibility and weak processability [209]
Ferricyanide	+440 (at pH 7)	1040 M^{-1} cm^{-1} (at 420 nm)	Low toxicity	Unstable at pH>12 [211]	Soluble in water	Inconspicuous color changes
Prussian blue	+500	30000 M^{-1} cm^{-1} (at 700 nm) [212]	Low toxicity	Stable at pH between 1 and 6.4	Notable change of color and biocompatibility	High insolubility in water

On the other hand, the use of conducting polymers as electrochromic sensors of living bacteria has gained interest recently. Among them, polyaniline (PANI) is one of the most employed due to its capacity to provide clear and intense color changes at different potentials. A smart chip for bacterial detection containing PANI as bacterial-sensing molecule has been recently reported.[223] The device reports on bacterial presence with clear color change after selective recognition with specific antibodies. Different electrochromic responses are obtained by applying a constant potential to the functionalized electrodes, being proportional to bacterial concentration and thus enabling quantification. Additionally, it provides low limits of detection of 10^2 colony forming units per 1 mL (CFU mL^{-1}) of *E. coli* with the naked eye and 10^1 CFU mL^{-1} by using specific software. Main limitations of the device are: (i) the low-stability of the electrodeposited PANI layers on the electrode; and (ii) the need for incorporating biorecognition elements, e.g., antibodies, to detect selective bacterial strains. In addition, the device requires external instrumentation for the measurement, which makes its implementation in situ very difficult.

Alternatively, PANI has been also employed as pH metabolic indicator due to its capacity to report on pH changes associated to bacterial metabolism.[224] Nevertheless, its low solubility and the instability of pristine polyaniline in aqueous solutions make again very difficult to implement it for in-situ sensing. Furthermore, and as commented previously, pH metabolic indicators are susceptible to change in response to environmental conditions, being thus highly prone to false positives.

Other conducting electrochromic polymer, such as the poly(3,4-propylenedioxythiophen-alt-3,4-ethylenedioxythiophene) (PPE), have been also used due to their capacity to react with reducing species released by metabolically active bacteria.[197] However, the implementation of conducting polymers in hospitals settings still requires extensive studies on their long-term toxicity.[225–227] In addition, conducting polymers already present important issues related to their electronic properties, stability and processability.[228]

A different approach is the use of iron derivatives as chromogenic electron acceptors of bacterial metabolism. Ferricyanide is among the most common iron-based metabolic indicator, reporting on both Gram-positive and Gram-negative bacteria.[229–232] Main advantages of ferricyanide are its high solubility, low toxicity and low cost. However, the metabolic reduction of ferricyanide involved a very weak color change from pale yellow to colorless ferrocyanide, which is hard to see with the naked eye. Alternatively, ferric hexacyanoferrate, also known as Prussian blue (PB), is a derivate from the previous molecule that keeps the good performing characteristics of ferricyanide (i.e. low toxicity, low redox potential able to interact with ETC proteins, etc.) but improve the chromatic change. In fact, PB presents an intense blue color, with an extinction molar coefficient almost 30 times higher than ferricyanide, becoming uncolored after bacterial reduction to Prussian white (PW).[233–235] Due to its intense color change and biocompatibility, PB has been already employed as a redox mediator in the development of sensors and biosensors.[236–238]

Since electrochromic metabolic indicators react with proteins/mediators present in the ETC of many bacterial species, they can be used to detect a wide variety of Gram-positive and Gram-negative bacteria. It is important to remark that this redox reaction between the electrochromic molecule and the proteins/mediators in the ETC only occurs only when bacteria are metabolizing and thus, when they are alive and viable. For this reason, electrochromic metabolic indicators are used in bacterial viability test, antibiotic susceptibility test and in the identification of resistant bacteria.[3,239–241]

As in the case of ATP, electrochromic metabolic indicators may be also used to identify contaminated surfaces with the limitation of requiring dispensing the precursor solution on the potentially contaminated surface. The presence of living bacteria results in the reduction of the electrochromic molecule and its color change. Contaminated surfaces may be thus identified using a simple and fast protocol, with the main limitation of requiring dedicated personnel to analyze the huge number of potentially risky surfaces. This is virtually impossible in large facilities such as hospitals or schools. In fact, different studies found pathogenic bacteria in hospital fabrics and in water systems,[8,242] but, in practice, there is no way of knowing if a textile in use is contaminated or not.

The implementation of such molecules directly on the textile may result in smart materials able to report in situ the presence of living organisms. Such strategy has been already proposed and explored, generating a number of smart materials that will be discussed below.

1.4 Smart Materials

By definition, a smart material is a material designed to change one or more properties in response to external stimuli, e.g. the presence of bacteria. What makes these materials so attractive is that the change takes place in situ, and without the need for employing additional reagents or experienced personnel. This phenomenon, generally reversible, confers them actuation and/or sensing capacity,[243] which widely useful in several applications such as smart windows, smart textiles or biosensing. Smart materials generally combine two or more materials, commonly (i) a support material providing structural integrity and robustness, and (ii) one or more dopants responsible for the smart material activity (i.e. responsibility to stimuli). Support materials such as polymers,[244] gels,[245] paper,[246] glass[247] or fabrics[248] have been already produced, which are normally combined with dopants of different natures including molecular switches,[249] magnetic particles,[250] pH indicators,[251] or electrochromic metabolic indicators, among others.

Smart materials are generally classified according to their activity. One of the most common classifications divides them into:

- **Passive smart materials**, when the material can transfer energy but without responding to it, e.g. optical fibers that transfer electromagnetic waves.
- **Active smart materials**, when it responds to stimuli by one of the following mechanisms:[252,253]
  (i) modifying their geometry or properties after application of electric, thermal or magnetic fields, for example photochromic glasses that change of color by the presence of sunlight;
  (ii) changing energy from one form to another, like the solar cells that convert solar energy into electricity.

Another classification considers the response of the smart material to the applied stimuli. They are categorized into:

- **Thermo-responsive materials** or **shape memory alloys**, smart materials that can reach different shapes and return to the original one by varying the temperature or stress.[254] Applications of these materials are found in many varied areas, like textile industry, automotive applications, biomedicine, aerospace engineering, etc.[255,256]

- **Piezoelectric materials**, which are able to produce electrical signals when a mechanical pressure is applied on them and vice versa. These materials can be used in optical-tracking devices, magnetic heads, computer keyboards, sensors and energy harvesting devices, among others.[254,257]

- **Magneto restrictive materials**, which also respond to mechanical pressure but with magnetic fields rather than electric ones. Some applications of these materials are motors, hydraulic actuators and small-frequency high-power sonar transducers.[258]

- **pH-sensitive materials**, which change of color with the pH. There is a wide range of applications for these materials such as sensors,[259] smart packaging of food,[260] smart insulin delivery,[261] and others.

- **Chromogenic systems**, which experience a color change in response to electrical, optical or thermal changes. These include: (i) thermochromic materials that change of color with the temperature; (ii) electrochromic materials that respond to an applied potential; and (iii) photochromic materials, when the change of color is produced in response to the exposure to light at a specific wavelength. Many applications are based on these materials in a wide range of fields, such as automotive or information displays, architectural market, smart textiles or biosensors, among many others.[262–264]

Based on that classification, smart materials with capacity to respond to the presence of microorganism will be discussed in the next section, and concretely those based on fabrics and water filters.

1.4.1 Smart Materials for Bacterial Detection

A wide range of smart materials have been used in different fields of application for bacterial detection, such as smart colorimetric biosensors,[265] smart graphene biosensing systems,[266] piezoelectric polymers[267] or smart microfluidics devices for contaminated food detection,[268] among many others. This section will be focused on the studies developed in smart textiles, wound dressings (in the form of hydrogels or cellulose-based materials) and membranes for bacterial detection.

Smart textiles and wound dressings with capacity to report on bacterial colonization have been explored and already reported. Main strategies in the development of smart bacterial-sensing textiles consist of the coating of the textile with organic constructs (e.g., phospholipid vesicles), hydrogels or pH-sensitive compounds (e.g. polymers or organic dyes), which storing colorimetric and/or fluorescent substances inside. The presence of bacteria results in the breakage of the organic construct, which releases the colorimetric/fluorescent indicator producing the subsequent color change of the textile. As an example, phospholipid vesicles (liposomes) strategy has been used for wound dressings fabrication.[269] Vesicles were stabilized with a synthetic polymerizable lipid by lateral cross-linking within the lipid bilayer. The released colorimetric/fluorescent indicator was produced after a toxin-mediated breakdown of the vesicle secreted by bacteria, which conferred the textile with selectivity against some specific virulent bacterial strains. In this sense, the liposome composition could be tuned by altering the lipid and fatty acid composition of the membranes, to make the vesicle selective to specific toxins/enzymes produced by some pathogens. Different types of vesicles were tested and most of them shown changes in color and fluorescence signals after 6 h of incubation. The same strategy was used in the development of a smart hydrogel wound dressing prototype, designed by the same authors.[270] In this case, the dressing was made of hydrated agarose film and the fluorescent dye within the vesicles were mixed with agarose and dispersed into the hydrogel matrix. Fluorescent and color detections were achieved in 4 h for some pathogenic strains. The sensitivity was dependent on the facility of the strain to grown in biofilm form. However, strategies based on the use of vesicles

are prone to false positives since changes on environmental conditions may produce the breakdown of liposomes inducing the release of the indicator.

Analogously, hydrogel film coatings (e.g. chitosan) with chromogenic or fluorogenic reporter moieties have been used by exploiting the activity of characteristic alpha-glucosidase or elastase enzymes to metabolize these gels.[271] The fluorogenic and chromogenic substrates were covalently conjugated to a matrix of chitosan-derived hydrogel. In the presence of these bacterial enzymes, the substrates were cleaved and the existence of bacteria was revealed by colorimetric and fluorescence responses. Presence of both, Gram-positive and Gram-negative bacteria was detected in 1 h and the limits of detection of the enzymes were of the order of 10^{-9} M. Nevertheless, enzymes have poor stability and the reproducibility of the results is difficult to achieve.

Recently, the organic molecule tricyanofuran hydrazine (TCFH) chromophore has been incorporated into cotton fabrics for smart textile production sensitive to pH and temperature changes.[272] Changes in pH and temperature produced a switching in the TCFH molecule. TCFH was cross-linked in situ with calcium alginate (to avoid steric hindrance of its molecular switching) forming a thin layer on the cotton textiles by dip-coating method. Resulting textiles showed color changes from red to yellow after 24 h of incubation with Gram-positive bacteria and from red to purple after 6 h of incubation with Gram-negative bacteria. Bacterial concentration used for the experiments was not reported and textiles showed no cytotoxicity. Analogously, the same authors used anthocyanin chromic dye (sensible to pH variations) for its immobilization into cotton fabrics using potassium alum as mordant.[273] After 12 h of incubation with Gram-negative bacteria, textile shown color changes from blue to purple. Similarly, textile color changes from purple to green were obtained for 18 h with Gram-positive bacteria.

In the same context, a smart bandage sensitive to pH for optical determination of wound status has been developed.[274] The bandage was fabricated by immobilizing cellulose particles covalently modified with a pH indicator dye into a biocompatible hydrogel. Thin layers of the obtained hydrogel were casted into commercial wound dressings and the pH variations were monitored with a novel radio-frequency identification-based-contact-less readout platform via a

low cost optoelectronic interface. Resulting smart bandage presented color changes well correlated with pH variation. Similarly, a smart self-assembled multilayer film was fabricated as pH and temperature sensor for wound dressings.[275] The film was developed by formation of hydrogen bonds and hydrophobic interactions between hydroxypropyl methylcellulose (HPMC) and epigallocatechin-3-gallate (EGCG). The release of EGCG from the resulting complex was produced in basic pH, accompanied by a color change and H_2O_2 generation, which allowed both, detecting and killing bacteria respectively. However, as in the strategies based on the use of vesicles, changes in pH conditions can be produced by environmental conditions, resulting in false positives. Furthermore, in most of cases, these sensing compounds are also susceptible to temperature changes, which decrease even more the selectivity of the method to the presence of live bacteria.

In a different approach, Eu^{3+}-induced polyelectrolyte nano-aggregates (EIPAs), a light-emitting nanomaterial, have been incorporated into cotton fabrics for the detection of bacteria.[276] EIPAs were chemically bonded into cotton textiles through pentaerythritol crosslinking agent by grafting process. Obtained smart fabrics showed durable and bright fluorescence, and toxicity assays were negative towards mammalian cells. Besides, after 24 h of incubation, they exhibited antibacterial activity against Gram-positive bacteria and sensing properties with Gram-negative bacteria via fluorescence quenching. The same compound was used in the production of a smart wearable fabric material with sensing and antimicrobial properties.[277] In this sense, sodium alginate was used as substrate for layer-by-layer assembly of Eu and Ag-NPs, endowing the textile with antibacterial activity. The sodium alginate improved the biocompatibility of the complex, which was combined with pentaerythritol and embedded into cotton fabrics by grafting. Resulting textiles showed sensing properties against Gram-positive bacteria, Gram-negative bacteria and transition metals through a dynamic fluorescence quenching mechanism, in addition to good antibacterial properties. Thus, the use of Eu provides a new and potentially attractive strategy to fabricate smart sensing and antibacterial textiles. However, this approach also presents some drawbacks. First, Eu has to be coordinated with organic ligands since the emission from an isolated Eu ion is weak because of its tight absorption on UV light. It also shows slight cytotoxicity,[278] so the release of such ions from the textiles may difficult their real application. Furthermore, color

changes are related to the presence of bacteria and transition metals, making it susceptible to false positives in the case of real samples.

Recently, another approach has been published, which developed on cellulose derivative membranes. The method consisted of a multi-layer wound dressing made of polyvinyl alcohol (PVA) foam and electrospun sodium carboxymethylcellulose (CMC) surface mesh with bacterial sensing and antibacterial properties.[279] Antibacterial function was endowed by adding stearyl trimethyl ammonium chloride (STAC) into the PVA foam. The sensing capacity was produced with a laser photodynamic response of methylene blue (MB), which also enhance the antibacterial activity of the dressing. MB is an organic antimicrobial cationic dye, which lose its blue color when in contact with bacteria due to the absence of oxygen by bacterial metabolism. Obtained wound dressings showed good antibacterial and sensing capacities against Gram-positive and Gram-negative bacteria. Color changes were observed after 6 h of incubation with both bacteria for samples without antibacterial agent (optical density = 0.8). When this was present, samples took more than 48 hours to change their color. Compared to the previous approaches, this method offers an antibacterial and sensing system for itself, with no need of adding external reagents or hydrogels. However, MB dye has harmful impact on water quality. In fact, several methods are being developed for its removal,[280] what difficulty its implantation in water treatment membranes.

As a conclusion, interesting smart materials have been developed with antimicrobial/antifouling, bacterial sensing or combining both antibacterial and bacterial sensing capacities, but still presenting important limitation in terms of scalability (capacity to produce them with mass production technologies) and stability of the biocide/sensing molecules. New approaches are thus necessary to tackle this important societal challenge in the near future.

1.5 References

(1) World Health Organization (WHO). The top 10 causes of death https://www.who.int/news-room/fact-sheets/detail/the-top-10-causes-of-death.

(2) World Health Organization (WHO). WHO Estimates of the Global Burden of Foodborne Diseases: Foodborne Disease Burden Epidemiology Reference Group 2007-2015. *WHO Libr. Cat. Data* **2015**. https://doi.org/10.1007/978-3-662-43978-4_3884.

(3) Dietvorst, J.; Vilaplana, L.; Uria, N.; Marco, M. P.; Muñoz-Berbel, X. Current and Near-Future Technologies for Antibiotic Susceptibility Testing and Resistant Bacteria Detection. *Trends Anal. Chem.* **2020**, *127*, 1–13. https://doi.org/10.1016/j.trac.2020.115891.

(4) Khan, H. A.; Baig, F. K.; Mehboob, R. Nosocomial Infections: Epidemiology, Prevention, Control and Surveillance. *Asian Pac. J. Trop. Biomed.* **2017**, *7* (5), 478–482. https://doi.org/10.1016/j.apjtb.2017.01.019.

(5) Neely, A. N.; Maley, M. P. Survival of Enterococci and Sthaphylococci on Hospital Fabrics and Plastics. *J. Clin. Microbiol.* **2000**, *38* (2), 724–726. https://doi.org/http://jcm.asm.org/.

(6) Tacconelli, E.; Cataldo, M. A. Vancomycin-Resistant Enterococci (VRE): Transmission and Control. *Int. J. Antimicrob. Agents* **2008**, *31* (2), 99–106. https://doi.org/10.1016/j.ijantimicag.2007.08.026.

(7) Frakking, F. N. J.; Bril, W. S.; Sinnige, J. C.; Klooster, J. E. va. t.; de Jong, B. A. W.; van Hannen, E. J.; Tersmette, M. Recommendations for the Successful Control of a Large Outbreak of Vancomycin-Resistant Enterococcus Faecium in a Non-Endemic Hospital Setting. *J. Hosp. Infect.* **2018**, *100* (4), e216–e225. https://doi.org/10.1016/j.jhin.2018.02.016.

(8) Fijan, S.; Turk, S. Š. Hospital Textiles, Are They a Possible Vehicle for Healthcare-Associated Infections? *Int. J. Environ. Res. Public Health* **2012**, *9* (9), 3330–3343. https://doi.org/10.3390/ijerph9093330.

(9) Allegranzi, B.; Nejad, S. B.; Combescure, C.; Graafmans, W.; Attar, H.; Donaldson, L.; Pittet, D. Burden of Endemic Health-Care-Associated Infection in Developing Countries: Systematic Review and Meta-Analysis. *Lancet* **2011**, *377* (9761), 228–241. https://doi.org/10.1016/S0140-6736(10)61458-4.

(10) European Centre for Disease Prevention and Control (ECDC). Healthcare associated infections - a threat to patient safety in Europe https://www.ecdc.europa.eu/en/publications-data/infographic-healthcare-associated-infections-threat-patient-safety-europe.

(11) WHO. Report on the Burden of Endemic Health Care-Associated Infection Worldwide Clean Care Is Safer Care. *World Heal. Organ.* **2011**, 1–40.

(12) Miller, I. F.; Schneider-Crease, I.; Nunn, C. L.; Muehlenbein, M. P. Estimating Infection Prevalence : Best Practices and Their Theoretical Underpinnings. *Ecol. Evol.* **2018**, *8*, 6738–

6747. https://doi.org/10.1002/ece3.4179.

(13) Kamat, U.; Ferreira, A.; Savio, R.; Motghare, D. Antimicrobial Resistance among Nosocomial Isolates in a Teaching Hospital in Goa. *Indian J. Community Med.* **2008**, *33* (2), 89–92. https://doi.org/10.4103/0970-0218.40875.

(14) Alemu, A. Y.; Endalamaw, A.; Bayih, W. A. The Burden of Healthcare-Associated Infection in Ethiopia: A Systematic Review and Meta-Analysis. *Trop. Med. Health* **2020**, *48* (77), 1–11. https://doi.org/10.1186/s41182-020-00263-2.

(15) Khan, H. A.; Ahmad, A.; Mehboob, R. Nosocomial Infections and Their Control Strategies. *Asian Pac. J. Trop. Biomed.* **2015**, *5* (7), 509–514. https://doi.org/10.1016/j.apjtb.2015.05.001.

(16) Sydnor, E. R. M.; Perl, T. M. Hospital Epidemiology and Infection Control in Acute-Care Settings. *Clin. Microbiol. Rev.* **2011**, *24* (1), 141–173. https://doi.org/10.1128/CMR.00027-10.

(17) Jenkins, D. R. Nosocomial Infections and Infection Control. *Medicine (Baltimore).* **2017**, 1–5. https://doi.org/10.1016/j.mpmed.2017.07.005.

(18) World Health Organization (WHO). *Prevention of Hospital-Acquired Infections*; 2002.

(19) Danasekaran, R.; Mani, G.; Annadurai, K. Prevention of Healthcare-Associated Infections: Protecting Patients, Saving Lives. *Int. J. Community Med. Public Heal.* **2014**, *1* (1), 67. https://doi.org/10.5455/2394-6040.ijcmph20141114.

(20) Römling, U.; Balsalobre, C. Biofilm Infections, Their Resilience to Therapy and Innovative Treatment Strategies. *J. Intern. Med.* **2012**, *272* (6), 541–561. https://doi.org/10.1111/joim.12004.

(21) Meticulous Research. Top 10 companies in antimicrobial coating market https://meticulousblog.org/top-10-companies-in-antimirobial-coating-market.

(22) Juanga-labayen, J. P.; Labayen, I. V; Yuan, Q. A Review on Textile Recycling Practices and Challenges. *Textiles* **2022**, *2*, 174–188. https://doi.org/https://doi.org/10.3390/textiles2010010.

(23) Morais, D. S.; Guedes, R. M.; Ascensao Lopes, M. Antimicrobial Approaches for Textiles: From Research to Market. *Materials (Basel).* **2016**, *9* (489), 1–21. https://doi.org/10.3390/ma9060498.

(24) Zhao, T.; Sun, G.; Song, X. An Antimicrobial Cationic Reactive Dye: Synthesis and Applications on Cellulosic Fibers. *J. Appl. Polym. Sci.* **2008**, *108*, 1917–1923. https://doi.org/10.1002/app.

(25) Owusu-Adom, K.; Guymon, C. A. Photopolymerization Kinetics of Poly (Acrylate)-Clay Composites Using Polymerizable Surfactants. *Polymer (Guildf).* **2008**, *49*, 2636–2643. https://doi.org/10.1016/j.polymer.2008.03.045.

(26) Liu, S.; Ma, J.; Zhao, D. Synthesis and Characterization of Cationic Monoazo Dyes

Incorporating Quaternary Ammonium Salts. *Dye. Pigment.* **2007**, *75*, 255–262. https://doi.org/10.1016/j.dyepig.2006.05.004.

(27)   Ranganath, A. S.; Sarkar, A. K. Evaluation of Durability to Laundering of Triclosan and Chitosan on a Textile Substrate. *J. Text.* **2014**, 1–5.

(28)   Karaszewska, A.; Kami, I.; Kiwa, M. Preparation and Properties of Textile Materials Modified with Triclosan-Loaded Polylactide Microparticles. *Polym. Adv. Technol.* **2017**, *28*, 1185–1193. https://doi.org/10.1002/pat.4030.

(29)   Orhan, M. Triclosan Applications for Biocidal Functionalization of Polyester and Cotton Surfaces. *J. Eng. Fiber. Fabr.* **2020**, *15*, 1–11. https://doi.org/10.1177/1558925020940104.

(30)   Zhao, T.; Chen, Q. *Halogenated Phenols and Polybiguanides as Antimicrobial Textile Finishes*; Elsevier Ltd, 2016. https://doi.org/10.1016/B978-0-08-100576-7.00009-2.

(31)   Blackburn, R. S.; Harvey, A.; Kettle, L. L.; Payne, J. D.; Russell, S. J. Sorption of Poly(Hexamethylenebiguanide) on Cellulose: Mechanism of Binding and Molecular Recognition. *Langmuir* **2006**, *22* (13), 5636–5644.

(32)   Enescu, D. Use of Chitosan in Surface Modification of Textile Materials. *Roum. Biotechnol. Lett.* **2008**, *13* (6), 4037–4048.

(33)   Zhou, B. C.; Kan, C.; Hong, T.; Polytechnic, K.; Sun, C. A Review of Chitosan Textile Applications. *AATCC J. Res.* **2019**, *6*, 8–14. https://doi.org/10.14504/ajr.6.S1.2.

(34)   Lim, S.-H.; Hudson, S. M. Review of Chitosan and Its Derivatives as Antimicrobial Agents and Their Uses as Textile Chemicals. *J. Macromol. Sci. Part C Polym. Rev.* **2003**, *43* (2), 223–269. https://doi.org/10.1081/MC-120020161.

(35)   Ren, X.; Jiang, Z.; Liu, Y.; Li, L.; Fan, X. N-Halamines as Antimicrobial Textile Finishes. In *Antimicrobial Textiles*; 2016; pp 125–140. https://doi.org/10.1016/B978-0-08-100576-7.00008-0.

(36)   Dong, A.; Wang, Y.; Gao, Y.; Gao, T.; Gao, G. Chemical Insights into Antibacterial N-Halamines. *Chem. Rev.* **2017**, *117*, 4806–4862. https://doi.org/10.1021/acs.chemrev.6b00687.

(37)   Chen, Y.; Wang, Y.; Feng, C.; He, Q.; Chen, Q.; Wang, Z.; Han, Q. Novel Quat/Di-N-Halamines Silane Unit with Enhanced Synergism Polymerized on Cellulose for Development of Superior Biocidability. *Int. J. Biol. Macromol.* **2020**, *154*, 173–181. https://doi.org/10.1016/j.ijbiomac.2020.03.117.

(38)   Perelshtein, I.; Applerot, G.; Perkas, N.; Hasmann, A.; Guebitz, G. M. Antibacterial Properties of an In Situ Generated and Simultaneously Deposited. *Optimization* **2009**, 361–366. https://doi.org/10.1021/am8000743.

(39)   Ravindra, S.; Murali Mohan, Y.; Narayana Reddy, N.; Mohana Raju, K. Fabrication of Antibacterial Cotton Fibres Loaded with Silver Nanoparticles via " Green Approach." *Colloids Surfaces A Physicochem. Eng. Asp.* **2010**, *367* (1–3), 31–40.

https://doi.org/10.1016/j.colsurfa.2010.06.013.

(40)   Perelshtein, I.; Applerot, G.; Perkas, N. Sonochemical Coating of Silver Nanoparticles on Textile Fabrics (Nylon , Polyester and Cotton) and Their Antibacterial Activity. **2008**. https://doi.org/10.1088/0957-4484/19/24/245705.

(41)   Ahammed, H. A. M.; Jayakumar, S.; Vaideki, K. Use of Zinc Oxide Nano Particles for Production of Antimicrobial Textiles. **2010**, *2* (1), 202–208. https://doi.org/10.4314/ijest.v2i1.59113.

(42)   Antunes, L.; Faustino, G.; Mouro, C.; Vaz, J.; Gouveia, I. C. Bioactive Microsphere-Based Coating for Biomedical-Textiles with Encapsulated Antimicrobial Peptides (AMPs). *Ciência Tecnol. dos Mater.* **2014**, *26* (2), 118–125. https://doi.org/10.1016/j.ctmat.2015.03.006.

(43)   Hajipour, M. J.; Fromm, K. M.; Akbar Ashkarran, A.; Jimenez de Aberasturi, D.; Larramendi, I. R. de; Rojo, T.; Serpooshan, V.; Parak, W. J.; Mahmoudi, M. Antibacterial Properties of Nanoparticles. *Trends Biotechnol.* **2012**, *30* (10), 499–511. https://doi.org/10.1016/j.tibtech.2012.06.004.

(44)   Gao, Y.; Cranston, R. Recent Advances in Antimicrobial Treatments of Textiles. *Text. Res. J.* **2008**, *78* (1), 60–72. https://doi.org/10.1177/0040517507082332.

(45)   Hegstad, K.; Langsrud, S.; Lunestad, B. T.; Scheie, A. A.; Sunde, M.; Yazdankhah, S. P. Does the Wide Use of Quaternary Ammonium Compounds Enhance the Selection and Spread of Antimicrobial Resistance and Thus Threaten Our Health? *Microb. Drug Resist.* **2010**, *16* (2), 91–104.

(46)   Marini, M.; Bondi, M.; Iseppi, R.; Toselli, M.; Pilati, F. Preparation and Antibacterial Activity of Hybrid Materials Containing Quaternary Ammonium Salts via Sol-Gel Process. *Eur. Polym. J.* **2007**, *43*, 3621–3628. https://doi.org/10.1016/j.eurpolymj.2007.06.002.

(47)   Chadeau, E.; Brunon, C.; Degraeve, P.; Leonard, D.; Grossiord, C.; Bessueille, F.; Cottaz, A.; Renaud, F.; Ferreira, I.; Darroux, C.; Simon, F.; Rimbault, F.; Oulahal, N. Evaluation of Antimicrobial Activity of a Polyhexamethylene Biguanide-Coated Textile by Monitoring Both Bacterial Growth (ISO 20743/2005 Standard) and Viability (Live/Dead Backlight Kit). *J. Food Saf.* **2012**, *32*, 141–151. https://doi.org/10.1111/j.1745-4565.2011.00361.x.

(48)   Hardin, I. R.; Kim, Y. *Nanotechnology for Antimicrobial Textiles*; Elsevier Ltd, 2016. https://doi.org/10.1016/B978-0-08-100576-7.00006-7.

(49)   Kohen, R.; Nyska, A. Oxidation of Biological Systems: Oxidative Stress Phenomena, Antioxidants, Redox Reactions, and Methods for Their Quantification. *Toxicol. Pathol.* **2002**, *30* (6), 620–650. https://doi.org/10.1080/0192623029016672.

(50)   Martínez-gutierrez, F.; Thi, E. P.; Silverman, J. M.; Oliveira, C. C. De; Svensson, S. L.; Hoek, A. Vanden; Sánchez, E. M.; Reiner, N. E.; Gaynor, E. C.; Pryzdial, E. L. G.; Conway, E. M.; Orrantia, E.; Ruiz, F.; Av-gay, Y.; Bach, H. Antibacterial Activity, Inflammatory Response, Coagulation and Cytotoxicity Effects of Silver Nanoparticles. *Nanomedicine Nanotechnology, Biol. Med.* **2012**, *8*, 328–336.

https://doi.org/10.1016/j.nano.2011.06.014.

(51) Lee, S. M.; Song, K. C.; Lee, B. S. Antibacterial Activity of Silver Nanoparticles Prepared by a Chemical Reduction Method. *Korean J. Chem. Eng.* **2010**, *27* (2), 688–692. https://doi.org/10.1007/s11814-010-0067-0.

(52) Marius, S.; Lucian, H.; Marius, M.; Daniela, P.; Irina, G.; Simona, D.; Viorel, M. Enhanced Antibacterial Effect of Silver Nanoparticles Obtained by Electrochemical Synthesis in Poly (Amide-Hydroxyurethane) Media. *J. Mater. Sci. Mater. Med.* **2011**, *22*, 789–796. https://doi.org/10.1007/s10856-011-4281-z.

(53) Domènech, B.; Muñoz, M.; Muraviev, D. N.; Macanás, J. Polymer-Silver Nanocomposites as Antibacterial Materials. *Microb. Pathog. Strateg. Combat. them Sci. Technol. Educ.* **2013**, *1* (December), 630–640.

(54) Mills, A.; Hodgen, S.; Lee, S. O. O. K. Self-Cleaning Titania Films: An Overview of Direct, Lateral and Remote Photo-Oxidation Processes. *Res. Chem. Intermed.* **2005**, *31* (4–6), 295–308. https://doi.org/10.1163/1568567053956644.

(55) Shilpa, S. A.; Subbulakshmi, M. S.; Hikku, G. S. Nanoparticles of Metal/Metal Oxide Embedded Fabrics to Impart Antibacterial Activity to Counteract Hospital Acquired Infections. *Eng. Res. Express* **2022**, *4*, 032002. https://doi.org/10.1088/2631-8695/ac8f1c.

(56) Rokitskaya, T. I.; Kolodkin, N. I.; Kotova, E. A.; Antonenko, Y. N. Indolicidin Action on Membrane Permeability: Carrier Mechanism versus Pore Formation. *Biochim. Biophys. Acta - Biomembr.* **2011**, *1808* (1), 91–97. https://doi.org/10.1016/j.bbamem.2010.09.005.

(57) Emam, H. E. Antimicrobial Cellulosic Textiles Based on Organic Compounds. *3 Biotech* **2019**, *9* (29), 1–14. https://doi.org/10.1007/s13205-018-1562-y.

(58) Russell, A. D. Introduction of Biocides into Clinical Practice and the Impact on Antibiotic-Resistant Bacteria. *J. Appl. Microbiol. Symp. Suppl.* **2002**, *92* (2001), 121–135. https://doi.org/10.1046/j.1365-2672.92.5s1.12.x.

(59) Windler, L.; Height, M.; Nowack, B. Comparative Evaluation of Antimicrobials for Textile Applications. *Environ. Int.* **2013**, *53*, 62–73. https://doi.org/10.1016/j.envint.2012.12.010.

(60) Percival, S. L.; Bowler, P. G.; Russell, D. Bacterial Resistance to Silver in Wound Care. *J. Hosp. Infect.* **2005**, *60*, 1–7. https://doi.org/10.1016/j.jhin.2004.11.014.

(61) Silver, S.; Phung, L. T.; Silver, G. Silver as Biocides in Burn and Wound Dressings and Bacterial Resistance to Silver Compounds. *J. Ind. Microbiol. Biotechnol.* **2006**, *33*, 627–634. https://doi.org/10.1007/s10295-006-0139-7.

(62) Sobczak, M.; Debek, C.; Oledzka, E.; Kozlowski, R. Polymeric Systems of Antimicrobial Peptides—Strategies and Potential Applications. *Molecules* **2013**, *18*, 14122–14137. https://doi.org/10.3390/molecules181114122.

(63) Alves, D.; Olívia Pereira, M. Mini-Review: Antimicrobial Peptides and Enzymes as Promising Candidates to Functionalize Biomaterial Surfaces. *Biofouling J. Bioadhesion Biofilm Res.*

2014, *30* (4), 483–499. https://doi.org/10.1080/08927014.2014.889120.

(64)   Aymonier, C.; Schlotterbeck, U.; Antonietti, L.; Zacharias, P.; Thomann, R.; Tiller, J. C.; Mecking, S. Hybrids of Silver Nanoparticles with Amphiphilic Hyperbranched Macromolecules Exhibiting Antimicrobial Properties. *Chem. Commun.* **2002**, *24*, 3018–3019. https://doi.org/10.1039/b208575e.

(65)   Choi, S.; Lee, K.; Park, S. Preparation and Characterization of Poly(Ester)-Silver and Nylon-Silver Nanocomposites. *Stud. Surf. Sci. Catal.* **2003**, *146*, 93–96. https://doi.org/10.1016/S0167-2991(03)80335-X.

(66)   Raffi, M.; Akhter, J. I.; Hasan, M. M. Effect of Annealing Temperature on Ag Nano-Composite Synthesized by Sol-Gel. *Mater. Chem. Phys.* **2006**, *99* (2–3), 405–409. https://doi.org/10.1016/j.matchemphys.2005.11.012.

(67)   Zeng, R.; Rong, M. Z.; Zhang, M. Q.; Liang, H. C.; Zeng, H. M. Laser Ablation of Polymer-Based Silver Nanocomposites. *Appl. Surf. Sci.* **2002**, *187* (3–4), 239–247. https://doi.org/10.1016/S0169-4332(01)00991-6.

(68)   Abramov, O. V.; Gedanken, A.; Koltypin, Y.; Perkas, N.; Perelshtein, I.; Joyce, E.; Mason, T. J. Pilot Scale Sonochemical Coating of Nanoparticles onto Textiles to Produce Biocidal Fabrics. *Surf. Coatings Technol.* **2009**, *204* (5), 718–722. https://doi.org/10.1016/j.surfcoat.2009.09.030.

(69)   Poulter, N.; Munoz-berbel, X.; Johnson, A. L.; Dowling, A. J.; Waterfield, N.; Jenkins, A. T. A. An Organo-Silver Compound That Shows Antimicrobial Activity against Pseudomonas Aeruginosa as a Monomer and Plasma Deposited Film W. *Chem. Commun.* **2009**, 7312–7314. https://doi.org/10.1039/b915467a.

(70)   Domènech, B.; Ziegler, K. K.; Carrillo, F.; Muñoz, M.; Muraviev, D. N.; Macanás, J. Development of Novel Catalytically Active Polymer-Metal-Nanocomposites Based on Activated Foams and Textile Fibers. *Nanoscale Res. Lett.* **2013**, *8* (1), 238. https://doi.org/10.1186/1556-276X-8-238.

(71)   Perelshtein, I.; Perkas, N.; Gedanken, A. The Sonochemical Functionalization of Textiles. In *The Impact and Prospects of Green Chemistry for Textile Technology*; Elsevier Ltd., 2019; pp 161–198. https://doi.org/10.1016/B978-0-08-102491-1.00007-1.

(72)   Gomoll, F. IUPAC Top Ten Emerging Technologies in Chemistry 2021. *Chem. Int.* **2021**, No. October, 13–20. https://doi.org/10.1515/ci-2021-0404.

(73)   Lévêque, J.-M.; Cravotto, G.; Delattre, F.; Cintas, P. *Organic Sonochemistry. Challenges and Perspectives for the 21st Century*; 2018.

(74)   Alonso, A.; Muñoz-berbel, X.; Vigués, N.; Rodríguez-rodríguez, R.; Macanás, J.; Muñoz, M.; Mas, J.; Muraviev, D. N. Superparamagnetic Ag@Co-Nanocomposites on Granulated Cation Exchange Polymeric Matrices with Enhanced Antibacterial Activity for the Environmentally Safe Purifi Cation of Water. *Adv. Funct. Mater.* **2013**, *23*, 2450–2458. https://doi.org/10.1002/adfm.201202663.

(75) Alonso, A.; Muñoz-Berbel, X.; Vigués, N.; Rodríguez-Rodríguez, R.; Macanás, J.; Mas, J.; Muñoz, M.; Muraviev, D. N. Intermatrix Synthesis of Monometallic and Magnetic Metal/Metal Oxide Nanoparticles with Bactericidal Activity on Anionic Exchange Polymers. *RSC Adv.* **2012**, *2* (3), 4596–4599. https://doi.org/10.1039/c2ra20216f.

(76) Alonso, A.; Mu, X.; Macan, J.; Mu, M.; Mas, J.; Muraviev, D. N. Characterization of Fibrous Polymer Silver/Cobalt Nanocomposite with Enhanced Bactericide Activity. *Langmuir* **2012**, *28*, 783–790. https://doi.org/10.1021/la203239d.

(77) Green, D. E.; Close JR., L. G.; Van Hyning, D. L. Textiles Having a Wash-Durable Silver-Ion Based Antimicrobial Topical Treatment, 2003.

(78) Green, D. E.; Van Hyning, D. L.; Close JR., L. G.; Li, S.; Goulet, R. J. Method of Manufacturing Yarns and Fabrics Having a Wash-Durable Non-Electrically Conductive Topically Applied Metal-Based Finish, 2003.

(79) Ghoranneviss, M.; Shahidi, S. Effect of Various Metallic Salts on Antibacterial Activity and Physical Properties of Cotton Fabrics. *J. Ind. Text.* **2012**, *42* (3), 193–203. https://doi.org/10.1177/1528083711433230.

(80) Zheng, X.; Zhang, Y.; Wang, Z.; Wang, Y.; Zou, L. Highly Effective Antibacterial Zeolitic Imidazolate Framework-67/Alginate Fibers. *Nanotechnology* **2020**, *31*, 375707. https://doi.org/10.1088/1361-6528/ab978a.

(81) Zhang, D.; Chen, L.; Zang, C.; Chen, Y.; Lin, H. Antibacterial Cotton Fabric Grafted with Silver Nanoparticles and Its Excellent Laundering Durability. *Carbohydr. Polym.* **2013**, *92* (2), 2088–2094. https://doi.org/10.1016/j.carbpol.2012.11.100.

(82) Zhang, Y.; Yu, X.; Gong, S.; Ye, C.; Fan, Z.; Lin, H. Antibiofilm Activity of Bacillus Pumilus SW9 against Initial Biofouling on Microfiltration Membranes. *Appl. Microbiol. Biotechnol.* **2014**, *98* (3), 1309–1320. https://doi.org/10.1007/s00253-013-4991-x.

(83) Abbas, A.; Al-amer, A. M.; Laoui, T.; Al-marri, M. J.; Nasser, M. S.; Khraisheh, M.; Ali, M. Heavy Metal Removal from Aqueous Solution by Advanced Carbon Nanotubes: Critical Review of Adsorption Applications. *Sep. Purif. Technol.* **2016**, *157*, 141–161. https://doi.org/10.1016/j.seppur.2015.11.039.

(84) Denstedt, J. D.; Wollin, T. A.; Reid, G. Biomaterials Used in Urology: Current Issues of Biocompatibility, Infection and Encrustation. *J. Endourol.* **1998**, *12* (6), 493–500. https://doi.org/10.1089/end.1998.12.493.

(85) Li, M.; Neoh, K. G.; Kang, E. T.; Lau, T.; Chiong, E. Surface Modification of Silicone with Covalently Immobilized and Crosslinked Agarose for Potential Application in the Inhibition of Infection and Omental Wrapping. *Adv. Funct. Mater.* **2014**, *24* (11), 1631–1643. https://doi.org/10.1002/adfm.201302242.

(86) Harris, C. A.; Resau, J. H.; Hudson, E. A.; West, R. A.; Moon, C.; Black, A. D.; McAllister, J. P. Reduction of Protein Adsorption and Macrophage and Astrocyte Adhesion on Ventricular Catheters by Polyethylene Glycol and N-Acetyl-L-Cysteine. *J. Biomed. Mater. Res. - Part A*

2011, *98 A* (3), 425–433. https://doi.org/10.1002/jbm.a.33130.

(87)   Zhou, J.; Yuan, J.; Zang, X.; Shen, J.; Lin, S. Platelet Adhesion and Protein Adsorption on Silicone Rubber Surface by Ozone-Induced Grafted Polymerization with Carboxybetaine Monomer. *Colloids Surfaces B Biointerfaces* **2005**, *41* (1), 55–62. https://doi.org/10.1016/j.colsurfb.2004.11.006.

(88)   Kochkodan, V.; Hilal, N. A Comprehensive Review on Surface Modified Polymer Membranes for Biofouling Mitigation. *Desalination* **2015**, *356*, 187–207. https://doi.org/10.1016/j.desal.2014.09.015.

(89)   Otitoju, T. A.; Ahmad, A. L. Recent Advances in Hydrophilic Modi Fi Cation and Performance of Polyethersulfone (PES) Membrane via Additive Blending. *RSC Adv.* **2018**, *8*, 22710–22728. https://doi.org/10.1039/c8ra03296c.

(90)   Aslam, M.; Ahmad, R.; Kim, J. Recent Developments in Biofouling Control in Membrane Bioreactors for Domestic Wastewater Treatment. *Sep. Purif. Technol.* **2018**, *206*, 297–315. https://doi.org/10.1016/j.seppur.2018.06.004.

(91)   Agrawal, A.; Sharma, A.; Kant, K.; Awasthi, A. Metal Oxides Nanocomposite Membrane for Biofouling Mitigation in Wastewater Treatment. *Mater. Today Chem.* **2021**, *21*, 100532. https://doi.org/10.1016/j.mtchem.2021.100532.

(92)   Maximous, N.; Nakhla, G.; Wong, K.; Wan, W. Optimization of Al2O3/PES Membranes for Wastewater Filtration. *Sep. Purif. Technol.* **2010**, *73* (2), 294–301. https://doi.org/10.1016/j.seppur.2010.04.016.

(93)   Bottino, A.; Capannelli, G.; Asti, V. D.; Piaggio, P. Preparation and Properties of Novel Organic – Inorganic Porous Membranes. *Sep. Purif. Technol.* **2001**, *22–23*, 269–275. https://doi.org/10.1016/S1383-5866(00)00127-1.

(94)   Pendergast, M. T. M.; Nygaard, J. M.; Ghosh, A. K.; Hoek, E. M. V. Using Nanocomposite Materials Technology to Understand and Control Reverse Osmosis Membrane Compaction. *Desalination* **2010**, *261* (3), 255–263. https://doi.org/10.1016/j.desal.2010.06.008.

(95)   Bae, T.; Tak, T. Effect of TiO2 Nanoparticles on Fouling Mitigation of Ultrafiltration Membranes for Activated Sludge Filtration. *J. Memb. Sci.* **2005**, *249*, 1–8. https://doi.org/10.1016/j.memsci.2004.09.008.

(96)   Qu, X.; Alvarez, P. J. J.; Li, Q. Applications of Nanotechnology in Water and Wastewater Treatment. *Water Res.* **2013**, *47* (12), 3931–3946. https://doi.org/10.1016/j.watres.2012.09.058.

(97)   Zhu, J.; Hou, J.; Zhang, Y.; Tian, M.; He, T.; Liu, J.; Chen, V. Polymeric Antimicrobial Membranes Enabled by Nanomaterials for Water Treatment. *J. Memb. Sci.* **2018**, *550*, 173–197. https://doi.org/10.1016/j.memsci.2017.12.071.

(98)   Zhang, A.; Zhang, Y.; Pan, G.; Xu, J.; Yan, H.; Liu, Y. In Situ Formation of Copper Nanoparticles in Carboxylated Chitosan Layer: Preparation and Characterization of Surface Modified TFC

Membrane with Protein Fouling Resistance and Long-Lasting Antibacterial Properties. *Sep. Purif. Technol.* **2017**, *176*, 164–172. https://doi.org/10.1016/j.seppur.2016.12.006.

(99)   Balta, S.; Sotto, A.; Luis, P.; Benea, L.; Van der Bruggen, B.; Kim, J. A New Outlook on Membrane Enhancement with Nanoparticles: The Alternative of ZnO. *J. Memb. Sci.* **2012**, *389*, 155–161. https://doi.org/10.1016/j.memsci.2011.10.025.

(100) Yu, Y.; Zhou, Z.; Huang, G.; Cheng, H.; Han, L.; Zhao, S.; Chen, Y.; Meng, F. Purifying Water with Silver Nanoparticles (AgNPs)-Incorporated Membranes: Recent Advancements and Critical Challenges. *Water Res.* **2022**, *222*, 118901. https://doi.org/10.1016/j.watres.2022.118901.

(101) Ašmonaite, G.; Boyer, S.; de Souza, K. B.; Wassmur, B.; Sturve, J. Behavioural Toxicity Assessment of Silver Ions and Nanoparticles on Zebrafish Using a Locomotion Profiling Approach. *Aquat. Toxicol.* **2016**, *173*, 143–153. https://doi.org/10.1016/j.aquatox.2016.01.013.

(102) Al-Hinai, M. H.; Sathe, P.; Al-Abri, M. Z.; Dobretsov, S.; Al-Hinai, A. T.; Dutta, J. Antimicrobial Activity Enhancement of Poly(Ether Sulfone) Membranes by in Situ Growth of ZnO Nanorods. *ACS Omega* **2017**, *2* (7), 3157–3167. https://doi.org/10.1021/acsomega.7b00314.

(103) Chadha, U.; Selvaraj, S. K.; Vishak Thanu, S.; Cholapadath, V.; Abraham, A. M.; Zaiyan M, M.; Manoharan, M.; Paramsivam, V. A Review of the Function of Using Carbon Nanomaterials in Membrane Filtration for Contaminant Removal from Wastewater. *Mater. Res. Express* **2022**, *9* (1), 012003. https://doi.org/10.1088/2053-1591/ac48b8.

(104) Jani, M.; Arcos-Pareja, J. A.; Ni, M. Engineered Zero-Dimensional Fullerene/Carbon Dots-Polymer Based Nanocomposite Membranes for Wastewater Treatment. *Molecules* **2020**, *25* (21), 1–28. https://doi.org/10.3390/molecules25214934.

(105) Daer, S.; Kharraz, J.; Giwa, A.; Hasan, S. W. Recent Applications of Nanomaterials in Water Desalination: A Critical Review and Future Opportunities. *Desalination* **2015**, *367*, 37–48. https://doi.org/10.1016/j.desal.2015.03.030.

(106) Katouzian, I.; Mahdi, S. Protein Nanotubes as State-of-the-Art Nanocarriers: Synthesis Methods, Simulation and Applications. *J. Control. Release* **2019**, *303*, 302–318. https://doi.org/10.1016/j.jconrel.2019.04.026.

(107) Goh, K.; Karahan, H. E.; Wei, L.; Bae, T. H.; Fane, A. G.; Wang, R.; Chen, Y. Carbon Nanomaterials for Advancing Separation Membranes: A Strategic Perspective. *Carbon N. Y.* **2016**, *109*, 694–710. https://doi.org/10.1016/j.carbon.2016.08.077.

(108) Yin, Z.; Chu, R.; Zhu, L.; Li, S.; Mo, F.; Hu, D. Application of Chitosan-Based Flocculants to Harvest Microalgal Biomass for Biofuel Production: A Review. *Renew. Sustain. Energy Rev.* **2021**, *145*, 111159. https://doi.org/10.1016/j.rser.2021.111159.

(109) Macczak, P.; Kaczmarek, H.; Ziegler-Borowska, M.; Wegrzynowska-Drymalska, K.; Burkowska-But, A. The Use of Chitosan and Starch-Based Flocculants for Filter Backwash

Water Treatment. *Materials (Basel).* **2022**, *15*, 1056. https://doi.org/10.3390/ma15031056.

(110) Cooper, A.; Floreani, R.; Ma, H.; Bryers, J. D.; Zhang, M. Chitosan-Based Nanofibrous Membranes for Antibacterial Filter Applications. *Carbohydr. Polym.* **2013**, *92* (1), 254–259. https://doi.org/10.1016/j.carbpol.2012.08.114.

(111) Rajendran, R.; Abirami, M.; Prabhavathi, P.; Premasudha, P.; Kanimozhi, B.; Manikandan, A. Biological Treatment of Drinking Water by Chitosan Based Nanocomposites. *African J. Biotechnol.* **2015**, *14* (11), 930–936. https://doi.org/10.5897/AJB2015.14469.

(112) Feng, Y.; Lin, X.; Li, H.; He, L.; Sridhar, T.; Suresh, A. K.; Bellare, J.; Wang, H. Synthesis and Characterization of Chitosan-Grafted BPPO Ultrafiltration Composite Membranes with Enhanced Antifouling and Antibacterial Properties. *Ind. Eng. Chem. Res.* **2014**, *53* (39), 14974–14981. https://doi.org/10.1021/ie502599p.

(113) Soenen, S. J.; Rivera-gil, P.; Montenegro, J.; Parak, W. J.; Smedt, S. C. De; Braeckmans, K. Cellular Toxicity of Inorganic Nanoparticles: Common Aspects and Guidelines for Improved Nanotoxicity. *Nano Today* **2011**, *6*, 446–465. https://doi.org/10.1016/j.nantod.2011.08.001.

(114) Khan, M.; Danielsen, S.; Johansen, K.; Lorenz, L.; Nelson, S.; Camper, A. Enzymatic Cleaning of Biofouled Thin-Film Composite Reverse Osmosis (RO) Membrane Operated in a Biofilm Membrane Reactor. *Biofouling J. Bioadhesion Biofilm Res.* **2014**, *30* (2), 153–167. https://doi.org/10.1080/08927014.2013.852540.

(115) Maartens, A.; Swart, P.; Jacobs, E. P. An Enzymatic Approach to the Cleaning of Ultrafiltration Membranes Fouled in Abattoir Effluent. *J. Memb. Sci.* **1996**, *119* (1), 9–16. https://doi.org/10.1016/0376-7388(96)00015-4.

(116) Chen, J.; Wang, L.; Zhu, Z. Preparation of Enzyme Immobilized Membranes and Their Self-Cleaning and Anti-Fouling Abilities in Protein Separations. *Desalination* **1992**, *86* (3), 301–315. https://doi.org/10.1016/0011-9164(92)80040-G.

(117) Koseoglu-Imer, D. Y.; Dizge, N.; Koyuncu, I. Enzymatic Activation of Cellulose Acetate Membrane for Reducing of Protein Fouling. *Colloids Surfaces B Biointerfaces* **2012**, *92*, 334–339. https://doi.org/10.1016/j.colsurfb.2011.12.013.

(118) Hou, J.; Dong, G.; Luu, B.; Sengpiel, R. G.; Ye, Y.; Wessling, M.; Chen, V. Hybrid Membrane with TiO2 Based Bio-Catalytic Nanoparticle Suspension System for the Degradation of Bisphenol-A. *Bioresour. Technol.* **2014**, *169*, 475–483. https://doi.org/10.1016/j.biortech.2014.07.031.

(119) Zhao, Q.; Liu, C.; Liu, J.; Zhang, Y. Development of a Novel Polyethersulfone Ultrafiltration Membrane with Antibacterial Activity and High Flux Containing Halloysite Nanotubes Loaded with Lysozyme. *RSC Adv.* **2015**, *5* (48), 38646–38653. https://doi.org/10.1039/c5ra05062f.

(120) Duan, L.; Wang, Y.; Zhang, Y.; Liu, J. Graphene Immobilized Enzyme/Polyethersulfone Mixed

Matrix Membrane: Enhanced Antibacterial, Permeable and Mechanical Properties. *Appl. Surf. Sci.* **2015**, *355*, 436–445. https://doi.org/10.1016/j.apsusc.2015.07.127.

(121) Azizi-lalabadi, M.; Hashemi, H.; Feng, J.; Mahdi, S. Carbon Nanomaterials against Pathogens; the Antimicrobial Activity of Carbon Nanotubes, Graphene/Graphene Oxide, Fullerenes, and Their Nanocomposites. *Adv. Colloid Interface Sci.* **2020**, *284*, 102250. https://doi.org/10.1016/j.cis.2020.102250.

(122) Dizaj, S. M.; Mennati, A.; Jafari, S.; Khezri, K.; Adibkia, K. Antimicrobial Activity of Carbon-Based Nanoparticles. *Adv. Pharm. Bull.* **2015**, *5* (1), 19–23. https://doi.org/10.5681/apb.2015.003.

(123) Fang, J.; Lyon, D. Y.; Wiesner, M. R.; Dong, J.; Alvarez, P. J. J. Effect of a Fullerene Water Suspension on Bacterial Phospholipids and Membrane Phase Behavior. *Environ. Sci. Technol.* **2007**, *41* (7), 2636–2642. https://doi.org/10.1021/es062181w.

(124) Deryabin, D. G.; Davydova, O. K.; Yankina, Z. Z.; Vasilchenko, A. S.; Miroshnikov, S. A.; Kornev, A. B.; Ivanchikhina, A. V.; Troshin, P. A. The Activity of [60]Fullerene Derivatives Bearing Amine and Carboxylic Solubilizing Groups against Escherichia Coli: A Comparative Study. *J. Nanomater.* **2014**, *2014*, 1–9. https://doi.org/10.1155/2014/907435.

(125) Fabbro, C.; Montellano Lopez, A.; Prato, M.; Da Ros, T. *Medicinal Chemistry and Pharmacological Potential of Fullerenes and Carbon Nanotubes*; 2008; Vol. 1.

(126) Baby, R.; Saifullah, B.; Zobir Hussein, M. Carbon Nanomaterials for the Treatment of Heavy Metal-Contaminated Water and Environmental Remediation. *Nanoscale Res. Lett.* **2019**, *14* (341), 1–17. https://doi.org/10.1186/s11671-019-3167-8.

(127) Penkova, A. V.; Polotskaya, G. A.; Toikka, A. M.; Trchová, M.; Šlouf, M.; Urbanová, M.; Brus, J.; Brožová, L.; Pientka, Z. Structure and Pervaporation Properties of Poly(Phenylene- Iso-Phthalamide) Membranes Modified by Fullerene C60. *Macromol. Mater. Eng.* **2009**, *294* (6–7), 432–440. https://doi.org/10.1002/mame.200800362.

(128) Li, H.; Chen, S.; Peng, X.; Sun, J.; Shu, C.; Jiang, L.; Wang, C. Fabrication of C60 Tri-Diethyl Malonate Membrane via an Electrospinning Method and Its Antibacterial Property. *J. Nanosci. Nanotechnol.* **2016**, *16* (3), 2504–2508. https://doi.org/10.1166/jnn.2016.10797.

(129) Chen, J.; Wang, X.; Han, H. A New Function of Graphene Oxide Emerges: Inactivating Phytopathogenic Bacterium Xanthomonas Oryzae Pv. Oryzae. *J. Nanoparticle Res.* **2013**, *15* (5), 1658. https://doi.org/10.1007/s11051-013-1658-6.

(130) Joz Majidi, H.; Babaei, A.; Arab Bafrani, Z.; Shahrampour, D.; Zabihi, E.; Jafari, S. M. Investigating the Best Strategy to Diminish the Toxicity and Enhance the Antibacterial Activity of Graphene Oxide by Chitosan Addition. *Carbohydr. Polym.* **2019**, *225*, 115220. https://doi.org/10.1016/j.carbpol.2019.115220.

(131) Bolotin, K. I.; Sikes, K. J.; Jiang, Z.; Klima, M.; Fudenberg, G.; Hone, J.; Kim, P.; Stormer, H. L. Ultrahigh Electron Mobility in Suspended Graphene. *Solid State Commun.* **2008**, *146* (9–10), 351–355. https://doi.org/10.1016/j.ssc.2008.02.024.

(132) Akhavan, O.; Ghaderi, E. Toxicity of Graphene and Graphene Oxide Nanowalls against Bacteria. *ACS Nano* **2010**, *4* (10), 5731–5736. https://doi.org/10.1021/nn101390x.

(133) Xie, Y. Y.; Hu, X. H.; Zhang, Y. W.; Wahid, F.; Chu, L. Q.; Jia, S. R.; Zhong, C. Development and Antibacterial Activities of Bacterial Cellulose/Graphene Oxide-CuO Nanocomposite Films. *Carbohydr. Polym.* **2020**, *229*, 115456. https://doi.org/10.1016/j.carbpol.2019.115456.

(134) Lin, D.; Qin, T.; Wang, Y.; Sun, X.; Chen, L. Graphene Oxide Wrapped SERS Tags: Multifunctional Platforms toward Optical Labeling, Photothermal Ablation of Bacteria, and the Monitoring of Killing Effect. *Appl. Mater. Interfaces* **2014**, *6*, 1320–1329. https://doi.org/10.1021/am405396k.

(135) Phys, J. A. Photocatalytic and Antibacterial Properties of Au-TiO2 Nanocomposite on Monolayer Graphene: From Experiment to Theory. *J. Appl. Phys.* **2013**, *114*, 204701. https://doi.org/10.1063/1.4836875.

(136) Yang, X.; Zhang, X.; Ma, Y.; Huang, Y.; Chen, Y. Superparamagnetic Graphene Oxide – Fe3O4 Nanoparticles Hybrid for Controlled Targeted Drug Carriers. *J. Mater. Chem.* **2009**, *19*, 2710–2714. https://doi.org/10.1039/b821416f.

(137) Zhang, H.; Zhang, C.; Zeng, G.; Gong, J.; Ou, X.; Huan, S. Easily Separated Silver Nanoparticle-Decorated Magnetic Graphene Oxide: Synthesis and High Antibacterial Activity. *J. Colloid Interface Sci.* **2016**, *471*, 94–102. https://doi.org/10.1016/j.jcis.2016.03.015.

(138) Celebi, K.; Buchheim, J.; Wyss, R. M.; Droudian, A.; Gasser, P.; Shorubalko, I.; Kye, J.-I.; Lee, C.; Park, H. G. Ultimate Permeation Across Atomically Thin Porous Graphene. *Science (80-.).* **2014**, *344*, 289–292. https://doi.org/10.1126/science.1249097.

(139) Karnik, R. Nano Filtration across Defect-Sealed Nanoporous Monolayer Graphene. *Nano Lett.* **2015**, *15*, 3254–3260. https://doi.org/10.1021/acs.nanolett.5b00456.

(140) Perreault, F.; Tousley, M. E.; Elimelech, M. Thin-Film Composite Polyamide Membranes Functionalized with Biocidal Graphene Oxide Nanosheets. *Environ. Sci. Technol. Lett.* **2014**, *1*, 71–76. https://doi.org/10.1021/ez4001356.

(141) Wang, Z.; Yu, H.; Xia, J.; Zhang, F.; Li, F.; Xia, Y.; Li, Y. Novel GO-Blended PVDF Ultra Fi Ltration Membranes. *Desalination* **2012**, *299*, 50–54. https://doi.org/10.1016/j.desal.2012.05.015.

(142) Yu, L.; Zhang, Y.; Zhang, B.; Liu, J.; Zhang, H.; Song, C. Preparation and Characterization of HPEI-GO/PES Ultrafiltration Membrane with Antifouling and Antibacterial Properties. *J. Memb. Sci.* **2013**, *447*, 452–462. https://doi.org/10.1016/j.memsci.2013.07.042.

(143) Zhang, J.; Xu, Z.; Shan, M.; Zhou, B.; Li, Y.; Li, B. Synergetic Effects of Oxidized Carbon Nanotubes and Graphene Oxide on Fouling Control and Anti-Fouling Mechanism of Polyvinylidene Fluoride Ultrafiltration Membranes. *J. Memb. Sci.* **2013**, *448*, 81–92. https://doi.org/10.1016/j.memsci.2013.07.064.

(144) Aslam, A.; Khan, P.; Khan, A.; Rahman, M. M.; Asiri, A. M. Lead Sensors Development and Antimicrobial Activities Based on Graphene Oxide/Carbon Nanotube/Poly (O-Toluidine)

Nanocomposite. *Int. J. Biol. Macromol.* **2016**, *89*, 198–205. https://doi.org/10.1016/j.ijbiomac.2016.04.064.

(145) Maksimova, Y. G. Microorganisms and Carbon Nanotubes: Interaction and Applications (Review). *Appl. Biochem. Microbiol.* **2019**, *55* (1), 1–12. https://doi.org/10.1134/S0003683819010101.

(146) Lee, B.; Baek, Y.; Lee, M.; Jeong, D. H.; Lee, H. H.; Yoon, J.; Kim, Y. H. A Carbon Nanotube Wall Membrane for Water Treatment. *Nat. Commun.* **2015**, *6*, 1–7. https://doi.org/10.1038/ncomms8109.

(147) Baek, Y.; Kim, C.; Kyun, D.; Kim, T.; Seok, J.; Hyup, Y.; Hyun, K.; Seek, S.; Cheol, S.; Lim, J.; Lee, K.; Yoon, J. High Performance and Antifouling Vertically Aligned Carbon Nanotube Membrane for Water Purification. *J. Memb. Sci.* **2014**, *460*, 171–177. https://doi.org/10.1016/j.memsci.2014.02.042.

(148) Goh, K.; Setiawan, L.; Wei, L.; Jiang, W.; Wang, R. Fabrication of Novel Functionalized Multi-Walled Carbon Nanotube Immobilized Hollow Fiber Membranes for Enhanced Performance in Forward Osmosis Process. *J. Memb. Sci.* **2013**, *446*, 244–254. https://doi.org/10.1016/j.memsci.2013.06.022.

(149) Liu, C. X.; Zhang, D. R.; He, Y.; Zhao, X. S.; Bai, R. Modification of Membrane Surface for Anti-Biofouling Performance: Effect of Anti-Adhesion and Anti-Bacteria Approaches. *J. Memb. Sci.* **2010**, *346*, 121–130. https://doi.org/10.1016/j.memsci.2009.09.028.

(150) Mei, Y.; Yao, C.; Li, X. A Simple Approach to Constructing Antibacterial and Anti-Biofouling Nanofibrous Membranes. *Biofouling* **2014**, *30* (3), 313–322. https://doi.org/10.1080/08927014.2013.871540.

(151) Gu, Q.; Jia, Z. Preparation of Quaternized Poly (Vinylidene Fluoride) Membranes by c-Ray Irradiation Induced Graft Polymerization and Their Antibacterial Property. *React. Funct. Polym.* **2013**, *73* (8), 1114–1121. https://doi.org/10.1016/j.reactfunctpolym.2013.04.009.

(152) Yu, H.; Zhang, X.; Zhang, Y.; Liu, J.; Zhang, H. Development of a Hydrophilic PES Ultra Filtration Membrane Containing SiO2@N-Halamine Nanoparticles with Both Organic Antifouling and Antibacterial Properties. *Desalination* **2013**, *326*, 69–76. https://doi.org/10.1016/j.desal.2013.07.018.

(153) Xueli, G.; Haizeng, W.; Jian, W.; Xing, H.; Congjie, G. Surface-Modified PSf UF Membrane by UV-Assisted Graft Polymerization of Capsaicin Derivative Moiety for Fouling and Bacterial Resistance. *J. Memb. Sci.* **2013**, *445*, 146–155. https://doi.org/10.1016/j.memsci.2013.05.026.

(154) Wu, Z.; Ye, C.; Guo, F.; Zhang, S.; Yu, X. Evidence for Broad-Spectrum Biofilm Inhibition by the Bacterium Bacillus Sp. Strain SW9. *Appl. Environ. Microbiol.* **2013**, *79* (5), 1735–1738. https://doi.org/10.1128/AEM.02796-12.

(155) Karkhanechi, H.; Takagi, R.; Ohmukai, Y.; Matsuyama, H. Enhancing the Antibiofouling Performance of RO Membranes Using Cu(OH)2 as an Antibacterial Agent. *Desalination*

2013, *325*, 40–47. https://doi.org/10.1016/j.desal.2013.06.015.

(156) Sile-yuksel, M.; Tas, B.; Koseoglu-imer, D. Y.; Koyuncu, I. Effect of Silver Nanoparticle (AgNP) Location in Nanocomposite Membrane Matrix Fabricated with Different Polymer Type on Antibacterial Mechanism. *Desalination* **2014**, *347*, 120–130. https://doi.org/10.1016/j.desal.2014.05.022.

(157) Fu, Q.; Wong, E. H. H.; Kim, J.; Scofield, J. M. P.; Gurr, P. A.; Kentish, S. E.; Qiao, G. G. The Effect of Soft Nanoparticles Morphologies on Thin Film Composite Membrane Performance. *J. Mater. Chem. A* **2014**, *2* (42), 17751–17756. https://doi.org/10.1039/c4ta02859g.

(158) Ben-Sasson, M.; Zodrow, K. R.; Genggeng, Q.; Kang, Y.; Giannelis, E. P.; Elimelech, M. Surface Functionalization of Thin-Film Composite Membranes with Copper Nanoparticles for Antimicrobial Surface Properties. *Environ. Sci. Technol.* **2014**, *48* (1), 384–393. https://doi.org/10.1021/es404232s.

(159) Munnawar, I.; Iqbal, S. S.; Anwar, M. N.; Batool, M.; Tariq, S.; Faitma, N.; Khan, A. L.; Khan, A. U.; Nazar, U.; Jamil, T.; Ahmad, N. M. Synergistic Effect of Chitosan-Zinc Oxide Hybrid Nanoparticles on Antibiofouling and Water Disinfection of Mixed Matrix Polyethersulfone Nanocomposite Membranes. *Carbohydr. Polym.* **2017**, *175*, 661–670. https://doi.org/10.1016/j.carbpol.2017.08.036.

(160) Xi, Z. Y.; Xu, Y. Y.; Zhu, L. P.; Wang, Y.; Zhu, B. K. A Facile Method of Surface Modification for Hydrophobic Polymer Membranes Based on the Adhesive Behavior of Poly(DOPA) and Poly(Dopamine). *J. Memb. Sci.* **2009**, *327* (1–2), 244–253. https://doi.org/10.1016/j.memsci.2008.11.037.

(161) Luppi, L.; Babut, T.; Petit, E.; Rolland, M.; Quemener, D.; Soussan, L.; Moradi, M. A.; Semsarilar, M. Antimicrobial Polylysine Decorated Nano-Structures Prepared through Polymerization Induced Self-Assembly (PISA). *Polym. Chem.* **2019**, *10* (3), 336–344. https://doi.org/10.1039/c8py01351a.

(162) Yoosefi Booshehri, A.; Wang, R.; Xu, R. The Effect of Re-Generable Silver Nanoparticles/Multi-Walled Carbon Nanotubes Coating on the Antibacterial Performance of Hollow Fiber Membrane. *Chem. Eng. J.* **2013**, *230*, 251–259. https://doi.org/10.1016/j.cej.2013.06.068.

(163) He, L.; Dumée, L. F.; Feng, C.; Velleman, L.; Reis, R.; She, F.; Gao, W.; Kong, L. Promoted Water Transport across Graphene Oxide-Poly(Amide) Thin Film Composite Membranes and Their Antibacterial Activity. *Desalination* **2015**, *365*, 126–135. https://doi.org/10.1016/j.desal.2015.02.032.

(164) Raaijmakers, M. J. T.; Benes, N. E. Current Trends in Interfacial Polymerization Chemistry. *Prog. Polym. Sci.* **2016**, *63*, 86–142. https://doi.org/10.1016/j.progpolymsci.2016.06.004.

(165) Cheng, C.; He, A.; Nie, C.; Xia, Y.; He, C.; Zhao, C. One-Pot Cross-Linked Copolymerization for the Construction of Robust Antifouling and Antibacterial Composite Membranes. *J. Mater. Chem. B* **2015**, *3*, 4170–4180. https://doi.org/10.1039/c5tb00136f.

(166) Liu, X.; Qi, S.; Li, Y.; Yang, L.; Cao, B.; Tang, C. Y. Synthesis and Characterization of Novel Antibacterial Silver Nanocomposite Nanofiltration and Forward Osmosis Membranes Based on Layer-by-Layer Assembly. *Water Res.* **2013**, *47*, 3081–3092. https://doi.org/10.1016/j.watres.2013.03.018.

(167) Ben-sasson, M.; Lu, X.; Bar-zeev, E.; Zodrow, K. R.; Nejati, S.; Qi, G.; Giannelis, E. P.; Elimelech, M. In Situ Formation of Silver Nanoparticles on Thin-Film Composite Reverse Osmosis Membranes for Biofouling Mitigation. *Water Res.* **2014**, *62*, 260–270. https://doi.org/10.1016/j.watres.2014.05.049.

(168) Zimmermann, T.; Rietdorf, J.; Pepperkok, R. Spectral Imaging and Its Applications in Live Cell Microscopy. *FEBS Lett.* **2003**, *546* (1), 87–92. https://doi.org/10.1016/S0014-5793(03)00521-0.

(169) Arora, M. Cell Culture Media: A Review. *Mater. Methods* **2013**, *3*, 1–29. https://doi.org/10.13070/mm.en.3.175.

(170) Yadav, B. S.; Ronda, V.; Vashista, D. P.; Sharma, B. Sequencing and Computational Approaches to Identification and Characterization of Microbial Organisms. *Biomed. Eng. Comput. Biol.* **2013**, *5*, BECB.S10886. https://doi.org/10.4137/becb.s10886.

(171) Park, S. J.; Onizuka, S.; Seki, M.; Suzuki, Y.; Iwata, T.; Nakai, K. A Systematic Sequencing-Based Approach for Microbial Contaminant Detection and Functional Inference. *BMC Biol.* **2019**, *17* (1), 72. https://doi.org/10.1186/s12915-019-0690-0.

(172) Roszak, D. B.; Colwell, R. R. Metabolic Activity of Bacterial Cells Enumerated by Direct Viable Count. *Appl. Environ. Microbiol.* **1987**, *53* (12), 2889–2893. https://doi.org/10.1128/aem.53.12.2889-2893.1987 169 6,567 Metrics Total Citations 169 Last 6 Months 1 Last 12 Months 6 Total Downloads 6,650 Last 6 Months 45 Last 12 Months 127.

(173) Chiquet, C.; Cornut, P.; Benito, Y.; Thuret, G.; Maurin, M.; Lafontaine, P.; Pechinot, A.; Palombi, K.; Lina, G.; Bron, A.; Denis, P.; Carricajo, A.; Creuzot, C. Eubacterial PCR for Bacterial Detection and Identification in 100 Acute Postcataract Surgery Endophthalmitis. *Investig. Ophthalmol. Vis. Sci.* **2008**, *49*, 1971–1978. https://doi.org/10.1167/iovs.07-1377.

(174) Wyatt, G. M.; Langley, M. N.; Lee, H. A.; Morgan, M. R. A. Further Studies on the Feasibility of One-Day Salmonella Detection by Enzyme-Linked Immunosorbent Assay. *Appl. Environ. Microbiol.* **1993**, *59* (5), 1383–1390. https://doi.org/10.1128/aem.59.5.1383-1390.1993.

(175) Tong, R.; Zhang, L.; Song, Q.; Hu, C.; Chen, X.; Lou, K.; Gong, X.; Gao, Y.; Wen, W. A Fully Portable Microchip Real-Time Polymerase Chain Reaction for Rapid Detection of Pathogen. *Electrophoresis* **2019**, *40* (12–13), 1699–1707. https://doi.org/10.1002/elps.201900090.

(176) Mao, X.; Yang, L.; Su, X. L.; Li, Y. A Nanoparticle Amplification Based Quartz Crystal Microbalance DNA Sensor for Detection of Escherichia Coli O157:H7. *Biosens. Bioelectron.* **2006**, *21* (7), 1178–1185. https://doi.org/10.1016/j.bios.2005.04.021.

(177) Shirasu, K. The HSP90-SGT1 Chaperone Complex for NLR Immune Sensors. *Annu. Rev. Plant*

Biol. **2009**, *60* (1), 139–164. https://doi.org/10.1146/annurev.arplant.59.032607.092906.

(178) Yamanaka, K.; Sekine, S.; Uenoyama, T.; Wada, M.; Ikeuchi, T.; Saito, M.; Yamaguchi, Y.; Tamiya, E. Quantitative Detection for Porphyromonas Gingivalis in Tooth Pocket and Saliva by Portable Electrochemical DNA Sensor Linked with PCR. *Electroanalysis* **2014**, *26* (12), 2686–2692. https://doi.org/10.1002/elan.201400447.

(179) Naimushin, A. N.; Soelberg, S. D.; Bartholomew, D. U.; Elkind, J. L.; Furlong, C. E. A Portable Surface Plasmon Resonance (SPR) Sensor System with Temperature Regulation. *Sensors Actuators, B Chem.* **2003**, *96* (1–2), 253–260. https://doi.org/10.1016/S0925-4005(03)00533-1.

(180) Soejima, T.; Iida, K. I.; Qin, T.; Taniai, H.; Seki, M.; Yoshida, S. I. Method to Detect Only Live Bacteria during PCR Amplification. *J. Clin. Microbiol.* **2008**, *46* (7), 2305–2313. https://doi.org/10.1128/JCM.02171-07.

(181) Vang, Ó. K.; Corfitzen, C. B.; Smith, C.; Albrechtsen, H. J. Evaluation of ATP Measurements to Detect Microbial Ingress by Wastewater and Surface Water in Drinking Water. *Water Res.* **2014**, *64*, 309–320. https://doi.org/10.1016/j.watres.2014.07.015.

(182) Tambi, A.; Brighu, U.; Gupta, A. B. MColiPAT Kit for Early Detection of Coliforms in Water. *Water Sci. Technol. Water Supply* **2020**, *20* (3), 871–877. https://doi.org/10.2166/ws.2020.008.

(183) Pujol-Vila, F.; Dietvorst, J.; Gall-Mas, L.; Díaz-González, M.; Vigués, N.; Mas, J.; Muñoz-Berbel, X. Bioelectrochromic Hydrogel for Fast Antibiotic-Susceptibility Testing. *J. Colloid Interface Sci.* **2018**, *511*, 251–258. https://doi.org/10.1016/j.jcis.2017.09.004.

(184) Tanaka, H.; Shinji, T.; Sawada, K.; Monji, Y.; Seto, S.; Yajima, M.; Yagi, O. Development and Application of a Luminiscence ATP Assay Method for Rapid Detection of Coliform Bacteria. *Water Res.* **1997**, *31* (8), 1913–1918. https://doi.org/10.1016/S0043-1354(97)00032-8.

(185) Pourciel-Gouzy, M. L.; Sant, W.; Humenyuk, I.; Malaquin, L.; Dollat, X.; Temple-Boyer, P. Development of PH-ISFET Sensors for the Detection of Bacterial Activity. *Sensors Actuators, B Chem.* **2004**, *103* (1–2), 247–251. https://doi.org/10.1016/j.snb.2004.04.056.

(186) Uria, N.; Abramova, N.; Bratov, A.; Muñoz-Pascual, F. X.; Baldrich, E. Miniaturized Metal Oxide PH Sensors for Bacteria Detection. *Talanta* **2016**, *147*, 364–369. https://doi.org/10.1016/j.talanta.2015.10.011.

(187) Lu, Y.-C.; Chuang, Y.-S.; Chen, Y.-Y.; Shu, A.-C.; Hsu, H.-Y.; Chang, H.-Y.; Yew, T.-R. Bacteria Detection Utilizing Electrical Conductivity. *Biosens. Bioelectron.* **2008**, *23*, 1856–1861. https://doi.org/10.1016/j.bios.2008.03.005.

(188) Uria, N.; Moral-Vico, J.; Abramova, N.; Bratov, A.; Muñoz, F. X. Fast Determination of Viable Bacterial Cells in Milk Samples Using Impedimetric Sensor and a Novel Calibration Method. *Electrochim. Acta* **2016**, *198*, 249–258. https://doi.org/10.1016/j.electacta.2016.03.060.

(189) Richter, K.; Schicklberger, M.; Gescher, J. Dissimilatory Reduction of Extracellular Electron

Acceptors in Anaerobic Respiration. *Appl. Environ. Microbiol.* **2012**, *78* (4), 913–921. https://doi.org/10.1128/AEM.06803-11.

(190) Straub, K. L.; Benz, M.; Schink, B. Iron Metabolism in Anoxic Environments at near Neutral PH. *FEMS Microbiol. Ecol.* **2001**, *34* (3), 181–186. https://doi.org/10.1016/S0168-6496(00)00088-X.

(191) Kracke, F.; Vassilev, I.; Krömer, J. O. Microbial Electron Transport and Energy Conservation - The Foundation for Optimizing Bioelectrochemical Systems. *Front. Microbiol.* **2015**, *6* (JUN), 1–18. https://doi.org/10.3389/fmicb.2015.00575.

(192) Rampersad, S. N. Multiple Applications of Alamar Blue as an Indicator of Metabolic Function and Cellular Health in Cell Viability Bioassays. *Sensors* **2012**, *12*, 12347–12360. https://doi.org/10.3390/s120912347.

(193) Murillo-Sierra, J. C.; Hernández-Ramírez, A.; Hinojosa-Reyes, L.; Guzmán-Mar, J. L. A Review on the Development of Visible Light-Responsive WO3-Based Photocatalysts for Environmental Applications. *Chem. Eng. J. Adv.* **2021**, *5*, 100070. https://doi.org/10.1016/j.ceja.2020.100070.

(194) Johansson, M. B.; Niklasson, G. A.; Österlund, L. Structural and Optical Properties of Visible Active Photocatalytic WO3 Thin Films Prepared by Reactive Dc Magnetron Sputtering. *J. Mater. Res.* **2012**, *27* (24), 3130–3140. https://doi.org/10.1557/jmr.2012.384.

(195) Tijani, J. O.; Abdullahi, M. N.; Bankole, M. T.; Mustapha, S.; Egbosiuba, T. C.; Ndamitso, M. M.; Abdulkareem, A. S.; Muzenda, E. Photocatalytic and Toxicity Evaluation of Local Dyeing Wastewater by Aluminium/Boron Doped WO3 Nanoparticles. *J. Water Process Eng.* **2021**, *44*, 102376. https://doi.org/10.1016/j.jwpe.2021.102376.

(196) Enesca, A.; Andronic, L.; Duta, A.; Manolache, S. Optical Properties and Chemical Stability of WO3 and TiO2 Thin Films Photocatalysts. *Rom. J. Inf. Sci. Technol.* **2007**, *10* (3), 269–277.

(197) Wu, J.; Zhu, Y.; You, L.; Dong, P.; Mei, J.; Cheng, J. Polymer Electrochromism Driven by Metabolic Activity Facilitates Rapid and Facile Bacterial Detection and Susceptibility Evaluation. *Adv. Funct. Mater.* **2020**, *30*, 2005192. https://doi.org/10.1002/adfm.202005192.

(198) Smith, J. J.; Mcfeters, G. a. Mechanisms of INT (2-(4-Iodophenyl)-3-(4-Nitrophenyl)-5-Phenyl Tetrazolium Chloride), and CTC (5-Cyano-2,3-Ditolyl Tetrazolium Chloride) Reduction in Escherichia Coli K-12. *J. Microbiol. Methods* **1997**, *29*, 161–175. https://doi.org/10.1016/S0167-7012(97)00036-5.

(199) Ullrich, S.; Karrasch, B.; Hoppe, H.; Jeskulke, K.; Kiel, D.-; Gmbh, U. F. Z. L.; Icrobiol, A. P. P. L. E. N. M. Toxic Effects on Bacterial Metabolism of the Redox Dye 5-Cyano-2, 3-Ditolyl Tetrazolium Chloride. *Appl. Environ. Microbiol.* **1996**, *62* (12), 4587–4593. https://doi.org/10.1128/aem.62.12.4587-4593.1996.

(200) Yoshida, N.; Hiraishi, A. An Improved Redox Dye-Staining Method Using 5-Cyano-2,3-Ditoryl Tetrazolium Chloride for Detection of Metabolically Active Bacteria in Activated Sludge.

Microbes Environ. **2004**, *19* (1), 61–70. https://doi.org/10.1264/jsme2.19.61.

(201) Bueno, C.; Villegas, M. L.; Bertolotti, S. G.; Previtali, C. M.; Neumann, M. G.; Encinas, M. V. The Excited-State Interaction of Resazurin and Resorufin with Amines in Aqueous Solutions. Photophysics and Photochemical Reaction. *Photochem. Photobiol.* **2002**, *76* (4), 385–390. https://doi.org/10.1562/0031-8655(2002)0760385TESIOR2.0.CO2.

(202) Pace, R. T.; Burg, K. J. L. Toxic Effects of Resazurin on Cell Cultures. *Cytotechnology* **2015**, *67* (1), 13–17. https://doi.org/10.1007/s10616-013-9664-1.

(203) Pettit, R. K.; Weber, C. A.; Kean, M. J.; Hoffmann, H.; Pettit, G. R.; Tan, R.; Franks, K. S.; Horton, M. L. Microplate Alamar Blue Assay for Staphylococcus Epidermidis Biofilm Susceptibility Testing. *Antimicrob. Agents Chemother.* **2005**, *49* (7), 2612–2617. https://doi.org/10.1128/AAC.49.7.2612-2617.2005.

(204) Hamid, R.; Rotshteyn, Y.; Rabadi, L.; Parikh, R.; Bullock, P. Comparison of Alamar Blue and MTT Assays for High Through-Put Screening. *Toxicol. Vitr.* **2004**, *18* (5), 703–710. https://doi.org/10.1016/j.tiv.2004.03.012.

(205) Marmisollé, W. A.; Florit, M. I.; Posadas, D. Coupling between Proton Binding and Redox Potential in Electrochemically Active Macromolecules. the Example of Polyaniline. *J. Electroanal. Chem.* **2013**, *707*, 43–51. https://doi.org/10.1016/j.jelechem.2013.08.012.

(206) Ramohlola, K. E.; Monana, G. R.; Hato, M. J.; Modibane, K. D.; Molapo, K. M.; Masikini, M.; Mduli, S. B.; Iwuoha, E. I. Polyaniline-Metal Organic Framework Nanocomposite as an Efficient Electrocatalyst for Hydrogen Evolution Reaction. *Compos. Part B Eng.* **2018**, *137*, 129–139. https://doi.org/10.1016/j.compositesb.2017.11.016.

(207) Kucekova, Z.; Humpolicek, P.; Kasparkova, V.; Perecko, T.; Lehocký, M.; Hauerlandová, I.; Sáha, P.; Stejskal, J. Colloidal Polyaniline Dispersions: Antibacterial Activity, Cytotoxicity and Neutrophil Oxidative Burst. *Colloids Surfaces B Biointerfaces* **2014**, *116*, 411–417. https://doi.org/10.1016/j.colsurfb.2014.01.027.

(208) Bhandari, S. *Polyaniline Blends, Composites, and Nanocomposites*; Elsevier Inc., 2018. https://doi.org/10.1016/b978-0-12-809551-5.00002-3.

(209) Zare, E. N.; Makvandi, P.; Ashtari, B.; Rossi, F.; Motahari, A.; Perale, G. Progress in Conductive Polyaniline-Based Nanocomposites for Biomedical Applications: A Review. *J. Med. Chem.* **2020**, *63* (1), 1–22. https://doi.org/10.1021/acs.jmedchem.9b00803.

(210) Howes, P.; Green, M.; Levitt, J.; Suhling, K.; Hughes, M. Phospholipid Encapsulated Semiconducting Polymer Nanoparticles: Their Use in Cell Imaging and Protein Attachment. *J. Am. Chem. Soc.* **2010**, *132* (11), 3989–3996. https://doi.org/10.1021/ja1002179.

(211) Luo, J.; Sam, A.; Hu, B.; DeBruler, C.; Wei, X.; Wang, W.; Liu, T. L. Unraveling PH Dependent Cycling Stability of Ferricyanide/Ferrocyanide in Redox Flow Batteries. *Nano Energy* **2017**, *42*, 215–221. https://doi.org/10.1016/j.nanoen.2017.10.057.

(212) Hatamie; Amir; Zargar; Behrooz; Jalali, A.; Ameri, H. Colorimetric Assay for 4-

Phenylthiosemicarbazide Detection in Environmental Samples Based on Prussian Blue Nanoparticles Formation Ion. *Iran. J. Chem. Chem. Eng* **2017**, *36* (1), 125–133.

(213) Yang, Z.; Cheng, Y.; Zhang, F.; Li, B.; Mu, Y.; Li, W.; Yu, H. Rapid Detection and Enumeration of Exoelectrogenic Bacteria in Lake Sediments and Wastewater Treatment Plant Using a Coupled WO3 Nanoclusters and Most Probable Number Method. *Environ. Sci. Technol. Lett.* **2016**, *3* (4), 133–137. https://doi.org/10.1021/acs.estlett.6b00112.

(214) Yuan, S.; Li, W.; Cheng, Y.; He, H.; Chen, J.; Tong, Z.; Lin, Z.; Zhang, F.; Sheng, G.; Yu, H. A Plate-Based Electrochromic Approach for the High-Throughput Detection of Electrochemically Active Bacteria. *Nat. Protoc.* **2014**, *9* (1), 112–119. https://doi.org/10.1038/nprot.2013.173.

(215) González, A.; Gálvez, N.; Clemente-León, M.; Dominguez-Vera, J. M. Electrochromic Polyoxometalate Material as a Sensor of Bacterial Activity. *Chem. Commun.* **2015**, *51* (50), 10119–10122. https://doi.org/10.1039/c5cc03301b.

(216) Berridge, M. V; Herst, P. M.; Tan, A. S. Tetrazolium Dyes as Tools in Cell Biology: New Insights into Their Cellular Reduction. *Biotechnol. Annu. Rev.* **2005**, *11* (05), 127–152. https://doi.org/10.1016/S1387-2656(05)11004-7.

(217) Rodriguez, G. G.; Phipps, D.; Ishiguro, K. Use of a Fluorescent Redox Probe for Direct Visualization of Actively Respiring Bacteria. *Appl. Environ. Microbiol.* **1992**, *58* (6), 1801–1808. https://doi.org/10.1128/aem.58.6.1801-1808.1992.

(218) Asma, N. I.; Berridge, M. V; Tan, A. S. Trans-Plasma Membrane Electron Transport: A Cellular Assay for NADH- and NADPH-Oxidase Based on Extracellular, Superoxide-Mediated Reduction of the Sulfonated Tetrazolium Salt WST-1. *Protoplasma* **1998**, *205*, 74–82. https://doi.org/10.1007/BF01279296.

(219) Baudoux, A.; Bertru, G.; Rouzic, B. Le. Direct Estimate of Active Bacteria: CTC Use and Limitations. *J. Microbiol. Methods* **2003**, *52*, 19–28. https://doi.org/10.1016/S0167-7012(02)00128-8.

(220) Chang, J.; Chen, B.; Lin, Y. S. Stimulation of Bacterial Decolorization of an Azo Dye by Extracellular Metabolites from Escherichia Coli Strain NO3. *Bioresour. Technol.* **2004**, *91*, 243–248. https://doi.org/10.1016/S0960-8524(03)00196-2.

(221) Palomino, J.; Martin, A.; Camacho, M.; Guerra, H.; Swings, J.; Portaels, F. Resazurin Microtiter Assay Plate : Simple and Inexpensive Method for Detection of Drug Resistance in Mycobacterium Tuberculosis. *Antimicrob. Agents Chemother.* **2002**, *46* (8), 2720–2722. https://doi.org/10.1128/AAC.46.8.2720.

(222) Lian, J.; Tian, X.; Guo, J.; Guo, Y.; Song, Y.; Yue, L.; Wang, Y.; Liang, X. Effects of Resazurin on Perchlorate Reduction and Bioelectricity Generation in Microbial Fuel Cells and Its Catalysing Mechanism. *Biochem. Eng. J.* **2016**, *114* (4), 164–172. https://doi.org/10.1016/j.bej.2016.06.028.

(223) Ranjbar, S.; Amin, M.; Nejad, F.; Parolo, C.; Shahrokhian, S. Smart Chip for Visual Detection

of Bacteria Using the Electrochromic Properties of Polyaniline. *Anal. Chem.* **2019**, *91*, 14960–14966. https://doi.org/10.1021/acs.analchem.9b03407.

(224) Thakur, B.; Amarnath, C. A.; Mangoli, S. H.; Sawant, S. N. Polyaniline Nanoparticle Based Colorimetric Sensor for Monitoring Bacterial Growth. *Sensors Actuators B Chem.* **2015**, *207*, 262–268. https://doi.org/10.1016/j.snb.2014.10.045.

(225) Luo, S. Conducting Polymers as Biointerfaces and Biomaterials: A Perspective for a Special Issue of Polymer Reviews. *Polym. Rev.* **2013**, *53* (3), 303–310. https://doi.org/10.1080/15583724.2013.805773.

(226) Green, R. A.; Lovell, N. H.; Wallace, G. G.; Poole-warren, L. A. Conducting Polymers for Neural Interfaces: Challenges in Developing an Effective Long-Term Implant. *Biomaterials* **2008**, *29*, 3393–3399. https://doi.org/10.1016/j.biomaterials.2008.04.047.

(227) Ravichandran, R.; Sundarrajan, S.; Venugopal, J. R.; Mukherjee, S.; Ramakrishna, S. Applications of Conducting Polymers and Their Issues in Biomedical Engineering. *J. R. Soc. Interface* **2010**, *7*, S559–S579. https://doi.org/10.1098/rsif.2010.0120.focus.

(228) Ouyang, J. Recent Advances of Intrinsically Conductive Polymers. *Acta Physico-Chimica Sin.* **2018**, *34* (11), 1211–1220. https://doi.org/10.3866/PKU.WHXB201804095.

(229) Rawson, F. J.; Downard, A. J.; Baronian, K. H. Electrochemical Detection of Intracellular and Cell Membrane Redox Systems in Saccharomyces Cerevisiae. *Sci. Rep.* **2014**, 1–9. https://doi.org/10.1038/srep05216.

(230) Morris, K.; Catterall, K.; Zhao, H.; Pasco, N.; John, R. Ferricyanide Mediated Biochemical Oxygen Demand - Development of a Rapid Biochemical Oxygen Demand Assay. *Anal. Chim. Acta* **2001**, *442* (1), 129–139. https://doi.org/10.1016/S0003-2670(01)01133-3.

(231) Morris, K.; Zhao, A. H.; A, R. J. Ferricyanide-Mediated Microbial Reactions for Environmental Monitoring. *Aust. j. Chem.* **2005**, *58*, 237–245. https://doi.org/10.1071/CH05038.

(232) Yoshida, N.; Yano, K.; Morita, T.; Mcniven, S. J.; Nakamura, H.; Karube, I. A Mediator-Type Biosensor as a New Approach to Biochemical Oxygen Demand Estimation. *Analyst* **2000**, *125*, 2280–2284. https://doi.org/10.1039/b005995l.

(233) Rosseinsky, D. R.; Glasser, L.; Jenkins, H. D. B. Thermodynamic Clarification of the Curious Ferric/Potassium Ion Exchange Accompanying the Electrochromic Redox Reactions of Prussian Blue, Iron(III) Hexacyanoferrate(II). *J. Am. Chem. Soc.* **2004**, *126* (33), 10472–10477. https://doi.org/10.1021/ja040055r.

(234) Ding, P.; Song, G.; Zhou, J.; Song, Q. Collection of Rolling Fingerprints by the Electrochromism of Prussian Blue. *Dye. Pigment.* **2015**, *120*, 169–174. https://doi.org/10.1016/j.dyepig.2015.04.019.

(235) Itaya, K.; Uchida, I.; Neff, V. D. Electrochemistry of Polynuclear Transition Metal Cyanides: Prussian Blue and Its Analogues. *Acc. Chem. Res.* **1986**, *19* (6), 162–168. https://doi.org/10.1021/ar00126a001.

(236) Ricci, F.; Palleschi, G. Sensor and Biosensor Preparation, Optimisation and Applications of Prussian Blue Modified Electrodes. *Biosens. Bioelectron.* **2005**, *21* (3), 389–407. https://doi.org/10.1016/j.bios.2004.12.001.

(237) Karyakin, A. A. Advances of Prussian Blue and Its Analogues in (Bio)Sensors. *Curr. Opin. Electrochem.* **2017**, *5* (1), 92–98. https://doi.org/10.1016/j.coelec.2017.07.006.

(238) Koncki, R. Chemical Sensors and Biosensors Based on Prussian Blues. *Crit. Rev. Anal. Chem.* **2002**, *32* (1), 79–96. https://doi.org/10.1080/10408340290765452.

(239) Ghatole, M.; Kashetty, V.; Ghule, A. Resazurin Assay for Rapid Drug Susceptibility Testing of Mycobacterium Tuberculosis. *Indian J. Microbiol. Res.* **2018**, *5* (1), 138–142. https://doi.org/10.18231/2394-5478.2018.0028.

(240) Jia, H.; Fang, R.; Lin, J.; Tian, X.; Zhao, Y.; Chen, L.; Cao, J.; Zhou, T. Evaluation of Resazurin-Based Assay for Rapid Detection of Polymyxin-Resistant Gram-Negative Bacteria. *BMC Microbiol.* **2020**, *20* (7), 1–11. https://doi.org/10.1186/s12866-019-1692-3.

(241) Hsieh, K.; Zec, H. C.; Chen, L.; Kaushik, A. M.; Mach, K. E.; Liao, J. C.; Wang, T. Simple and Precise Counting of Viable Bacteria by Resazurin- Amplified Picoarray Detection. *Anal. Chem.* **2018**, *90*, 9449–9456. https://doi.org/10.1021/acs.analchem.8b02096.

(242) Sehulster, L.; Chinn, R. Y. W. Centers for Disease Control Ans Prevention. Guidelines for Environmental Infection Control in Health-Care Facilities: Recommendations of CDC and the Healthcare Infection Control Practices Advisory Committee (HICPAC). *Morb. Mortal. Wkly. Rep.* **2003**, *52* (RR10), 1–48.

(243) Drossel, W. G.; Kunze, H.; Bucht, A.; Weisheit, L.; Pagel, K. Smart3 - Smart Materials for Smart Applications. *Procedia CIRP* **2015**, *36*, 211–216. https://doi.org/10.1016/j.procir.2015.01.055.

(244) Kumar, B.; Noor, N.; Thakur, S.; Pan, N.; Narayana, H.; Yan, S.; Wang, F.; Shah, P. Shape Memory Polyurethane-Based Smart Polymer Substrates for Physiologically Responsive, Dynamic Pressure (Re) Distribution. *ACS Omega* **2019**, *4*, 15348–15358. https://doi.org/10.1021/acsomega.9b01167.

(245) Chaterji, S.; Kwon, K. Il; Park, K. Smart Polymeric Gels: Redefining the Limits of Biomedical Devices. *Prog. Polym. Sci.* **2007**, *32*, 1083–1122. https://doi.org/10.1016/j.progpolymsci.2007.05.018.

(246) Dichiara, A. B.; Song, A.; Goodman, S. M.; He, D.; Bai, J. Smart Papers Comprising Carbon Nanotubes and Cellulose Microfibers for Multifunctional Sensing Applications. *J. Mater. Chem. A* **2017**, *5*, 20161. https://doi.org/10.1039/c7ta04329e.

(247) Gao, Y.; Luo, H.; Zhang, Z.; Kang, L. Nanoceramic VO2 Thermochromic Smart Glass: A Review on Progress in Solution Processing. *Nano Energy* **2012**, *1*, 221–246. https://doi.org/10.1016/j.nanoen.2011.12.002.

(248) Phys, J. A. Smart Textiles: Challenges and Opportunities. *J. Appl. Phys.* **2012**, *112*, 091301.

https://doi.org/doi.org/10.1063/1.4742728.

(249) Natali, M.; Giordani, S. Molecular Switches as Photocontrollable '"Smart"' Receptors. *Chem. Soc. Rev.* **2012**, *41*, 4010–4029. https://doi.org/10.1039/c2cs35015g.

(250) Ramanujan, R. V.; Lao, L. L. The Mechanical Behavior of Smart Magnet-Hydrogel Composites. *Smart Mater. Struct.* **2006**, *15*, 952. https://doi.org/10.1088/0964-1726/15/4/008.

(251) Alizadeh-sani, M.; Mohammadian, E.; Rhim, J.; Mahdi, S. PH-Sensitive (Halochromic) Smart Packaging Films Based on Natural Food Colorants for the Monitoring of Food Quality and Safety. *Trends Food Sci. Technol.* **2020**, *105*, 93–144. https://doi.org/10.1016/j.tifs.2020.08.014.

(252) Qader, I. N.; KöK, M.; Dagdelen, F.; Aydogdu, Y. A Review of Smart Materials: Researches and Applications. *El-Cezeri J. Sci. Eng.* **2019**, *6* (3), 755–788. https://doi.org/10.31202/ecjse.562177.

(253) Bahl, S.; Nagar, H.; Singh, I.; Sehgal, S. Smart Materials Types, Properties and Applications : A Review. *Mater. Today Proc.* **2020**, *28*, 1302–1306. https://doi.org/10.1016/j.matpr.2020.04.505.

(254) Kamila, S. Introduction , Classification and Applications of Smart Materials : An Overview. *Am. J. Appl. Sci.* **2013**, *10* (8), 876–880. https://doi.org/10.3844/ajassp.2013.876.880.

(255) Leng, J.; Lu, H.; Liu, Y.; Huang, W. M.; Du, S. Shape-Memory Polymers — A Class of Novel Smart Materials. *Mrs Bull.* **2009**, *34* (848–855). https://doi.org/10.1557/mrs2009.235.

(256) Leng, J.; Lan, X.; Liu, Y.; Du, S. Shape-Memory Polymers and Their Composites: Stimulus Methods and Applications. *Prog. Mater. Sci.* **2011**, *56*, 1077–1135. https://doi.org/10.1016/j.pmatsci.2011.03.001.

(257) Mahapatra, S. Das; Mohapatra, P. C.; Aria, A. I.; Christie, G.; Mishra, Y. K.; Hofmann, S.; Thakur, V. K. Piezoelectric Materials for Energy Harvesting and Sensing Applications: Roadmap for Future Smart Materials. *Adv. Sci.* **2021**, *8*, 2100864. https://doi.org/10.1002/advs.202100864.

(258) Basheer, A. A. Advances in the Smart Materials Applications in the Aerospace Industries. *Aircr. Eng. Aerosp. Technol.* **2020**, *92* (7), 1027–1035. https://doi.org/10.1108/AEAT-02-2020-0040.

(259) Richter, A.; Bund, A.; Keller, M.; Arndt, K. Characterization of a Microgravimetric Sensor Based on PH Sensitive Hydrogels. *Sensors Actuators B* **2004**, *99*, 579–585. https://doi.org/10.1016/j.snb.2004.01.011.

(260) Alizadeh, M.; Tavassoli, M.; Hamishehkar, H.; Julian, D. Carbohydrate-Based Films Containing PH-Sensitive Red Barberry Anthocyanins: Application as Biodegradable Smart Food Packaging Materials. *Carbohydr. Polym.* **2021**, *255*, 117488. https://doi.org/doi.org/10.1016/j.carbpol.2020.117488.

(261) Xie, J.; Li, A.; Li, J. Advances in PH-Sensitive Polymers for Smart Insulin Delivery. *Macromol. Rapid Commun.* **2017**, *38*, 1700413. https://doi.org/10.1002/marc.201700413.

(262) Lampert, C. M. Chromogenic Smart Materials. *Mater. Today* **2004**, 28–35. https://doi.org/doi.org/10.1016/S1369-7021(04)00123-3.

(263) Song, Y.; Wei, W.; Qu, X. Colorimetric Biosensing Using Smart Materials. *Adv. Mater.* **2011**, *23*, 4215–4236. https://doi.org/10.1002/adma.201101853.

(264) Ding, Y.; Invernale, M. A.; Sotzing, G. A. Conductivity Trends of PEDOT-PSS Impregnated Fabric and the Effect of Conductivity on Electrochromic Textile. *Appl. Mater. Interfaces* **2010**, *2* (6), 1588–1593. https://doi.org/10.1021/am100036n.

(265) Song, J.; Cheng, Q.; Zhu, S. "Smart''' Materials for Biosensing Devices: Cell-Mimicking Supramolecular Assemblies and Colorimetric Detection of Pathogenic Agents." *Biomed. Microdevices* **2002**, *4* (3), 213–221. https://doi.org/doi.org/10.1023/A:1016000530783.

(266) Pal, K.; Asthana, N.; Aljabali, A. A.; Bhardwaj, S. K.; Kralj, S.; Penkova, A.; Thomas, S.; Zaheer, T.; Souza, F. G. De. A Critical Review on Multifunctional Smart Materials ' Nanographene ' Emerging Avenue: Nano-Imaging and Biosensor Applications. *Crit. Rev. Solid State Mater. Sci.* **2022**, *47* (5), 691–707. https://doi.org/10.1080/10408436.2021.1935717.

(267) Carvalho, E. O.; Fernandes, M. M.; Padrao, J.; Nicolau, A.; Marqués-Marchán, J.; Asenjo, A.; Gama, F. M.; Ribeiro, C.; Lanceros-Mendez, S. Tailoring Bacteria Response by Piezoelectric Stimulation. *Appl. Mater. Interfaces* **2019**, *11*, 27297–27305. https://doi.org/10.1021/acsami.9b05013.

(268) Tominaga, T. Rapid Detection of Klebsiella Pneumoniae, Klebsiella Oxytoca, Raoultella Ornithinolytica and Other Related Bacteria in Food by Lateral-Flow Test Strip Immunoassays. *J. Microbiol. Methods* **2018**, *147*, 43–49. https://doi.org/10.1016/j.mimet.2018.02.015.

(269) Thet, N. T.; Hong, S. H.; Marshall, S.; Laabei, M.; Toby, A.; Jenkins, A. Visible, Colorimetric Discrimination between Pathogenic Strains of Staphylococcus Aureus and Pseudomonas Aeruginosa Using Fluorescent Dye Containing Lipid Vesicles. *Biosens. Bioelectron.* **2013**, *41* (1), 538–543. https://doi.org/10.1016/j.bios.2012.09.019.

(270) Thet, N. T.; Alves, D. R.; Bean, J. E.; Booth, S.; Nzakizwanayo, J.; Young, A. E. R.; Jones, B. V.; Jenkins, A. T. A. Prototype Development of the Intelligent Hydrogel Wound Dressing and Its Efficacy in the Detection of Model Pathogenic Wound Biofilms. *ACS Appl. Mater. Interfaces* **2016**, *8* (24), 14909–14919. https://doi.org/10.1021/acsami.5b07372.

(271) Ebrahimi, M.-M. S.; Laabei, M.; Jenkins, A. T. A.; Schönherr, H. Autonomously Sensing Hydrogels for the Rapid and Selective Detection of Pathogenic Bacteria. *Macromol. Rapid Commun.* **2015**, *36* (24), 2123–2128. https://doi.org/10.1002/marc.201500485.

(272) Snari, R. M.; Alsahag, M.; Alisaac, A.; Bayazeed, A.; Alsoliemy, A.; Khalifa, M. E.; El-metwaly, N. M. Smart Textiles Immobilized with Hydrazone Probe for Colorimetric Recognition of Bacteria. *J. Mol. Liq.* **2022**, *366*, 120149. https://doi.org/10.1016/j.molliq.2022.120149.

(273) Alisaac, A.; Alsahag, M.; Alshareef, M.; Snari, R. M.; Alhasani, M.; Abumelha, H. M.; El-metwaly, N. M. Development of Smart Cotton Fabrics Immobilized with Anthocyanin and Potassium Alum for Colorimetric Detection of Bacteria. *Inorg. Chem. Commun.* **2022**, *145*, 110023. https://doi.org/doi.org/10.1016/j.inoche.2022.110023.

(274) Kassal, P.; Zubak, M.; Scheipl, G.; Mohr, G. J.; Steinberg, M. D. Smart Bandage with Wireless Connectivity for Optical Monitoring of PH. *Sensors Actuators B Chem.* **2017**, *246*, 455–460. https://doi.org/10.1016/j.snb.2017.02.095.

(275) Huang, T.; Lu, H.; Ho, Y.; Lu, K.; Wang, P. A Smart and Active Film with Tunable Drug Release and Color Change Abilities for Detection and Inhibition of Bacterial Growth. *Mater. Sci. Eng. C* **2021**, *118*, 111396. https://doi.org/10.1016/j.msec.2020.111396.

(276) Wang, J.; Wang, J.; Liu, J.; Wang, X.; Raheem, A.; Song, Z.; Kipper, M. J.; Tang, J. Smart Sensing of Bacterial Contamination on Fluorescent Cotton Fabrics (FCF) by Nontoxic Eu 3+-Induced Polyelectrolyte Nano-Aggregates (EIPAs). *Dye. Pigment.* **2020**, *181*, 108536. https://doi.org/doi.org/10.1016/j.dyepig.2020.108536.

(277) Li, C.; Tang, Q.; Wei, H.; Liu, J.; Wang, Q.; Wang, Y.; Du, Z.; Wang, J.; Xu, R.; Bi, Y.; Snow, C. D.; Bel, L. A.; Tang, J. Smart Wearable Fluorescence Sensing of Bacterial Pathogens and Toxic Contaminants by Eu3+ -Induced Sodium Alginate/Ag Nanoparticle Aggregates. *ACS Appl. Nano Mater.* **2022**, *5* (6), 8393–8403. https://doi.org/10.1021/acsanm.2c01525.

(278) Raheem, A.; Liu, J.; Wang, J.; Wang, J.; Zhao, Y.; Wang, Y.; Wang, Y.; Wang, W.; Ul, F.; Kipper, M. J.; Tang, J. Selective Sensing of Cu2+ and Fe3+ Ions with Vis-Excitation Using Fluorescent Eu3+-Induced Aggregates of Polysaccharides (EIAP) in Mammalian Cells and Aqueous Systems. *J. Hazard. Mater.* **2020**, *399*, 122991. https://doi.org/10.1016/j.jhazmat.2020.122991.

(279) He, M.; Ou, F.; Wu, Y.; Sun, X.; Chen, X.; Li, H.; Sun, D.; Zhang, L. Smart Multi-Layer PVA Foam/CMC Mesh Dressing with Integrated Multi-Functions for Wound Management and Infection Monitoring. *Mater. Des.* **2022**, *194*, 108913. https://doi.org/10.1016/j.matdes.2020.108913.

(280) Zamel, D.; Hassanin, A. H.; Ellethy, R.; Singer, G.; Abdelmoneim, A. Novel Bacteria-Immobilized Cellulose Acetate/Poly(Ethylene Oxide) Nanofibrous Membrane for Wastewater Treatment. *Sci. Rep.* **2019**, *9*, 18994. https://doi.org/10.1038/s41598-019-55265-w.

2
Objectives

The main objective of this PhD thesis is the development of smart materials based on the use of electrochromic metabolic indicators for the control and prevention of bacterial infections. To achieve this objective, two smart materials, i.e., textiles and water filters, will be studied and endowed with bacterial-sensing and antibacterial properties through the incorporation of Prussian blue nanoparticles and bactericidal agents, respectively. In this context, the following specific objectives have been envisioned:

- To determine the most suitable sensing probe to be implemented in smart materials, which has to be sensitive only to live bacteria, to produce clear color change detectable with the bare eye, to be biocompatible, to present stability and durability in the material and to be easy to implement by mass-production technologies.

- To study and characterize the electrochromogenic properties of the two forms of Prussian blue, namely soluble and insoluble and their response to bacterial metabolism in both, suspension and after electrodepostion into ITO-PET transparent electrodes.

- To achieve homogeneous and stable coatings of Prussian blue into polyester-cotton textiles and study their bacterial-sensing capacity against both, Gram-negative and Gram-positive bacteria.

- To develop smart textile by the implementation of the sensing molecule into antibacterial fabrics for the determination of the self-life of the bactericide textile.

- To improve the sensitivity and time of response of the smart textiles by testing different modification methods, such as cyanotype process.

- To develop smart membrane filters able to detect the presence of live bacteria in water by a simple color change produced on the filter surface.

- To endow the filter samples with antibacterial and sensing capacities for the development of smart filters.

3

Materials and Methods

3.1 Reagents

All chemicals used in this thesis are listed below. All of them were used as received unless it stated. All aqueous solutions were always prepared using deionized water (water conductivity = 17 MΩ).

Potassium ferricyanide ($K_3[Fe(CN)_6]$), iron(II) chloride ($FeCl_2$), hydrogen chloride (HCl 37%), phosphate buffer saline (PBS), ammonium iron (III) citrate, Mueller-Hinton broth 2 (MH), 2-(N-morpholino)ethane-sulfonic acid hydrate (MES hydrate), 2-hydroxyethyl cellulose with an average molecular mass of 380 kDa, Dulbecco's Modified Eagle's Medium (DMEM, supplemented with 10% fetal bovine serum, 1% penicillin/ streptomycin solution), cooper (II) acetate, ammonia, nitrocellulose membranes - 0.2 µm (Whatman) and mixed cellulose esters membranes (MF-Millipore) were purchased from Sigma-Aldrich (Spain).

Iron (III) chloride anhydrous ($FeCl_3$), Zobell Marine Broth and Live/Dead BacLight Bacterial Viability Kit (Invitrogen) were obtained from Fischer Scientific (Spain).

Glucose, sodium borohydride ($NaBH_4$), potassium phosphate dibasic trihydrate ($K_2HPO_4 \cdot 3H_2O$), potassium dihydrogen phosphate (KH_2PO_4), hydrogen peroxide (H_2O_2) and Silver nitrate ($AgNO_3$) were from Panreac (Spain).

Soya Casein Digest Lecithin Polysorbate Broth (SCDLP) medium was obtained from Scharlab S.L (Spain).

Potassium chloride (KCl) and oxalic acid were purchased from Probus.

3.1.1 Solutions and media preparation

Phosphate Buffer 0.1 M was prepared by mixing 2.625 g of KH_2PO_4 and 7.010 g of $K_2HPO_4 \cdot 3H_2O$ in 500 mL of milli-Q water.

PBS 0.1 M was obtained by dissolving one tablet in 200 mL of deionized water, as specified by the supplier.

MH medium was prepared according to the supplier: 22 g were diluted in 1 L of deionized water. The pH was adjusted to 6.2 with HCl 0.1 M.

MES 0.1 M was obtained by diluting 1.95 g in 100 mL of deionized water. The pH of the solution was adjusted to 6.2 with HCl 0.1 M.

For Zobell Broth preparation, 37.4 g of the solid broth reagent were diluted in 1 L of deionized water, as indicated by the supplier.

All the media were sterilized in an autoclave from Selecta before use (autoclave conditions: 121 $^{\circ}$C in wet environment for 25 minutes).

3.2 Synthesis of PB-NPs

Depending on the counter-ion used for charge compensation, two forms of PB can be synthetized: the one called "insoluble" (PB$_{Ins}$), which incorporates iron as counter-ion, and the "soluble" (PB$_{Sol}$) containing potassium ions. Both PB forms are composed of insoluble PB particles and result in blue-colored suspensions, but they present important structural and functional differences, e.g. in the deposition kinetics. That is, while PB$_{Sol}$-NPs present slow deposition kinetics by the small size of the particles, PB$_{Ins}$-NPs, containing aggregations of NPs, precipitate quickly.[1–3]

PB-NPs were synthetized by a chemical reaction of ferric and hexacyanoferrate ions in aqueous solution (i.e. water) until a dark blue colloid is formed.[3,4] For PB$_{Sol}$ synthesis, equimolar solutions (30 mM) of FeCl$_2$ and K$_3$[Fe(CN)$_6$] were used. Concretely, 25 mL of the ferricyanide solution were slowly added to 25 mL of the iron dichloride resulting in a dark blue solution corresponding to PB$_{Sol}$ formation. On the other hand, PB$_{Ins}$ was synthesized by mixing 50 mL of 15 mM K$_3$[Fe(CN)$_6$] with an excess of FeCl$_2$ (30 mL, 0.1 M). In this case, the iron dichloride solution which was added dropwise to the ferricyanide producing the formation of the dark blue precipitate corresponding to the PB$_{Ins}$. The precipitate was left to deposit and cleaned twice with distilled water. Figure 3.1 shows the differences between the deposition kinetics of the soluble and insoluble forms after their synthesis, which confirmed the correct synthesis of both PB forms.

As previously demonstrated, light can affect PB-NPs stability,[5] hence synthetized NPs were stored protected from light until used.
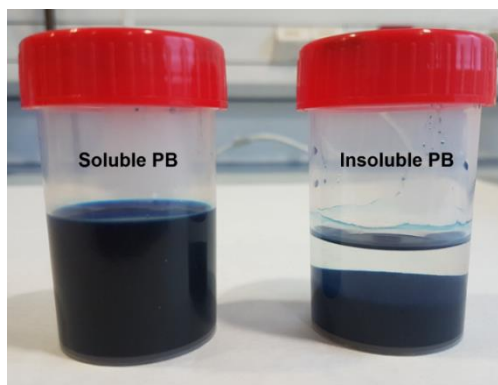

Figure 3.1. Shyntesis of PB$_{Sol}$ and PB$_{Ins}$. Picture of the two-synthetized forms of PB: soluble and insoluble.

3.3 Coating Technologies

3.3.1 PB-NPs electrodeposition on ITO-PET electrodes

Electrochemical studies required the electrodeposition of PB-NPs on the working electrode (WE) surface. In this case, a three-electrode spectroelectrochemical cell was used (Figure 3.2), where poly(ethylene terephthalate) sheets coated with conductive indium tin oxide (ITO-PET) substrates were used as WE, a platinum wire was the counter electrode (CE) and Ag/AgCl (3M KCl) was used as the reference electrode (RE).

Two different PB electrodeposition procedures were performed and compared, namely potentiostatic and galvanostatic electrodeposition. Potentiostatic electrodeposition was based on previous publications.[6,7] Briefly, a solution containing equimolar concentrations of $K_3[Fe(CN)_6]$ and $FeCl_3$ (10 mM) in 1 M HCl was prepared and immediately electrodeposited at a constant potential of 0.4 V *vs.* Ag/AgCl (3M KCl). Electrodeposition times between 20 and 120 seconds were evaluated.

In the galvanostatic electrodeposition, the previous solution was electrodeposited but this time at a constant charge of 40 µA cm^{-2} (24 µA, when considering the active area of the WE, i.e.

0.6 cm^2). For comparison with potentiostatic electrodeposition, this charge was applied between 20 and 120 seconds.

Between the processes, the solution was agitated under constant stirring to ensure homogeneous distribution of the components of the precursor reagent among the solution. Once electrodeposited, both potentionstatically and galvanostatically PB-modified ITO-PET electrodes were rinsed with deionized water to remove non-electrodeposited molecules and air-dried before electrochemical studies. Finally, the electrodeposited PB was transformed into its K$^+$-containing PB$_{Sol}$ form[7] in order to improve its stability and homogeneity. To this end, PB-ITO-PET electrodes were incorporated again in the electrochemical cell together with the platinum wire CE and the Ag/AgCl (3M KCl) RE. Ten cyclic voltammetries were then performed in 1 M KCl (pH ≈ 2.5) by scanning the potential between 0.7 and -0.4 V (vs. Ag/AgCl RE) at a scan rate of 20 mV s^{-1} to induce its transformation into PB$_{sol}$. Electrochemical measurements were conducted with the electrochemical workstation μ-Autolab Type III and controlled with the software Nova 2.1.4 (Metrohm Autolab B.V.).
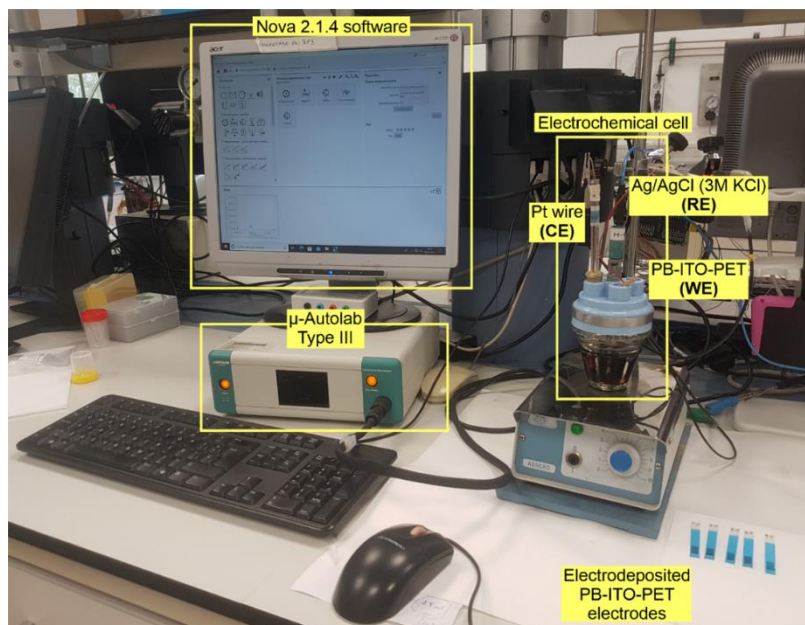
Figure 3.2. Electrochemical set-up used for the PB-NPs electrodeposition on ITO-PET electrodes.

3.3.2 Sonochemical coating on polyester-cotton textiles of PB and CuO-NPs

PB and CuO-NPs were deposited on polyester-cotton textiles using the sonochemical coating processes described below.

For the PB-NPs coating, polyester-cotton fabrics (KLOPMAN, Italy) from industrial production of hospital pyjamas were used as model hospital textiles. The sonochemical coating process is illustrated in Figure 3.3 and employed an ultrasonic transducer (Ti-horn, 20 kHz, 750 W, Sonics and Materials CV334, USA). The power (21.5 W) and intensity (0.43 W/ cm^3) were determined calorimetrically by measuring the temperature increase in the ultrasonic vessel, as reported previously.[8]

Polyester-cotton fragments (3 × 3 cm; approx. 0.18 g each) were immersed in the ultrasonic pot already containing 50 mL of the PB-NPs aqueous suspension. In the optimization of the sonochemical coating process, PB (of both soluble and insoluble forms) at concentrations from 0.03 to 0.3 mM and sonication times of 5, 15 and 30 min were evaluated at a temperature of 20 °C keeping the amplitude of the ultrasonic probe at a 35 %. This amplitude was high enough to provide textiles with a homogeneous distribution of NPs, resulting in color homogeneity, but without compromising the integrity of the textile. Higher amplitudes were observed to produce textile damage.
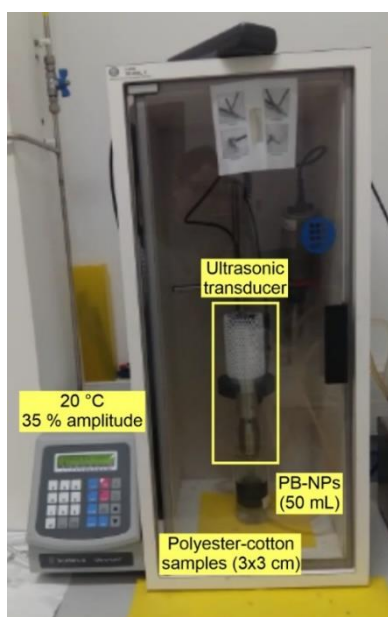
Figure 3.3. Set-up used for the sonochemical coating of the polyester-cotton textiles with PB.

Besides the PB-NPs coating, some fabric samples were previously sonochemically coated with antibacterial CuO-NPs in order to endow the textiles with both bacterial-sensing capacity and antimicrobial activity.

This antibacterial coating was performed in Klopman Int. SRL (Italy) with an industrial sonochemical coating machine designed under the EU-funded project PROTECT, using the following protocol. A 0.01 M copper acetate water solution was introduced in the ultrasonic reactor (0.2 g copper acetate for each 100 mL reaction volume). Polyester-cotton fabric sample (50 cm width, 5 meter length) was immersed in that solution and the sonicator was turned on (90 % amplitude) until the temperature reached 60 ⁰C (5-7 min). Then, ammonia was added dropwise until pH 8. The initial color of the solution was blue and it turned to brown after ammonia addition. The sonochemical process resulted in homogeneous and highly colored textile samples.

3.3.3 PB coating on polyester-cotton textiles and filters by cyanotyping process

In addition to the sonochemical coating process, PB-NPs were also introduced on polyester-cotton textiles and water-treatment filters using cyanotype-based technology.

For that purpose, the following solutions were prepared, following the protocol detailed in:[9] i) 25 grams of ferric ammonium citrate diluted in 100 mL of water and ii) 10 grams of potassium ferricyanide diluted in 100 mL of water. Equal amounts of each solution were mixed, always in this order, and the process was performed in the dark or in very low light to avoid photo-chemical reaction. The substrates under study were then immersed in the precursor solution and then left to dry in an induction oven (Model FD-53, Binder, DE) at 40 ⁰C for 30 minutes, and in the dark. Three types of substrates were employed, namely (i) polyester-cotton fabrics, (ii) nitrocellulose (NC) filters with 0,2 μm pore size and (iii) mixed cellulose ester (MCE) filters with 0,22 μm and 0,45 μm pore size. After drying, all substrates presented a yellowish coloration by the adsorption of iron-based molecules. Samples were then irradiated at a wavelength of 365 nm with an UV light supplying a power density 52 mW cm^{-2} (UV lamp Dymax Model 5000 UV Flood). Several irradiation times between 10 and 120 seconds were evaluated to optimize cyanotyping. After irradiation, filters were revealed by immersion in an acidified water solution, producing the almost immediate

appearance of an intense blue color associated to PB formation. The samples were kept in the solution during 10-15 min to remove all the impurities and stored at room temperature.

A scheme of the cyanotype-based synthesis is illustrated in Figure 3.4, taking the modification of the filters as example. Textiles modification protocol was completely analogous to it.
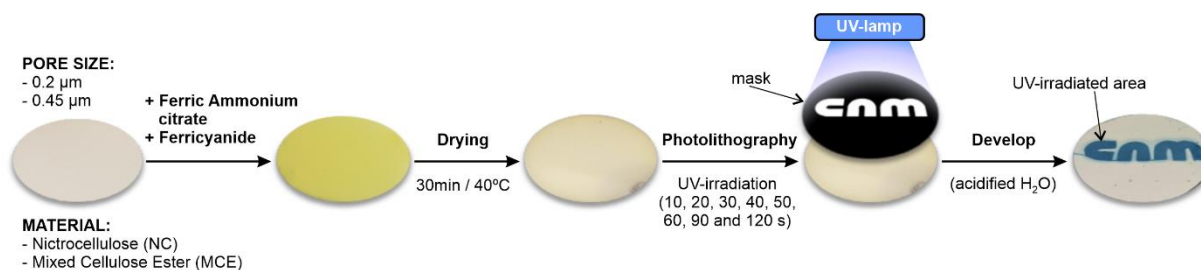

Figure 3.4. Scheme of the cyanotyping process followed for the modification of the filters with PB-NPs.

3.3.3.1 Optimization of the cyanotype process in NC filters

Filters of different composition, i.e. MCE and NC, and pore size, i.e. 0.22 and 0.45 µm, were coated using the cyanotype process described above. The UV irradiation time was optimized by analyzing the range between 10 and 90 s of UV irradiation. Reflectance measurements were performed after irradiation and developing, in order to study the homogeneity and color intensity of the PB-modified samples. Reflectance measurements were performed with a reflection/backscatter probe (QR600-7-SR125BX, Ocean Insights) simultaneously connected to the light source (DH-200-BAL, Mikropack GmbH, Ocean Optics, Largo, FL, USA) as well as to an external spectrophotometer (WE6500; Ocean Optics, Largo, FL, USA). The following experimental conditions were used for the experiment: wavelength range between 420 and 910 nm and integration time of 250 ms. The absorbance spectrum was obtained in five different points of the modified filters in both surfaces, i.e., the front and the backsides, which enabled to evaluate light penetration in the material.

3.3.4 Intermatrix Synthesis of Ag-NPs on nitrocellulose filters

As commented in the Introduction chapter, the Intermatrix Synthesis (IMS) allows in-situ production and stabilization of metal/metal oxide NPs on polymeric substrates containing accessible functional groups. The IMS protocol involves the exchange of the counter ions of the accessible functional groups in the substrate by ionic precursors of the NPs of interest, e.g. Ag^+ in the case of Ag-NPs. Next, the ionic precursors are reduced with a chemical reducing agent, resulting in the in situ formation of the NPs in the polymeric substrate.

In this case, Ag-NPs were produce in situ on NC filters by following the IMS protocol detailed in [10,11], aiming to confer them antimicrobial activity. The IMS protocol involved the immersion of NC filters (25 mm diameter) with a pore size of 0.2 μm in a precursor solution containing $AgNO_3$ in a concentration between 0.4 to 100 mM for 30 minutes. Then, 0.05 M $NaBH_4$ solution was added to the samples for 15 minutes, reducing Ag ions into metallic Ag and producing the adhesion of the Ag-NPs to the NC fibers. Finally, samples were washed with distilled water to remove non-reacted compound and unattached molecules and left to dry at 37 ⁰C for 18 hours.

3.4. Bacterial cultures

Escherichia coli ATCC 25922 (E. coli) and *Staphylococcus aureus (ATCC 29213) (S. aureus)* were used as model Gram-negative and Gram-positive bacteria, respectively. *Pseudomonas putida CAE 95 % Azti 1942 (P. putida)*, *Alteromonas sp. SED-606 (Alteromonas)* and *Vibrio SED-513 (Vibrio)* were also employed in the case of filters for being some of the most common bacterial strains present in water samples [12–14].

E. coli and *S. aureus* were grown aerobically in a Luria-Bertani (LB) broth overnight (18 h) at 37 °C under constant shaking (Infors CH-4103 Bottingen). After centrifugation (5804 R Eppendorf centrifuge, Germany) at 2700xg for 10 min, the supernatant was removed and the pellet was re-suspended in different media depending on the experiment, namely: MH medium, 0.1 M MES (pH adjusted to 6.2 in both cases with 1 M HCl), phosphate buffer (pH 7.2) or water.

Conversely, *P. putida*, *Alteromonas* and *Vibrio* were incubated aerobically in a Zobell Marine broth overnight (18 h) at 25 °C under constant shaking. Then, the same process as described above was followed, re-suspending the pellet in water.

The bacterial concentration was initially determined spectroscopically by measuring the optical density at 600 nm of the suspension with a Smartspec Plus spectrometer (Bio-rad, California, US) and adjusting it between 0.16 – 0.17 A.U., which corresponded to a concentration of around 10^8 CFU mL^{-1}. The real bacterial concentration of the suspension was determined by cell culturing in either LB (for *E. coli* and *S. aureus*) or Zobell Marine Agar plates (for *P. putida*, *Alteromonas* and *Vibrio*), and counting.

3.5 Electrochromic Properties of PB Materials

Spectroelectrochemistry was used to study the electrochromic capacity of free PB-NPs in suspension and after coating polyester-cotton fabrics and ITO-PET electrodes. In the case of PB$_{Sol}$-NPs suspensions, the position and intensity of the redox potential peaks, their reversibility and stability were evaluated by using the spectroelectrochemical cell showed in Figure 3.5. The cell combined an electrochemical cell and a spectroscopic cuvette, which implemented in a single structure. The electrochemical cell was composed by a three-electrode configuration, with (i) a platinum mesh WE to avoid the physical adsorption of colloidal PB on the electrode surface, (ii) a platinum wire CE and (iii) an Ag/AgCl (3M KCl) RE. The spectroscopic cuvette integrated in the previous one consisted of a thin layer quartz glass with two different optical paths (BAS Inc). In this case, a 0.5 mm optical path cuvette was employed to analyze PB$_{Sol}$ samples in suspension. To perform the measurements, the cuvette was introduced in a holder from Ocean Optics coupled with optical fibers while the electrodes were connected to the potentiostat. Electrochemical measures were conducted by applying CVs at 20 mV s^{-1} from -0.25 to 0.5 V to a PB$_{Sol}$ suspension of 1 mM in 0.1 KCl and 0.1 M oxalic acid medium. In addition, the reduction of PB to PW was obtained by applying -0.5 V for 2 min in the same previous conditions.
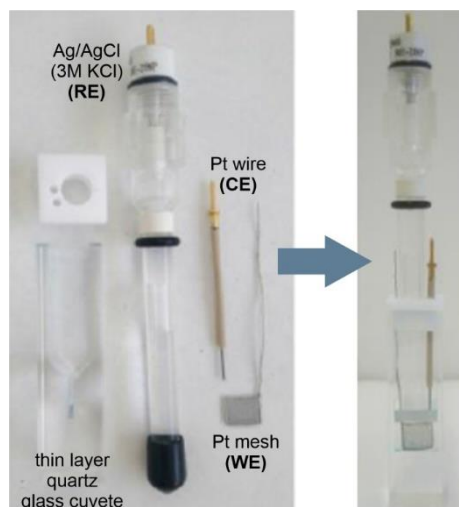
Figure 3.5. Three-electrode spectroelectrochemical cell used for the PB-NPs study in suspension.

On the other hand, the sandwich configuration illustrated in Figure 3.6a was employed to study the electrochromic behavior of PB-NPs deposited on polyester-cotton fabrics. This configuration allowed the study of the electrochemical properties of solid materials without the need for using solvents. In the sandwich configuration (Figure 3.6b), platinum electrodes were located in front of the PB-coated textiles, with a solid hydrogel electrolyte layer in between, i.e. 2-hydroxyethyl cellulose. The working electrode was the Pt mesh used in the previous experiment. Cellulose-based electrolytes were prepared by dissolving 2-hydroxyethyl cellulose (380 kDa) in 1 M KCl to a final concentration of 6.5% (w/v). Reagents were mixed under magnetic stirring, increasing the temperature until boiling. The solution was then left to dry at room temperature and then implemented in the sandwich. Electrochemical measurements were conducted by CVs developed between 0.4 and -0.3 V at different scan rates (1, 5, 10 and 20 mV s^{-1}). Furthermore, an electrolysis was conducted on fresh and old prepared samples by applying -0.5 V during 15 min. Spectrochemical measures were coordinated by using a trigger and developed at a wavelength range between 420 and 910 nm with an integration time of 200 ms.
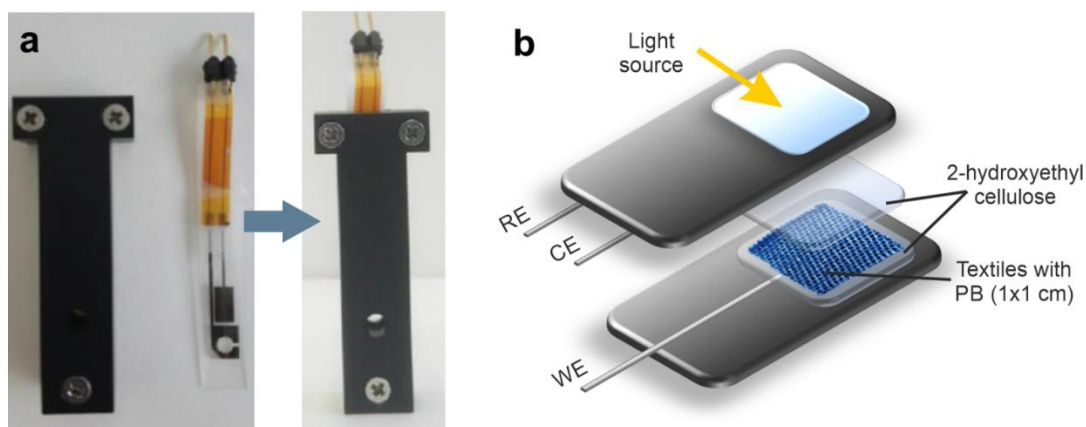
Figure 3.6. Cell used for the spectroelectrochemical study of the PB-modified textiles. a) Picture of the spectroelectrochemical cell. b) Scheme of the assembly of the spectroelectrochemical cell, PB-modified textiles and the solid hydrogel electrolyte.

In the case of PB-ITO-PET electrodes, spectroscopic and electrochemical analysis were conducted sequentially, and not simultaneously as in the previous cases, by using the set-up illustrated in Figure 3.7. This set-up was composed by a holder to introduce the spectrochemical cuvette coupled with optical fibers, which were connected to the light source and to an external spectrophotometer. Spectrochemical measurements were controlled by Ocean View software. These measures were combined with the electrochemical ones, conducted with the electrochemical workstation µ-Autolab Type III and controlled with the software Nova 2.1.4. Electrochemical measurements were performed in the same three-electrode electrochemical cell used for the electrodeposition of the ITO-PET electrodes.

Experimentally, on the already electrodeposited PB-ITO-PET electrodes (see section 3.3.1), spectroelectrochemical and electrochemical measurements were conducted at different times (0, 1, 5, 10 and 24 h) of incubation with *E. coli* bacterial suspensions of 10^8 CFU mL^{-1} to study the electrochromic reduction of the electrodeposited PB layer produced by bacteria.

Spectrochemical measurements were performed first, by introducing the quartz cuvette containing the PB-modified electrodes in MH (pH 6.2) medium into an Ocean Optics holder that ensured a fixed position for the optical fibers and avoided the interference of the incident light during the measurement. Absorbance measurements were then performed in the wavelength

76

range between 420 and 910 nm, with an integration time of 200 ms. As a control, electrodes were submerged in MH medium and the absorbance was measured after 24 h of incubation.

Immediately thereafter, electrodes were introduced in the electrochemical cell containing 25 mL of MH and measured chronoamperometrically by applying a constant potential of 0.6 V vs. Ag/AgCl (3M KCl) for 80 s. ITO-PET electrodes in MH without any treatment were used as controls. All the measurements were carried out at room temperature.
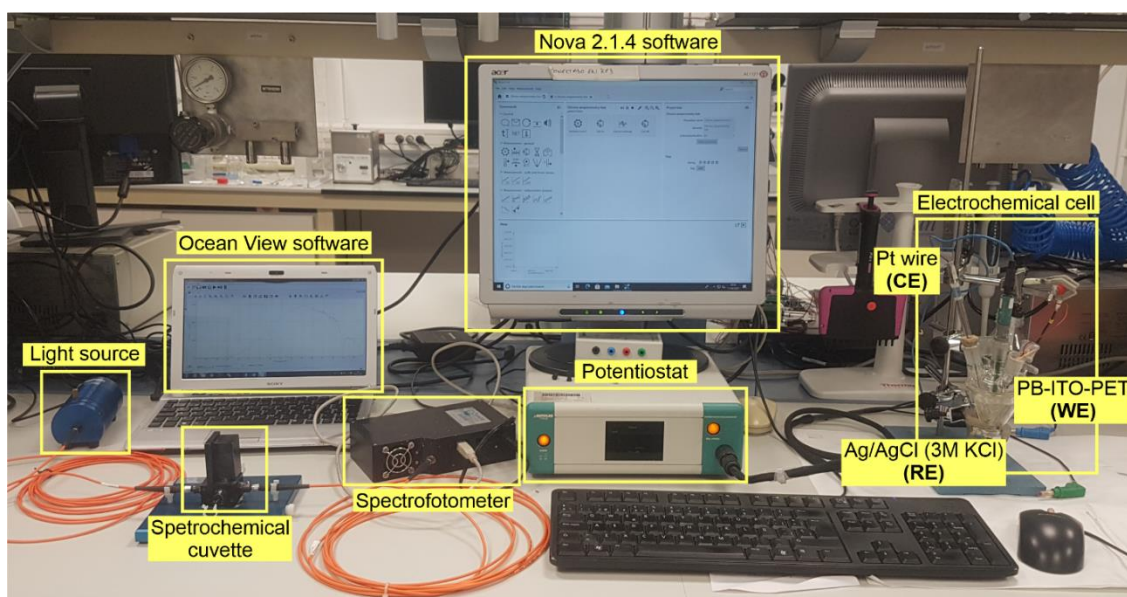

Figure 3.7. Experimental set-up used for electrochemical and spectrochemical measurements on PB-ITO-PET electrodes.

3.6 Bacterial Sensing Activity of PB Materials

The evaluation of the bacterial sensing capacity of the PB-based materials and NPs suspensions has been one of the main objectives of the current thesis. For this reason, a number of techniques and protocols have been employed, which detailed below. It is important to remark that the protocols detailed below were applied to both PB-based materials and materials containing PB and antimicrobials NPs.

3.6.1 PB-NPs suspensions

The bacterial-sensing capacity of PB-NP suspensions, either in their soluble or insoluble forms was evaluated spectroscopically. Absorbance measurements of PB-NP suspensions were performed in 96-well plates using the Thermo Electron Multiskan EX plate reader (VWR International, Pennsylvania, US) and Ascent software (VWR International, Pennsylvania, US) for data recording. PB and bacterial solutions were freshly prepared every day. Their concentrations were adjusted to the magnitudes detailed in each experiment and mixed in MH medium just before starting the experiment. Absorbance spectra in the wavelength range between 400 and 900 nm were acquired every hour for the duration of the experiment, obtaining three replicates for each condition. In PB data analysis, the contribution of bacterial scattering was subtracted from absorbance spectra to simplify results interpretation. Spectrum lines were additionally smoothed by using the Savitzky-Golay algorithm to remove background noise.

The capacity of PB-ITO-PET electrodes to respond to bacteria was evaluated electrochemical and spectroscopically. PB-ITO-PET electrodes were incubated in 10^8 CFU mL^{-1} *E. coli* suspensions in MH medium (pH = 6.2) for either 0, 1, 5, 10 or 24 h at 37 °C. After the incubation, the electrodes were implemented into the setup presented in Figure 3.7 and the metabolic transformation of PB to PW was evaluated chronoamperometrically and by absorbance analysis. Chronoamperometrically, a potential of 0.6 V vs. (Ag/AgCl RE) was applied to the PB-ITO-PET electrode for 80 seconds, which corresponded to the reduction potential of PW. The current generated and the charge, this understood as the area under the current vs. potential curve, was determined and used to study bacterial reduction. In parallel, the change in the absorbance magnitude at 680-720 nm, which corresponded to the maximum absorption of PB, was determined as also used to evaluate bacterial reduction and thus, the capacity of these electrodes to sense bacteria.

3.6.2 PB-modified textiles

The bacterial-sensing activity of PB-modified polyester-cotton textiles containing either PB alone or PB/antimicrobial-NPs was evaluated by image acquisition after immersion of the samples into bacterial suspensions. Samples were always analyzed during the first 15 days of preparation to ensure repeatability of the results. In all cases, color changes were monitored in real time with a digital microscope camera DigiMicro 2.0 Scale. Images were taken every 10 minutes and analyzed using the freeware *ImageJ*. The three RGB channels were separated choosing the red one for quantification since it was the most sensitive. The percentage of color lost was calculated by comparison with the initial color of the unmodified sample.

Textiles samples were analyzed in wet and dry conditions. In the first case, 1×1 cm modified samples (approx. 0.02 g) were immersed in bacterial suspensions containing 10^5 to 10^9 CFU mL^{-1}. The effect of different solutions/buffers on the bacterial sensing capacity of the textiles was evaluated first. Water, LB, 0.1 M PBS at pH 6.2, 0.1 M PBS at pH 7.2, and 0.1 M MES buffer (pH 6.2) supplemented with 0.1 % glucose, to ensure bacterial metabolism, were incubated with the samples for 4 days and continuously monitored. In a second study, samples containing PB-NPs, CuO-NPs or both NPs were incubated with *E. coli* suspensions containing a concentration of 10^9, 10^8 and 10^7 CFU mL^{-1} either in MES medium (pH 6.2) or in phosphate buffer (pH 7.2), both supplemented with 0.1 % of glucose. The incubation process lasted 9 days, refreshing the bacterial suspension every 72 h of incubation to guarantee the presence of living microorganisms in the medium.

On the other hand, cyanotype-based modified textiles were also analyzed in dry conditions by incorporating 1 x 1 cm samples in plate dishes containing LB medium with agar. Different *E. coli* suspensions were prepared (from 10^2 to 10^8 CFU mL^{-1}) in MH medium at pH 6.2 and 100 µL aliquots were added to different areas of the textile samples. As control, MH medium with no bacteria was also tested. The experiment was performed into an oven (Conterm, P. Selecta) at a constant temperature of 37 °C.

3.6.3 PB-modified filters

The bacterial-sensing activity of the PB-modified filters with and without antibacterial Ag-NPs was evaluated by measuring the color change of the filters at different experimental conditions, i.e. UV irradiation times between 30 and 120 s, the filters material and the pore size. For that purpose, 10 mL of *E. coli* suspensions containing 10^7 CFU mL^{-1} in MH medium (pH 6.2) were passed through modified filters, either NC (pore size = 0.2 μm) or MCE ones (pore size = 0.22 or 0.45 μm), using a holder that allowed the filtration of the samples. After filtration, the activity of the bacteria retained on the filters was evaluated by immersing them into 2 mL of MH broth medium. During the incubation, the color change was monitored for 50 h using a micro camera. Modified filters without bacteria were used as control. The experiment was repeated three times to study the repeatability of the assay. Once the optimal conditions were selected, the color change of the filters was tested with different concentrations of bacteria in the range between 10^2 - 10^7 CFU mL^{-1} in MH (pH 6.2) by following the previous protocol.

3.7 Confocal microscopy

Confocal images of the smart textiles and filters were used to evaluate the number of live and dead bacteria attached to the sample, and thus their contact killing capacity. To this end, smart samples were incubated with *E. coli* suspensions containing 10^9 CFU mL^{-1} at 37 °C for 72 hours. After that, the samples were rinsed with distilled water and stained with the Live/Dead BacLight Bacterial Viability Kit (Invitrogen), as detailed by the supplier. Concretely, 1.5 μL of 3.34 mM SYTO9 and 1.5 μL of 20 mM propidium iodide were diluted with water up to a final volume of 1 mL. After that, 100 μL of the previous Live/Dead staining solution was dispensed on the textile surface and incubated for 30 min. After washing the excess of stain with PBS, confocal images of the smart textiles were taken with a confocal microscope (Leica TCS SP5) at an excitation wavelength of 470 nm. Three-dimensional reconstruction was performed with the *Image J* software, where live bacteria (stained with SYTO9) appeared in green (emission wavelength = 630 nm) and dead bacteria (stained with propidium iodide) emitted in the red region of the visible

spectra (emission wavelength = 530 nm). The percentage of live bacteria was obtained as the average of five different areas of identical surface.

3.8 Bactericide NPs Release Evaluation

The stability of the bactericide NPs on the smart materials (i.e. CuO-NPs polyester-cotton fabrics and Ag-NPs on NC filters) was studied by Inductively-Coupled Plasma – Optical Emission Spectrometry (ICP-OES) with an optical emission spectrometer (Perkin-Elmer, optima 4300DV) and a microwave digestion station (Milestone, Ultrawave). Colony counting assays were also conducted through the protocol detailed in Figure 3.8 to complement the previous ICP-OES assays.

In the case of CuO-modified textiles, samples were submerged in MES medium for 24 h and an aliquot (1 mL) was analysed by ICS-OES to determine Cu^{2+} concentration in Cu^{2+} mg per mL of MES. Simultaneously, a second aliquot of 1.5 mL of the medium was incubated with a bacterial suspension initially containing 10^8 CFU mL^{-1} *E. coli* for 24 h at 37 °C. After incubation, the final bacterial concentration was determined by plating in agar dishes and colony counting. Textiles without antibacterial treatment were used as control samples.
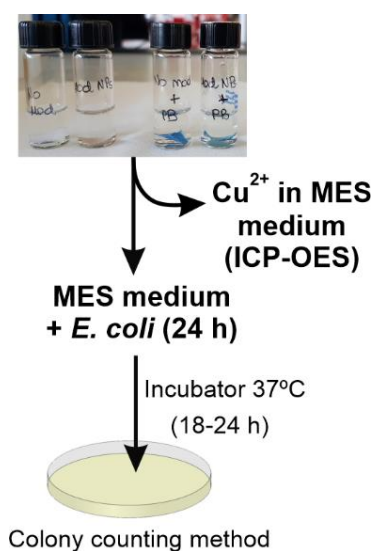
Figure 3.8. CuO-NPs release study. Scheme of the process followed to study the CuO-NPs release to the medium

81

In the case of the NC filters, the ICP-OES, 10 mL of *E. coli* suspensions containing between 10^4 and 10^8 CFU mL^{-1} bacteria in water were filtered using the different samples: NC filters modified with only PB-NPs, with only Ag-NPs and containing both PB and Ag-NPs. Each filter was cut in four parts and incubated in 2 mL of MH medium. Filter samples without bacteria were used as control. The ICP-OES analyses of the medium were performed in duplicate after different incubation times, namely 2, 7, 10 and 28 h.

3.9 Structural and Compositional Studies

This section details the techniques and protocols employed to study the structure and composition changes of the PB-electrodes and the smart materials.

3.9.1 SEM and EDX measurements

The surfaces topology of PB-electrodeposited layer and the smart textiles were studied by Field Emission Scanning Electron Microscopy (FE-SEM) using an AURIGA® series en04 SEM (CarlZeiss) coupled to Oxford Inca Energy Dispersive X-Ray Analysis (EDX).

The smart filters were metalized with Au-NPs previously to their study in the FE-SEM (Carl ZEISS Merlin).

3.9.2 AFM measurements

The layer thickness of the PB-modified electrodes was analyzed by atomic force microscopy (AFM) using a Nanoscope IV Dimension 3100 (Veeco Instruments). Measurements were performed in tapping mode by using a probe (OTESPA-R3) from Bruker.

3.9.3 XAS analysis

X-ray absorption (XAS) spectra at Fe K-edge were measured for the characterization of the smart textiles modified with either PB and/or CuO NPs, employing the CLAESS beamline at the ALBA synchrotron using a Si (311) double crystal monochromator [16]. The harmonic rejection was

achieved by a proper combination of angle and coating of collimating and focusing mirrors. The beam size at the sample position was adjusted to 300 x 300 μm^2. The beamline was calibrated using a Fe foil measured in transmission mode and the energy of the first maximum in the derivative spectrum was taken at 7112 eV. The incident and transmitted intensity were detected by two ionization chambers filled with a mixture of $He/N_2/Kr$. The samples were placed at 45 degrees to the incident beam and measured at room temperature in fluorescence mode. The fluorescence signal (Fe Kα) was detected by a six-channel silicon-drift detector. Data analysis was performed using ATHENA and ARTEMIS software [17].

3.10 Cytotoxicity Tests

PB-NPs cytotoxicity was determined in the human fibroblast cell line MRC-5 (ATCC Line Bank, Virginia, USA) by using the colorimetric MTT (3-(4,5-dimethylthiazol-2-yl)-2,5-diphenyltetrazolium bromide) assay. The protocol was based on a previous publication [18]. Concretely, MRC-5 cells were cultured in complete Dulbecco's Modified Eagle's Medium (DMEM, supplemented with 10% foetal bovine serum, 1% penicillin/ streptomycin solution). When confluent, cells were exposed to different concentrations of PB_{Sol} and PB_{Ins}. After 24 h of incubation, wells were washed with PBS, and the MTT solution (5 mg mL^{-1}) was added and incubated for 1 h (37 °C, 5% CO_2). After washing with PBS, the purple formazan generated by MTT metabolism of viable cells was solubilized with DMSO. The optical density of each well was determined at 570 nm in a spectrophotometer reader (BioTek® Synergy HT, Vermont, USA). Cell viability was expressed as percentage in relation to non-treated cells.

3.11 References

(1)   Ricci, F.; Palleschi, G. Sensor and Biosensor Preparation, Optimisation and Applications of Prussian Blue Modified Electrodes. *Biosens. Bioelectron.* **2005**, *21* (3), 389–407. https://doi.org/10.1016/j.bios.2004.12.001.

(2)   Ellis, D.; Eckhoff, M.; Neff, V. D. Electrochromism in the Mixed-Valence Hexacyanides. 1. Voltammetric and Spectral Studies of the Oxidation and Reduction of Thin Films of Prussian Blue. *J. Phys. Chem.* **1981**, *85* (9), 1225–1231. https://doi.org/10.1021/j150609a026.

(3)   Karyakin, A. A. Prussian Blue and Its Analogues: Electrochemistry and Analytical Applications. *Electroanalysis* **2001**, *13* (10), 813–819. https://doi.org/https://doi.org/10.1002/1521-4109(200106)13:10<813::AID-ELAN813>3.0.CO;2-Z.

(4)   Davidson, D.; Welo, L. A. The Nature of Prussian Blue. *J. Phys. Chem.* **1928**, *32* (8), 1191–1196. https://doi.org/10.1021/j150290a007.

(5)   Gervais, C.; Languille, M. A.; Reguer, S.; Garnier, C.; Gillet, M. Light and Anoxia Fading of Prussian Blue Dyed Textiles. *Herit. Sci.* **2014**, *2* (1). https://doi.org/10.1186/s40494-014-0026-x.

(6)   Pellitero, M. A.; Guimerà, A.; Kitsara, M.; Villa, R.; Rubio, C.; Lakard, B.; Doche, M. L.; Hihn, J. Y.; Del Campo, F. J. Quantitative Self-Powered Electrochromic Biosensors. *Chem. Sci.* **2017**, *8* (3), 1995–2002. https://doi.org/10.1039/c6sc04469g.

(7)   Garcia-Jareno, J. J.; Benito, D.; Navarro-Laboulais, J.; Vicente, F. Electrochemical Behavior of Electrodeposited Prussian Blue Films on ITO Electrode: An Attractive Laboratory Experience. *J. Chem. Educ.* **1998**, *75* (7), 881. https://doi.org/10.1021/ed075p881.

(8)   Petkova, P.; Francesko, A.; Fernandes, M. M.; Mendoza, E.; Perelshtein, I.; Gedanken, A.; Tzanov, T. Sonochemical Coating of Textiles with Hybrid ZnO/Chitosan Antimicrobial Nanoparticles. *ACS Appl. Mater. Interfaces* **2014**, *6* (2), 1164–1172. https://doi.org/10.1021/am404852d.

(9)   Farber, R. *Historic Photographic Processes*; 1998. https://doi.org/10.1017/CBO9781107415324.004.

(10)   Domènech, B.; Muñoz, M.; Muraviev, D. N.; Macanás, J. Polymer-Silver Nanocomposites as Antibacterial Materials. *Microb. Pathog. Strateg. Combat. them Sci. Technol. Educ.* **2013**, *1* (December), 630–640.

(11)   Muraviev, D. N.; Macanás, J.; Parrondo, J.; Muñoz, M.; Alonso, A.; Alegret, S.; Ortueta, M.; Mijangos, F. Cation-Exchange Membrane as Nanoreactor: Intermatrix Synthesis of Platinum-Copper Core-Shell Nanoparticles. *React. Funct. Polym.* **2007**, *67*, 1612–1621. https://doi.org/10.1016/j.reactfunctpolym.2007.07.052.

(12)   Kouremenos, K. A.; Beale, D. J.; Antti, H.; Palombo, E. A. Liquid Chromatography Time of

Flight Mass Spectrometry Based Environmental Metabolomics for the Analysis of Pseudomonas Putida Bacteria in Potable Water. *J. Chromatogr. B* **2014**, *966*, 179–186. https://doi.org/10.1016/j.jchromb.2014.02.058.

(13)   Access, O. Water Microbiology. Bacterial Pathogens and Water. *Int. J. Environ. Res. Public Health* **2010**, 3657–3703. https://doi.org/10.3390/ijerph7103657.

(14)   Chen, Z.; Li, Z.; Liu, P.; Liu, Y.; Wang, Y.; Li, Q.; He, N. Characterization of a Novel Bioflocculant from a Marine Bacterium and Its Application in Dye Wastewater Treatment. *BMC Biotechnol.* **2017**, *17* (84), 1–11. https://doi.org/10.1186/s12896-017-0404-z.

(15)   Ezenarro, J. J.; Uria, N.; Castillo-fernández, Ó.; Párraga, N. Development of an Integrated Method of Concentration and Immunodetection of Bacteria. *Anal. Bioanal. Chem.* **2017**, *410* (1), 105–113.

(16)   Simonelli, L.; Marini, C.; Olszewski, W.; Ávila Pérez, M.; Ramanan, N.; Guilera, G.; Cuartero, V.; Klementiev, K. CLAESS: The Hard X-Ray Absorption Beamline of the ALBA CELLS Synchrotron. *Cogent Phys.* **2016**, *3* (1), 1231987. https://doi.org/10.1080/23311940.2016.1231987.

(17)   Ravel, B.; Newville, M. ATHENA, ARTEMIS, HEPHAESTUS: Data Analysis for X-Ray Absorption Spectroscopy Using IFEFFIT. *J. Synchrotron Radiat.* **2005**, *12* (4), 537–541. https://doi.org/10.1107/S0909049505012719.

(18)   Alonso, A.; Muñoz-Berbel, X.; Vigués, N.; Rodríguez-Rodríguez, R.; MacAnás, J.; Muñoz, M.; Mas, J.; Muraviev, D. N. Superparamagnetic Ag@Co-Nanocomposites on Granulated Cation Exchange Polymeric Matrices with Enhanced Antibacterial Activity for the Environmentally Safe Purification of Water. *Adv. Funct. Mater.* **2013**, *23* (19), 2450–2458. https://doi.org/10.1002/adfm.201202663.

4

Results and Discussion

4.1

Soluble and Insoluble PB-NPs for Electrochromogenic Bacterial-Sensing

Abstract

Among the techniques developed for bacterial detection, those based on metabolic indicators are progressively gaining interest due to their simplicity, adaptability, and, most importantly, their capacity to differentiate between live and dead bacteria. PB may act as a metabolic indicator, being reduced by bacterial metabolism, producing a visible color change from blue to colorless. This molecule can be present in two main forms, namely, the soluble and the insoluble, having different properties and structures. In the current chapter, the bacterial-sensing capacity of soluble and insoluble PB will be tested and compared both in suspensions as PB-NPs and after deposition on transparent ITO-PET electrodes. In the presence of live bacteria, both soluble and insoluble PB forms are metabolized and completely reduced to the PW state in less than 10 h. However, when electrodeposited on ITO-PET electrodes, bacterial reduction of PB is detected in less than 1 h, being the soluble PB form the one presenting the fastest metabolic reduction kinetics. This study paves the way to the use of PB as a metabolic indicator for the early detection of bacterial infection in fields like microbial diagnostics, surface sterilization, food and beverage contamination, and environmental pollution, among others.
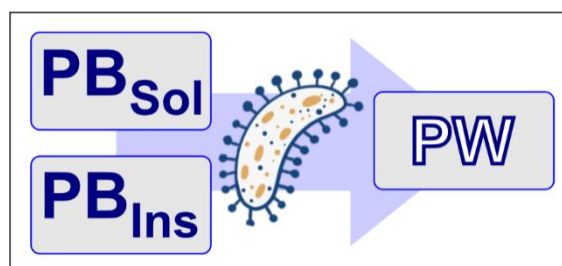
This chapter contains results previously published in:

Congresses:

Oral presentation entitled "**Smart Sensing Electrochromic Textiles for Live Bacteria Detection**", presented at the **XXXIX Reunión del Grupo de Electroquímica de la Real Sociedad Española de Química & 3rd E3 Mediterranean Symposium.** University Complutense of Madrid. 2018.

Journals:

Electrochromogenic Detection of Live Bacteria Using Soluble and Insoluble Prussian Blue. Amparo Ferrer-Vilanova, Yasmine Alonso, Josune J. Ezenarro, Sara Santiago, Xavier Muñoz-Berbel and Gonzalo Guirado. *ACS Omega*. 2021, 6, 30989-30997.

This chapter contains results related to these publications:

Bacterial-sensing platform based on iSIMPLE system. Amparo Ferrer-Vilanova, Wannes Verbist, Francesco Dal Dosso, Jeroen Lammertyn and Xavier Muñoz-Berbel. (Article to be submitted).

Ultrasensitive bacterial biosensing using a disposable all-in-one amperometric platform with self-noise cancellation. Joan Aymerich, Amparo Ferrer-Vilanova, Jose Cisneros-Fernández, Roger Escudé-Pujol, Gonzalo Guirado, Lluís Terés, Michele Dei, Xavier Muñoz-Berbel. (Article submitted to *Biosensors and Bioelectronics*).

International academic visit:

This work was partially performed in a **3 months academic visit to the MeBioS group leaded by Prof. Jeroen Lammertyn at the Katholieke Universiteit Leuven (Belgium).**

4.1.1 Selection of the Sensing Probe Based on the Knowhow of the Group

To develop smart materials for bacteria detection, different issues should be taken into account. **First, the detection should be performed in situ**, by the own material, without the need for sample collection and transport to central laboratories. Related to the former, the material should detect bacteria directly and without the need for employing reagents or products that require manipulation or human intervention. This is fundamental in the case of large infrastructures, e.g. hospitals, since the control of the high number of surfaces present there may be virtually impossible.

Second, the material should be sensitive only to live bacteria. Bacteria, due to their high colonization capacity and ability to attach and form complex biological structures such as biofilms, are expected to be almost everywhere. In the case of antimicrobial materials, bacterial presence may be even higher since bacteria in contact with them die and remained attached to their surfaces, acting as a pre-layer that may benefit the attachment of new bacteria. However, dead bacteria are not infective and their detection may result in false positive results. For this reason, all sensing strategies sensitive to bacterial antigens, enzymes and DNA are discarded since they are sensitive to both, live and dead bacteria.

Considering the previous requirements, the sensing methodology used along this thesis will be focused on the use of metabolic indicators directly implemented in the material surface, which directly respond to live bacteria though a color change, without requiring any additional reagent or manipulation. From the myriad of metabolic indicators, those based on electrochromic molecules are selected here for being the only ones directly interacting with proteins/mediators of the ETC. Since these proteins/mediators involved in catabolic processes are quite conservative and present similar redox potentials, metabolic indicators of bacterial metabolism may be considered a general sensing mechanism able to report on the presence of many living Gram-positive or Gram-negative bacteria. Additionally, electrochromic molecules present other properties that make them very attractive in the production of smart materials, such as (i) being able to report on the presence of live bacteria though a simple and intense color change detectable even with the bare eye; (ii) being stable and low cost; (iii) presenting low toxicity; and

(iv) being susceptible of implementation into the end products through simple and scalable coating technologies.

Keeping this in mind, several studies have been conducted in our research group related to the use of electrochromic molecules as metabolic indicators. The first one was developed in the framework of Ferran Pujol's thesis. In this sense, fast and sensitive chromic toxicity bioassays based on the metabolic reduction of ferricyanide when in contact with *E. coli* were developed either, in solution[1] and after ferricyanide entrapment on cellulose-paper discs.[2] In both cases, a color change from yellow to colorless was produced. However, this molecule was discarded in this thesis since ferricyanide color changes are not intense enough to be easily detected with the bare eye. Moreover, the implementation of small ferricyanide particles on polymeric substrates, electrodes or textiles is not simple, and would make the smart textile development very complex.

As a step forward, an electrochromic iron (III)-complexed alginate hydrogel sensitive to bacterial metabolism was developed in a collaboration between Ferran Pujol and Jiri Dietvorst.[3] In this case, bacteria were entrapped into the hydrogel matrix, producing the oxidation of Fe (II) ions to Fe (III) and forming the hydrogel in situ. Then, the mixture was incubated with an antibiotic and after some time, ferricyanide was added. Remaining living bacteria could reduce ferricyanide to ferrocyanide, which reacted to the Fe (III) ions present in the hydrogel producing PB. With this approach, the color change was produced from yellow to blue, which was much more notable than in the previous case.

Improving previous protocol, a new bacterial detection methodology based on the cyanotype method was developed in the framework of Jiri's thesis. The detection of low concentrations of bacteria was achieved with a photocatalytic-based reaction in which iron-based compounds were metabolically reduced in the presence of light, resulting in the formation of PB and a strongly blue colored precipitate.[4] Metabolic activity of live bacteria was detected in 3 h of reaction with a sensitivity close to single bacterium. This fundament was applied for developing a sepsis kit for fast detection of bacteria in whole blood.[5] Thus, viable bacteria was entrapped on filter fibers and incubated with iron compounds with constant illumination. Then, living bacteria reduced part of the Fe (III), producing a blue color on the filters surface due to PB formation.

However, the illumination of the sample required during the process, as well as the manipulation of reagents to complete the assay or the high solubility of ferricyanide, are drawbacks that difficult the implementation of these approaches in textiles or filters for the in situ detection of bacterial infections.

Considering these previous results, alternative sensing molecules should be considered as metabolic indicators to be implemented into textiles and/or filters. For the selection of the most suitable electrochromic molecule, ferricyanide, Presto blue, PB and PB precursors (ferricyanide + iron chloride) were evaluated and compared for being non-toxic, and presenting low reduction potentials that made them susceptible of metabolic reduction. In a preliminary test, *E. coli* and *Staphylococcus aureus* (*S. aureus*) were used as model Gram-negative and Gram-positive bacteria, respectively, to evaluate the suitability of the selected electrochromic molecules. Metabolic indicators were incubated with *E. coli* concentrations from 10 to 10^{10} CFU mL^{-1} at 37 °C. Results after 24 h of incubation are illustrated in Figure 4.1.1.
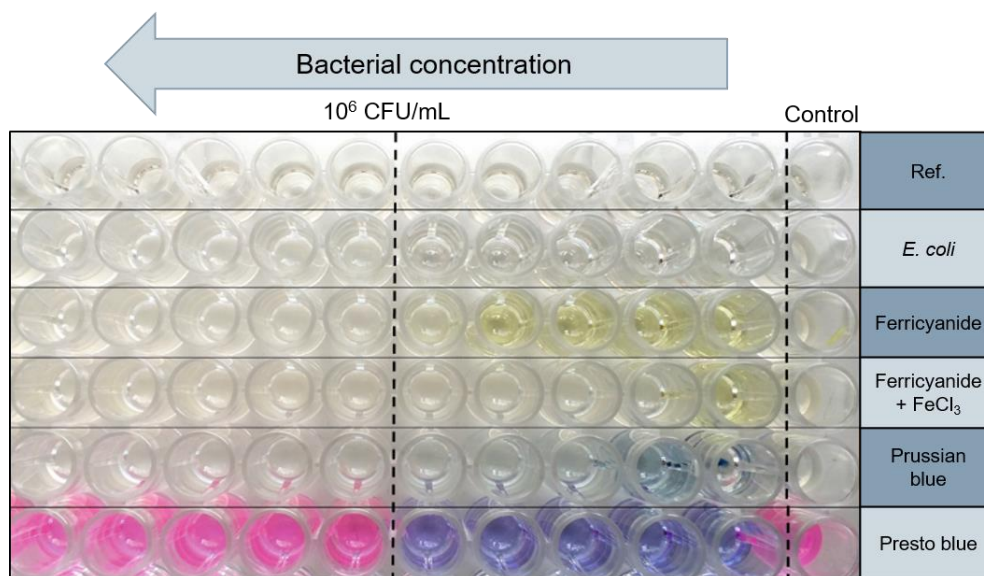
Figure 4.1.1. Initial test for selecting the most suitable electrochromic metabolic indicator. ELISA-plate illustrating the color change of the three electrochromic molecules ferricyanide, Presto blue and PB 24 h after incubation with *E. coli* bacterial suspensions from 10 to 10^{10} CFU mL^{-1}.

Important color changes were observed by bacterial concentrations above 10^6 CFU mL^{-1} in all cases, which associated to bacterial metabolism. Below such concentration, Presto blue samples remained with the same initial color while some slight reduction of colour intensity was

observed in the ferricyanide and PB samples between 10^3 and 10^5 CFU mL^{-1}. PB formation from the precursor solution was not observed in any case. Similar results were obtained after incubation of the electrochromic molecules with *S. aureus*, demonstrating the potential application of the sensing mechanism to these two bacterial families. As commented above, most electrochromic metabolic indicators were soluble molecules, not able to be implemented in the textile. Thus, only PB was considered in future implementation assays since based on insoluble NPs is easy to implement to textiles and filters.

4.1.1.1 Prussian blue

PB is one of the most used and ancient coordination materials known nowadays. It was discovered accidentally by Diesbach in 1704, and since then it has been widely used as pigment in paints, lacquers, printing inks and laundry dyes due to the high intensity and durability of its color [6] (Figure 4.1.2).
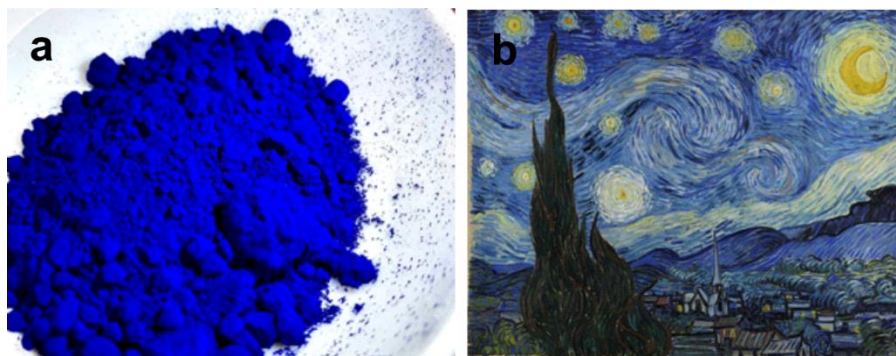
Figure 4.1.2. Prussian blue in pigments and paints. a) Picture showing the intense blue color of a PB pigment. b) Paint made of PB (Starry Night by Vincent Van Gogh, 1889).

PB can be synthesized chemically following two protocols:[7]

(i)   mixing ferric ions and hexacyanoferrate (II) ions: $Fe^{3+} + [Fe^{II}(CN)_6]^{4-}$;

(ii)   mixing ferrous ions and hexacyanoferrate (III) ions: $Fe^{2+} + [Fe^{III}(CN)_6]^{3-}$.

In both cases, an immediate formation of a dark blue colloid is observed.

Ferric hexacyanoferrate or PB complex has a tridimensional polymeric network structure consisting of alternate Fe (II) and Fe (III) located on a face centered lattice in where the Fe (III) ions are surrounded octahedrically by nitrogen atoms and Fe (II) ions by carbon atoms.[6] The remaining

charge is compensated by either potassium or ferric ions. When the charge is compensated by potassium ions, PB is known as "soluble" (PB_{Sol}) and ferric counterions lead to what is called "insoluble" PB (PB_{Ins}). Nevertheless, both compounds are highly insoluble in water and, in fact, these terms refer to how fast PB-NPs are deposited. That is, for PB_{Sol}, the PB-NPs are suspended for long times due to their small size, which results in low deposition kinetics. Conversely, PB_{Ins} contains NP aggregates that tend to precipitate quickly.[8,9] Schemes for the two structures are shown in Figure 4.1.3.[10] Both forms of PB present similar, but not identical, color changes and standard redox potentials.
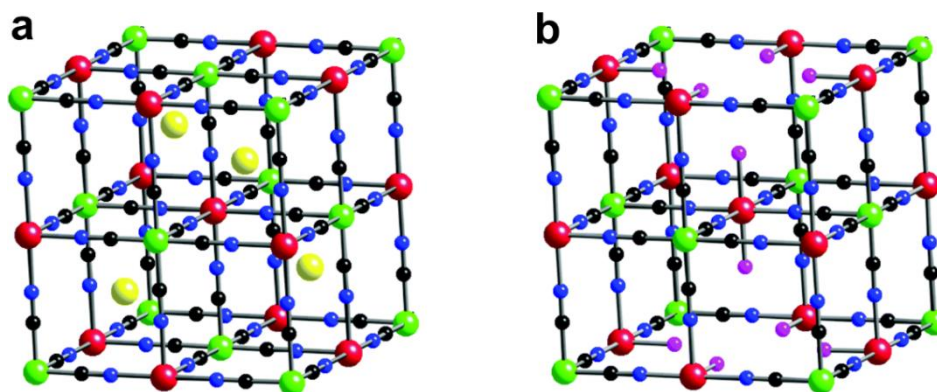
Figure 4.1.3. Structures of the PB forms. a) Structure of PB_{Sol}, with the centers of the cubic cells occupied by K^+ ions. b) Structure of PB_{Ins}, where the coordinative sphere of Fe^{III} is completed by water. Colors of the atoms: Fe^{II} (green), Fe^{III} (red), C (black), N (blue), K (yellow), and H_2O (purple). The figure reproduced from ref [10], with permission from the Royal Society of Chemistry.

Electrochemical and optical properties of PB have also been widely studied. PB presents a deep blue color, connected with an intense charge-transfer absorption band of the compound around 700 nm. When the iron atoms present in PB structure are reduced from Fe (III) to Fe (II), the formation of PW or also known as Everitt's salt is produced, which is colorless. On the contrary, the oxidation of Fe (II) to Fe (III) in the PB complex produces the formation of Berlin green, with a greenish-yellow color and a characteristic absorption band at 420 nm.[11–14]

Due to its multiple and varied properties, PB has proven to be suitable for a wide range of application fields such as energy, biomedicine, biosensing or smart materials. Some examples include the production of alkaline ion ($Li^+/Na^+/K^+$) batteries,[15,16] hydrogen storage,[17] drug

delivery,[18] biomedical imaging,[19] therapeutic hyperthermia,[20] self-powered electrochromic windows[21] or as artificial enzyme peroxidase,[22] among many others.

Therefore, PB has been selected as sensing indicator for the development of this thesis because of its ideal properties, namely:

- A high redox potential, which make it able to interact with proteins and mediators from the ETC.[23] Preliminary results support this statement.[24]

- Simplicity of implementation in textiles and filters, as demonstrated by the fast that it has been used as a traditional textile dye.[25,26]

- High extinction molar coefficient and evident color change after reduction, which visible with naked eye.[27,28]

- Low or null toxicity and biocompatibility, as demonstrated by a number of publications where it is used as redox mediator in biosensors.[6,14,27,29,30]

However, the differences between the soluble and insoluble forms of PB and their influence on its capacity as a bacterial electron acceptor have been poorly studied.

In this chapter, the electrochromic differences of the two PB forms in bacterial detection are extensively studied and discussed both in suspension and when immobilized in electrodes for optical and/or electrochemical transduction.

4.1.2 Study of the electrochromic properties of soluble and insoluble PB-NPs

For a better understanding of the PB bacterial-sensing mechanism, optical and electrochemical properties of both PB_{Sol} and PB_{Ins} were studied. Although both forms of PB were insoluble in most solvents, PB_{Sol} was partially peptized and solubilized in oxalic acid for its analysis.[31] To avoid the physical adsorption of colloidal PB on the electrode surface, a platinum mesh was used as working electrode (WE). In these experimental conditions, 1 mM PB_{Sol} was

measured by cyclic voltammetry (CV) at 20 mV s^{-1} in 0.1 M KCl supplemented with 0.1 M oxalic acid, obtaining repeatable and reliable electrochemical recordings (Figure 4.1.4a).
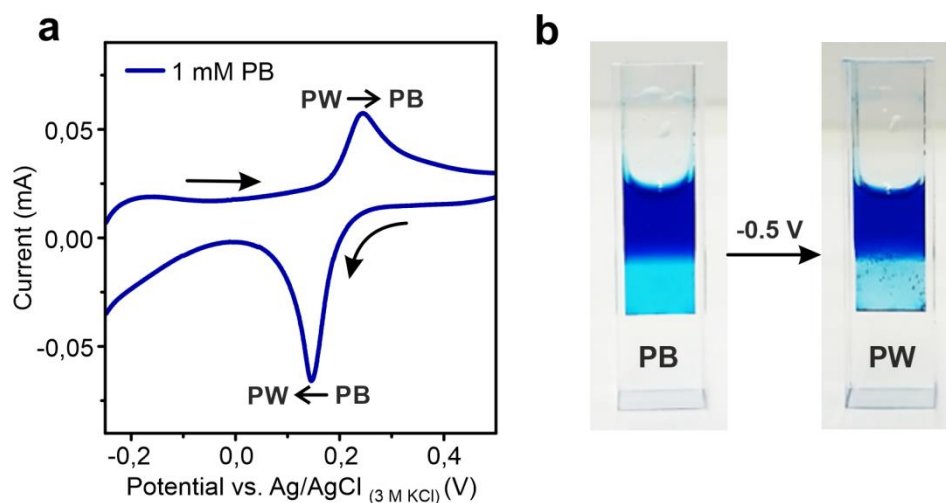
Figure 4.1.4. Electrochemical and optical characterization of PB$_{Sol}$ in suspension. a) CV of an aqueous suspension of 1 mM PB$_{Sol}$ in a 0.1 M KCl and 0.1 M oxalic acid medium at 20 mV s^{-1}. b) Suspension color change obtained after applying -0.5 V for 2 min in the same previous conditions.

In the ETC of *E. coli*, the exchange of electrons is produced between several primary dehydrogenases and terminal reductases, which are linked by three quinones: ubiquinone (E° = 0.1 V vs. NHE), demethyl menaquinone (MQ) (E° = 0.04 V vs. NHE), and MQ (E° = -0.08 V vs. NHE).[32] From Figure 4.1.4a, a standard redox potential of 0.2 V vs. Ag/AgCl (3M KCl) (0.4 V vs. NHE) was obtained, which should be appropriated to oxidize the proteins and mediators involved in the ETC. Even cytochrome d, the most positive component of *E. coli* ECT with a midpoint potential of 0.27 V vs. NHE,[33] should be oxidized by PB-NPs.

To simulate the metabolic reduction of colloidal PB-NPs by bacterial metabolism, a potential of −0.5 V (vs. Ag/AgCl (3 M KCl)) was applied to the NP suspension for 2 min. As shown in Figure 4.1.4b, a lighter color of the suspension was obtained, associated with the PB reduction, where the typical colloidal nature of the PB$_{Sol}$ suspension could also be appreciated with the bare eye.

On the other hand, PB$_{Ins}$ could not be peptized/solubilized with oxalic acid and presented fast sedimentation kinetics that impeded its characterization directly in suspension. For this reason, PB$_{Ins}$ was electrodeposited on conductive and transparent ITO-PET electrodes for electrochemical and optical analysis. Two PB$_{Ins}$ electrodeposition procedures were performed and

compared, namely, potentiostatic (constant potential) and galvanostatic (constant charge). Electrodeposition results are presented in Figure 4.1.5, including (i) images of the electrodeposited electrodes at different electrodeposition times, (ii) scanning electron microscopy (SEM) images of electrodes electrodeposited for 80 s, and (iii) CVs obtained from all electrodeposited electrodes.

The thickness of the electrodeposited layers performed at each electrodeposition time was determined by atomic force microscopy (AFM) and the images are presented in Figure 4.1.6 for the potentiostatic electrodeposition and in Figure 4.1.7 for the galvanostatic electrodeposition.
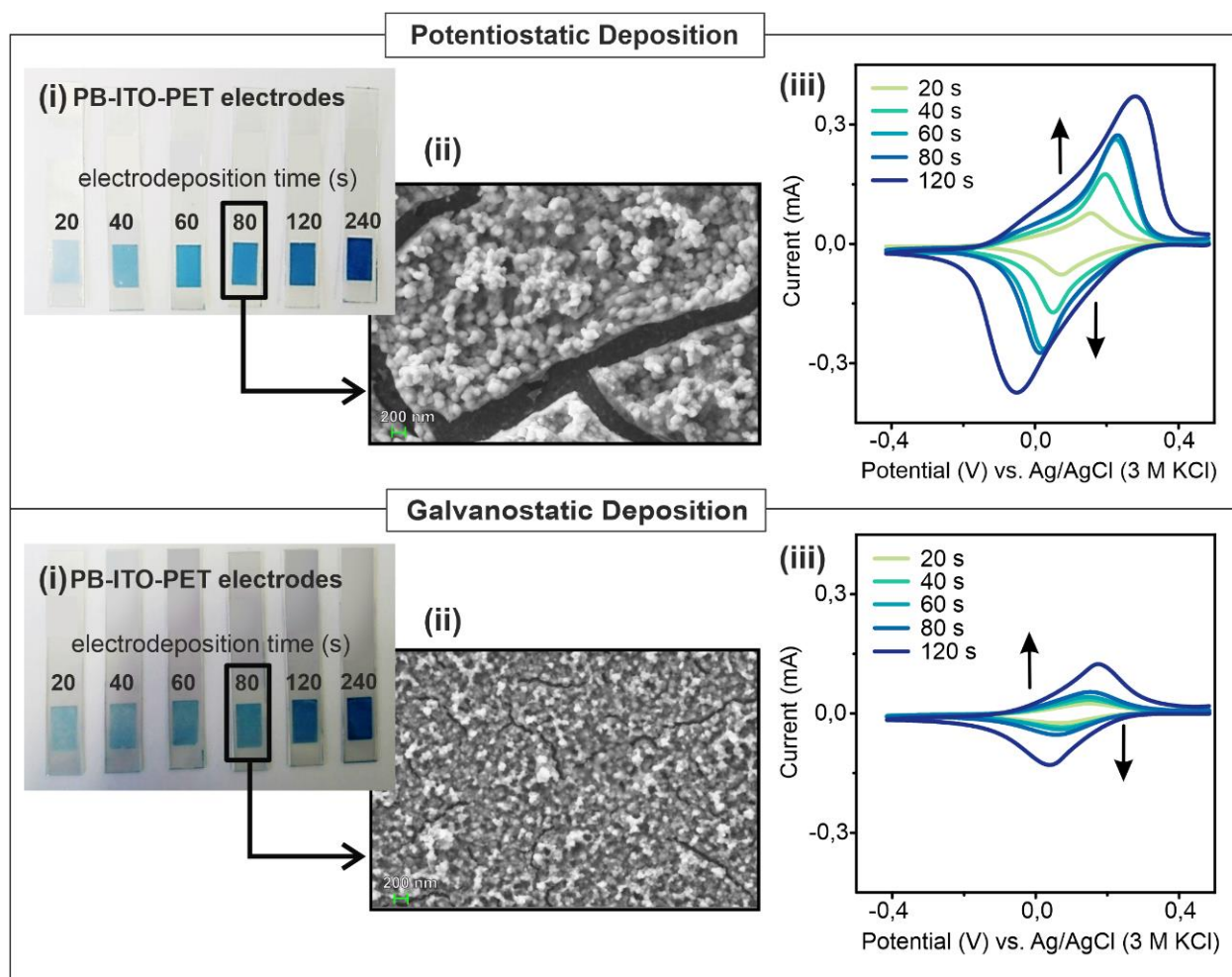
Figure 4.1.5. Comparative scheme for PB_{Ins} electrodeposition on ITO-PET electrodes by potentiostatic and galvanostatic techniques. Different parameters are shown, such as (i) images of the PB-electrodeposited electrodes at different deposition times, (ii) SEM images of PB electrodeposited for 80 s, and (iii) CVs recorded from PB-deposited electrodes.

Figure 4.1.6. AFM images of potentiostatic PB layers. AFM images of PB electrodeposited on ITO-PET electrodes by potentiostatic technique at different electrodeposition times (from 20 to 240 s).
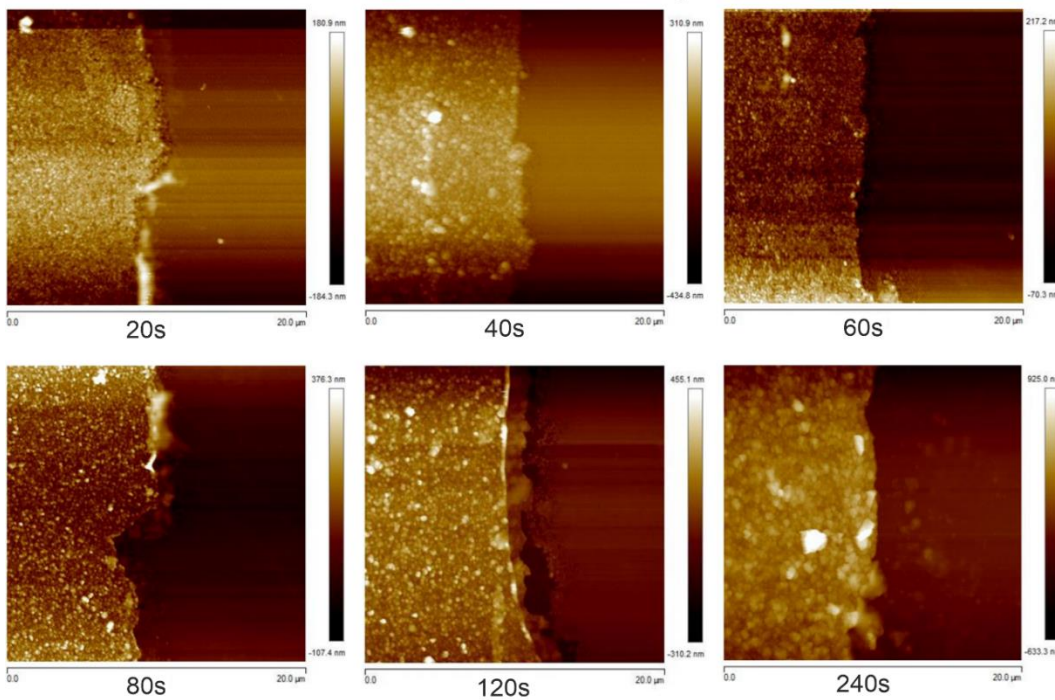
Figure 4.1.7. AFM images of galvanostatic PB layers. AFM images of PB electrodeposited on ITO-PET electrodes by galvanostatic technique at different electrodeposition times (from 20 to 240 s).

With both electrodeposition strategies, longer electrodeposition times produced thicker PB films with deeper color intensities and larger current magnitudes in the CVs. Conversely, peak separation also increased with the electrodeposition time by a reduction of charge transfer capacity when increasing the thickness of the electrodeposited layer. The relationship between the PB-layer thickness and the electrodeposition time is represented in Figure 4.1.8. In both cases, an E° of 0.12 V vs. Ag/AgCl (3M KCl) (0.32 vs. NHE) was obtained. This redox potential value was slightly smaller than the one obtained by the soluble form in suspension, but sufficiently high to react with most of the redox components of the bacterial ETC. Comparing both techniques, potentiostatic electrodeposition provided higher peak and color intensities, which were associated with the formation of larger particles and a thicker PB layer, as observed by SEM (Figure 4.1.5) and AFM (Figure 4.1.6 and Figure 4.1.7).

Considering previous results, 80 s of potentiostatic electrodeposition, which corresponded to a PB layer of around 200 nm (Figure 4.1.8), was chosen as the optimal condition for spectroelectrochemical studies.
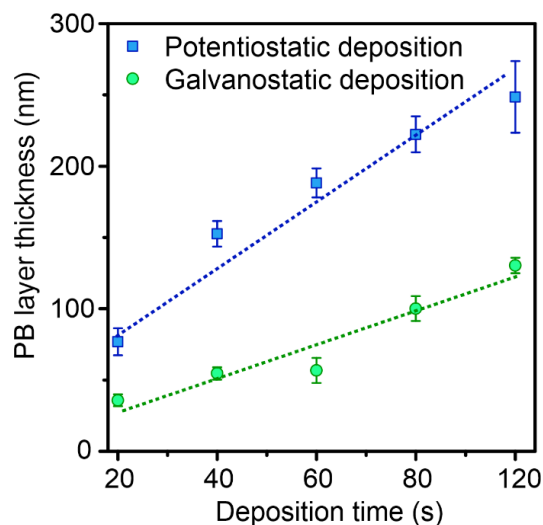
Figure 4.1.8. PB-layer thickness for potentiostatic and galvanostatic electrodeposition techniques. PB-layer thickness measured on all of the modified electrodes by the AFM technique vs. the deposition time (n = 5).

In spectroelectrochemical assays, the electrodeposited electrodes were submerged in the cell containing 1 M KCl, and 10 CVs were registered between 0.7 and -0.4 V (vs. Ag/ AgCl (3M KCl)) at 20 mV s^{-1}. Along the cycles, small differences were observed between the first scan and the other nine. Regarding the standard redox potential value, it was a clear shift of approximately 20 mV (Figure 4.1.9a). The spectroscopic change was more evident, where the PB band initially at 720 nm was shifted to 710 nm, showing a decrease in the absorbance peak value after the development of 10 cycles (Figure 4.1.9b).[34] The shift in the peak potential and absorbance magnitude suggested structural changes in PB along with the reduction to PW and subsequent re-oxidation. The following mechanism was proposed based on previous studies,[35–38] which is illustrated in equations (4.1.1) and (4.1.2):

$$Fe_4^{III}[Fe^{II}(CN)_6]_3 + 4K^+ + 4e^- \rightleftarrows K_4Fe_4^{II}[Fe^{II}(CN)_6]_3 \tag{4.1.1}$$
$$\text{PB}_{\text{Ins}} \qquad\qquad\qquad\qquad\qquad \text{PW}$$

$$KFe^{III}[Fe^{II}(CN)_6] + K^+ + e^- \rightleftarrows K_2Fe^{II}[Fe^{II}(CN)_6] \tag{4.1.2}$$
$$\text{PB}_{\text{Sol}} \qquad\qquad\qquad\qquad \text{PW}$$
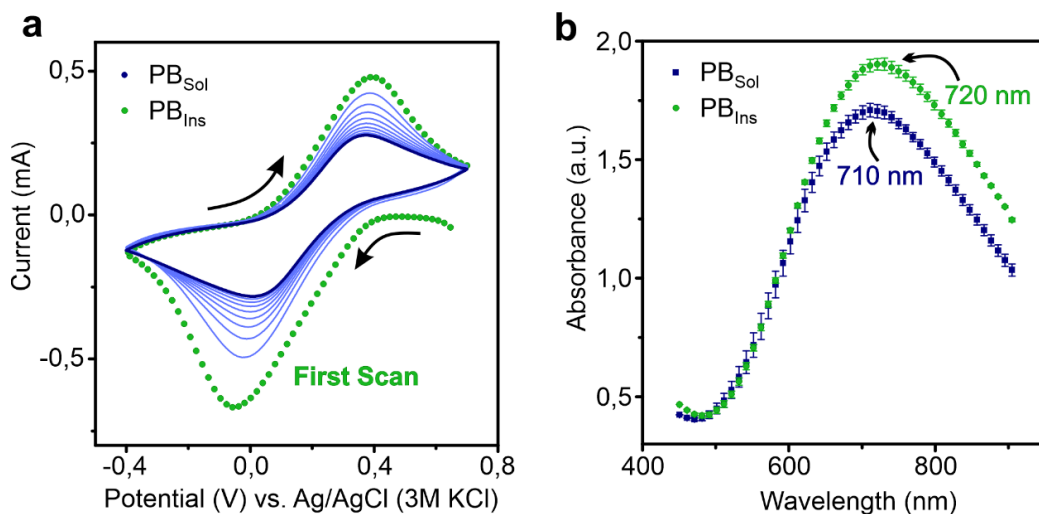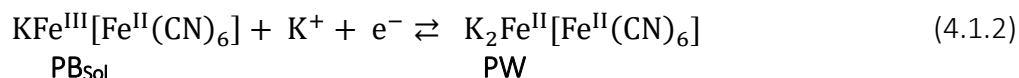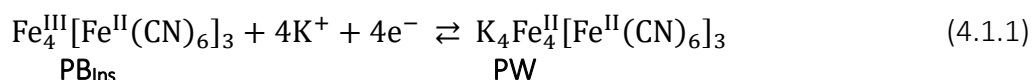
Figure 4.1.9. Spectroelectrochemical differences between PB$_{\text{Sol}}$ and PB$_{\text{Ins}}$. a) Development of 10 CVs from 0.7 to −0.4 V vs Ag/AgCl (3M KCl) at 20 mV s^{-1} to the electrodeposited PB films. The first scan corresponds to PB$_{\text{Ins}}$ (green), while the rest correspond to the progressive formation of PB$_{\text{Sol}}$ (dark blue). b) Absorbance spectrum obtained from freshly electrodeposited PB (PB$_{\text{Ins}}$, in green) and after applying 10 CVs (PB$_{\text{Sol}}$, in blue).

PB$_{Ins}$ was first electrodeposited on the ITO-PET electrodes. When potential cycles were applied in K$^+$-rich media, potassium cations occupied the PB cavities during PW oxidation, turning the initial PB$_{Ins}$ into PB$_{Sol}$ in the following cycles. Furthermore, the decrease in the value of the peak current among cycles, as shown in Figure 4.1.9a, confirmed the loss of iron atoms in the PB structure when PB$_{Ins}$ was converted into PB$_{Sol}$. Although indistinguishable by the bare eye, both soluble and insoluble forms of electrodeposited PB presented slightly different optical and electrochemical properties (a difference of about 20 mV in the standard redox potential, 10 nm in the absorbance peak, and a decrease in current and absorbance values), which may affect their capacity to react with proteins in the ETC and thus, to sense bacteria.

4.1.3 Bacterial-sensing activity of soluble and insoluble PB-NPs in suspension.

Bacterial-sensing activity of both soluble and insoluble forms of PB was analyzed and compared using *E. coli* as a model microorganism. PB suspensions were prepared with the same initial absorbance magnitude, i.e. 0.9 AU at wavelength of 716 nm, in order to be produce comparable spectroscopic responses. To determine the concentration present in the PB suspension after the synthetic process, the extinction molar coefficient (ε) of both suspensions was determined using the spectrochemical cell with different light paths illustrated in Figure 4.1.10a by applying the Beer-Lambert law (equation (4.1.3):

$$A = \varepsilon \cdot c \cdot l \tag{4.1.3}$$

where, *A* is the absorbance (AU), ε is the extinction molar coefficient (M^{-1} cm^{-1}), *c* is the molar concentration (M) and *l* is the optical path length (cm).

The molar extinction coefficient was estimated as the slope of the plot illustrated in Figure 4.1.10b, where the absorbance magnitude of each PB suspension is represented versus the length of the light path. It is important to remark that the concentration in the measurements is constant and only the path length change between measurements.

Molar extinction coefficient values of 8.4×10^3 and 3.4×10^4 M^{-1} cm^{-1} were obtained for soluble and insoluble PB, respectively, which were in agreement with those theoretically reported in[39], i.e.

3.0×10^4 M^{-1} cm^{-1} for the PB$_{Sol}$ at a wavelength of 700 nm. Based on these coefficients magnitude, the concentrations of the PB suspensions were estimated to be 0.28 mM for the PB$_{Sol}$ and 0.07 mM for the PB$_{Ins}$.
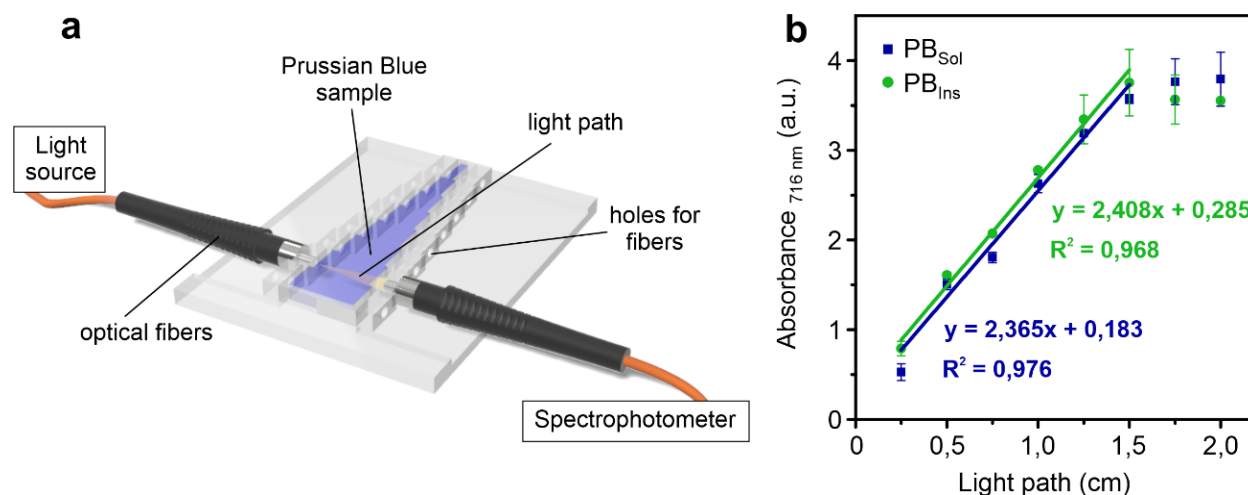

Figure 4.1.10. Scheme of the spectrochemical cell used to determine the molar extinction coefficient of PB$_{Sol}$ and PB$_{Ins}$ suspensions. b) Absorbance measurements obtained at 716 nm for PB$_{Sol}$ and PB$_{Ins}$ by varying the light path and linear regression values (n = 3).

PB-NP suspensions were incubated with *E. coli* concentrations between 10 and 10^8 CFU mL^{-1} for 24 h, and acquiring absorbance spectra between 420 and 900 nm every hour for the duration of the experiment with a plate reader. The results from the incubation of both soluble and insoluble PB with a bacterial concentration of 10^8 CFU mL^{-1} are illustrated in Figure 4.1.11a and Figure 4.1.11b, respectively. In both cases, initially, the PB peak around 700 nm is observed, which disappeared over time due to PB reduction to PW by bacterial metabolism. However, a general increment of absorbance in the full wavelength range was observed, which was associated to bacterial scattering and their growth along the experiment. To better observe the color shift produced by bacterial metabolic reduction of PB-NPs, the contribution of bacterial scattering was subtracted from the spectra. After scattering subtraction, the peak decrease at 700 nm corresponding to the reduction from PB to PW was clearly observed for both PB$_{Sol}$ and PB$_{Ins}$, as shown in Figure 4.1.11c and Figure 4.1.11d, respectively. However, some scattering was still present in the PB spectra after bacterial scattering subtraction at low wavelengths, which was associated to the formation of PB-NPs aggregates. The magnitude of this aggregate NPs scattering

was more intense in the case of PB$_{Ins}$, which, in fact, produced larger particles more susceptible to scatter light.
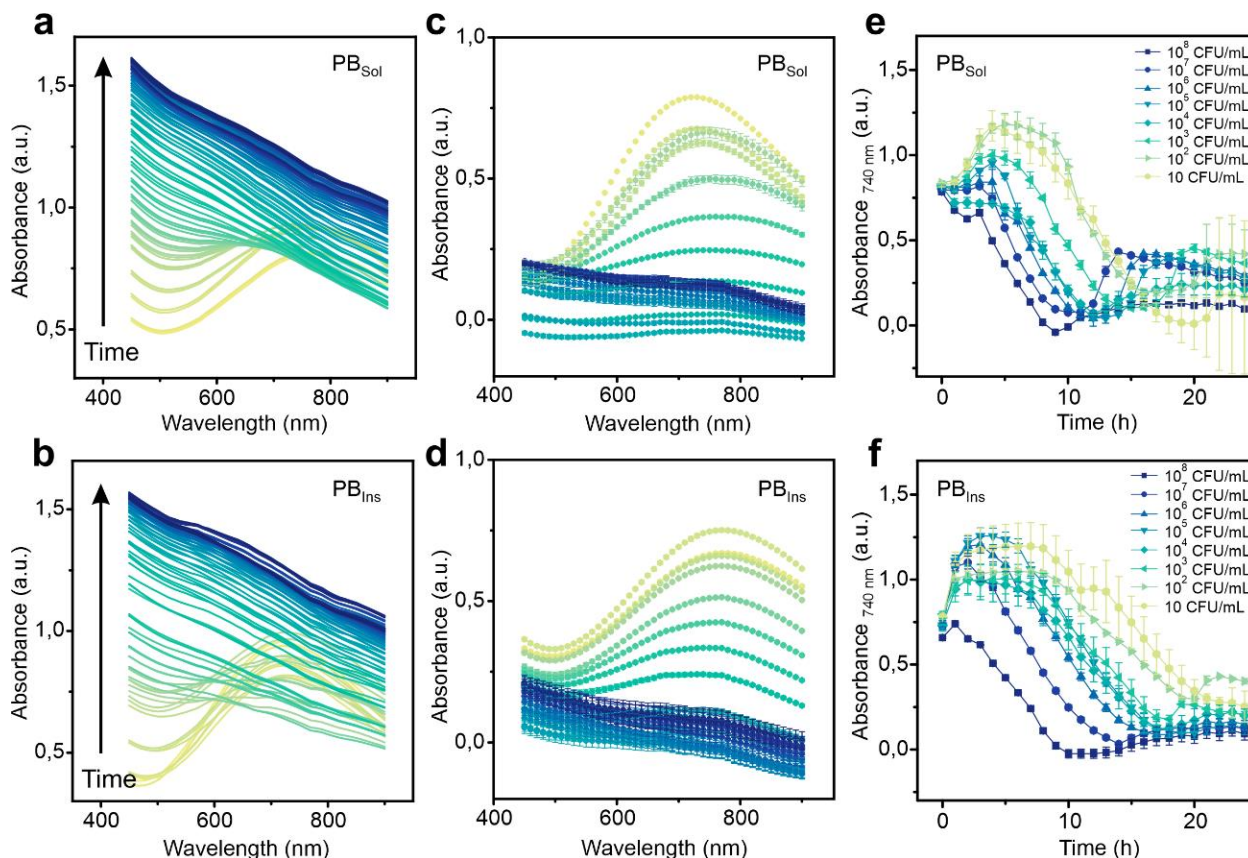

Figure 4.1.11. Bacterial-sensing activity of PB-NPs in suspension. Absorbance spectra obtained over time for: a) PB$_{Sol}$ and, b) PB$_{Ins}$, when incubated with a bacterial concentration of 10^8 CFU mL^{-1} in MH medium (pH 6.2). Absorbance spectra resulting when data from bacterial scattering was extracted, for: c) PB$_{Sol}$ and, d) PB$_{Ins}$. Absorbance values at 740 nm obtained from the previous graphs versus reaction time after *E.coli* inoculation at different concentrations (between 10 and 10^8 CFU mL^{-1}) with (e) PB$_{Sol}$ and (f) PB$_{Ins}$, during 24 hours in MH medium (pH 6.2). For all graphs shown, n = 3.

Although the rates of color change were larger for higher bacterial concentrations, metabolic reduction activity was observed in all bacterial samples under study, even the more diluted ones. The peak reduction kinetics at 740 nm after 24 h of incubation is represented in Figure 4.1.11e and Figure 4.1.11f for soluble and insoluble PB, respectively. In the case of 10^8 CFU mL^{-1}, a complete reduction to PW was achieved in less than 10 h in both cases, while the lowest concentration (10 CFU mL^{-1}) required 20 h of incubation for a total color change. It should be also

remarked that, at the beginning of the experiment the absorbance values tended to increase before decreasing due to metabolic reduction of PB. This increment was higher at the lowest bacterial concentrations and may be related to the scattering produced by PB-NPs since these low concentrations required more time to metabolize PB. Although both PB forms presented similar changes and kinetics, the reduction to PW was in general faster in the case of PB_{Sol}. Although still controversial, this fact was associated with its higher solubility, which facilitated the PB-NP diffusion in the medium to accept electrons from bacterial ETC., the reactivity with bacteria and other components of the medium such as potassium ions, of the different compositions of both PB forms.

4.1.4 Bacterial-sensing activity of PB-NPs electrodeposited on ITO-PET electrodes.

After the potentiostatic electrodeposition of soluble and insoluble PB on ITO-PET electrodes, their bacterial-sensing activity was also studied and compared. Electrodes freshly electrodeposited were used as PB_{Ins}, while those cycled in a 1 M KCl medium were used to test the PB_{Sol} behavior. The two PB-modified ITO-PET electrodes were incubated with a 10^8 CFU mL^{-1} *E. coli* suspension and their metabolic reduction activity was analyzed both optically and electrochemically after different incubation times of 0, 1, 5, 10, and 24 h. As a control, electrodes were submerged in MH medium (pH 6.2) and the absorbance was measured after 24 h of incubation. Spectra obtained at these times are shown in Figure 4.1.12a and Figure 4.1.12b for the soluble and insoluble PBs forms, respectively. The reduction in the PB absorbance peak by bacterial metabolism was already observed clearly after 1 h of incubation. To compare the reduction rates for both forms of PB, Figure 4.1.12c shows the absorbance value at 716 nm for the control and the samples in contact with bacteria. PB_{Sol} showed faster kinetics of reduction to PW when in contact with bacteria, while both controls remained constant over the experimental time.

Consecutively, electrochemical measurements were carried out with PB-modified ITO-PET electrodes after incubation with bacterial suspensions. After incubation at the incubation times described previously, electrodes were measured chronoamperometrically by applying a constant potential of 0.6 V vs. Ag/AgCl (3M KCl) for 80 s. ITO-PET electrodes without any treatment were used as controls. The resulting graphs for soluble and insoluble PBs are illustrated in Figure 4.1.12d

and Figure 4.1.12e, respectively. In the graphs, the area below the chronamperometric curve corresponded to the amount PW produced by bacterial metabolism. According to the results, few PB molecules were reduced after short incubation times, resulting in small areas under the amperometric curve. However, this magnitude progressively increased with the incubation time since bacteria had more time to metabolize PB and reduce it to PW. This progressive increasing with the incubation time was observed in both cases, PB_{Sol} and PB_{Ins}.
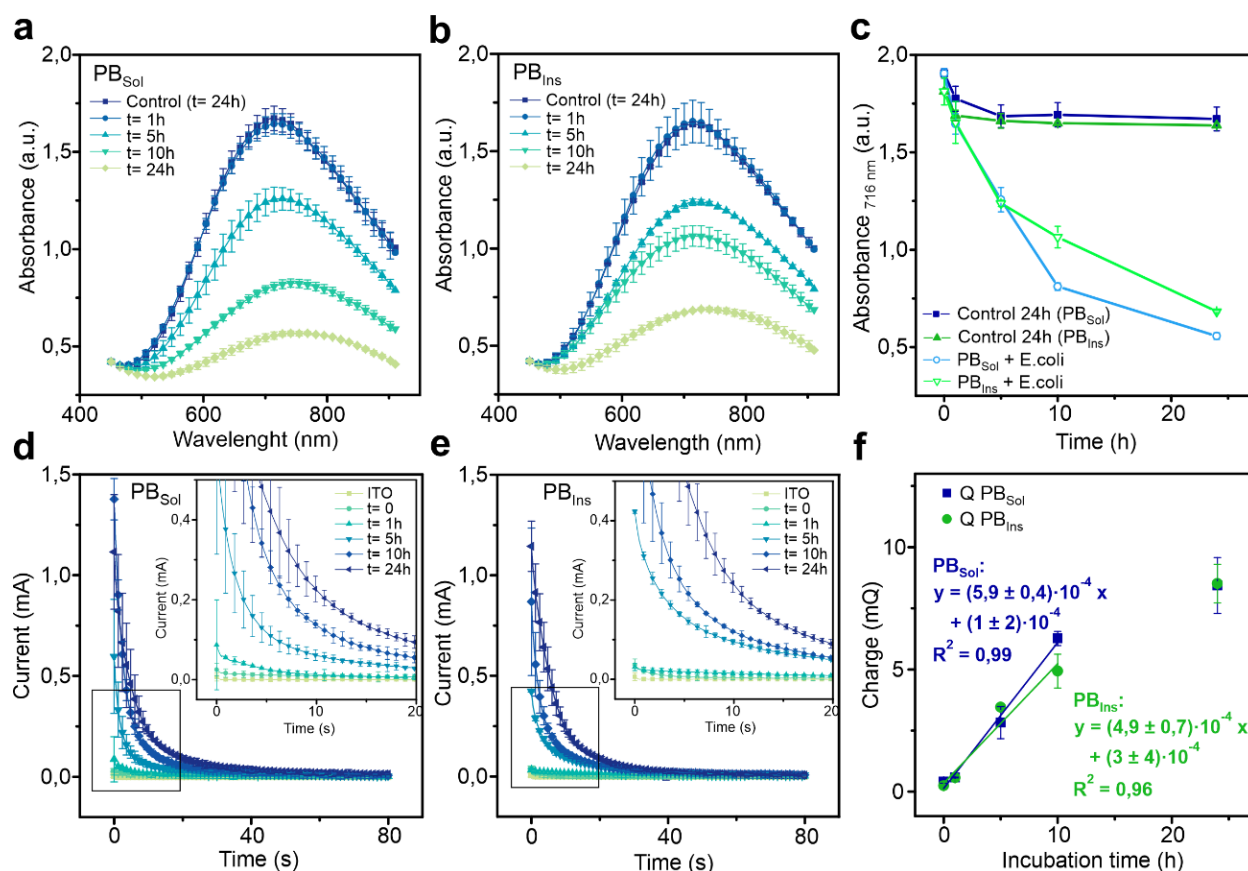
Figure 4.1.12. Bacterial-sensing activity of PB-NPs electrodeposited on ITO-PET electrodes. Absorbance spectra of the PB-electrodeposited electrodes, obtained after incubation with a bacterial concentration of 10^8 CFU·mL^{-1} at different times (1, 5, 10 and 24 h) for (a) PB_{Sol} and (b) PB_{Ins}. As control, PB-electrodes were submerged in MH medium (pH 6.2) (n=3). (c) Absorbance values at 716 nm (obtained from the previous graphs) over incubation time for PB_{Sol} and PB_{Ins} electrodeposited electrodes and their respective controls (n=3). Chronoamperometry curve of the PB-electrodeposited electrodes, obtained by applying 0.6 V for 80 s after incubation with a bacterial concentration of 10^8 CFU·mL^{-1} at different times (1, 5, 10 and 24 h) for (d) PB_{Sol} and (e) PB_{Ins} (n=3). (f) Relationship between the charge obtained by integrating the curve at the chronoamperometry versus the incubation time for PB_{Sol} (blue squares) and PB_{Ins} (green circles)

To study the kinetics of the process, the charge obtained after the chronoamperometry was calculated by integrating those areas. The relationship between the charge obtained and the incubation times is plotted in Figure 4.1.12f for both PB_{Sol} and PB_{Ins}. As already commented, longer incubation times resulted in higher amounts of PB reduced by bacteria and larger charges (measured as the area below the curve in the chronoamperometric measurement). In both cases, the metabolic reduction of PB by bacteria was detectable amperometrically after only 1 h of incubation. However, the slope for PB_{Sol} was 18% higher than for PB_{Ins}, which indicated faster reduction kinetics and larger sensing capacities for the soluble form of PB. In addition, the limit of detection was calculated based on the standard deviation of the blank and the slope for both processes ($3\ \sigma_{(t=0)}$/slope) in terms of time necessary to detect a bacterial concentration of 10^8 CFU mL^{-1}. Using this estimation, the limit of detection was 4 min for the soluble and 8 min for the insoluble one. Analogously, the limit of quantification ($10\ \sigma_{(t=0)}$/slope) calculated from the regression data of Figure 4.1.12 was of 28 min for the PB_{Ins} and 14 min for the PB_{Sol}.

These discrepancies may be related to the different structures presented for both PB forms. As shown in equations (4.1.1) and (4.1.2), they differ in the molecular mass, the number of iron atoms in the structure and in the number of electrons exchanged. According to Faraday's Law, the charge understood as the area under the curve in the chronoamperometric analysis could be related to the number of moles of PB reduced by bacterial metabolism (4.1.4):

$$n = \frac{Q}{zF} \tag{4.1.4}$$

where n is the number of moles of PB, Q is the calculated charge of the curve (C), z is the number of electrons involved in the electrochemical process, and F is the Faraday constant (96485 C mol^{-1}).

When applying the previous equation to the metabolic reduction of PB and considering the same value of charge for both PB forms, the following relationship between the number of moles of soluble and insoluble PB was obtained (4.1.5):

$$\frac{n_S}{n_I} = 4 \qquad (4.1.5)$$

Although the amount of charge obtained in the reduction of PB by bacterial metabolism is similar for PB_{Sol} and PB_{Ins}, there was a difference between the number of moles reduced in both cases.

Figure 4.1.13 illustrates the electron pathway through the electrochemical detection process. In aerobic conditions, bacteria metabolize the carbon source, i.e., nutrients in the form of organic matter like glucose, which are oxidized to carbon dioxide to obtain energy. Electrons derived from this process are then passed through the bacterial electron transport chain in the plasma membrane to finally reduce the electrodeposited PB to the colorless PW state. PW on the electrode is re-oxidized to its initial PB, generating a current flow proportional to the concentration of metabolically produced PW (or to the amount of PB metabolized by bacteria during the incubation period). Considering this mechanism, four moles of PB_{Ins} are needed for each mole of PB_{Sol} metabolized by bacteria to produce the same amount of charge. This fact is closely linked to the number of iron atoms presented in each structure. Thus, the PB_{Ins} structure presents four iron (III) atoms, thus four electrons are needed to switch PB to the PW form, while PB_{Sol} only needs one electron to achieve this reduction. Therefore, the metabolic reduction kinetics from PB to PW is four times faster for the soluble form than for the insoluble one.
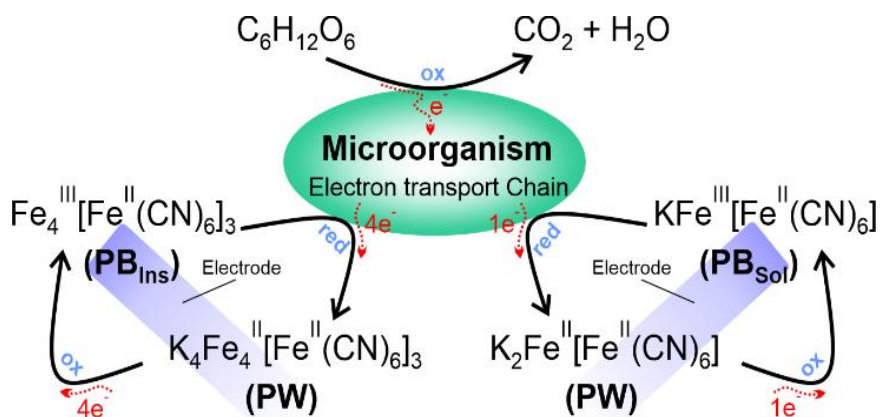
Figure 4.1.13. Scheme of the electrons pathway during the electrochemical detection process.

Compared to other live/dead detection methods, detection times may appear longer. However, this study is developed for the future application in smart materials, in which the detection will be produced in situ and without the need for sample collection, transport, and/or treatment/processing. Other works present shorter detection times;[40,41] however, the time dedicated to samples' collection, transport, and preparation (24–48 h) is even longer than the one presented here. Although less than 1h is a reasonable time when considering a practical application, e.g., detection of microbial pollution, bacterial concentrations necessary to produce this change are still high. To reach the small detection limits required in current regulations, the use of more sensitive transduction mechanisms, e.g., amperometric detection by incorporating electrodes on different substrates, and/or pre-concentration processes will be explored and discussed in the following sections.

4.1.5 Conclusions

PB, due to its optical (high molar extinction coefficient) and electrochemical (suitable redox potential) properties, is an excellent candidate for bacterial detection either in solution or after deposition in solid-state, transparent ITO-PET electrodes. The two main forms of PB, namely, soluble and insoluble, present differences in terms of the structure (the counter ion in the insoluble form is an iron atom and in the soluble form is potassium), absorption capacity (a difference in the absorption peak of 10 nm is shown, and the molar absorption coefficient for the insoluble is four times higher than for the soluble one), and redox activity (both present a difference of approximately 20 mV, having the soluble form a smaller redox potential, more suitable to react with the proteins in the ETC). Both forms are metabolized by bacteria, changing their redox state and producing an intense color change observable even with the bare eye. However, the soluble form presents some advantages in electrochemical detection, i.e., faster metabolic reduction kinetics observed at a higher slope value obtained from the quantification of the charge produced by the process. This difference may be attributed to more suitable redox potential and the presence of a single iron ion in the structure of the soluble form, while the insoluble form requires the reduction of four iron atoms for producing the color change. Therefore, this study elucidates the potential of PB-NPs to be used as metabolic indicators for the

detection of the presence of living bacteria in different environments, e.g., liquids, solids, or air, with potential application in many sectors such as clinical diagnostics, food and beverage contamination, or water pollution, among others.

4.1.6 References

(1) Pujol-Vila, F.; Vigués, N.; Díaz-González, M.; Muñoz-Berbel, X.; Mas, J. Fast and Sensitive Optical Toxicity Bioassay Based on Dual Wavelength Analysis of Bacterial Ferricyanide Reduction Kinetics. *Biosens. Bioelectron.* **2015**, *67*, 272–279. https://doi.org/10.1016/j.bios.2014.08.030.

(2) Pujol-Vila, F.; Vigués, N.; Guerrero-Navarro, A.; Jiménez, S.; Gómez, D.; Fernández, M.; Bori, J.; Vallès, B.; Riva, M. C.; Muñoz-Berbel, X.; Mas, J. Paper-Based Chromatic Toxicity Bioassay by Analysis of Bacterial Ferricyanide Reduction. *Anal. Chim. Acta* **2016**, *910*, 60–67. https://doi.org/10.1016/j.aca.2016.01.006.

(3) Pujol-Vila, F.; Dietvorst, J.; Gall-Mas, L.; Díaz-González, M.; Vigués, N.; Mas, J.; Muñoz-Berbel, X. Bioelectrochromic Hydrogel for Fast Antibiotic-Susceptibility Testing. *J. Colloid Interface Sci.* **2018**, *511*, 251–258. https://doi.org/10.1016/j.jcis.2017.09.004.

(4) Dietvorst, J.; Ferrer-Vilanova, A.; Iyengar, S. N.; Russom, A.; Mas, J.; Marco, M.; Guirado, G. Bacteria Detection at a Single-Cell Level through a Cyanotype-Based Photochemical Reactioń. *Anal. Chem.* **2022**, *94*, 787–792. https://doi.org/10.1021/acs.analchem.1c03326.

(5) Narayana Iyengar, S.; Dietvorst, J.; Ferrer-Vilanova, A.; Guirado, G.; Muñoz-Berbel, X.; Russom, A. Toward Rapid Detection of Viable Bacteria in Whole Blood for Early Sepsis Diagnostics and Susceptibility Testing. *ACS Sensors* **2021**, *6*, 3357–3366. https://doi.org/10.1021/acssensors.1c01219.

(6) Koncki, R. Chemical Sensors and Biosensors Based on Prussian Blues. *Crit. Rev. Anal. Chem.* **2002**, *32* (1), 79–96. https://doi.org/10.1080/10408340290765452.

(7) Karyakin, A. A. Prussian Blue and Its Analogues: Electrochemistry and Analytical Applications. *Electroanalysis* **2001**, *13* (10), 813–819. https://doi.org/10.1002/1521-4109(200106)13:10<813::AID-ELAN813>3.0.CO;2-Z.

(8) Ellis, D.; Eckhoff, M.; Neff, V. D. Electrochromism in the Mixed-Valence Hexacyanides. 1. Voltammetric and Spectral Studies of the Oxidation and Reduction of Thin Films of Prussian Blue. *J. Phys. Chem.* **1981**, *85* (9), 1225–1231. https://doi.org/10.1021/j150609a026.

(9) Lundgren, C. A.; Murray, R. W. Observations on the Composition of Prussian Blue Films and Their Electrochemistry. *Inorg. Chem.* **1988**, *27* (5), 933–939. https://doi.org/10.1021/ic00278a036.

(10) Grandjean, F.; Samain, L.; Long, G. J. Characterization and Utilization of Prussian Blue and Its Pigments. *Dalt. Trans.* **2016**, *45*, 18018–18044. https://doi.org/10.1039/c6dt03351b.

(11) Itaya, K.; Uchida, I.; Neff, V. D. Electrochemistry of Polynuclear Transition Metal Cyanides: Prussian Blue and Its Analogues. *Acc. Chem. Res.* **1986**, *19* (6), 162–168. https://doi.org/10.1021/ar00126a001.

(12) Ding, P.; Song, G.; Zhou, J.; Song, Q. Collection of Rolling Fingerprints by the Electrochromism of Prussian Blue. *Dye. Pigment.* **2015**, *120*, 169–174. https://doi.org/10.1016/j.dyepig.2015.04.019.

(13) Rosseinsky, D. R.; Glasser, L.; Jenkins, H. D. B. Thermodynamic Clarification of the Curious Ferric/Potassium Ion Exchange Accompanying the Electrochromic Redox Reactions of Prussian Blue, Iron(III) Hexacyanoferrate(II). *J. Am. Chem. Soc.* **2004**, *126* (33), 10472–10477. https://doi.org/10.1021/ja040055r.

(14) Karyakin, A. A. Advances of Prussian Blue and Its Analogues in (Bio)Sensors. *Curr. Opin. Electrochem.* **2017**, *5* (1), 92–98. https://doi.org/10.1016/j.coelec.2017.07.006.

(15) Peng, J.; Wang, J.; Yi, H.; Hu, W.; Yu, Y.; Yin, J.; Shen, Y. A Dual-Insertion Type Sodium-Ion Full Cell Based on High-Quality Ternary-Metal Prussian Blue Analogs. *Adv. Energy Mater.* **2018**, *8*, 1702856. https://doi.org/10.1002/aenm.201702856.

(16) Shi, D.; Fu, J.; Shadike, Z.; Cao, M.; Wang, W.; Fu, Z. All-Solid-State Rechargeable Lithium Metal Battery with a Prussian Blue Cathode Prepared by a Nonvacuum Coating Technology. *ACS Omega* **2018**, *3*, 7648–7654. https://doi.org/10.1021/acsomega.8b01102.

(17) Kaye, S. S.; Long, J. R. The Role of Vacancies in the Hydrogen Storage Properties of Prussian Blue Analogues. *Catal. Today* **2007**, *120*, 311–316. https://doi.org/10.1016/j.cattod.2006.09.018.

(18) Li, X.; Liang, X.; Ma, F.; Jing, L.; Lin, L.; Yang, Y. Chitosan Stabilized Prussian Blue Nanoparticles for Photothermally Enhanced Gene Delivery. *Colloids Surfaces B Biointerfaces* **2014**, *123*, 629–638. https://doi.org/10.1016/j.colsurfb.2014.10.001.

(19) Bui, N. Q.; Cho, S.; Moorthy, M. S.; Park, S. M.; Piao, Z.; Nam, S. Y.; Kang, H. W.; Kim, C. In Vivo Photoacoustic Monitoring Using 700-Nm Region Raman Source for Targeting Prussian Blue Nanoparticles in Mouse Tumor Model. *Sci. Rep.* **2018**, *8*, 2000. https://doi.org/10.1038/s41598-018-20139-0.

(20) Online, V. A.; Li, Z.; Zeng, Y.; Wu, M.; Wu, L.; Huang, A.; Yang, H.; Liu, X.; Liu, J. Glypican-3 Antibody Functionalized Prussian Blue Nanoparticles for Targeted MR Imaging and Photothermal Therapy of Hepatocellular Carcinoma. *J. Mater. Chem. B* **2014**, *2*, 3686–3696. https://doi.org/10.1039/c4tb00516c.

(21) Wang, J.; Zhang, L.; Yu, L.; Jiao, Z.; Xie, H.; Sun, X. W. A Bi-Functional Device for Self-Powered Electrochromic Window and Self-Rechargeable Transparent Battery Applications. *Nat. Commun.* **2014**, *5*, 4921. https://doi.org/10.1038/ncomms5921.

(22) Komkova, M. A.; Karyakina, E. E.; Karyakin, A. A. Catalytically Synthesized Prussian Blue Nanoparticles Defeating Natural Enzyme Peroxidase. *J. Am. Chem. Soc.* **2018**, *140* (1), 11302–11307. https://doi.org/10.1021/jacs.8b05223.

(23) Ertl, P.; Unterladstaetter, B.; Bayer, K.; Mikkelsen, S. R. Ferricyanide Reduction by Escherichia Coli: Kinetics, Mechanism, and Application to the Optimization of Recombinant Fermentations. *Anal. Chem.* **2000**, *72* (20), 4949–4956. https://doi.org/10.1021/ac000358d.

(24) Jahn, M. K.; Haderlein, S. B.; Meckenstock, R. U. Reduction of Prussian Blue by the Two Iron-Reducing Microorganisms Geobacter Metallireducens and Shewanella Alga. *Environ. Microbiol.* **2006**, *8* (2), 362–367. https://doi.org/10.1111/j.1462-2920.2005.00902.x.

(25) Gervais, C.; Languille, M. A.; Réguer, S.; Gillet, M.; Pelletier, S.; Garnier, C.; Vicenzi, E. P.; Bertrand, L. Why Does Prussian Blue Fade? Understanding the Role(s) of the Substrate. *J. Anal. At. Spectrom.* **2013**, *28* (10), 1600–1609. https://doi.org/10.1039/c3ja50025j.

(26) Gervais, C.; Languille, M. A.; Reguer, S.; Garnier, C.; Gillet, M. Light and Anoxia Fading of Prussian Blue Dyed Textiles. *Herit. Sci.* **2014**, *2* (1). https://doi.org/10.1186/s40494-014-0026-x.

(27) Qin, Z.; Li, Y.; Gu, N. Progress in Applications of Prussian Blue Nanoparticles in Biomedicine. *Adv. Healthc. Mater.* **2018**, *7*, 1800347. https://doi.org/10.1002/adhm.201800347.

(28) Hatamie; Amir; Zargar; Behrooz; Jalali, A.; Ameri, H. Colorimetric Assay for 4-Phenylthiosemicarbazide Detection in Environmental Samples Based on Prussian Blue Nanoparticles Formation Ion. *Iran. J. Chem. Chem. Eng* **2017**, *36* (1), 125–133.

(29) Ricci, F.; Palleschi, G. Sensor and Biosensor Preparation, Optimisation and Applications of Prussian Blue Modified Electrodes. *Biosens. Bioelectron.* **2005**, *21* (3), 389–407. https://doi.org/10.1016/j.bios.2004.12.001.

(30) Fiorito, P. A.; Gonçales, V. R.; Ponzio, E. A.; Córdoba De Torresi, S. I. Synthesis, Characterization and Immobilization of Prussian Blue Nanoparticles. A Potential Tool for Biosensing Devices. *Chem. Commun.* **2005**, No. 3, 366–368. https://doi.org/10.1039/b412583e.

(31) Kohn, M. New Observations on the Solubility of Prussian Blue. *Anal. Chim. Acta* **1954**, *11*, 18–27. https://doi.org/10.1016/S0003-2670(00)87685-0.

(32) Kracke, F.; Vassilev, I.; Krömer, J. O. Microbial Electron Transport and Energy Conservation - The Foundation for Optimizing Bioelectrochemical Systems. *Front. Microbiol.* **2015**, *6* (JUN), 1–18. https://doi.org/10.3389/fmicb.2015.00575.

(33) G, R.; A.P.F., T. Development of an Electrochemical Method for the Rapid Determination of Microbial Concentration and Evidence for the Reaction Mechanism. *Anal. Chim. Acta* **1988**, *215*, 61–69. https://doi.org/10.1016/S0003-2670(00)85266-6.

(34) Dacarro, G.; Taglietti, A. Prussian Blue Nanoparticles as a Versatile Photothermal Tool. *Molecules* **2018**, *23*, 1414. https://doi.org/10.3390/molecules23061414.

(35) Mortimer, R. J.; Rosseinsky, D. R. Iron Hexacyanoferrate Films: Spectroelectrochemical Distinction and Electrodeposition Sequence of "Soluble" (K+-Containing) and "Insoluble"

(K+-Free) Prussian Blue, and Composition Changes in Polyelectrochromic Switching. *J. Chem. Soc. Dalt. Trans.* **1984**, No. 9, 2059–2062. https://doi.org/10.1017/CBO9781107415324.004.

(36) Bueno, P. R.; Ferreira, F. F.; Giménez-Romero, D.; Setti, G. O.; Faria, R. C.; Gabrielli, C.; Perrot, H.; Garcia-Jareño, J. J.; Vicente, F. Synchrotron Structural Characterization of Electrochemically Synthesized Hexacyanoferrates Containing K+: A Revisited Analysis of Electrochemical Redox. *J. Phys. Chem. C* **2008**, *112* (34), 13264–13271. https://doi.org/10.1021/jp802070f.

(37) Delongchamp, B. D. M.; Hammond, P. T. High-Contrast Electrochromism and Controllable Dissolution of Assembled Prussian Blue/Polymer Nanocomposites. *Adv. Funct. Mater.* **2004**, *14* (3), 224–232. https://doi.org/10.1002/adfm.200304507.

(38) García-Jareño, J. J.; Navarro-Laboulais, J.; Vicente, F. Electrochemical Study of Nafion Membranes/Prussian Blue Films on Ito Electrodes. *Electrochim. Acta* **1996**, *41* (17), 2675–2682. https://doi.org/10.1016/0013-4686(96)00121-1.

(39) Zargar, B.; Hatamie, A. Prussian Blue Nanoparticles: A Simple and Fast Optical Sensor for Colorimetric Detection of Hydralazine in Pharmaceutical Samples. *Anal. Methods* **2014**, *6* (15), 5951–5956. https://doi.org/10.1039/c4ay00618f.

(40) Liu, X.; Marrakchi, M.; Xu, D.; Dong, H.; Andreescu, S. Biosensors Based on Modularly Designed Synthetic Peptides for Recognition, Detection and Live/Dead Differentiation of Pathogenic Bacteria. *Biosens. Bioelectron.* **2016**, *80*, 9–16. https://doi.org/10.1016/j.bios.2016.01.041.

(41) Berney, M.; Hammes, F.; Bosshard, F.; Weilenmann, H. U.; Egli, T. Assessment and Interpretation of Bacterial Viability by Using the LIVE/DEAD BacLight Kit in Combination with Flow Cytometry. *Appl. Environ. Microbiol.* **2007**, *73* (10), 3283–3290. https://doi.org/10.1128/AEM.02750-06.
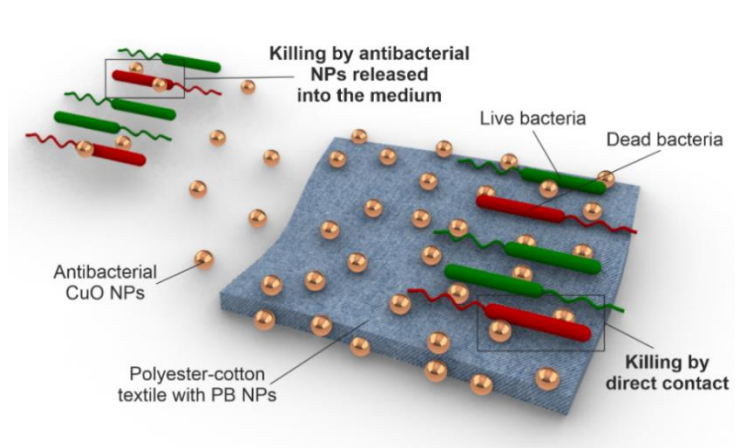
4.2

Prussian blue Modification of Polyester-Cotton Fabrics for the Production of Smart Textiles

Abstract

Bacterial contamination of surfaces is one of the main bacterial transmission and infection pathways in hospitals and other healthcare settings. Antimicrobial textiles are now being used to minimize bacterial transmissions and infections from contaminated surfaces. The main limitation of these materials is, however, their limited lifespan, since they lose antimicrobial activity progressively, being again susceptible of bacterial colonization. The detection of pathogens present on contaminated surfaces may minimize infection risks, but not always possible with current microbial detection technologies requiring sample collection and transport to central laboratories. And, although in situ bacterial detection is currently possible with colorimetric chemical reagents that detect ATP or other metabolically-related compounds, it is still necessary to spread the reagent on the material surface, being virtually impossible to cover the large number of surfaces present in these infrastructures.

In this chapter, smart hospital fabrics with the capacity to detect live bacteria by a simple change of color based on a single-step sonochemical coating process requiring less than 15 min are presented. The presence of PB-NPs confers the textile with an intensive blue color and with bacterial-sensing capacity. Live bacteria in the textile metabolize PB-NPs and reduce them to colorless PW, enabling in situ detection of bacterial presence in less than 6 h with the bare eye (complete color change requires 40 h), being sensitive to both Gram-positive and Gram-negative bacteria. The redox reaction is completely reversible and the textile recovers its initial blue color by re-oxidation with environmental oxygen when bacteria die, enabling its re-use.

As a step forward, this technology is also implemented in antibacterial textiles for the production of a smart textile able to report on the loss of its antimicrobial activity through a local change of color. The PB coating maintains the antimicrobial activity of the material (antibacterial activity > 4), while increasing the stability of the CuO-nanoparticles on the textile reducing the Cu^{2+} release. On the other hand, the CuO-nanoparticles did not compromise the bacterial sensing capacity of Prussian blue, which responds to bacterial presence with a color change, visually appreciable in less than 3 hours.

Finally, this technology is improved by modifying the polyester-cotton textiles through a photocatalytic cyanotype method, which confers an intense blue color to the samples. The bacterial sensing activity is improved, showing local color changes in the textiles after less than 6 h of incubation in bacterial concentrations two magnitude orders smaller than those used in the previous cases, even in dry conditions. Furthermore, cyanotype process confers more stability to the CuO-NPs on the textile fibers without affecting their antibacterial capacity. As a result, the smart material presents antimicrobial and bacterial sensing properties able to report on contaminated surfaces in hospitals, and other critical facilities such as schools or retirement homes, aiming to prevent bacterial infections.

This chapter contains results previously published in:

Congresses:

Oral presentation entitled "**Live Bacteria Sensing in Antimicrobial Textiles**", presented at the **11th Ibero-American Congress on Sensors.** Barcelona (Spain). 2018.

Poster contribution entitled "**Smart Sensing Textiles Based on Electrochromic Molecules for Live Bacteria Detection**", presented at the **69th Annual Meeting of the International Society of Electrochemistry.** Bologna (Italy). 2018.

Poster contribution entitled "**Smart Sensing Fabrics for Live Bacteria Detection**", presented at the **Eurosensors 32nd Conference.** Graz (Austria). 2018.

Oral presentation entitled "**Bacterial Detection in Smart Sensing Hospital Textiles**", presented at the **XXIVth Transfronttier Meeting of Sensors and Biosensors.** Perpignan (France). 2019.

Journals:

Smart Sensing Fabrics for Live Bacteria Detection. Amparo Ferrer-Vilanova, Kristina Ivanova, María Díaz-González, Yasmine Alonso, Gonzalo Guirado, Tzanko Tzanov and Xavier Muñoz-Berbel. *Proceedings*, 2018, 2:13, 916.

Sonochemical coating of Prussian Blue for the production of smart bacterial-sensing hospital textiles. Amparo Ferrer-Vilanova, Yasmine Alonso, Jiri Dietvorst, Marta Pérez-Montero, Rosalía Rodríguez-Rodríguez, Kristina Ivanova, Tzanko Tzanov, Núria Vigués, Jordi Mas, Gonzalo Guirado and Xavier Muñoz-Berbel. *Ultrasonics - Sonochemistry*. 2021, 70, 105317.

Smart biocide and chromogenic textile to prevent bacterial infections. Amparo Ferrer-Vilanova, Josune J. Ezenarro, Kristina Ivanova, Óscar Calvo, Ilana Perelshtein, Giulio Gorni, Maria Blanes, Núria Vigués, Jordi Mas, Aharon Gedanken, Tzanko Tzanov, Gonzalo Guirado and Xavier Muñoz-Berbel. *(Article submitted to Materials Horizons Journal)*.

4.2.1 PB-based bacterial-sensing textiles

PB-NPs were implemented into polyester-cotton textiles through a sonochemical coating process. Thus, polyester-cotton samples (3 x 3 cm) were immersed in aqueous suspensions of PB-NPs and sonochemically coated varying the sonication time (from 5 to 30 min), PB type (PB$_{Sol}$ or PB$_{Ins}$) and concentration (from 0.03 to 30 mM) (Figure 4.2.1). From the two forms of PB, only PB$_{Ins}$ was stably incorporated in the textile, while PB$_{Sol}$ was almost completely removed after a soft cleaning process involving the rinsing of the textile with buffer (Figure 4.2.2a).
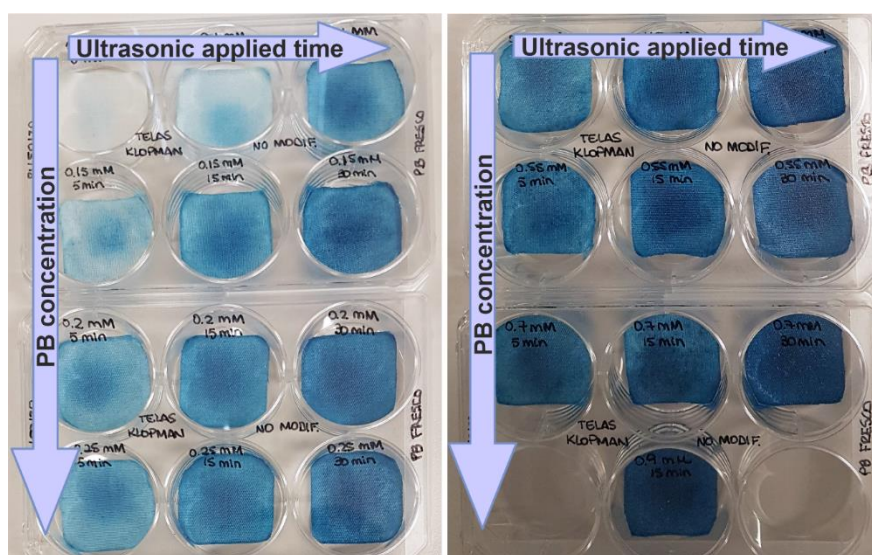
Figure 4.2.1. Polyester-cotton textiles sonochemically coated with PB. PB-polyester-cotton textiles modified at different PB concentrations (from 0.03 to 30 mM) and different times (from 5 to 15 minutes).

In addition, the ageing of the PB$_{Ins}$ suspension influenced the sonochemical coating. Freshly prepared samples presented more homogeneity and color intensity than their 4-days old counterparts (Figure 4.2.3). Homogeneous and highly-colored samples were obtained after coating with freshly-prepared PB suspensions containing 0.08 mM PB for at least 15 min of sonication. No relevant changes were observed when longer sonication times were applied. SEM image of this sample revealed the presence of homogeneously distributed NPs on the textile fibers, although mostly aggregated (Figure 4.2.2b). Accordingly, the single-step sonochemical coating of freshly-prepared PB samples containing 0.08 mM for 15 min was chosen as optimal coating conditions and used in further experiments.
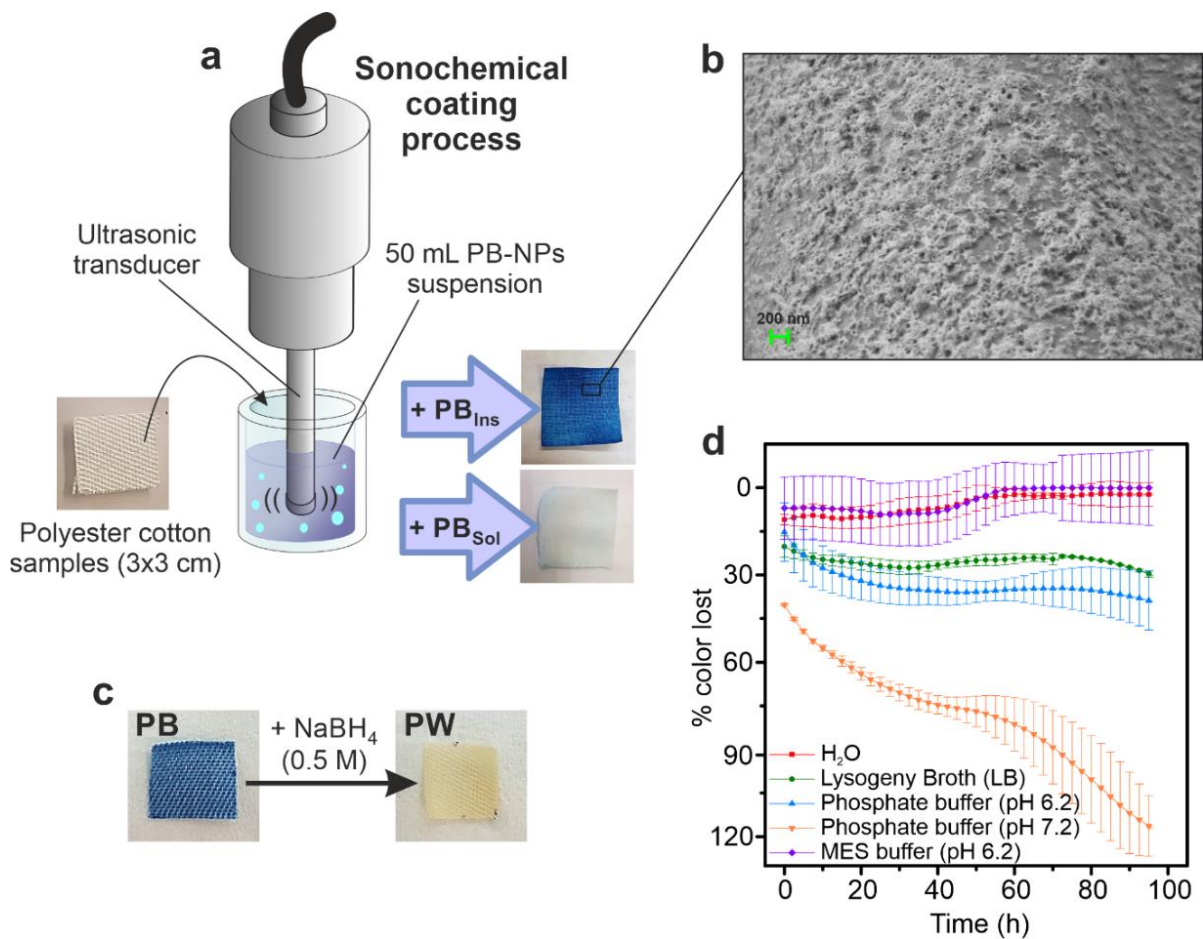
Figure 4.2.2 Sonochemical coating process and characterization of PB-modified textiles. a) Scheme of the sonochemical coating process and resulting textiles obtained after incorporation of PB_{Sol} or PB_{Ins}. b) SEM image of the samples modified with PB_{Ins} 0.08 mM. c) PB-modified textile reduced to PW after addition of $NaBH_4$ 0.5 M as reducing agent. d) Color stability of polyester-cotton textiles modified with PB_{Ins} 0.08 mM after 96 hours submerged in (i) water, (ii) LB, 0.1 M phosphate buffered saline (PBS) at (iii) pH 6.2 and (iv) pH 7.2, and (v) 0.1 M MES buffer (pH 6.2), all supplemented with 0.1% glucose. The color lost was expressed as percentage vs. unmodified textiles color (n=3).
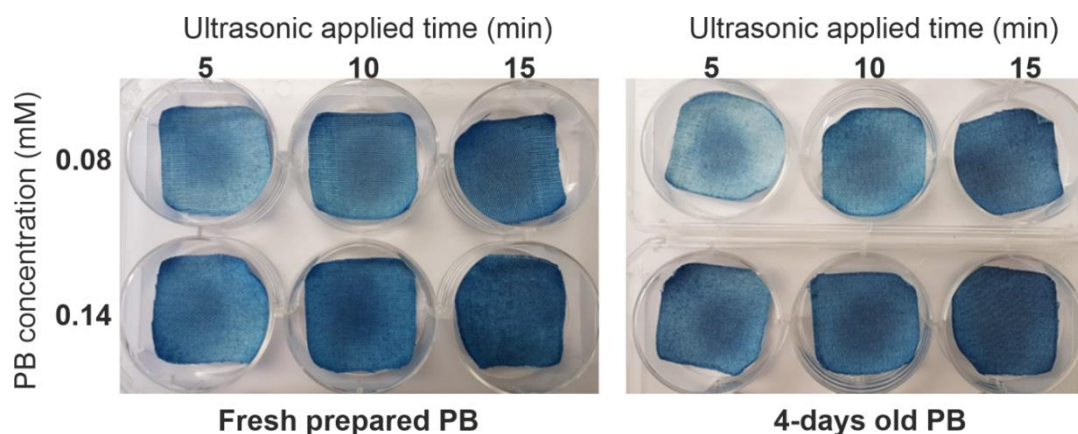
Figure 4.2.3. Fresh prepared PB-textiles vs. 4-days old. Comparison when polyester-cotton textiles were modified with fresh synthesized PB-NPs and the same solution prepared 4 days before.

The oxidative capacity of the coated textile was evaluated using $NaBH_4$ as reducing agent. When in contact with 0.5 M $NaBH_4$, textiles immediately lost the blue color by the formation of PW (Figure 4.2.2c), which confirmed the redox activity of the NPs immobilized in the smart textile, recovering the initial color when in contact with hydrogen peroxide. In dried conditions, coated samples were stable for more than four months with minimal discoloration.

The stability was lower in solution and depended on the medium (Figure 4.2.2d). First, the stability of PB-NPs in the textile was deeply influenced by the pH. It was clearly evidenced when comparing the samples incubated in the physiologic PBS buffer at pH 7.2, which showed an important decrease in color intensity, with those incubated in PBS at pH 6.2, which maintained more than 70 % of the initial color for 4 days. This was in agreement with previous results concluding that hydrolyzed ferric ions in the coordination sphere of PB could only be substituted at a pH lower than 6.4.[1–5] Apart from the pH, the medium composition also had a role in the stability of PB-NPs. Coated samples were more stable in MES than in PBS, even when both buffers had the same pH (pH 6.2). The reason for that may be in the monovalent ions content, e.g., sodium and potassium, which is much higher in PBS than in MES. The presence of such ions, which may substitute iron as counterion in the PB structure, might reduce the stability of NPs incorporated in the textile. In fact, overnight incubation of the textiles with KCl, LiCl or $NaNO_3$ led to the dissociation of the PB and color disappearance (Figure 4.2.4), probably due to the formation of PB$_{Sol}$ which, as commented before, was not stable on the textile fibers. LB medium, slightly acidic

and with monovalent ions in its composition, maintained around 70% of the initial color similarly to PBS at pH 6.2. On the other hand, distilled water, acidic on its own but without important concentration of monovalent counter ions, presented low color losses comparable to MES. Therefore, both ionic composition and pH influenced the stability of PB-NPs incorporated in the textile, but pH-mediated PB decomposition presented faster dissolution kinetics.
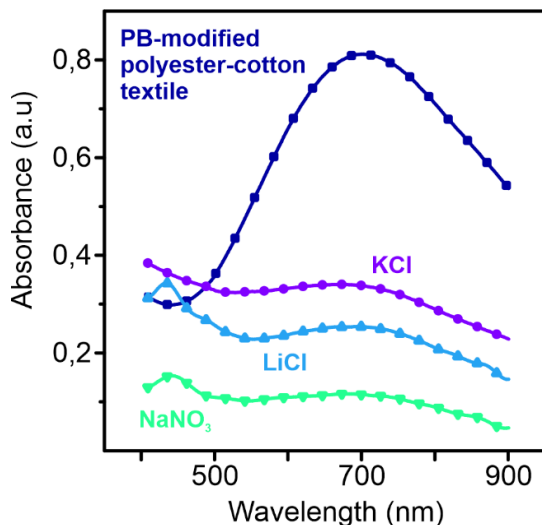

Figure 4.2.4. Color stability of PB-modified textiles depending on the medium composition. Absorbance spectra of PB-modified polyester-cotton textiles after overnight incubation in KCl, LiCl and NaNO₃ media.

The reversibility of PB-NPs incorporated in the textile was studied spectroelectrochemically to evaluate structural/compositional changes along reduction/oxidation cycles. A sandwich configuration with a solid electrolyte, i.e. 2-hydroxyethyl cellulose, was used to study the activity of the smart textiles without solvents (see this configuration in the Materials and Methods section; section number 3.5). CVs (between 0.4 to -0.3 V) at different scan rates (1, 5, 10 and 20 mV s^{-1}) clearly reported two peaks, corresponding to the reduction from PB to PW (at 0 V) and the subsequent re-oxidation of PW to PB at 0.13 V (Figure 4.2.5 a). Peak intensities increased directly with the scan rate and the relationship between intensity of the anodic and cathodic peaks was approximately 1, which corresponds to the behavior of a thin film system.[6] These samples were also very stable to electrolysis. After applying -0.5 V potential for 15 min, the sample only lost 20 % of the initial color. Much more significant color loss was observed in the case of samples prepared with old PB suspension, which lost more than 90 % of color due to the low stability of

the old PB-NPs in the textile (Figure 4.2.5b). It confirmed that freshly prepared PB-NPs in textiles were stable and reversible in solid state when monovalent cations were not present in the medium.
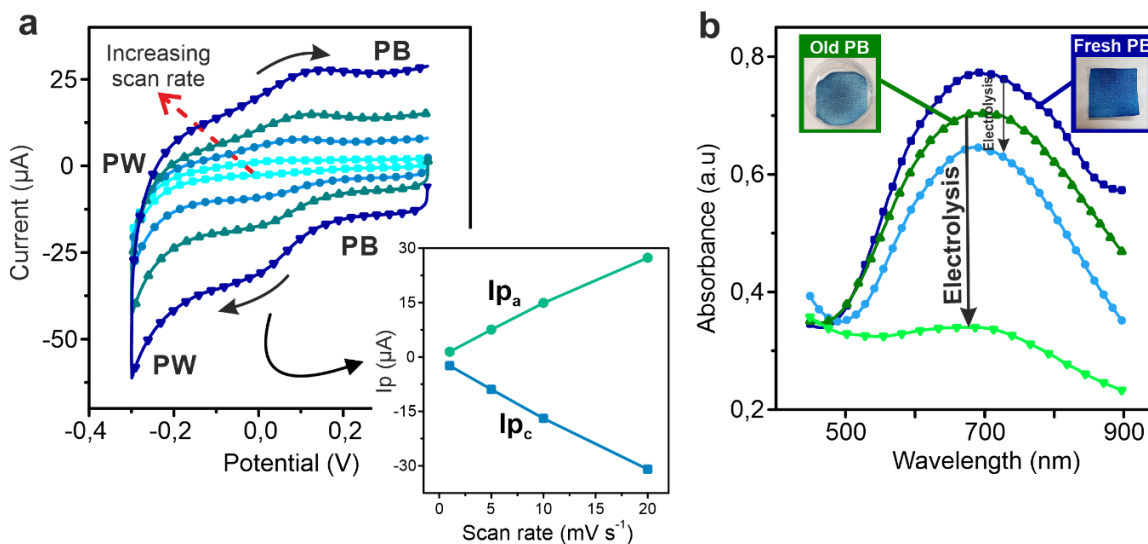

Figure 4.2.5. Spectroelectrochemical measurements on the modified textiles. a) Set-up scheme used for the spectroelectrochemical measurements on the textiles. b) CVs of PB-modified textiles developed between 0.4 and -0.3 V at different scan rates (1, 5, 10 and 20 mV s^{-1}) and representation of current peak values obtained vs scan rate. c) Comparative spectra obtained from textiles coated with PB$_{Ins}$ freshly prepared and PB$_{Ins}$ prepared 4 days before the coating process and corresponding spectra after apply -0.5 V during 15 min to each one of them.

4.2.1.1 Bacterial-sensing activity of the smart textiles modified with PB

As an already demonstrated metabolic bacterial indicator,[7] PB in the textile should confer it with bacterial-sensing activity through the mechanism illustrated in Figure 4.2.6. Once the sonochemical coating of PB-NPs provides the fabrics with an intense blue color, the attachment of live bacteria would change the smart fabric color by the metabolic reduction of PB to PW by proteins (e.g. cytochrome) and mediators (e.g. ubiquinone) from the bacterial electron transport chain.[8] Since the reaction is metabolic, dead bacteria would not be able to produce this change. If live bacteria died, for example by an antibacterial treatment, the atmospheric oxygen would re-oxidize PW to PB,[9] and the smart textile would recover its initial blue color.
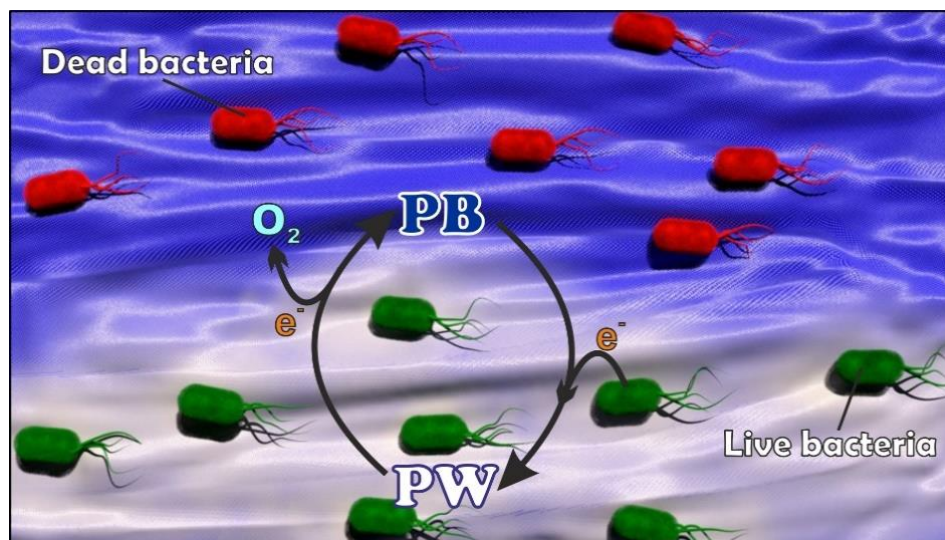
Figure 4.2.6. Scheme of the smart textile performance when in contact with live and dead bacteria. Living bacteria are represented in green color and the dead one in red.

Bacterial-sensing capacity of PB-coated textiles was evaluated spectroscopically (as the percentage of color change) in distilled H_2O, LB, PBS (at pH 6.2 and 7.2) and MES buffer (pH 6.2) containing *E. coli* concentrations between 10^8 and 10^9 CFU mL^{-1} (Figure 4.2.7a). Since bacterial proliferation depends on the medium composition, the evolution of this parameter over time was determined in each medium through plating (Figure 4.2.7b) and optical density measurements at 600 nm (Figure 4.2.7c).

All modified textiles presented important color changes over time, stronger than those observed in the stability studies with media without bacteria. Three different behaviors were observed depending on the solution composition. First, in LB, bacteria almost doubled the initial concentration in the sample during the experiment, enabling a fast metabolic reduction of PB resulting in a 60 % color loss after 72 h, being the largest reported. Second, in buffer, for either PBS or MES, bacterial concentration slightly decreased over time, which resulted in weaker color changes about 40-45 %. The higher color change observed in the PBS sample at pH 7.2 was again attributed to combination of metabolic reduction with the pH-mediated decomposition of PB. In fact, when set at the same pH, PBS and MES presented very similar color change kinetics, as well as analogous bacterial concentrations and bacterial proliferation rates. Finally, textiles incubated in distilled water presented an initial color loss of 30 %, followed by a fast color recovery by oxygen

re-oxidation when bacteria died (which was confirmed by cell counting). Therefore, these smart textiles were able to report on the presence/absence of living bacteria in real time thanks to its reversibility.
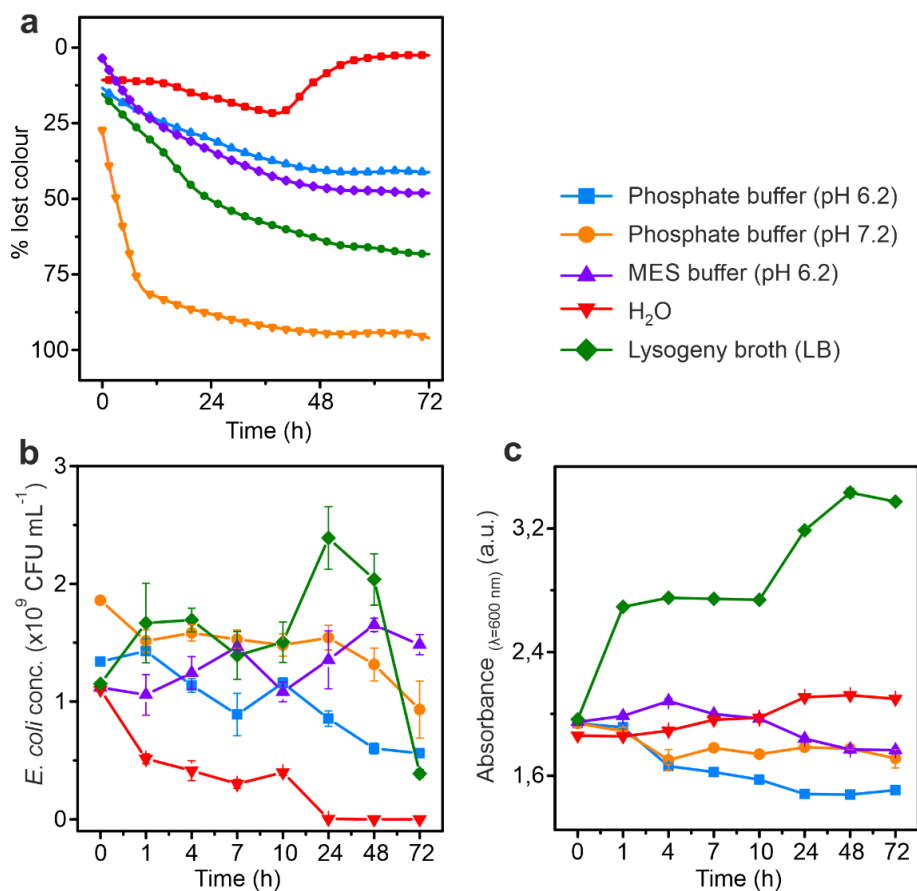

Figure 4.2.7. Relation between bacterial-sensing capacity of the textiles and bacterial proliferation. Different parameters obtained after PB-NPs modified textiles were incubated with *E. coli* for 72 hours, such as a) textile loss of color percentage; b) *E. coli* concentration by cell counting and c) absorbance values at 600 nm throughout the experiment. *E. coli* concentrations above 10^9 CFU mL^{-1} in 900 μL were incubated in different media (H$_2$O, LB, 0.1 M PBS (at pH 6.2 and 7.2) and 0.1 M MES (pH 6.2)) and 0.1% of glucose was used (n=3). A common legend for all the graphs is shown on the top.

To confirm that PB-NPs detected bacterial activity without affecting microbial structure and/or function, the antibacterial activity of the smart textiles was evaluated. Antibacterial activity was determined by incubation of the samples in *E. coli* suspensions in MES (pH 6.2) supplemented with 0.1 % glucose. Modified textiles, non-modified textiles (without PB-NPs) and control samples

(bacterial suspension without textile) were evaluated in compared in the study. The number of viable bacteria was represented as a survival percentage from the initial concentration (Figure 4.2.8a). No significant differences were observed between control, non-modified and modified textiles, confirming the low or null antibacterial activity of the PB-NPs in the textile.
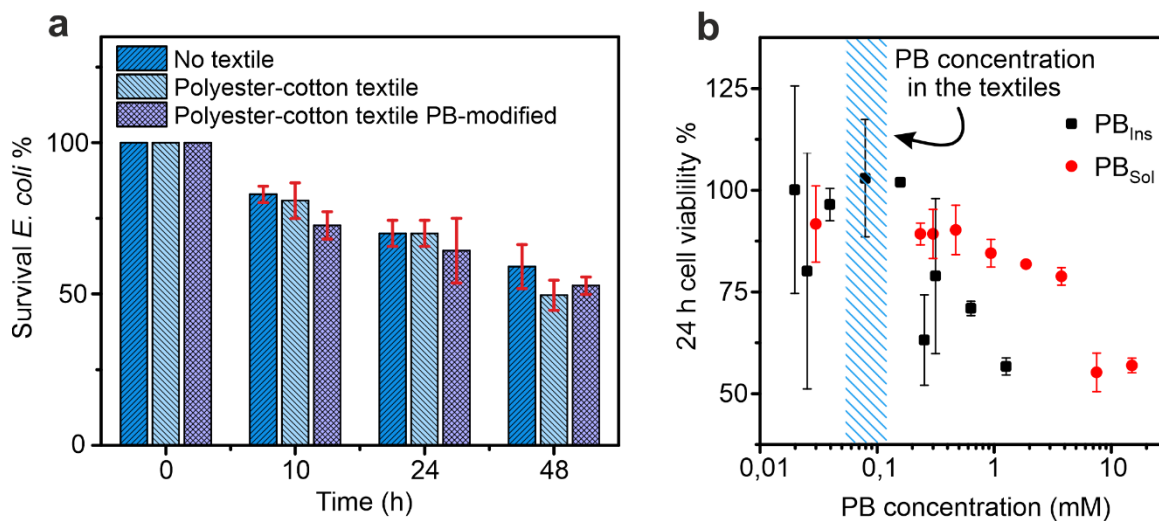

Figure 4.2.8. Antibacterial activity of PB-modified textiles and cytotoxicity. a) Survival percentage of *E. coli* measured at different incubation times for polyester-cotton textiles with and without PB in MES 0.1 M medium at pH 6.2 and with 0.1 % of glucose. As control, an inoculated solution in the same medium without textile sample was used (n=3). b) MTT cytotoxicity assay for PB_{Sol} (red circles) and PB_{Ins} (black squares) solutions at different concentrations. Concentrations are represented in a logarithmic scale and the one used in the textiles (0.08 mM PB) is highlighted in the graph with blue cross lines. Cell viability was determined after 24 hours of incubation with both solutions (n=3) and viability was expressed as percentage versus non-treated control samples.

On the other hand, because of the direct physical contact with skin, cytotoxicity assays of PB-NPs were performed to evaluate its potential risk for human health. Figure 4.2.8b shows that both, soluble and insoluble PB-NPs were cytotoxic when in high concentrations, with a decrease of the cell viability near to 50 %. However, the concentration implemented in the textiles was not cytotoxic and should not result in cytotoxic or inflammatory responses.

Finally, the capacity to detect different bacterial types was evaluated by comparing the response of the smart textile to the Gram-negative *E. coli* with the Gram-positive *S. aureus* bacteria. Experiments were performed in MES (pH 6.2) supplemented with 0.1% of glucose at bacterial concentrations of 10^7, 10^8 or 10^9 CFU mL^{-1}. Results are summarized in Figure 4.2.9. In

both cases, no detectable changes were observed in the control sample (without bacteria) or after 5 days of incubation in bacterial suspension with a concentration below 10^7 CFU mL^{-1}. Textiles incubated with 10^8 CFU mL^{-1} presented a small color change that was quickly reversed until it recovered the initial color. More pronounced and sustained changes were observed after incubation with 10^9 CFU mL^{-1}, which was even detectable with the bare eye after 6 h of incubation. The complete color lost required 48 h. In the case of *S. aureus*, the peptidoglycan layer typical in Gram-positive bacteria slows down the extracellular electron transfer to the PB-NPs [10], showing slower kinetics. After 90 hours, when most of bacteria in the sample were already dead due to nutrients depletion, the textiles started to recover their initial blue color through oxygen re-oxidation. The complete color recovery required a reaction with an oxidizing agent, i.e. hydrogen peroxide, as shown in the images, confirming the stability of PB-NPs in the textiles.
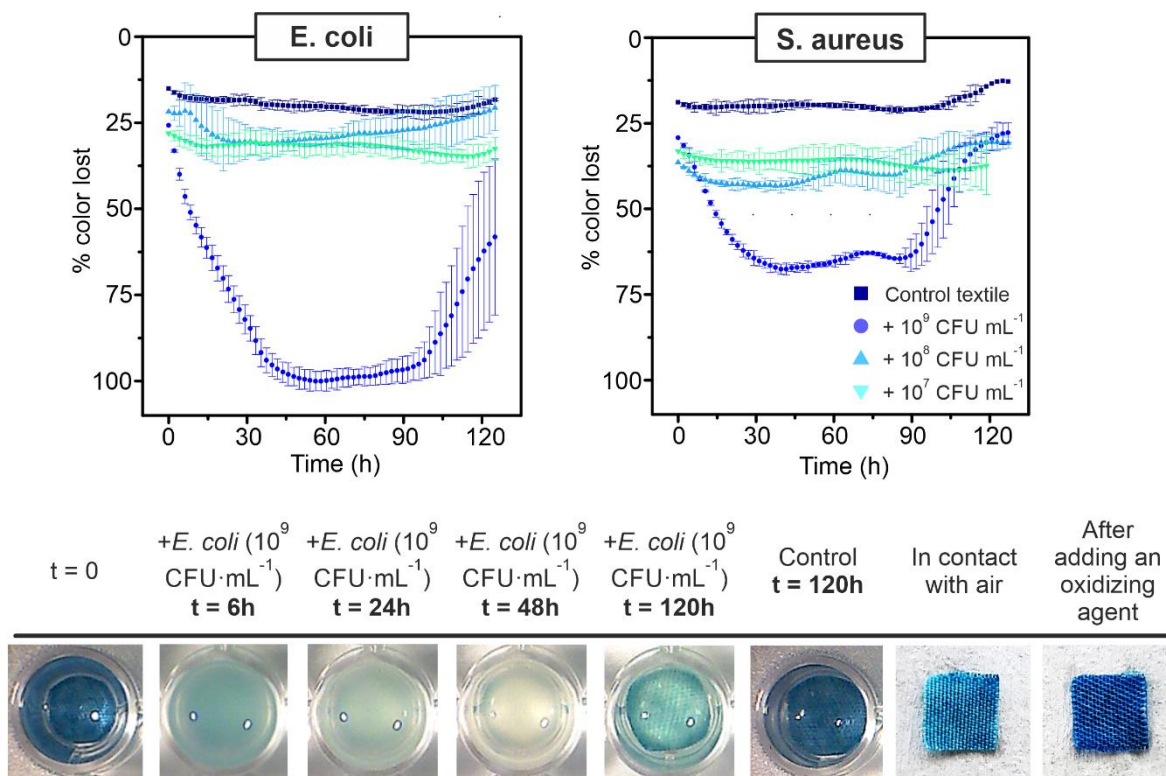

Figure 4.2.9. Bacterial-sensing activity of PB-modified textiles. Quantification of PB-modified textiles color loss after incubation with *E. coli* and *S. aureus* in MES medium (pH 6.2) and 0.1% of glucose. Bacteria concentrations are shown in a common legend. As control, PB-modified textiles were submerged in MES solution, without bacteria. Color loss was expressed as percentage versus unmodified-textiles color (n=3). In the schematic table, representative images from the textiles can be seen at different times of the experiment with *E. coli* inoculation, when they were in contact with air and after adding an oxidizing agent.

This technology is also implemented in textiles containing antibacterial NPs for the production of smart textiles with antibacterial and bacterial-sensing capacities to prevent bacterial infections. The characterization of these smart textiles, as well as their sensing and antibacterial activities are studied in the following sections.

4.2.2 Production of smart sensing and antibacterial textiles

The production of the smart textile was performed in two steps. First, antibacterial textiles were produced at Klopman facilities by incorporating CuO-NPs to the polyester-cotton fabrics with the ultrasonic coating equipment implemented in their production line. In a second step, the textiles were coated with PB-NPs through the sonochemical protocol described above, which took benefit of the cavitation phenomenon.

Figure 4.2.10shows images of the textile samples and individual fibers of pristine (Figure 4.2.10a and Figure 4.2.10b) and CuO-NPs-coated fabrics (Figure 4.2.10c and Figure 4.2.10d) before and after the coating with PB-NPs. It is clearly observed how the initially white cotton-polyester samples (Figure 4.2.10a) acquired an intense blue color (Figure 4.2.10b) after 15 minutes of sonication with freshly prepared 0.08 mM PB solutions. SEM images showed a dense coating of PB NPs on the fibers (total coverage > 95%), resulting in a strong and homogeneous textile coloration. Analogously, the coating of CuO-NPs-modified cotton-polyester textiles with PB-NP change their initial brownish color (Figure 4.2.10c) into deep blue (Figure 4.2.10d). PB-NPs distribution and aggregation was similar to that observed in the pristine samples, also presenting a high coverage percentage (coverage percentage > 95%). This result indicated that the initial presence of CuO-NPs did not affect the PB-NPs coating process.
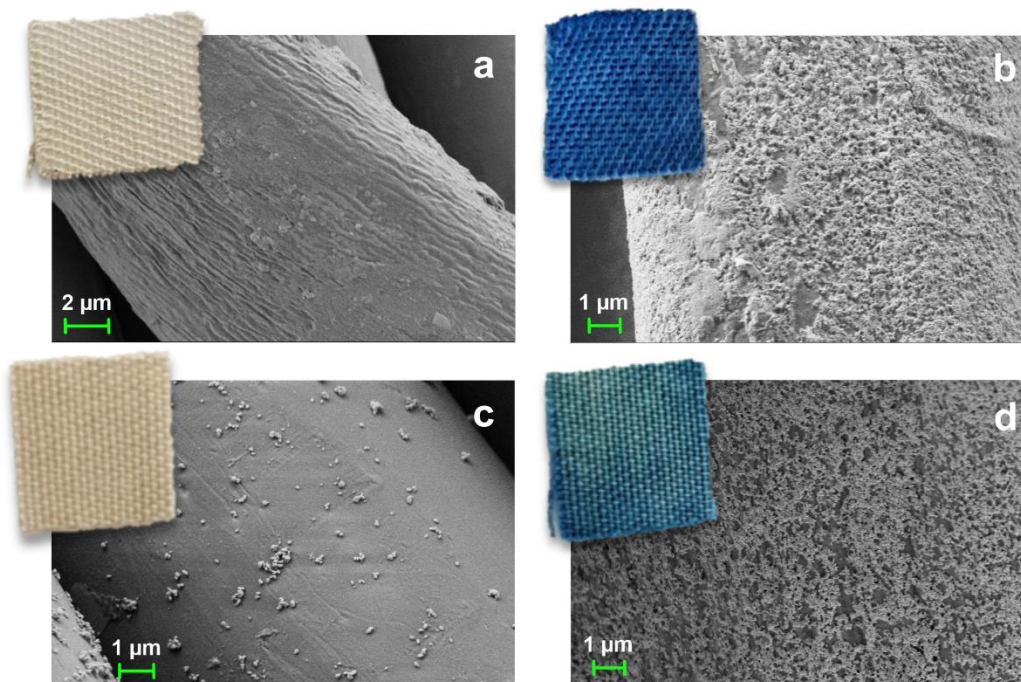
Figure 4.2.10. Fabrics and SEM images of a) polyester-cotton textile, b) polyester-cotton textile coated with PB-NPs, c) polyester-cotton textile coated with CuO-NPs, d) polyester-cotton textile coated with PB- and CuO-NPs.

The influence of the PB nano-coating on the stability and activity of the CuO-modified textiles was evaluated. Stability studies were conducted as illustrated in Figure 3.8 (in the Materials and Methods section). Briefly, CuO- and CuO/PB-modified samples were incubated with MES buffer for 24 h. The incubation solution was then split into two for further analysis. One aliquot was analyzed by ICP-OES to determine the amount of copper released from the textile to the medium during the incubation. The second one was incubated with *E. coli* (initial *E. coli* concentration in the medium = 10^8 CFU mL^{-1}) overnight (18-20 hours) at 37 °C to evaluate its antibacterial activity. Pristine non-modified cotton-polyester textiles were used as control samples in these studies. Textile samples only containing PB-NPs were also studied for completeness.

In the ICP-OES analysis, Cu was detected in the incubation solution of both CuO- and CuO/PB NPs-coated samples. The Cu^{2+} amount in the medium was, however, reduced to a half when the fabric was also coated with PB NPs, i.e. from 0.59 ± 0.04 mg/L for CuO samples to 0.34 ± 0.09 mg/L

for CuO/PB samples (Figure 4.2.11a). Apparently, the presence of PB nano-coating stabilized the CuO-NPs on the fabrics, reducing the copper release to the medium.
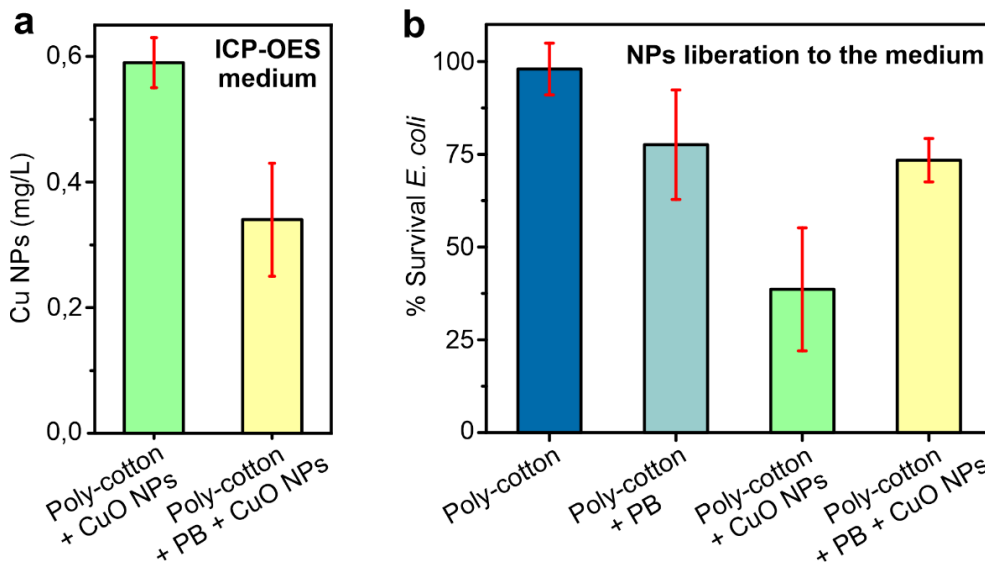

Figure 4.2.11. Cu NPs release to MES medium from sonochemically coated textiles. a) Amount of Cu^{2+} obtained from the ICP-OES analysis of the medium (n=3). b) Percentage of survived *E. coli* in the medium after 24 h incubation (n=3).

This effect was confirmed in the second experiment, where the medium containing Cu^{2+} released from the textiles was incubated overnight with *E. coli* suspensions. As shown in Figure 4.2.11b, the bacterial survival percentage was high (>75 % in average) for textiles only containing PB NPs or both PB/CuO NPs. Conversely, the survival percentage was much lower (40 % survival) for samples only containing CuO-NPs, which was in good agreement with the higher amounts of copper released to the medium and associated to a lower stability of CuO-NPs on the textile samples.

On the other hand, the antibacterial activity of the textiles was then evaluated according to ISO 20743:2021, as illustrated in Figure 4.2.12a. The ISO included a formula (Eq. 1 in Materials and Methods section) that enabled to classify the materials according to their antibacterial activity (A) in: i) significantly antibacterial, when providing A values between 2 and 3, and ii) strongly antibacterial when exceeding 4. Figure 4.2.12b shows the antibacterial values of the analyzed samples, i.e. pristine polyester-cotton textiles, textiles modified with CuO-NPs, with PB-NPs and

with both CuO/PB-NPs. The A value for non-modified polyester-cotton textiles used as control was close to 0, confirming that these materials did not present intrinsic antibacterial activity. Fabrics modified with PB NPs alone presented A values below 1, which suggested some antibacterial activity, probably due to the nano-size of the particles, although not enough to be considered significant. The two samples containing CuO NPs presented A values above 4, indicating a strong antibacterial activity. No significant differences were observed when comparing antibacterial activity of textiles containing only CuO NPs with those containing both CuO and PB NPs, indicating that the PB coating did not affect the antibacterial activity of the CuO NPs on the textile. Thus, the PB coating improved the performance of antibacterial textiles containing CuO NPs since increased the stability of CuO NPs in the textile, and its shelf-life, without compromising its bactericidal activity.
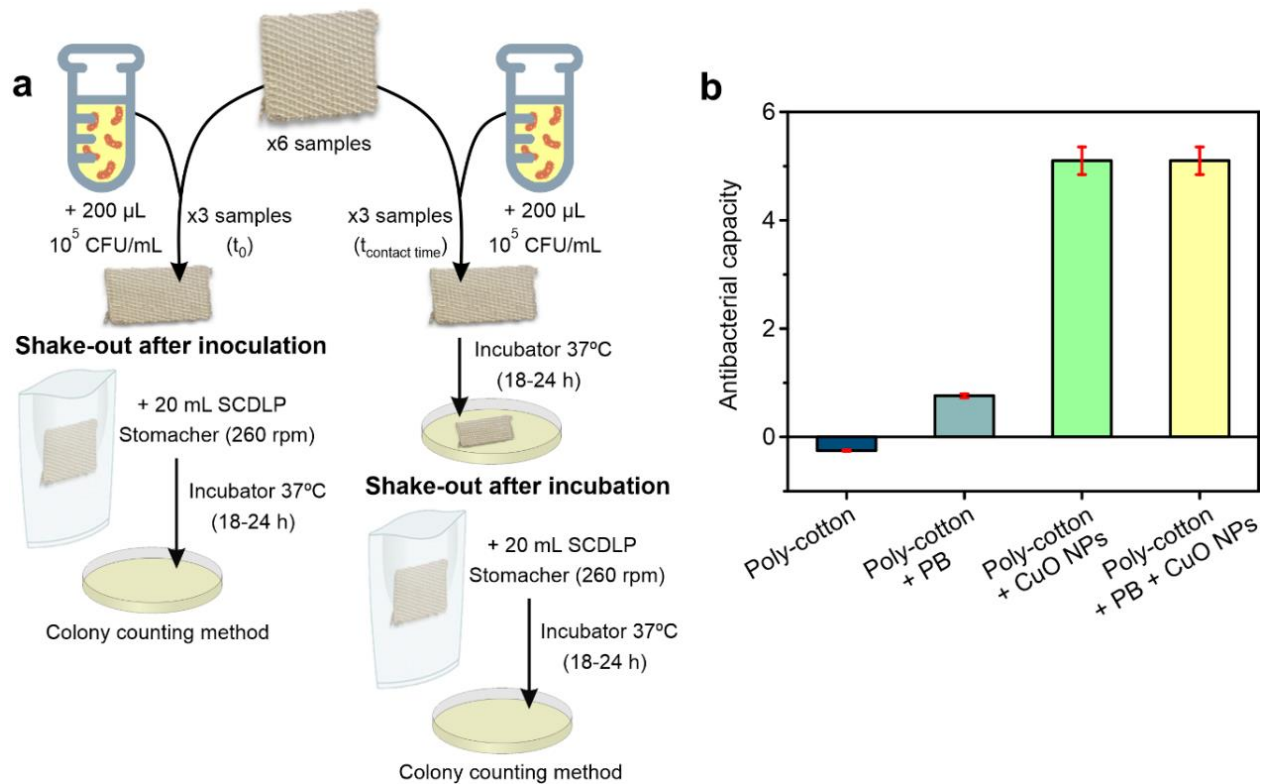

Figure 4.2.12. Antibacterial activity of the smart textiles. a) Scheme of the ISO 20743 procedure used for measuring the antibacterial capacity of the different types of textiles. As control, textiles with no antibacterial activity were used (n=3). b) Antibacterial capacity obtained when the ISO 20743 procedure was applied to the different types of textiles.

4.2.2.1 Electrochromic response and mechanisms of the smart textiles

The electrochromic properties of the PB-modified textiles were evaluated qualitatively by visual inspection after incubation of the textile with model chemical and microbiological redox agents. $NaBH_4$, H_2O_2 and *E. coli* were used as model reducing and oxidizing chemical agents, and reducing microorganism, respectively. Assays were performed with modified textiles containing either PB (shown in previous sections) or CuO/PB NPs for comparison. Results are presented in Figure 4.2.13, showing important differences between the chemical and the microbiological redox mechanism.
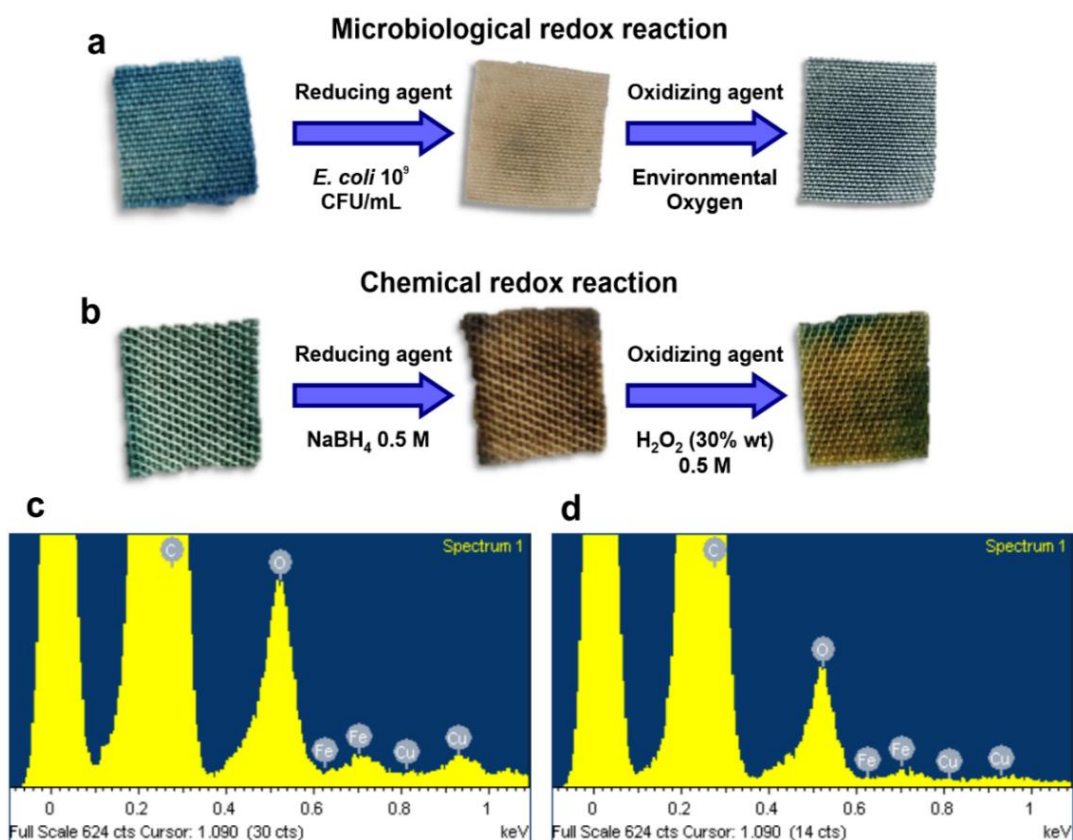

Figure 4.2.13. Smart textiles redox properties analysis. Samples pictures (containing PB- and CuO-NPs) after a) microbiological reduction with *E. coli* 10^9 CFUmL^{-1} and re-oxidation by environmental oxygen, and b) chemical redox reactions by addition of reducing ($NaBH_4$) and oxidizing (H_2O_2) agents. c) EDX spectrum of the textiles modified with PB- and CuO-NPs after reduction with $NaBH_4$ (10kV). d) EDX spectrum of the textiles modified with PB- and CuO-NPs after reduction with $NaBH_4$ and re-oxidation with H_2O_2 (10kV).

Microbiologically, living bacteria reduced PB to uncolored Prussian White (PW), producing the discoloration of the coated textile. The process required several hours and reverted spontaneously from PW to PB when bacteria died by the action of environmental oxygen (Figure 4.2.13a). Conversely, chemical reduction of PB-modified textiles with 0.5 M NaBH$_4$ resulted in immediate textile discoloration (Figure 4.2.13b). However, chemical re-oxidation with 30 % H$_2$O$_2$ did not revert to the initial state and part of the textile remained uncolored after incubation, even after long times. This lack of chemical reversibility of the immobilized PB could not be attributed to its dissolution or decomposition since the EDX analysis revealed the presence of comparable copper and iron amounts on the textile, the latter associated to PB, after NaBH$_4$ reduction (Figure 4.2.13c) and H$_2$O$_2$ re-oxidation (Figure 4.2.13d). Conversely, the irreversibility of the electrochromic system may be attributed to structural changes, which were studied through XAS at the Fe K-edge (around 7100 eV). This analysis provided information regarding the oxidative state and the coordination of the Fe atoms in the PB coating along the reduction/re-oxidation processes.

The X-ray absorption near edge structure (XANES) of the starting PB-modified textile is shown in Figure 4.2.14a, together with the spectrum of PB textile modified with CuO-NPs. The spectra of the soluble and the insoluble PB powders were also included for comprehension. In all cases, three main features were identified in the spectra: a pre-edge peak (A) around 7114 eV, a whiteline (B) around 7130 eV and another distinguished resonance (C) in the range between 7140 and 7150 eV. A great similarity of XAS spectra of soluble and insoluble PB compounds was clearly seen and it was in agreement with results reported by other authors.[12] Despite both forms of PB are insoluble, the term soluble is typically used to refer to how ease is the dispersion of the compound in an aqueous solution to form a colloidal suspension.[13] Structurally, their main difference is in the counterion compensating the remaining charge of PB iron complex, this being either potassium in soluble PB or ferric ions in the insoluble one.[14] The presence of alkali metal cations affected the global structure of the molecule, but no relevant differences were observed for what concerns to the local structure studied by XAS.
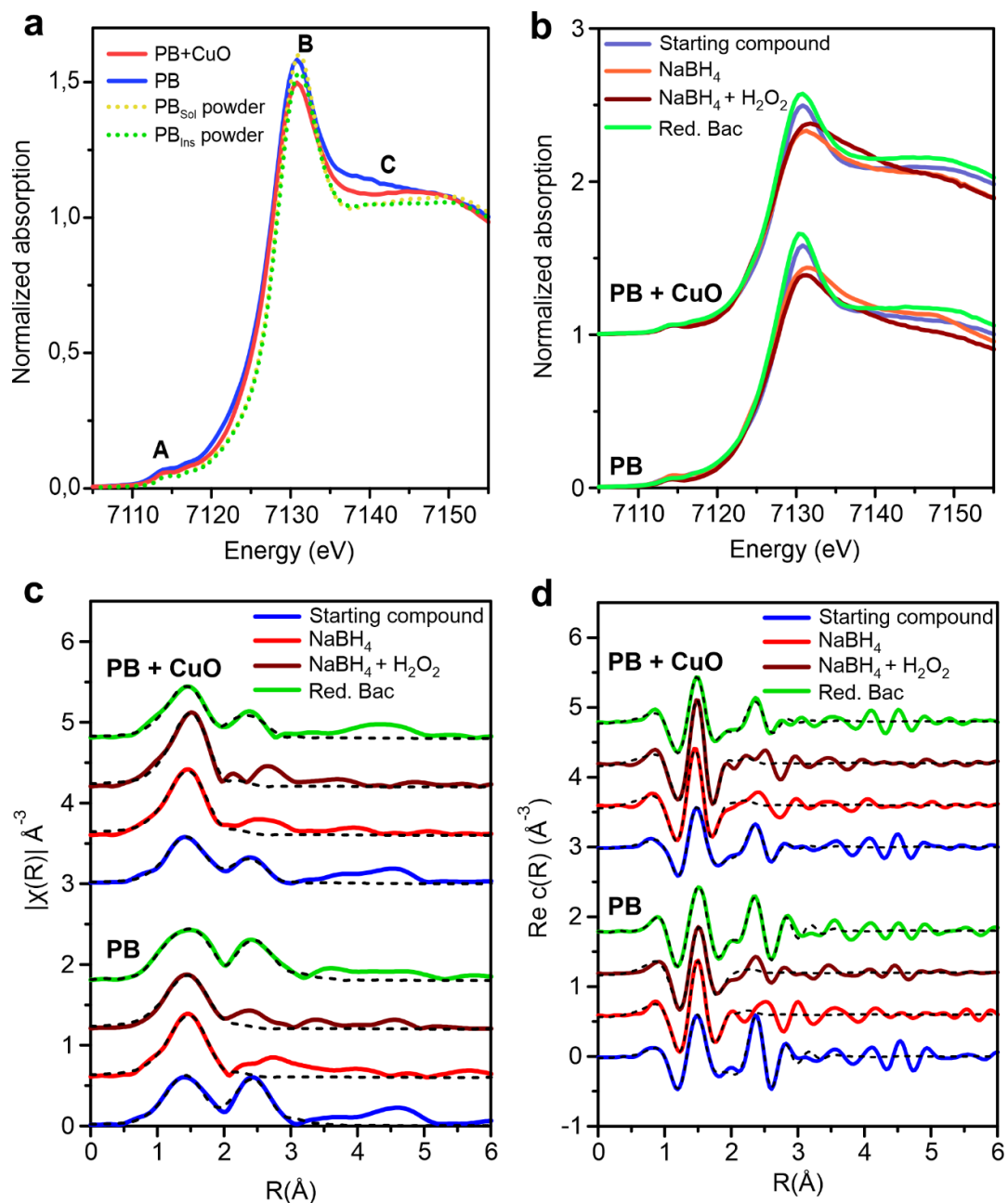
Figure 4.2.14. X-ray absorption spectra of the smart textiles. a) XANES spectra of soluble and insoluble PB powders and PB textile with and without CuO-NPs. b) XANES spectra of PB textiles with and without CuO-NPs after reduction with NaBH₄, re-oxidation with H₂O₂ and after reduction performed by bacteria. c) Fourier Transform moduli and (d) real part of $k^2\chi(k)$ signal obtained from EXAFS analysis. Data are represented by solid line and the fit by the dashed line.

The magnitude and shape of the pre-edge peaks were very similar in all samples. The low intensity of the pre-edge peak was consistent with the presence of Fe^{2+} and Fe^{3+} species in octahedral symmetry as reported in,[15] and concretely to weak 1s-3d electric quadrupole transitions. It is important to note here that 1s-3d transitions are electric-dipole forbidden unless there is a certain p-d orbital mixing, e.g. in tetrahedral or quite distorted structures.[16]

The edge position, taken as the maximum of the first derivative spectrum, was around 7129 eV for the soluble and insoluble PB powders, while it was slightly shifted towards lower energy values, i.e. 0.5 eV, for the textile samples. This result indicated the partial reduction of Fe^{3+} to Fe^{2+} in the textile. Another indication of the shifts towards lower oxidative states and energy values was observed in the whiteline position that shifted from 7131.1 eV to 7130.8 eV. Additionally, the soluble and insoluble PB powders presented a similar slope of the C feature in the region 7140-7150 eV, which differed from that obtained by the textile samples. The slope of this multiple scattering resonance was described to be sensitive to vacancies and/or a distortion of the Fe^{2+}–C–N–Fe^{3+} arrangement and its deviation from linearity,[12,17] confirming that the deposition on the textile altered the initial structure of the PB-NPs.

Figure 4.2.14b also incorporates the XANES spectra of the textiles after chemical reaction with $NaBH_4$ and H_2O_2, and microbiological reduction by bacteria. After reduction with $NaBH_4$, the absorption at 0.5 intensity of the PB-modified textile shifted towards lower energy values and the whiteline intensity decreased. The re-oxidation with H_2O_2 did not recover the original PB structure, and only minor changes were observed compared to the previous spectrum corresponding to $NaBH_4$ reduction. Conversely, microbiological reduction by bacteria produced XANES spectra very similar in shape to those obtained by the initial PB-modified textile. Main differences between them resided in the rising edge and the whiteline magnitude. Both parameters shifted by around 0.4 eV towards lower energy values, confirming the presence of slightly higher amounts of Fe^{2+} ions due to microbiological reduction. The small shift in magnitude indicated that bacteria were only reducing small amounts of Fe^{3+} to Fe^{2+}, while not affecting both the local structure of PB and the shape of the whole XANES spectra. Similar conclusions were obtained for textiles also incorporating CuO-NPs and treated in the same conditions, which confirmed that the presence of

the antibacterial particles did not interfere with the electron exchange between bacteria and PB molecules on the textile.

An analysis of the extended X-ray absorption fine structure (EXAFS) spectra was conducted in order to study the local changes around Fe^{3+}/Fe^{2+} ions after different reduction/oxidation processes. A multiple k-weight fit was performed in the k-range 3-10 Å^{-1} and R-range 1-3.1 Å and included in Figure 4.2.14c, Figure 4.2.14d and Table 4.2.1.

In previous studies, the local structure of Fe in PB was modelled considering several single scattering path, as well as intense multiple scattering paths.[13,18,19] The first shell was related to single scattering from Fe^{2+}–C and Fe^{3+}–N at distances around 1.9 and 2.0 Å, respectively. Instead, the main contribution used to model the second shell was a 3-leg path around 3.0 Å due to Fe^{2+}–C–N–Fe^{3+}, where the linear geometry made this contribution stronger than Fe–N and Fe–C single scattering paths at similar distance. In this study, only a maximum of three paths were considered to model the data due to the short k-range available. Despite C and N may not be distinguished in EXAFS for their similar scattering properties, the shorter bond of the first shell was referred as Fe–C and the longer one as Fe–N. The same Debye-Waller factor (σ^2) was imposed to these two scattering paths, following a procedure developed by other authors.[13]

As shown in Figure 4.2.14b, the first shell fit was performed considering a unique Fe–C/N bond distance and implementing the coordination number as a free parameter. The value obtained after fitting by the samples reduced with $NaBH_4$ was consistent with an octahedral coordination. On the other hand, the second shell was strongly reduced in intensity after chemical reduction. This strong decrease was a clear indication of the distortion or modification of the PB structure during chemical reduction, where the contribution from the multiple scattering path Fe^{2+}–C–N–Fe^{3+} was heavily attenuated. The structure of the starting textile was not recovered after chemical re-oxidation with H_2O_2, but the local structure around Fe ions remained similar to that after reduction with $NaBH_4$. This result was in agreement with XANES spectra analysis. Conversely, EXAFS spectra of PB-modified textiles after microbiological reduction were similar to those of the starting sample, maintaining clear features associated with the original PB structure. Thus, EXAFS analysis indicated that microbiological reduction of PB in textiles was not altering the

PB structure, confirming the XANES results. The presence of CuO-NPs on the textile did not modify the previous results significantly. Thus, textiles containing both CuO- and PB-NPs were structurally similar to those only containing PB-NPs, but with a larger disorder in second shell. This disorder was confirmed by the much higher Debye-Waller factor obtained with the samples containing both NPs. The changes reported after chemical and microbiological reduction/oxidation processes were in agreement with those discussed above in the case of textile without CuO-NPs, confirming that the presence of CuO-NPs did not affect the accessibility and reactivity of PB-NPs on the textile.

Table 4.2.1. Results of the EXAFS fit. *Deg* is the degeneracy of the scattering path (that corresponds to the coordination number for single scattering paths), *R* is the bond distance and σ^2 the Debye-Waller factor. The many body amplitude reduction factor S_0^2 was obtained from fitting the Fe foil and fixed to 0.8.

Sample	Shell	N/Deg	R (Å)	σ^2 (10^{-3} Å^2)
PB				
Starting compound	Fe-C	3	1.93 (2)	6 (2)
	Fe-N	3	2.04 (2)	6 (2)
	Fe-C-N	12	3.14 (3)	8 (1)
NaBH$_4$	Fe-C/N	7 (1)	1.98 (2)	12 (3)
NaBH$_4$ + H$_2$O$_2$	Fe-C/N	6 (1)	1.97 (1)	12 (3)
Reduced by bacteria	Fe-C	3	1.92 (2)	7 (3)
	Fe-N	3	2.11 (3)	7 (3)
	Fe-C-N	12	3.13 (3)	10 (2)
PB + CuO-NPs				
Starting compound	Fe-C	3	1.93 (2)	7 (2)
	Fe-N	3	2.10 (4)	7 (2)
	Fe-C-N	12	3.13 (3)	17 (2)
NaBH$_4$	Fe-C/N	6 (1)	1.98 (2)	12 (3)
NaBH$_4$ + H$_2$O$_2$	Fe-C/N	6 (1)	1.97 (1)	9 (2)
Reduced by bacteria	Fe-C	3	1.90 (2)	7 (4)
	Fe-N	3	2.05 (3)	7 (4)
	Fe-C-N	12	3.13 (3)	17 (2)

4.2.2.2 Smart textile response to bacterial colonization

The response of the smart textiles to bacteria was evaluated by incubation of the textile samples with *E. coli* suspensions containing 10^9, 10^8 and 10^7 CFU mL^{-1} in two different media, i.e. phosphate buffer (pH 7.2) and MES medium (pH 6.2). The experimental protocol consisted of three consecutive incubations of the sample with bacteria, each one lasting 72 h. After 72 h of incubation, the bacterial suspension was removed and refreshed to ensure high concentrations of living bacteria in contact with the textile. The number of living bacteria, both in suspension and on the textile surface, and the change of color of the textile associated to the metabolic reduction of PB-NPs were monitored over time. Concretely, the survival percentage in the medium was determined by collecting aliquots of the incubation sample, plating in agar and counting after overnight incubation. The survival percentage on the textile fibers was determined by confocal imaging, after staining with the live/dead dye. Images were acquired after each incubation process. Finally, the color change of the textiles was recorded with a microscopic camera acquiring images regularly for the duration of the experiment, and quantified using image analysis software.

Figure 4.2.15 shows the color changes associated with the metabolically-mediated reduction profiles at each experimental condition, as well as representative images of the smart textiles after incubation with 10^9 CFU mL^{-1} bacterial suspensions. It is worth mentioning that the textiles also containing CuO-NPs presented an initial brownish color before modification with PB, which influenced image acquisition and data analysis.
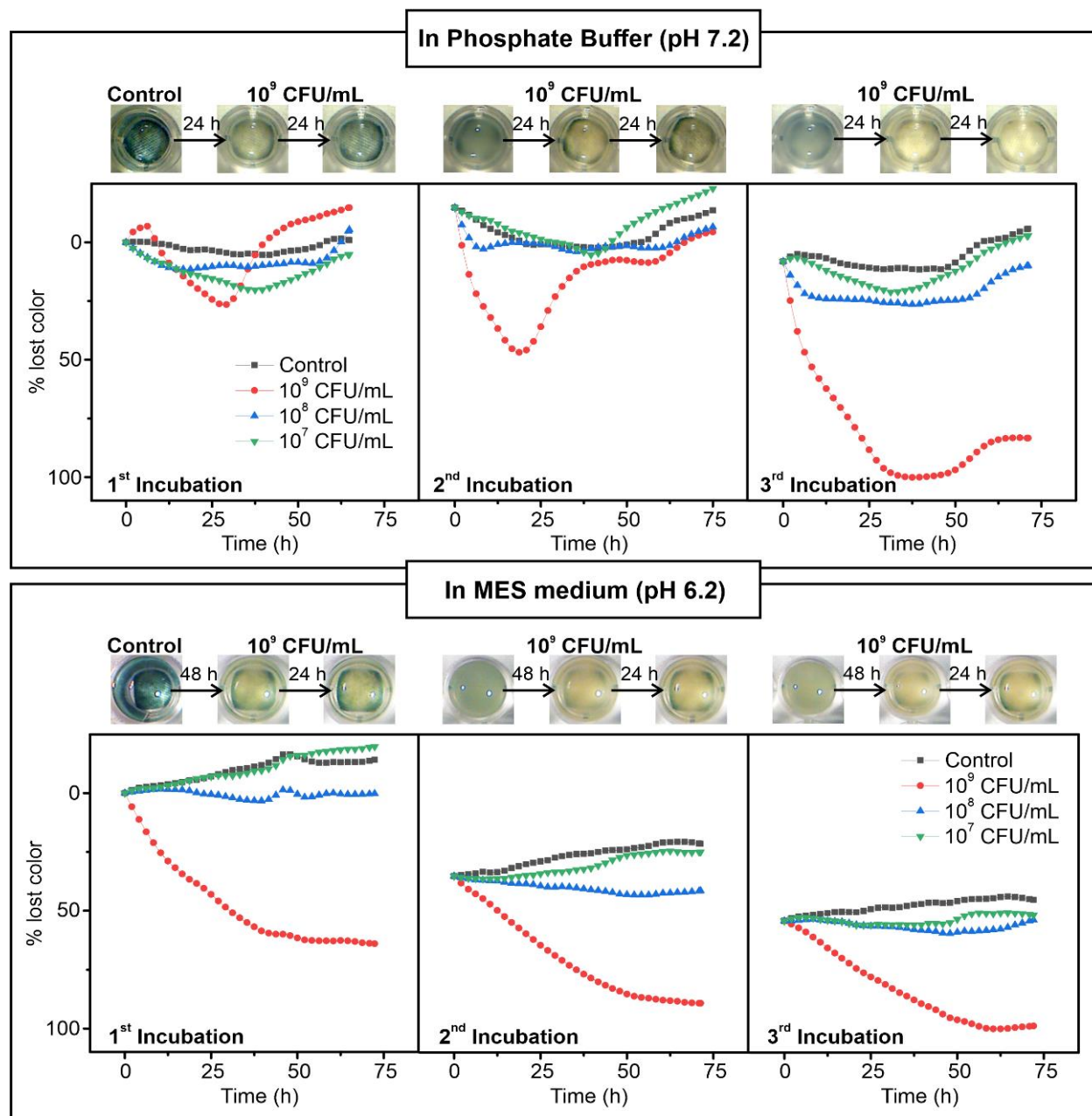
Figure 4.2.15. Sensing and antibacterial activities of the smart textiles. Color lost percentage of polyester-cotton textiles modified with PB- and CuO-NPs after three consecutive incubations of *E. coli* 10^9, 10^8 and 10^7 CFU mL^{-1}. The experiment was performed in two different media, phosphate buffer (pH 7.2) and MES medium (pH 6.2) and the images correspond to the smart textiles change of color upon contact with *E. coli* 10^9 CFU mL^{-1}.

During the first incubation in phosphate buffer, very small color changes were recorded by the three bacterial concentrations under study. Only the textiles incubated with the highest bacterial concentration (10^9 CFU mL^{-1}) presented an observable color change, distinguishable from the control, after 28 h of incubation (see pictures in Figure 4.2.15 top left). This small color change, corresponding to the loss of around 25 % of the initial color, may be associated to the presence of living bacteria on the textile surface that metabolically reduced PB to PW. Interestingly, after 50 h of incubation, all the samples recovered their initial blue color, probably by an oxygen-mediated re-oxidation of PW to PB produced once bacteria died. Confocal images of the textile samples after 72 h of incubation in phosphate buffer containing 10^9 CFU/mL *E. coli* revealed the attachment of high bacterial concentrations, covering more than 80 % of their surface (Figure 4.2.16). Around 47 % of the attached bacteria were dead, which is associated with the contact killing activity of the smart textile (Figure 4.2.17a), while the number of dead bacteria in the medium was much larger, reaching 99.7 % of the total (Figure 4.2.17b). This result was in agreement with the previous observation that large amounts of CuO-NPs were released from the textile to the medium, being the diffusion of CuO-NPs the main antibacterial mechanism followed in this case. A second important aspect to be considered is the enhanced resistance to CuO-NPs of attached bacteria. Even when the contact killing mechanism may be less efficient than the diffusion, bacteria attached to the textile surface would also be in contact with the released CuO-NPs. However, their sensitivity to these antibacterial agents was reduced by the extra protection provided by the biofilm-like structure that they were forming on the textile surface.[20] As a result, at high bacterial concentrations and in phosphate buffer (pH 7.2) containing glucose, the sensing capacity showed faster kinetics than the antibacterial one, and some metabolic reduction of PB produced by the live bacteria attached to the textile could be observed after short incubation times.
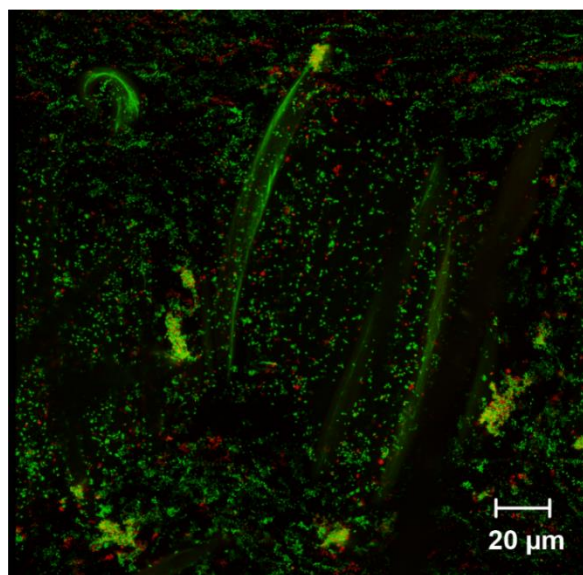
Figure 4.2.16. Live/dead bacteria image. Three-dimensional reconstruction of the confocal image of the smart textile incubated with *E. coli* (10^9 CFU mL^{-1}) in phosphate buffer (pH 7.2) after 72 h (first incubation step).
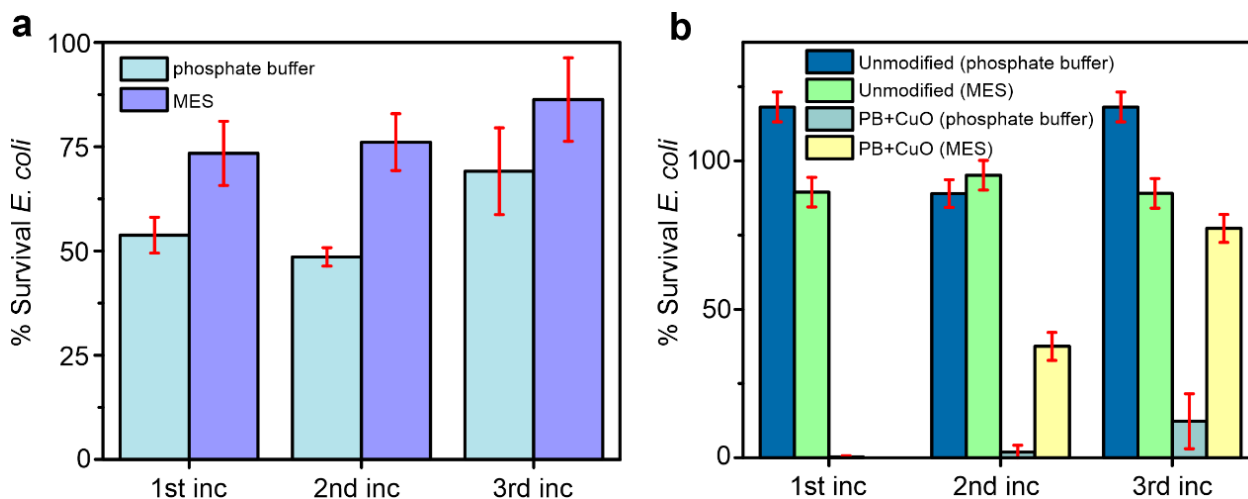

Figure 4.2.17. Live bacteria counts on the textile and in the medium. a) Survival E. coli percentage on the textile fibres obtained from confocal microscopy images (n=5). b) Survival E. coli percentage obtained on the medium (Phosphate buffer and MES) after being in contact with the non-modified textiles and textiles with PB- and CuO-NPs for 72 h during three incubation steps (n=2).

In the second incubation, the survival percentage of bacteria on the textile surface and in solution was very similar to that obtained in the first incubation (53 % vs 49 % on surface; 0.3 % vs. 1.9 % in solution). However, the color change for the 10^9 CFU mL^{-1} *E. coli* suspensions was faster and deeper, losing around 50 % of the initial color in less than 20 h. As before, after 24 h the textiles started to recover the blue color by oxygen re-oxidation, reaching 90 % recovery after 40 h. This difference may be attributed to a faster bacterial recruitment and attachment. It has been widely reported that during bacterial colonization of a surface, the recruitment of new bacteria is faster when a bacterial pre-layer is already present on that.[21,22] In this case, previous incubation resulted in the formation of a biofilm-like structure covering more than 80 % of the textile surface. The presence of this bacterial pre-layer accelerated the recruitment of new bacteria, accentuating the kinetic difference previously observed between the sensing and the antibacterial mechanisms, and resulting in a faster and deeper color change.

The antibacterial activity of the textiles decreased in the third incubation, with survival percentages of 69 % on the textile surface and 12 % in suspension. This was in agreement with colorimetric changes. Lower antibacterial activities resulted in larger color changes, being the first time that PB reduction was detectable in 10^8 CFU mL^{-1} sample. The color change produced by the 10^9 CFU mL^{-1} sample was also faster and deeper than in the previous incubation, and this time the textile did not recover the initial color after incubation, probably by the large number of living bacteria present on its surface.

In a second study, the response of the smart textile was evaluated in MES medium. The experimental protocol was identical than with phosphate buffer, with three consecutive incubations of 72 h. Main difference between media were: i) phosphate buffer (pH 7.2) provided a more physiological medium than MES (pH 6.2), which may benefit bacterial proliferation,[23] and ii) the lower pH of MES increased the stability of PB-NPs in the textile.[5]

The three incubation experiments in MES presented similar responses, with color changes only observed in the 10^9 CFU mL^{-1} sample. Along the 72 h of experiment (either during the first, second or third incubation), the textile was progressively losing color until stabilization around 50 h of incubation. In contrast with phosphate buffer experiments, textiles incubated with bacterial

suspension in MES did not recover their initial color during the experiment. The lack of recovery suggested the presence of high concentrations of living bacteria on the textile, which was confirmed by confocal microscopy. Confocal images showed high bacterial concentrations in both phosphate and MES experiments, but the bacterial survival percentage was much higher in the case of MES (73 % vs 53 % in the first incubation; 76 % vs. 49 % in the second incubation; 86 % vs. 69 % in the third incubation). This decrease in the contact killing efficiency may be associated to the lower stability of the antibacterial CuO-NPs on the textile when incubated in MES. This observation was in agreement with current bibliography, suggesting that the acidic pH of MES favored CuO-NPs release to the medium,[24] and with the studies of bacterial survival in the medium presented below.

As shown in Figure 4.2.17b, the amount of live bacteria in the medium was close to 0 (i.e. 0.03 %) after the first incubation, but rapidly increasing to 37.5 % in the second incubation, and 77 % in the third one. This result indicated that most antibacterial CuO-NPs were released to the medium during the first incubation, and only few remained on the textile, which responsible of the low antibacterial activity of the material. However, it was not a problem in this application of the smart textile, since this lack of antibacterial activity resulted in deeper color changes indicating the presence of living bacteria in the textile and the potential risk of infection of this bacterial contaminated surface.

The full activity of the textile in the prevention of nosocomial infection resulting from the contact with contaminated surfaces is summarized in Figure 4.2.18. On the one hand, the smart textile responds to microbial colonization by killing bacteria through two mechanisms, namely i) contact killing of attached bacteria, and ii) diffusion of released antibacterial particles. The efficiency of these mechanisms depends on the physic-chemical characteristics of the medium and the experimental conditions, which determine the stability of the antibacterial NPs on the textile. When the material is losing antibacterial efficiency, a second mechanism is activated in the smart textile, which changes of color in response to the presence of living bacteria. This second mechanism is based on the capacity of bacteria to metabolize PB reducing it to colorless PW. This change of color is then informing on the bacterial colonization of the textile surface and its potential infectiveness,

141

and thus, on the need for its removal and/or disinfection. This dual mechanism may contribute to reduce bacterial infection risk in sensitive environments, such as hospitals, schools or healthcare centers, among others.
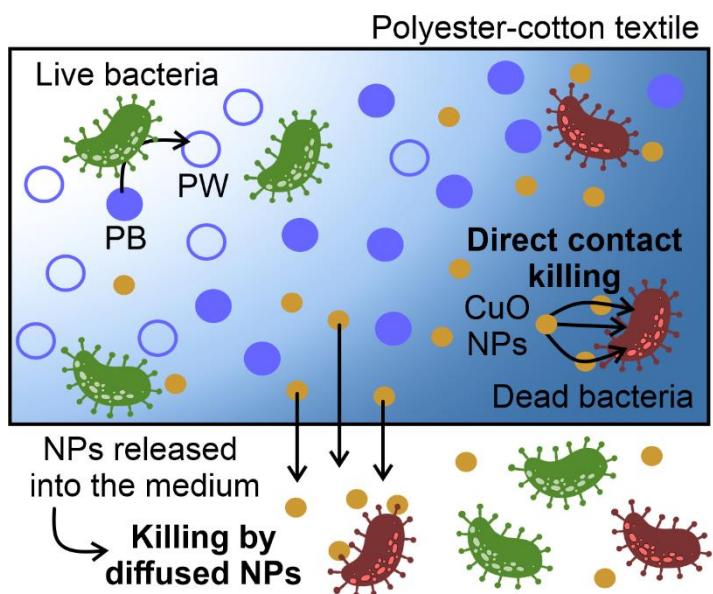

Figure 4.2.18. Smart textiles antibacterial mechanisms. Antibacterial mechanisms scheme of the smart textiles: by direct contact killing on the textile surface and by CuO-NPs release to the medium. Live and dead bacteria are represented in green and red colors, respectively. PB- and PW-NPs are represented respectively by blue and white circles and CuO-NPs by yellow ones.

However, the efficient implementation of this technology in real environments requires additional analysis, e.g. evaluation of the response in dry conditions, and improvements to enhance the sensitivity of the material, making it responsive to smaller bacterial concentration after shorter incubation times. These drawbacks were improved by testing alternative methods for the modification of the textiles, e.g. cyanotype method, which is presented below.

4.2.3 Production of cyanotype-based smart textiles

The cyanotype process was invented by Herschel in 1842, and since then it has been widely used in many paintings and photographic processes due to its dark and intense blue color (Figure 4.2.19).[25] Cyanotype is a photocatalytic process in which, UV light is used to photoactivate ammonium ferric citrate, which reacts with ferricyanide to produce PB and its characteristic blue color.[26]


Figure 4.2.19. Example of a cyanotype impression (by Rachel E. Church, 2019).

In this case, PB was synthetized directly on the textiles. During the synthesis, UV irradiation causes a photochemical redox reaction in the ferric ammonium citrate complex, whereby the iron (III) is reduced to iron (II) and the citrate is oxidized initially to acetone dicarboxylic acid,[27] as shown in equation (4.2.1):

$$2\ Fe^{3+} + C(OH)COOH(CH_2COOH)_2 \xrightarrow{h\nu} 2\ Fe^{2+} + CO(CH_2COOH)_2 + CO_2 + 2H^+ \qquad (4.2.1)$$
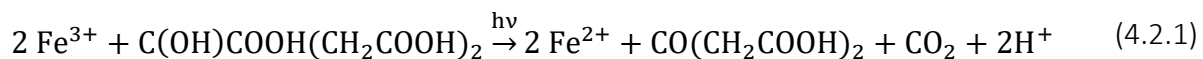
Then, according to the equation (4.2.2), the iron (II) couples with the ferricyanide to precipitate PB, producing an intense blue color on the substrate.

$$Fe^{2+} + [Fe^{III}(CN)_6]^{3-} \rightarrow Fe^{III}[Fe^{II}(CN)_6]^- \qquad (4.2.2)$$
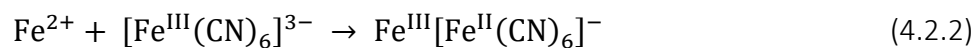
Thus, polyester-cotton samples (3 x 3 cm) were immersed in the solution containing ammonium iron citrate and ferricyanide. Then, samples were dried for 30 min and irradiated with UV light for different times from 30 s to 3 min. Finally, samples were washed with acidified water to remove impurities. In all conditions, samples with high homogeneity and color intensity were obtained, as shown in Figure 4.2.20.
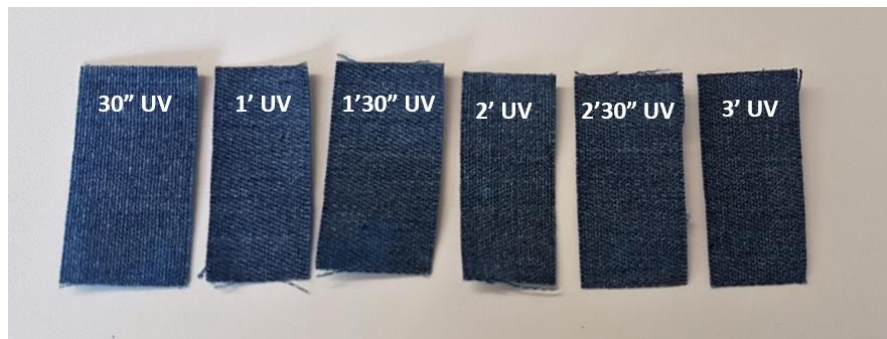

Figure 4.2.20. Different UV light irradiation times of the cyanotype process. Polyester-cotton textiles modified with PB by varying the UV irradiation time from 30 s to 3 min.

In an analogous procedure, polyester-cotton samples with sonochemically coated CuO-NPs were modified with PB by cyanotype process, endowing the textiles with both, sensing and antibacterial properties. SEM images were taken to characterize the obtained samples: textiles only containing PB-NPs and textiles modified with both PB and CuO-NPs (Figure 4.2.21).
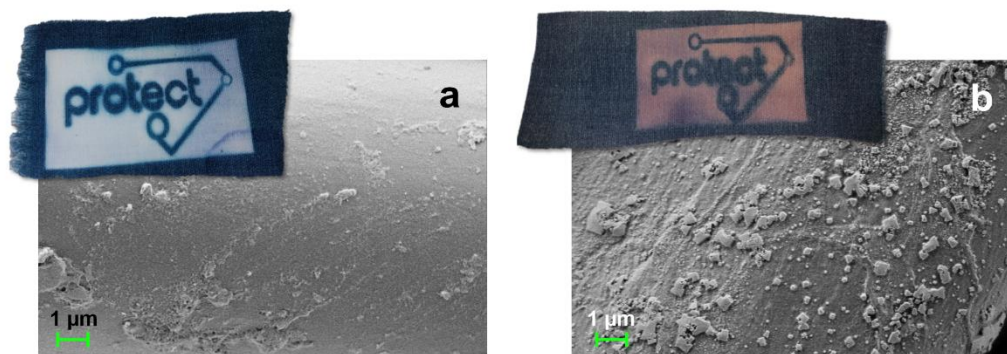

Figure 4.2.21. Cyanotyping fabrics and SEM images of a) polyester-cotton textile coated with PB by cyanotype, b) polyester-cotton textile coated first sonochemically with CuO-NPs and then with PB by cyanotype method.

In both cases, the particles distribution was homogeneous, covering most of the surface of the fibers. Compared to the sonochemical coating, the PB particles synthetized by cyanotype modification showed cubic structures adhered to the fibers. In Figure 4.2.21b, both types of particles could be easily differentiated. While PB presented cubic structures with an approximated area between 0.25 - 0.5 μm^2, CuO-NPs had spherical shape and the covered area was much smaller.

Cyanotype modification presented two main advantages compared to sonochemical coating. First, as observed in Figure 4.2.21, this coating protocol was compatible with photolithography and thus, with the use of masks, it was possible to produce patterns by only modifying selected areas of the textile. Second, the PB modification is produced on the surface of the textile (i.e. superficial) and as shown in Figure 4.2.20, the penetration of the light and thus the thickness of the PB layer could be adjusted by varying the UV irradiation time. This fact was highly decisive in the bacterial-sensing response of the textile, since a thinner and superficial layer of PB may be metabolized faster by bacteria, producing color changes in shorter incubation times than those obtained with sonochemically coated textiles where PB-NPs were distributed throughout the entire sample thickness. Due to their homogeneity, color intensity and low thickness of the PB layer, 30 s of UV light radiation were selected as the optimal textile production conditions and used in further experiments.

The electrochromic behavior of PB-modified textiles was tested chemically with a protocol completely analogous to the one used with sonochemically-coated textiles. That is, textile samples were immersed into a solution containing 0.5 M $NaBH_4$ as reducing agent and then, into a solution with 0.5M H_2O_2 as oxidizing agent. Pictures of the textiles after these processes are showed in Figure 4.2.22a and Figure 4.2.22b for textiles only containing PB and textiles with PB and CuO-NPs, respectively.
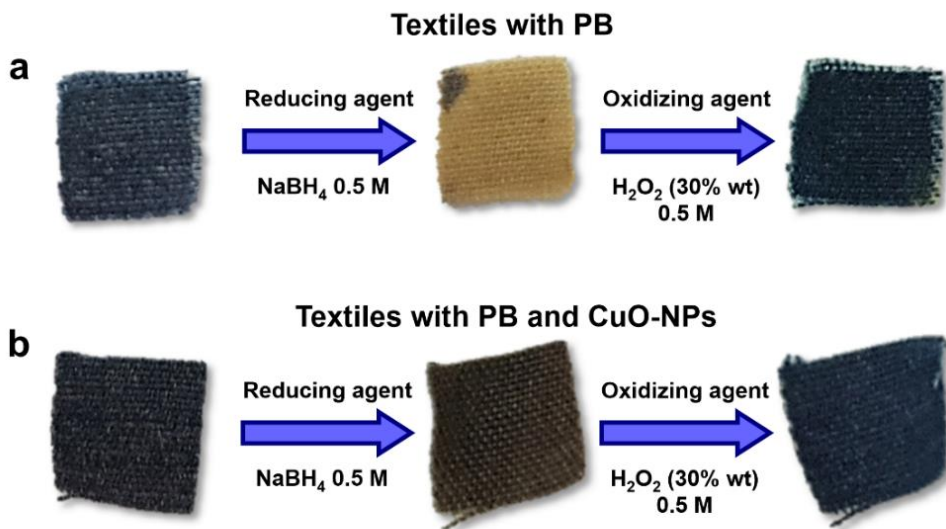
Figure 4.2.22. Smart cyanotyping textiles redox analysis. Samples pictures obtained with chemical redox reactions by addition of reducing (NaBH$_4$) and oxidizing (H$_2$O$_2$) agents for samples containing a) PB and b) PB- and CuO-NPs.

After addition of the reducing agent, modified textiles lost their blue color instantaneously, by the reduction of PB to PW. In the case of the samples modified with both, PB and CuO-NPs, the color change was also produced, but this time the change of color was less evident than with textiles only with PB due to the brownish color of the CuO-NPs. Then, in contrast to the sonochemical coated samples, the addition of H$_2$O$_2$ resulted in the full recovery of the initial blue color. This fact confirmed the higher structural stability of the PB particles synthetized by cyanotype method compared to those sonochemically produced.

These electrochromic properties of the smart textiles were evaluated in the presence of bacteria, to determine their bacterial-sensing activity after PB-modification through cyanotype process.

4.2.3.1 Bacterial-sensing capacity of the smart textiles

In a preliminary experiment, the bacterial-sensing capacity of textiles modified through cyanotype process was evaluated against the Gram-negative bacteria *E. coli* and the Gram-positive bacteria *S. aureus* in liquid media. For that purpose, PB-modified textiles were incubated with bacterial suspensions of 10^8 CFU mL^{-1} in LB broth media at 37 °C. Textile samples provided detectable color changes in less than 2 h and the complete color disappearance was achieved after 9 h of incubation for both types of bacteria (Figure 4.2.23).
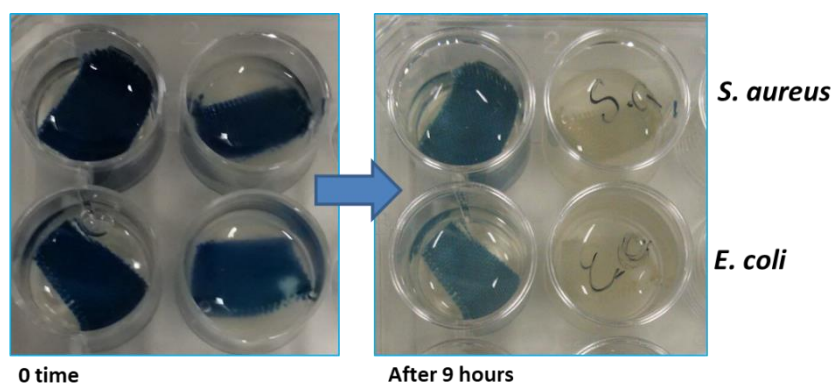

Figure 4.2.23. Bacterial-sensing capacity of the smart textiles in liquid medium. Pictures of PB-modified textiles after 9 h incubated in a LB nutrient media containing *E. coli* and *S. aureus* suspensions of 10^8 CFU mL^{-1}.

In a second experiment, the bacterial-sensing capacity of the PB-modified textiles was tested in dry conditions by optical inspection. Thus, polyester-cotton textile samples (1 x 1 cm) modified with PB through cyanotype method were placed in independent LB agar Petri dishes. Then, 100 µL of *E. coli* suspensions from 10^2 to 10^8 CFU mL^{-1} in MH medium were added to each textile sample. MH medium without bacteria was used as control. Then, the plates were introduced in an incubator and kept at 37 °C for the duration of the experiment. Textile images were acquired every 10 min with a micro camera during 24 h. The bacterial-sensing capacity was evaluated by calculating the percentage of color lost on the textiles, taking as the 100 % the initial color of the polyester-cotton textile samples without modification. The experiment was repeated three times and results were expressed with their standard deviations. The resulting graph and pictures of the textiles after 24 h of incubation are shown in Figure 4.2.24. The legend shows the real amount of

147

bacteria present on the textiles surface, which was calculated after plating and counting the initial bacterial samples.
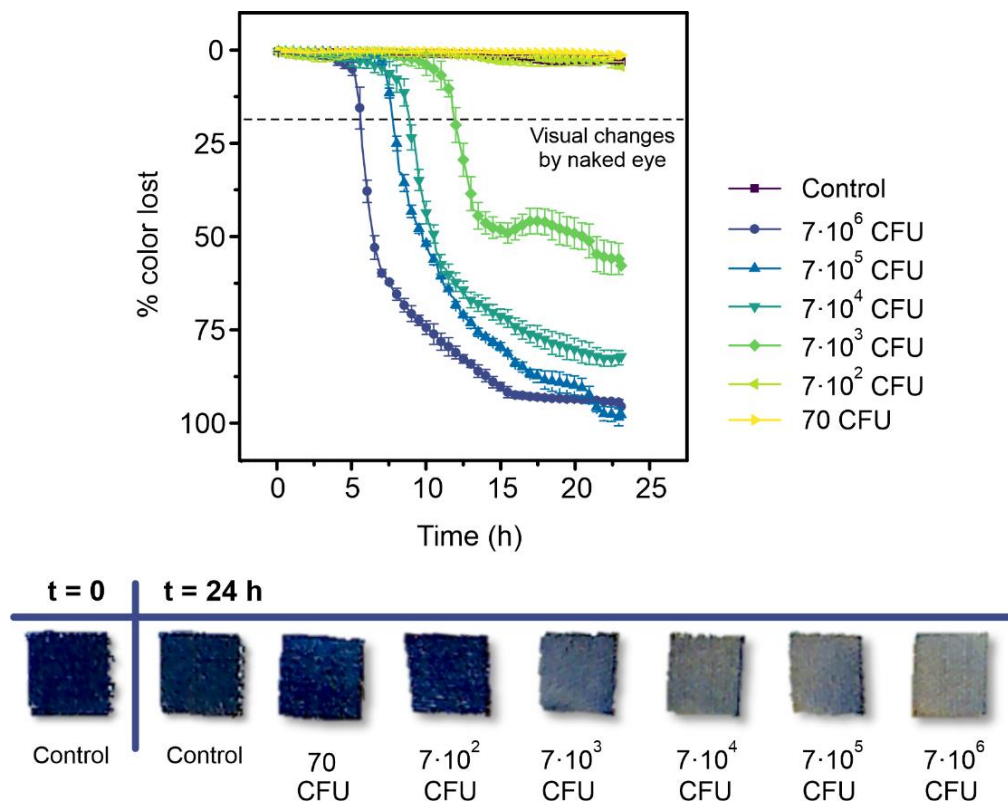

Figure 4.2.24. Bacterial-sensing activity of PB-modified textiles by cyanotype method. Quantification of PB-modified textiles color loss after being in contact with 100 μL of different concentrations of *E. coli* (from 10^2 to 10^7 CFU mL^{-1}) in MH medium (pH 6.2), placed in agar plates. Final amounts of bacteria on the textiles are shown the legend. As control, 100 μL of MH medium without bacteria were added to PB-modified textiles. Color loss was expressed as percentage versus unmodified-textiles color (n=3). In the schematic table, representative images from the textiles can be seen after 24 h of the experiment.

The color of the control samples remained constant along the experiment. Similarly, textiles in contact with 70 and 700 CFU also showed no detectable changes during the incubation time. It is important to remark, however, that both samples changed of color when increasing the incubation time the incubation time beyond 24 h, indicating that it may be possible to detect very low bacterial concentrations with the cyanotype-based textile.

Textiles in contact with bacterial samples above 10^2 CFU showed important color changes detectable with the bare eye after less than 15 h of incubation. Concretely, suspensions containing

$7 \cdot 10^3$ CFU produced an observable change after 12 h and for those containing $7 \cdot 10^6$ CFU it was visually detected in less than 6 h. Therefore, the detection time was shorter for higher bacterial concentrations. Thus, color changes with these samples were significantly faster than with those sonochemically probably due to the smaller thickness of the PB layer.

4.2.3.2 Smart biocide/bacterial sensing cyanotype-based textiles

Finally, the PB influence on the antibacterial activity and the stability of the antibacterial NPs on the smart textiles produced by the cyanotype method was evaluated with an analogous experiment to that performed with the textiles sonochemically coated. Thus, cyanotype textile samples were incubated in MES medium for 24 h and the solution was divided in two parts. One aliquot was analyzed by ICP-OES to determine the amount of Cu released form the textiles to the medium and the other was incubated with *E. coli* (initial *E. coli* concentration in the medium = 10^8 CFU mL^{-1}) overnight (18-20 hours) at 37 °C to evaluate its antibacterial activity. As in the previous case, textiles without any treatment were used as control samples.

The ICP-OES analysis of the medium revealed that Cu was released in both, textiles only containing CuO-NPs and PB/CuO-NPs (Figure 4.2.25a). As observed with the sonochemically coated samples, the amount of Cu^{2+} in the medium was much smaller when the textile was also modified with PB-NPs. However, with cyanotype method, the difference was even higher, reducing the amount of Cu almost five times when comparing with the textiles only modified with CuO-NPs, i.e., from 0.59 ± 0.04 mg L^{-1} to 0.13 ± 0.07 mg L^{-1}. This data confirmed that the textile modification with PB through the cyanotype method stabilize the CuO-NPs on the fabrics even more than when modified by sonochemical coating.
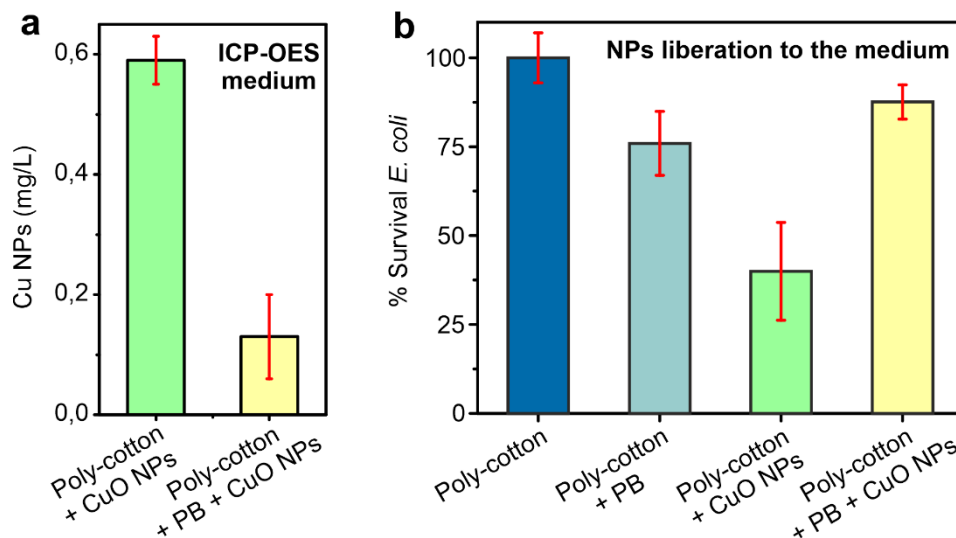
Figure 4.2.25. Cu NPs release to MES medium from cyanotype textiles. a) Amount of Cu^{2+} obtained from the ICP-OES analysis of the medium (n=3). b) Percentage of survived *E. coli* in the medium after 24 h incubation (n=3).

In a second experiment, the MES medium with the Cu^{2+} released from the textiles was was incubated overnight with *E. coli* suspensions. Accordingly to the previous experiment, the bacterial survival percentage for textiles modified with PB and CuO-NPs showed in Figure 4.2.25b was even higher than the obtained for the sonochemical coating process (almost 90 %), which confirmed the higher stability of this process. This fact indicates that probably, the main antimicrobial mechanism performed for this smart textiles is by direct contact killing, since most of the CuO-NPs remained in the textile fibers.

The antibacterial capacity of the smart textiles was evaluated after incubation of *E. coli* 10^8 CFU mL^{-1} in MES medium (pH 6.2) for 48 h with the textiles modified with PB, CuO-NPs and both, PB and CuO-NPs. Aliquots of the medium were taken at different times (7, 24 and 48 h) and plated on agar plates for cell counting. The percentage of *E. coli* survival was calculated by comparison with the *E. coli* concentration at the beginning of the experiment. Polyester-cotton textiles without any treatment were used as control samples. The results are illustrated in Figure 4.2.26.
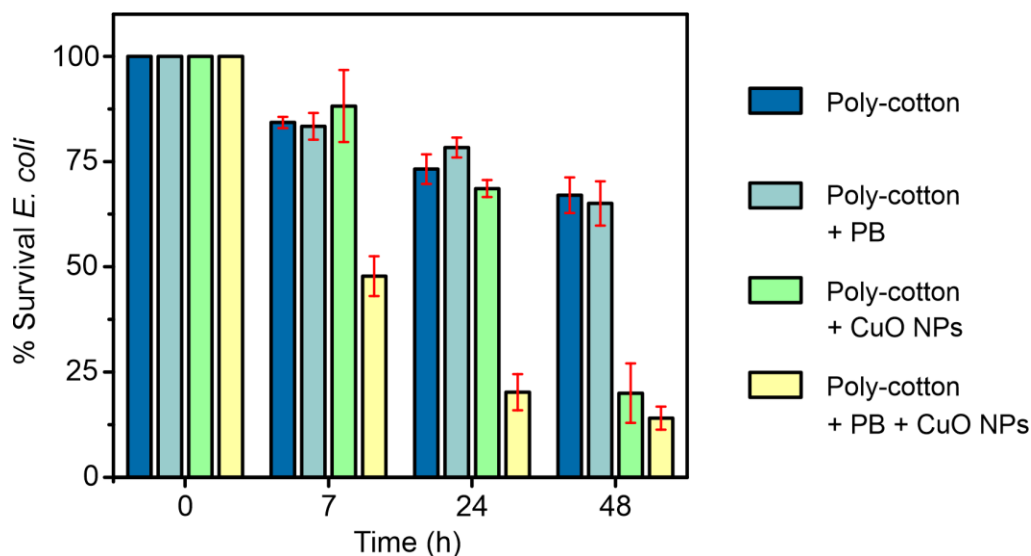
Figure 4.2.26. Antibacterial activity of the cyanotype-modified smart textiles. Percentage of survival *E. coli* after incubation with an *E. coli* suspension of 10^8 CFU mL^{-1} for 24 h. Live bacteria in the medium was counted at different times: 7, 24 and 48 h (n = 3). The percentage of survival *E. coli* was calculated by comparison with the initial concentration of bacteria.

Samples only containing PB-NPs showed low or null antibacterial activities, very similar to those obtained by the controls. On the other hand, samples containing CuO-NPs or both PB and CuO-NPs presented biocide activity, as expected by the presence of CuO, but with different antimicrobial kinetics. That is, the presence of PB-NPs increased the antimicrobial kinetics, being able to record bactericidal activities after only 7 h of incubation, while samples only containing CuO-NPs required more than 24 h to provide bactericidal activities significantly different than the control samples. After 48 h of incubation, both samples with CuO and PB/CuO presented a quite similar bactericide activity. From this experiment, it can be concluded that the PB-modification by cyanotype process accelerated the antibacterial capacity of the smart textiles, which may be associated to a synergistic effect of both NPs associated to inner redox processes between NPs and or to geometrical factors, such as an increase in the surface area or a higher attraction to bacteria by the surface charge of PB. The exact mechanism is still under discussion.

4.2.4 Conclusions

To prevent HAIs risks, a smart hospital fabric able to detect the presence of living bacteria by changing its own color is developed here based on the incorporation of PB-sensing NPs by two technologies, i.e., sonochemical coating and cyanotype process. In the first case, only freshly-prepared PB$_{Ins}$-NPs can be sonochemically incorporated in textile with sufficient concentration and homogeneity for bacterial sensing. Optimal conditions require sonication of 0.08 mM PB-NPs for 15 minutes in a single-step ultrasonic process. PB-NPs in the textile are not antibacterial or cytotoxic, and maintain the bacterial-sensing capacity reported in solution both for Gram-positive and Gram-negative bacteria. In the latter case, a detectable color change is observed after 5-6 hours of incubation in high bacterial concentrations (10^9 CFU mL^{-1}), with a total color change after 40 hours. The textile recovers the color when bacteria die by re-oxidation mediated by environmental oxygen. Thus, these smart textiles allow the detection of live bacteria in situ, which are even detectable with the naked eye. In addition, smart textiles with bactericidal and bacterial-sensing capacities have been developed. Sonochemical coating of polyester-cotton textiles with CuO- and PB-NPs resulted in a homogeneous distribution of both NPs, covering more than 95 % of the textile surface. Furthermore, the ICP-OES study revealed that the amount of CuO-NPs released to the media was reduced to half when PB was incorporated, while the antibacterial activity remained intact. Thus, the PB matrix stabilized CuO-NPs on the fibers, extending the shelf-life of the antibacterial material without compromising its antibacterial activity. SEM images, EDX and XAS analysis confirmed that after chemical reduction and oxidation processes with NaBH$_4$ and H$_2$O$_2$ respectively, textiles did not recover the initial PB structure. However, after reduction by bacteria and re-oxidation by environmental oxygen, the PB structure on the textiles had very similar response to that obtained by the initial textile with either PB, or PB- and CuO-NPs, which confirmed that the antibacterial NPs did not interfere the electron exchange between bacteria and PB. The electrochromic response of the smart textiles was evaluated in two different media, i.e. phosphate buffer and MES. In both conditions, the coated textiles showed color change from blue to colorless due to the metabolic reduction of PB caused by the presence of live bacteria. In phosphate, the CuO-NPs were more stable on the fibers and after killing bacteria, the textiles recovered the blue color due to re-oxidation from PW to PB. However, in MES medium, a large

amount of bactericidal NPs was released to the medium and the bacteria attached to the textile remained alive. The high living bacteria concentration in the textile due to the lack of antibacterial activity impeded the blue color recovery, indicating the risk of infection due to the presence of living bacteria on the textile surface. Based on that, two different mechanisms were elucidated to describe the antibacterial capacity of the smart textiles: (i) contact killing, and (ii) bacteria kill owing to release of antibacterial NPs. The efficiency of those mechanisms will depend on the medium and the experimental conditions. Once the antibacterial activity of the smart textile is reduced, the bacterial-sensing capacity will produce a color change due to the presence of live bacteria, warning for a risk of infection. Finally, the smart textile sensitivities and detection times were improved by modifying the textiles with PB through a photocatalytic cyanotype process. Smart textiles obtained by cyanotyping showed an intense blue color and a clear color change in presence of bacteria due to PB reduction to PW. Chemical redox reaction showed higher stability of the PB-NPs on the textile fibers. Besides, the antibacterial NPs release is diminished in the PB presence, even more than with the sonochemical coating method. Smart textiles showed faster sensing activities with color changes observable with naked eye in less than 6 h when in contact with 10^6 CFU in dry conditions, which closer to the real application of the textile. Antibacterial capacity of the smart textiles was also improved with the presence of PB on the fibers, killing almost a 40 % more than textiles only containing CuO-NPs in 7 h. This dual mechanism of the nano-enabled fabrics might contribute to the control and prevention of bacterial infections in hospitals, schools or healthcare centers, among others.

4.2.5 References

(1)   Ricci, F.; Palleschi, G. Sensor and Biosensor Preparation, Optimisation and Applications of Prussian Blue Modified Electrodes. *Biosens. Bioelectron.* **2005**, *21* (3), 389–407. https://doi.org/10.1016/j.bios.2004.12.001.

(2)   Karyakin, A. A. Prussian Blue and Its Analogues: Electrochemistry and Analytical Applications. *Electroanalysis* **2001**, *13* (10), 813–819. https://doi.org/10.1002/1521-4109(200106)13:10<813::AID-ELAN813>3.0.CO;2-Z.

(3)   Cheng, M.; Peng, W.; Hua, P.; Chen, Z.; Sheng, J.; Yang, J.; Wu, Y. In Situ Formation of PH-Responsive Prussian Blue for Photoacoustic Imaging and Photothermal Therapy of Cancer. *RSC Adv.* **2017**, *7* (30), 18270–18276. https://doi.org/10.1039/C7RA01879G.

(4)   Hatamie; Amir; Zargar; Behrooz; Jalali, A.; Ameri, H. Colorimetric Assay for 4-Phenylthiosemicarbazide Detection in Environmental Samples Based on Prussian Blue Nanoparticles Formation Ion. *Iran. J. Chem. Chem. Eng* **2017**, *36* (1), 125–133.

(5)   Zargar, B.; Hatamie, A. Prussian Blue Nanoparticles: A Simple and Fast Optical Sensor for Colorimetric Detection of Hydralazine in Pharmaceutical Samples. *Anal. Methods* **2014**, *6* (15), 5951–5956. https://doi.org/10.1039/c4ay00618f.

(6)   Bard, A. J.; Faulkner, L. R.; Swain, E.; Robey, C. *Electrochemical Methods. Fundamentals and Applications*; 1980.

(7)   Jahn, M. K.; Haderlein, S. B.; Meckenstock, R. U. Reduction of Prussian Blue by the Two Iron-Reducing Microorganisms Geobacter Metallireducens and Shewanella Alga. *Environ. Microbiol.* **2006**, *8* (2), 362–367. https://doi.org/10.1111/j.1462-2920.2005.00902.x.

(8)   Kracke, F.; Vassilev, I.; Krömer, J. O. Microbial Electron Transport and Energy Conservation - The Foundation for Optimizing Bioelectrochemical Systems. *Front. Microbiol.* **2015**, *6* (JUN), 1–18. https://doi.org/10.3389/fmicb.2015.00575.

(9)   Catterall, K.; Robertson, D.; Teasdale, P. R.; Welsh, D. T.; John, R. Evaluating Use of Ferricyanide-Mediated Respiration Bioassays to Quantify Stimulatory and Inhibitory Effects on Escherichia Coli Populations. *Talanta* **2010**, *80* (5), 1980–1985. https://doi.org/10.1016/j.talanta.2009.10.057.

(10)   Pankratova, G.; Hederstedt, L.; Gorton, L. Extracellular Electron Transfer Features of Gram-Positive Bacteria. *Anal. Chim. Acta* **2019**, *1076*, 32–47. https://doi.org/10.1016/j.aca.2019.05.007.

(11)   Ferrer-vilanova, A.; Alonso, Y.; Dietvorst, J.; Pérez-montero, M.; Rodríguez-rodríguez, R.; Ivanova, K.; Tzanov, T.; Vigués, N.; Mas, J.; Guirado, G.; Muñoz-berbel, X. Sonochemical Coating of Prussian Blue for the Production of Smart Bacterial- Sensing Hospital Textiles. *Ultrason. - Sonochemistry* **2021**, *70*, 105317. https://doi.org/10.1016/j.ultsonch.2020.105317.

(12) Samain, L.; Grandjean, F.; Long, G. J.; Martinetto, P.; Bordet, P.; Strivay, D. Relationship between the Synthesis of Prussian Blue Pigments, Their Color, Physical Properties, and Their Behavior in Paint Layers. *J. Phys. Chem. C* **2013**, *117* (19), 9693–9712. https://doi.org/10.1021/jp3111327.

(13) Samain, L.; Silversmit, G.; Sanyova, J.; Vekemans, B.; Salomon, H.; Gilbert, B.; Grandjean, F.; Long, G. J.; Hermann, R. P.; Vincze, L.; Strivay, D. Fading of Modern Prussian Blue Pigments in Linseed Oil Medium. *J. Anal. At. Spectrom.* **2011**, *26* (5), 930–941. https://doi.org/10.1039/c0ja00234h.

(14) Ellis, D.; Eckhoff, M.; Neff, V. D. Electrochromism in the Mixed-Valence Hexacyanides. 1. Voltammetric and Spectral Studies of the Oxidation and Reduction of Thin Films of Prussian Blue. *J. Phys. Chem.* **1981**, *85* (9), 1225–1231. https://doi.org/10.1021/j150609a026.

(15) Grandjean, F.; Samain, L.; Long, G. J. Characterization and Utilization of Prussian Blue and Its Pigments. *Dalt. Trans.* **2016**, *45*, 18018–18044. https://doi.org/10.1039/c6dt03351b.

(16) Yamamoto, T. Assigment of Pre-Edge Peaks in K-Edge x-Ray Absorption Spectra of 3d Transition Metal Compounds: Electroc Dipole or Quadrupole? *X-Ray Spectrom.* **2008**, *37*, 572–584. https://doi.org/10.1002/xrs.

(17) Kulesza, P. J.; Zamponi, S.; Berrettoni, M.; Marassi, R.; Malik, M. A. Preparation, Spectroscopic Characterization and Electrochemical Charging of the Sodium-Containing Analogue of Prussian Blue. *Electrochim. Acta* **1995**, *40* (6), 681–688. https://doi.org/10.1016/0013-4686(94)00348-5.

(18) Buser, H. J.; Ludi, A.; Schwarzenbach, D.; Petter, W. The Crystal Structure of Prussian Blue: Fe4[Fe(CN)6]3·xH2O. *Inorg. Chem.* **1977**, *16* (11), 2704–2710. https://doi.org/10.1021/ic50177a008.

(19) Glatzel, P.; Jacquamet, L.; Bergmann, U.; De Groot, F. M. F.; Cramer, S. P. Site-Selective EXAFS in Mixed-Valence Compounds Using High-Resolution Fluorescence Detection: A Study of Iron in Prussian Blue. *Inorg. Chem.* **2002**, *41* (12), 3121–3127. https://doi.org/10.1021/ic010709m.

(20) Singh, S.; Singh, S. K.; Chowdhury, I.; Singh, R. Understanding the Mechanism of Bacterial Biofilms Resistance to Antimicrobial Agents. *Open Microbiol. J.* **2017**, *11* (1), 53–62. https://doi.org/10.2174/1874285801711010053.

(21) Arnold, J. W.; Silvers, S. Comparison of Poultry Processing Equipment Surfaces for Susceptibility to Bacterial Attachment and Biofilm Formation. *Poult. Sci.* **2000**, *79* (8), 1215–1221. https://doi.org/10.1093/ps/79.8.1215.

(22) Sauer, K.; Stoodley, P.; Goeres, D. M.; Hall-Stoodley, L.; Burmølle, M.; Stewart, P. S.; Bjarnsholt, T. The Biofilm Life Cycle: Expanding the Conceptual Model of Biofilm Formation. *Nat. Rev. Microbiol.* **2022**, *20* (10), 608–620. https://doi.org/10.1038/s41579-022-00767-0.

(23) Davey, K. R. Modelling the Combined Effect of Temperature and PH on the Rate Coefficient for Bacterial Growth. *Int. J. Food Microbiol.* **1994**, *23* (3–4), 295–303.

https://doi.org/10.1016/0168-1605(94)90158-9.

(24)   von Moos, N.; Maillard, L.; Slaveykova, V. I. Dynamics of Sub-Lethal Effects of Nano-CuO on the Microalga Chlamydomonas Reinhardtii during Short-Term Exposure. *Aquat. Toxicol.* **2015**, *161*, 267–275. https://doi.org/10.1016/j.aquatox.2015.02.010.

(25)   Stulik, D. C.; Kaplan, A. *Cyanotype*; 2018. https://doi.org/10.5040/9781350088733.0067.

(26)   Dietvorst, J.; Ferrer-Vilanova, A.; Iyengar, S. N.; Russom, A.; Mas, J.; Marco, M.; Guirado, G. Bacteria Detection at a Single-Cell Level through a Cyanotype-Based Photochemical Reaction. *Anal. Chem.* **2022**, *94*, 787–792. https://doi.org/10.1021/acs.analchem.1c03326.

(27)   Ware, M. Prussian Blue: Artists' Pigment and Chemists' Sponge. *J. Chem. Educ.* **2008**, *85* (5). https://doi.org/10.1021/ed085p612.

<div style="text-align: right">

4.3

</div>

Smart Filters for in situ Live Bacteria Detection in Water

Abstract

To prevent the biofouling in membrane filters for water treatment, traditional techniques such as coagulation-flocculation, adsorption or ion exchange are used, relying in long protocols and low effectivity. Besides, most of times, bacterial contamination in water requires periodical analysis which result expensive. In this chapter, smart filters able to detect the presence of bacteria in situ are developed. Color changes are observed by naked eye in 9 hours for high bacterial concentrations. The sensitivity and time response of the method are improved by the use of a sensing platform, which allowed the pre-concentration of the sample and enhance the sensitivity of the method with the use of optical fibers. Hence, color changes are detected in 2 hours for bacterial concentrations of 10^4 CFU mL^{-1}. Smaller concentrations also produced color changes in less than 5 hours. In addition, Ag-NPs are introduced on the filters showing high antibacterial capacity. Filter samples change their color response when biocide NPs were present or not, informing of the presence of live bacteria in situ. This technology can be applied in real water samples analysis, reducing the formation of biofouling and allowing to sense the presence of bacteria in water.
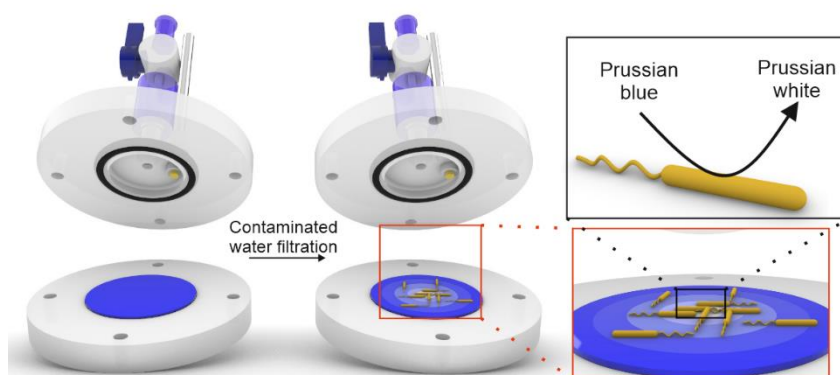
This chapter contains results related to these publications:

Toward Rapid Detection of Viable Bacteria in Whole Blood for Early Sepsis Diagnostics and Susceptibility Testing. Sharath Narayana Iyengar, Jiri Dietvorst, Amparo Ferrer-Vilanova, Gonzalo Guirado, Xavier Muñoz-Berbel and Aman Russom. *ACS Sensors*, 2021, 6, 3357-3366.

Bacteria Detection at a Single-Cell Level through a Cyanotype-Based Photochemical Reaction. Jiri Dietvorst, Amparo Ferrer-Vilanova, Sharath Narayana Iyengar, aman Russom, Núria Vigués, Jordi Mas, Lluïsa Vilaplana, Maria-Pilar Marco, Gonzalo Guirado and Xavier Muñoz-Berbel. *Analytical Chemistry*, 2022, 94, 787-792.

Smart electrochromic filters for in situ live bacteria detection in water. Amparo Ferrer-Vilanova, Josune J. Ezenarro, Núria Vigués, Jordi Mas, Javier del Campo, Xavier Borrisé, Gonzalo Guirado and Xavier Muñoz-Berbel. (Article to be submitted)

Acknowledgements

4.3.1 Filters modification with PB by cyanotype process and characterization

PB was introduced in the membrane filters through the same cyanotype process described for the polyester-cotton textiles. The procedure followed is schematized in Figure 3.4 (Materials and Methods section). After the cyanotype modification process, the characteristic and intense blue color from PB was observed on the samples. Figure 4.3.1 shows a picture of a nitrocellulose filter modified with PB and the SEM image of its surface, which reveals the characteristic cubes structures of PB also shown in the case of the textiles modified through cyanotype process.
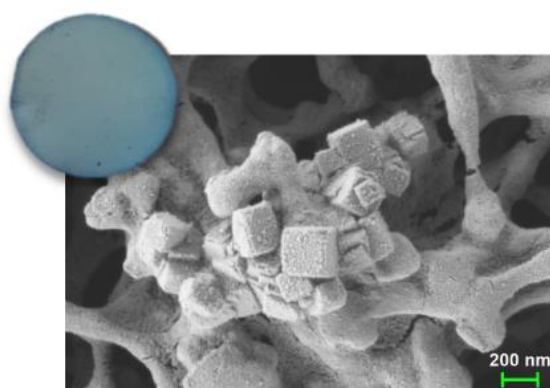

Figure 4.3.1. PB-modified filter. Picture of the filter modified with PB by cyanotype method and SEM image of its surface.

To optimize the method, two different types of materials were tested with different pore sizes, (i) nitrocellulose (NC) filters with 0,2 μm pore size and (ii) mixed cellulose ester (MCE) filters with 0,22 μm and 0.45 μm pore size, all of them with a diameter of 25 mm. The influence of applying different UV irradiation times to the filters surface (from 10 to 120 s) was also evaluated for the samples optimization.

The characterization of the obtained samples was developed by obtaining the visible-spectra in five different points of the filter by using a reflection/backscatter probe. In Figure 4.3.2, the images of the front and backsides of the filters are shown as well as the obtained spectra for four different irradiation times: 10, 30, 60 and 90s. These results were separated by material and pore size. For all the conditions, the characteristic peak of PB appeared around 700 nm. Comparing the front and backsides, the longer was the irradiation time the deeper was the PB layer. Thus, when filters were irradiated for 90s, the spectra of both sides were more similar than with shorter irradiation times. When comparing the type of material, more intense blue color was obtained for

MCE (Figure 4.3.2b and Figure 4.3.2c) than for NC filters (Figure 4.3.2a). However, the deviation bars provide information about the homogeneity of the PB-coating, being the NC samples the most homogeneous material. For this reason, the NC was the optimum filter material selected for further experiments.
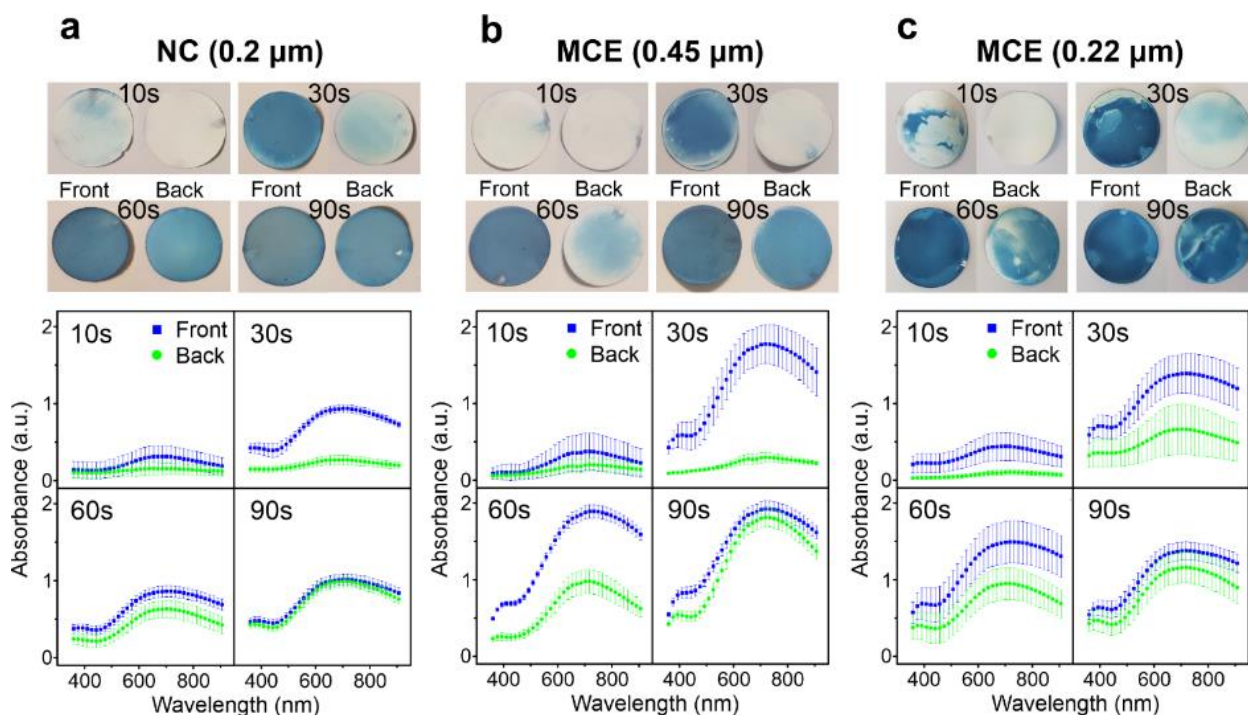

Figure 4.3.2. PB-modified filters and their optical characterization spectra. Pictures and absorbance spectra obtained in five different points of each sample in both, the front (in blue color) and the backsides (in green color) of the filters. The experiment was developed for three different types of samples: a) NC filters with 0.2 µm pore size, b) MCE filters with 0.45 µm pore size and c) MCE filters with 0.22 µm pore size. For each condition, different irradiation times were evaluated: 10, 30, 60 and 90s. For all the samples, n=3.

4.3.2 Optimization of the filters color change by UV irradiation time study

The principle of sensing is the same as studied in the previous chapters. When live bacteria is present on the filter surface, this will show a focalized color change from deep blue to colorless due to the PB reduction by bacterial metabolism (Figure 4.3.3a). For this purpose, it is important to maintain live bacteria adhered on the filters fibers. To study the bacterial retention on the filters surface, an *E.coli* suspension of 10^7 CFU mL^{-1} was passed through the smart filters of two different porous sizes (0.2 and 0.45 µm). The amount of live bacteria was evaluated with confocal images

of both types of filters and the filtered water was plated for counting. Confocal images are shown in Figure 4.3.3b and Figure 4.3.3c for pore sizes of 0.2 µm and 0.45 µm, respectively. Resulting images showed higher bacterial retention in the filters with a porous size of 0.2 µm. These results were in concordance to the counts made in the filtered medium, showing a 99 % of the amount of bacteria filtered vs. 2 % for pore sizes of 0.45 µm and 0.2 µm, respectively. For these reasons, the pore size used in further experiments was 0.2 µm.
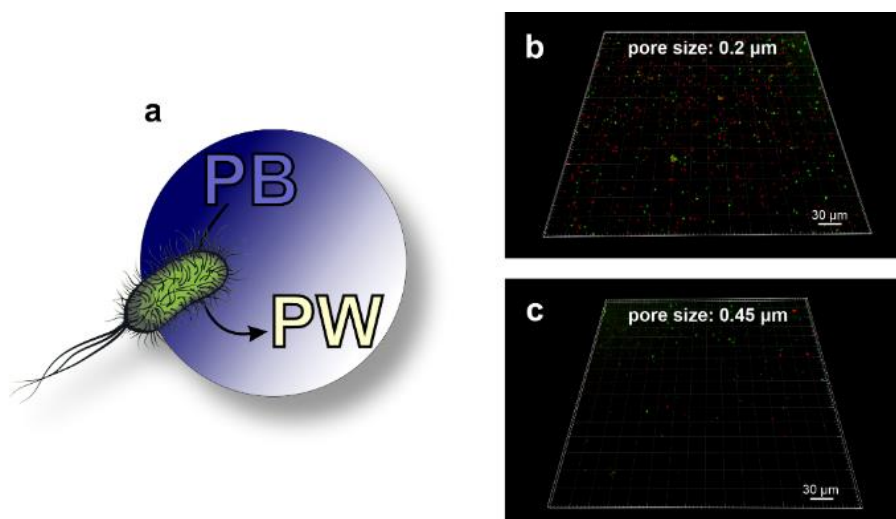

Figure 4.3.3. Principle of sensing and bacteria retention on the filters surface. a) Scheme of the principle of sensing of the smart filters. Confocal images after filtration of a 10^7 CFU mL^{-1} *E. coli* suspension through filters of two pore sizes: a) 0.2 µm and b) 0.45 µm.

The UV irradiation time applied during the cyanotype modification process was optimized by evaluation of the bacterial-sensing response of the smart filters at the different conditions. Thus, 10 mL of an *E.coli* bacterial suspension of 10^7 CFU mL^{-1} were passed through PB-modified filters coated at different UV irradiation times (30, 40, 50, 60, 90 and 120 s). Then, filters were incubated in 2 mL of MH medium (pH 6.2) and the color change of the filters was monitored during 50 h. As control, PB-modified filters in MH medium with no bacteria were used. The experiment was carried out three times to study the repetition of the results. The percentage of the color lost was calculated by comparison with the non-treated samples. Resulting graphs are shown in Figure 4.3.4.
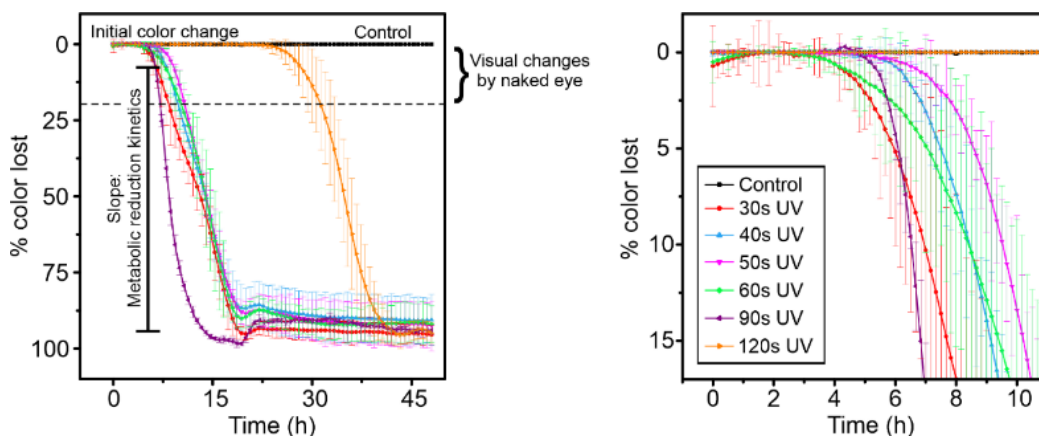
Figure 4.3.4. Bacterial-sensing response of the filters modified with different UV irradiation times. Percentage of color lost measured during 50 h in 2 mL of MH medium after filtering 10 mL of *E. coli* 10^7 CFU mL^{-1}. The percentage of color lost was calculated by comparison with the unmodified filters. As control, PB-modified filters without bacteria were used. The graph on the right side shows the results in the range visible by naked eye (below 20 % of color lost). For all the conditions, n=3.

Control samples remained stable throughout the experiment. For the rest of them, initially samples presented an intense blue color, which completely disappeared along the experiment. However, to observe the color changes by naked eye, only the 20 % of the color lost was necessary, which is represented at the graph in the right side. Two important parameters to take into account were the time when the sample started to change the color and the observed rate for the complete disappearance of color (the slope of the curve). These parameters are quantified in Table 4.3.1 for all the UV irradiation times tested, where the slope of the obtained curves represents the bacterial metabolic reduction kinetics of PB.

Table 4.3.1. Initial color change and slope parameters obtained for different UV irradiation times.

	UV irradiation time (s)					
	30	40	50	60	90	120
Initial color change (h)	2,5	5,1	4,7	2,7	4,7	20,7
Slope	6,09 ± 0,06	6,08 ± 0,09	5,39 ± 0,24	6,08 ± 0,1	11,19 ± 0,15	5,04 ± 0,07

162

Although color changes were observed earlier when filters were irradiated 30 s, the fastest reduction of PB coated on the filters by bacterial metabolism occurred when samples were irradiated for 90 s. This phenomenon may be related to the depth of the UV irradiation applied to the samples, which may produce a different distribution of PB-NPs throughout the thickness of the filter. To study that, SEM images were taken to the cross section of the filters. The composition of those parts was determined by EDX and a mapping of the iron atoms distribution was performed. Figure 4.3.5 illustrates the obtained results for control filters (nitrocellulose filters without PB) and for PB-modified filters irradiated with UV during 30 and 90 s.
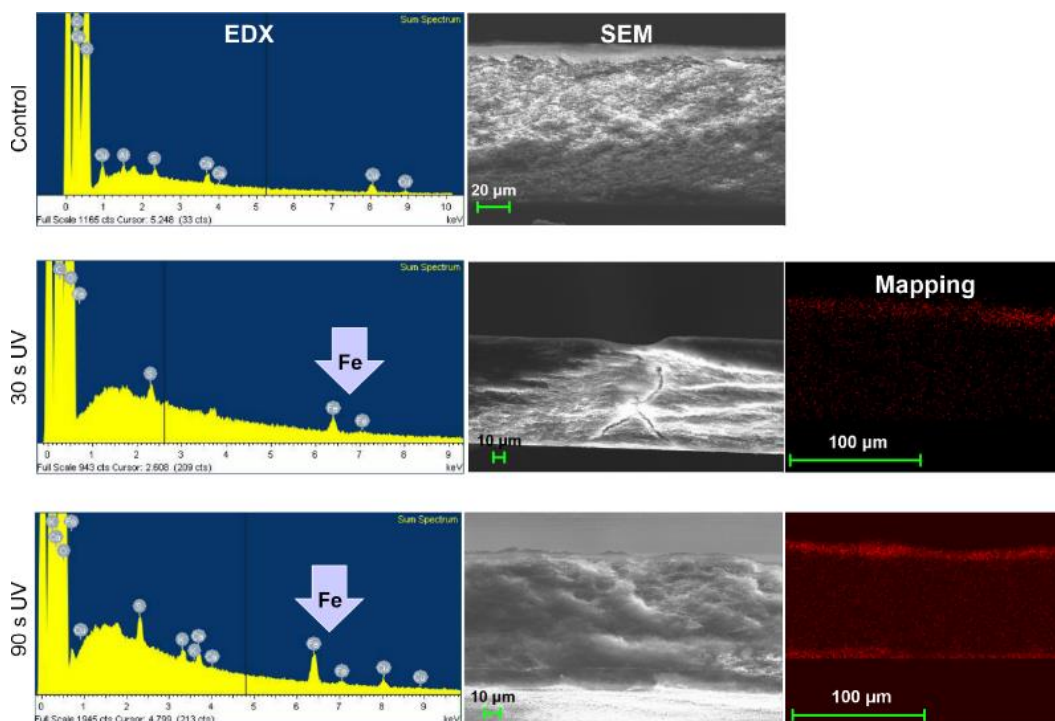

Figure 4.3.5. Cross section analysis of the smart filters. SEM images, EDX analysis and mapping of the Fe ions distribution through the cross section of NC filters modified with PB by UV irradiation times of 30 and 90s and filters without modification.

The EDX analysis of the SEM images revealed the presence of iron atoms in both samples containing PB, which was higher for filters irradiated 90s. In addition, the mapping distribution of the iron atoms through the cross section of the filters confirmed that when samples were irradiated with longer times, the PB-layer formed on the filters surface was deeper, covering the

163

full thickness of the filter when irradiated for 90 s. This fact may be related to the higher slopes showed in Figure 4.3.4, which produced faster PB reduction kinetics along the full experiment. This fact is probably due to an electrocatalytic process generated between PB- particles, in which, the transfer of electrons could be accelerated through the filter thickness, producing faster color changes. For this reason, UV irradiation of 90 s were chosen as the optimal conditions to test the filters color change produced by the presence of live bacteria, as long as the color change is evaluated by the naked eye.

With the optimal conditions already selected, the bacterial-sensing capacity of the smart filters was evaluated by using NC filters with 0.2 μm of pore size and modified with PB by UV irradiation during 90 s.

4.3.3 Bacterial-sensing evaluation of smart PB-modified filters

The bacterial-sensing capacity of the smart filters was evaluated for the filters modified with PB. Thus, 10 mL of different *E. coli* suspensions from 10^2 to 10^7 CFU mL^{-1} were passed through the filters and they were incubated in 2 mL of MH medium (pH 6.2). The color change was monitored for 75 h. As control, PB-modified filters without bacteria were incubated in MH. The resulting graphs are shown in Figure 4.3.6.
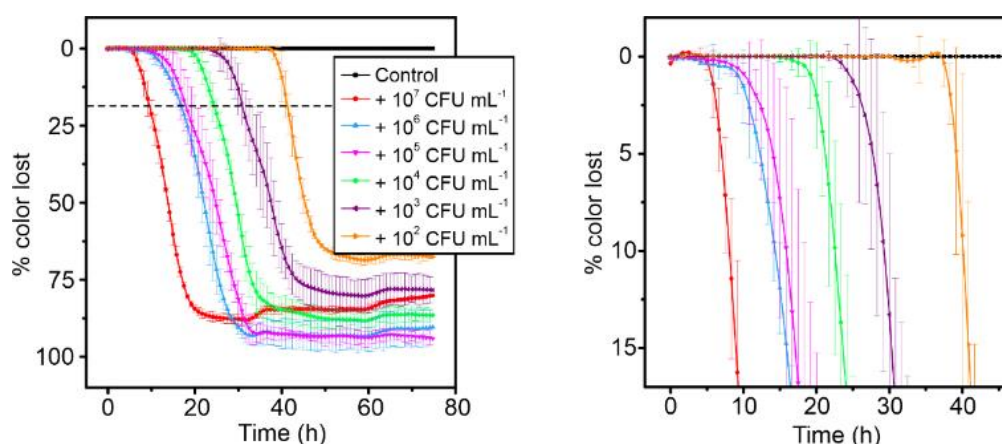
Figure 4.3.6. Bacterial-sensing evaluation of PB-modified filters. Color lost percentage of the PB-modified filters obtained after filtering 10 mL of *E. coli* suspensions from 10^2 to 10^7 CFU mL^{-1}. Samples were immersed in 2 mL of MH and images were taken every 10 min for color quantification. The percentage of color lost was calculated by comparison with the unmodified filters. The graph on the right side shows the results in the range visible by naked eye (below 20 % of color lost). For all the conditions, n=3.

For all the bacterial concentrations, the filters shown a color lost correlated with the bacterial concentration, while the control remained constant along the experiment. All the curves presented similar slopes. At the graph on the right side, color changes perceived by naked eye are represented. For the highest concentration of bacteria tested (10^7 CFU mL^{-1}), color changes were detected in 9 h and the lowest concentration of bacteria (10^2 CFU mL^{-1}) took 40 h in showing color changes. Therefore, the bacterial-sensing activity of the smart filters was proved. However, in order to apply the system to a real conditions, shorter detection times with lower bacterial concentrations are required.

It is important to remark that since bacteria was retained on the filter surface, the real amount of bacteria detected depends on the filtrated volume. For example, in the case of filtering 10 mL of a bacterial suspension of 10^7 CFU mL^{-1}, the real amount of bacteria on the filter corresponds to 10^8 CFU, thus by increasing the volume filtered, the detection could be achieved in shorter times. For this reason, a sensor platform was developed for further experiments, which allowed the pre-concentration of the samples by filtering higher volumes of sample. In addition, the system incorporated optical fibers, allowing sensing the color changes in situ and in shorter times. The design and implementation of this system will be explained in the next sections.

4.3.4 Sensor platform design and fabrication

Intending to reduce the detection time, a photonic prototype was designed based on previous works developed within the framework of Josune J. Ezenarro's PhD thesis. These works demonstrated the ability of the device to pre-concentrate different bacteria like *E. coli*,[12] *Legionella pneumophila*[13,14] and cyanobacteria[15] by flow-through membrane filtration. For this thesis, the device's design was adapted, especially the upper part, by including a permanently attached adapter fabricated in PMMA to introduce a reflection/backscatter probe inside the incubation chamber, increasing the sensitivity for detecting membrane colour changes produced by living bacteria. The sensor design and the experimental procedure followed are described below.

The design of the pre-concentration and sensing device is shown in Figure 4.3.7 and included all elements for fluid management and positioning the optical fiber required for absorbance measurement in situ. The holder consisted of 50 mm in diameter parts assembled by screws and sealed by a rubber O-ring (20 mm in inner diameter and 3 mm in width) to ensure water tightness. The upper part was composed of: (i) a 4 mm thread bolt for a universal Luer connector to connect a valve controlled double fluidic inlet for the water filtration and MH media incubation; (ii) a cavity to implement the rubber O-ring; (iii) a second cavity of 17.5 mm diameter and 2.8 mm of depth used as an incubation chamber with a hole of 4 mm for the incorporation of an additional polymeric structure, also fabricated in PMMA by milling and assembled and sealed by UV curable optical adhesive (Norland Optical Adhesive 68, Norland Products, inc. Cranbury, NJ 06512) to introduce a reflection/backscatter probe (QR600-7-SR125BX, Ocean Insights) inside the incubation chamber. This PMMA structure had external and inner diameters of 4 mm and 3.1 respectively and allowed positioning the optical fiber to a distance of 2 mm from the membrane. The fiber was simultaneously connected to the light source as well as to an external used as the optical detector, working as a light-emitting and collection source. The bottom part was a planar socket to place the modified NC membrane with evacuation channels facilitating water exit towards the outlet.
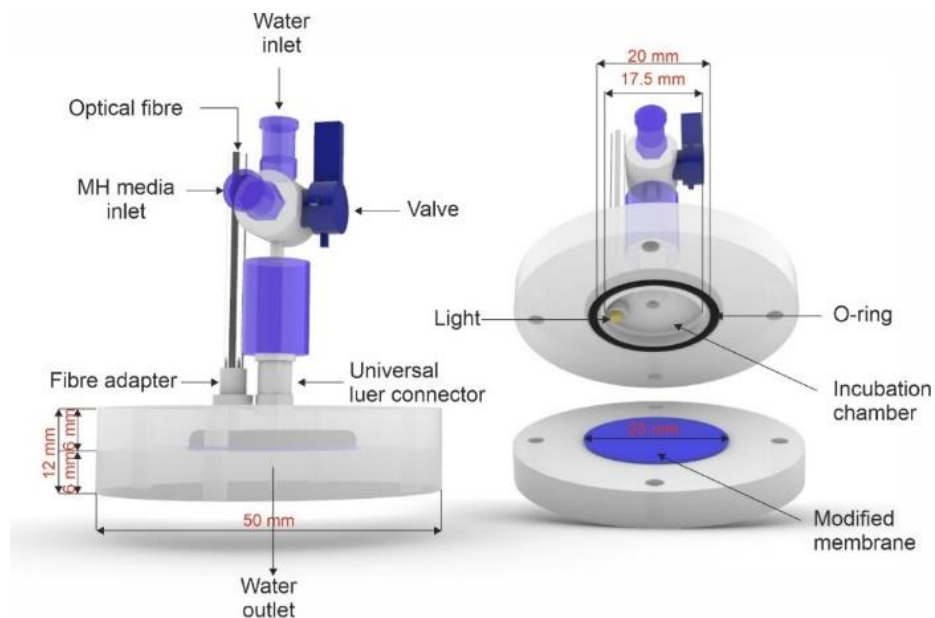

Figure 4.3.7. 3D design of the pre-concentration and sensing device. Design of the sensing platform used for measuring the bacterial-sensing capacity of the PB-modified filters. The design was performed by using Rhinoceros 6 software (Robert McNeel & Associates).

4.3.5 Bacterial-sensing evaluation of smart PB-modified filters on the sensor platform

Since the sensing platform allowed to detect the presence of bacteria in shorter times, a preliminary test was developed to evaluate the different response of filters irradiated with UV light for 30 and 90 s. Thus, 10 mL of a 10^5 CFU mL^{-1} *E. coli* suspension in water was filtered manually through both types of PB-modified samples by using the sensor platform. Once samples were filtered, by changing the valve positioning, the water inlet was closed to open the medium inlet. Then, 700 µm of MH medium (pH 6.2) were added to the chamber for enhance bacterial growth. The lamp was activated and the absorbance spectra of the filters surface was acquired each hour during 5 h. Between measurements, the light source was turned off because a large exposure to light affected the color of the samples.

Figure 4.3.8a shows the obtained spectra for PB-modified filters irradiated with UV light for 30 s. The peak centered at 700 nm typical from the PB color is decreasing over time due to the PB reduction by bacterial metabolism. It is important to notice that the time of response and the bacterial concentration were greatly reduced comparing with the previous results. The absorbance values at 700 nm for both samples were represented in a separate graph (Figure 4.3.8b) to compare the kinetics of their responses.
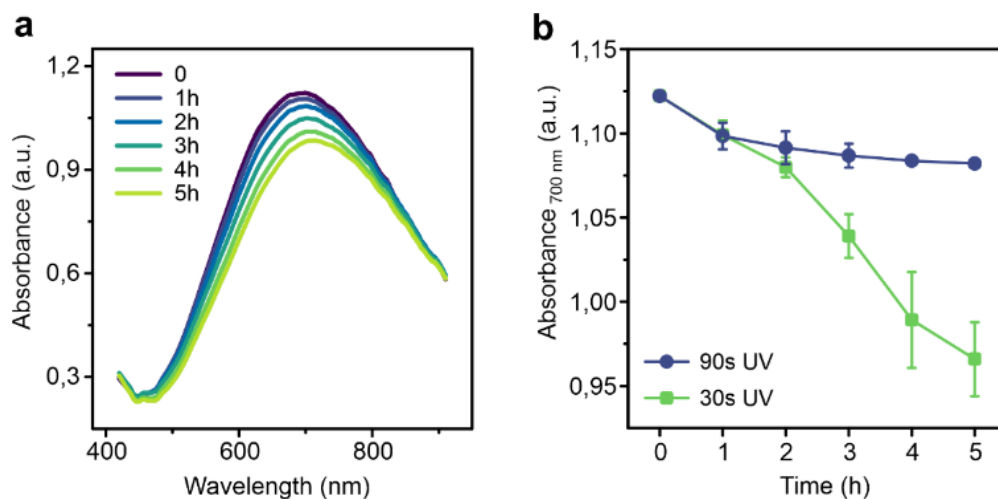

Figure 4.3.8. Sensing response of the pre-concentration system by varying the UV irradiation time. a) Absorbance spectra obtained when a PB-modified filter irradiated with UV light for 30 s was filtered with 10 mL of 10^5 CFU mL^{-1} *E. coli* suspension. b) Absorbance values at 700 nm for filters irradiated for 30 and 90 s with UV light (n = 2).

Both type of filters were reduced in presence of bacteria after 5 h. However, it was clearly seen that filters irradiated for 30 s showed faster responses to bacterial metabolism. In fact, this difference could be observed after 1 h of experiment, since their response within the first hour was the same. In summary, filters irradiated for 90 s showed the optimal properties for being used in a visual inspection, while those irradiated for 30 s were the most suitable for bacterial detection when using the pre-concentration device.

Therefore, the bacterial-sensing capacity of the PB-modified filters was studied in the pre-concentration system with filter samples irradiated with UV light for 30 s, using as model microorganism *E. coli*. Thus, different *E. coli* suspensions in a concentration range from 10^4 to 10^7 CFU mL^{-1} were filtered using different volumes of sample in each case. The selection of the volumes was determined by the pore saturation, since high concentrations of bacteria produced saturation when high volumes were employed. Bacterial suspensions were prepared in water media filtered twice, for avoiding the presence of other bacteria. This media was used for filtering the control PB-modified filters, without bacteria. Absorbance spectra of the filters' color was acquired each 10 min for 2 h. The slopes of the PB reduction kinetics were obtained from the values at 700 nm as in the previous case. The bacterial concentration, volume filtered and the slope obtained in each case are specified in Table 4.3.2.

Table 4.3.2. Data obtained for the measurement of the bacterial-sensing capacity of the smart filters.

E. coli concentration (CFU mL^{-1})	filtered volume (mL)	Total CFU on the filter	slope
0	100	0	$1,37 \cdot 10^{-4}$
0	100	0	$1,42 \cdot 10^{-5}$
$2,5 \cdot 10^4$	100	$2,5 \cdot 10^6$	$-8,15 \cdot 10^{-5}$
$6,7 \cdot 10^4$	100	$6,7 \cdot 10^6$	$-8,47 \cdot 10^{-5}$
$7,3 \cdot 10^5$	100	$7,3 \cdot 10^7$	$-2,55 \cdot 10^{-4}$
$7,1 \cdot 10^5$	100	$7,1 \cdot 10^7$	$-2,32 \cdot 10^{-4}$
$7,1 \cdot 10^6$	70	$5,97 \cdot 10^8$	$-7,30 \cdot 10^{-4}$
$4,1 \cdot 10^6$	70	$2,87 \cdot 10^8$	$-3,43 \cdot 10^{-4}$

The total CFU on the filter surface and the slope of the PB reduction kinetics were represented and the calibration curve was obtained. Results are illustrated in Figure 4.3.9.
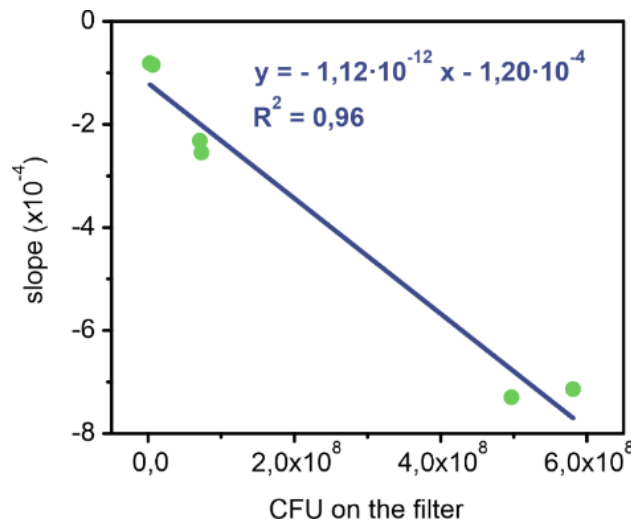

$$y = -1,12 \cdot 10^{-12} x - 1,20 \cdot 10^{-4}$$
$$R^2 = 0,96$$

Figure 4.3.9. Calibration curve of the bacterial-sensing capacity of the smart filters. Calibration curve obtained from the filtration of different bacterial suspensions of *E. coli* (from 10^4 to 10^6 CFU mL^{-1}) through the PB-modified filters. Depending on the filtered volume, the total CFU on the filter surface was calculated and represented versus the slope of the PB reduction kinetics of each sample (n = 2).

Results showed a good correlation (R^2 = 0.96) between the amount of CFU present on the filter and the slope obtained for each value. The limits of detection and quantification were calculated for these conditions (e.g. bacterial detection in two hours), being $2.33 \cdot 10^8$ and $7.75 \cdot 10^8$ (total CFU on the filter) respectively.

To evaluate the bacterial-sensing capacity against other microorganisms present in water, PB-modified filters were tested using three different types of bacteria, namely *p. putida, vibrio* and *alteromonas*. Thus, each bacteria was suspended in filtered water and 100 mL of 10^6 CFU mL^{-1} was passed through the smart filters. The experiment was repeated twice for each bacteria. The slopes of the color change obtained at 700 nm were $(-2,54 \pm 0,01) \cdot 10^{-4}$, $(-2,66 \pm 0,58) \cdot 10^{-4}$ and $(-2,43 \pm 0,79) \cdot 10^{-4}$ for *p. putida, vibrio* and *alteromonas*, respectively. These values are close between repetitions and show concordance with those obtained for *E. coli*, proving the repeatability of the method. Besides, it demonstrates that can be applied for a wild range of different bacteria types since PB metabolic reduction is produced by electrons acceptance from the ETC.

Finally, the bacterial-sensing response was evaluated for smaller concentrations of bacteria by increasing the time of the measure. Therefore, 100 mL of an *E. coli* bacterial suspension of 10^3 CFU mL^{-1} were passed through the PB-modified filters and the color change was measured for 5 h as previously described. The absorbance values at 700 nm obtained each 10 min are represented in Figure 4.3.10.
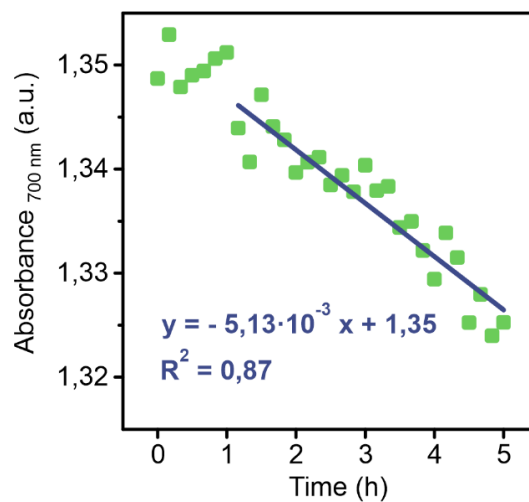

Figure 4.3.10. Bacterial-sensing response of PB-modified filters against an *E. coli* suspension of 10^3 CFU mL^{-1}. Absorbance values at 700 nm obtained by filtration of 100 mL of an *E. coli* suspension of 10^3 CFU mL^{-1}. Measurements were performed every 10 min and the color changes were recorded for 5 h.

In the resulting graph, it could be observed that there was not change of color during the first hour of the experiment. After that time, the filter was losing its color progressively. For this reason, the slope of the color change was determined after one hour of experiment, being of the order of 10^{-3}, which was much higher than the previous studied, taking into account that the real amount of CFU in contact with the filter surface was 10^5 CFU. This result indicates that the sensing system is able to detect the presence of living bacteria even with low concentrations and sensitivity of the method can be improved by both, filtering higher volumes or measuring for longer times.

4.3.6 Production of the smart antimicrobial filters

For the production of the smart filters with antimicrobial capacity, filter samples were modified first with the antimicrobial agent and then, with the PB by cyanotype process. Ag-NPs were used as the antimicrobial compound on the filters surface and were produced in situ by the IMS method explained in the materials and methods chapter. Briefly, filter samples were immersed in a precursor solution of $AgNO_3$ of different concentrations (from 0.4 to 100 mM) for 30 min. Then, 0.05 M $NaBH_4$ was added for 15 min to reduce Ag ions and promote the Ag-NPs adhesion into the fibers of the filters. Finally, samples were washed and let dry at 37 °C overnight. Obtained filters had an intense blue color (Figure 4.3.11) similar to those modified only with PB. In the SEM image, the cubic structures of the PB can be clearly identified as well as the Ag-NPs, forming aggregates of small spheres attached on the NC fibers of the filter.
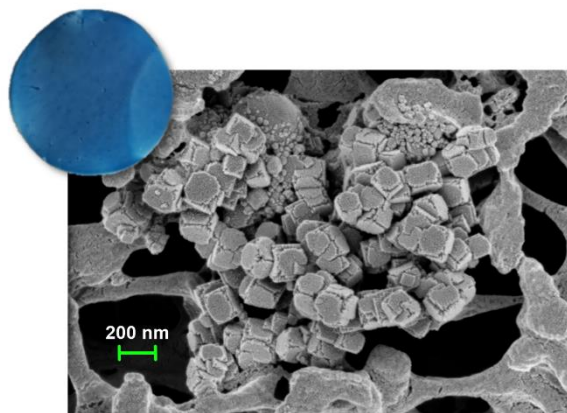

Figure 4.3.11. Smart filter and SEM image. Picture of the filter modified with PB and Ag-NPs (2mM) by cyanotype and IMS methods, respectively and SEM image of its surface

4.3.7 Antibacterial capacity of the smart filters

The selection of the optimal concentration of Ag-NPs on the filters was determined by an antibiogram test. Thus, MH agar plates were completely covered with *E. coli* bacteria and filters modified with PB and Ag-NPs at different concentrations were placed along the MH plates and kept at 37 °C overnight. After the incubation process, the zone of inhibition (e.g., the area around the filters where there was no living bacteria) was measured. 2 mM was the minimum concentration of Ag-NPs in which the zone of inhibition was observed, so it was selected as the optimal for further experiments.

For the determination of the antibacterial activity of the smart filters, the different samples were filtered with *E. coli* bacterial suspensions and placed in Eosin Methylene Blue (EMB) agar plates at 37 °C overnight for counting survival bacteria on the filter surface. The experiment was developed in three samples of each type: filters modified with PB and with PB and Ag-NPs. As control, NC filters were used. EMB plates were used in this experiment because they are fluorescent and facilitate the counting when illuminated with UV light (See Figure 4.3.12). The percentage of survival bacteria was calculated by comparing the CFU counted in the plates with the initial *E. coli* concentration filtered. Results showed survival percentages of (82.5 ± 3.5) % and (76.9 ± 6.2) % for the control and PB samples. However, in the samples modified with PB and Ag-NPs no live bacteria was found, which prove the good effectivity of the smart filters.
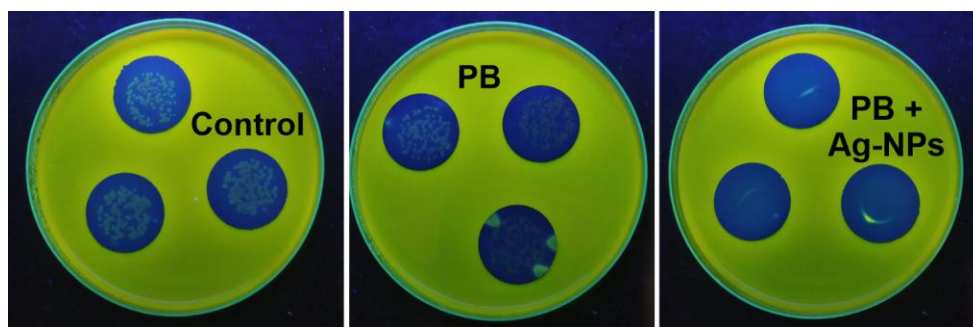

Figure 4.3.12. Antibacterial activity of the smart filters. Images of the different filter samples after filtration of E. coli suspensions and incubation at 37 °C overnight.

4.3.8 Smart-sensing activity and biocide NPs release study

Finally, the influence of the antibacterial NPs on the electrochromic response of the smart filters and their stability were evaluated. Filter samples with PB and PB/Ag-NPs were filtered with 10 mL of bacterial suspensions of 10^4 and 10^8 CFU mL^{-1} and cut in four equal parts. Two of them were incubated in 2 mL of MH medium and the color changes were recorded for 50 h (Figure 4.3.13). As controls, filters modified with PB and PB/Ag without bacteria were used. The other two parts were submerged in 2 mL of MH and the medium was analyzed by ICP-OES at different times to determine the amount of Ag-NPs released form the filters. For comparison, filters modified with Ag were also included.
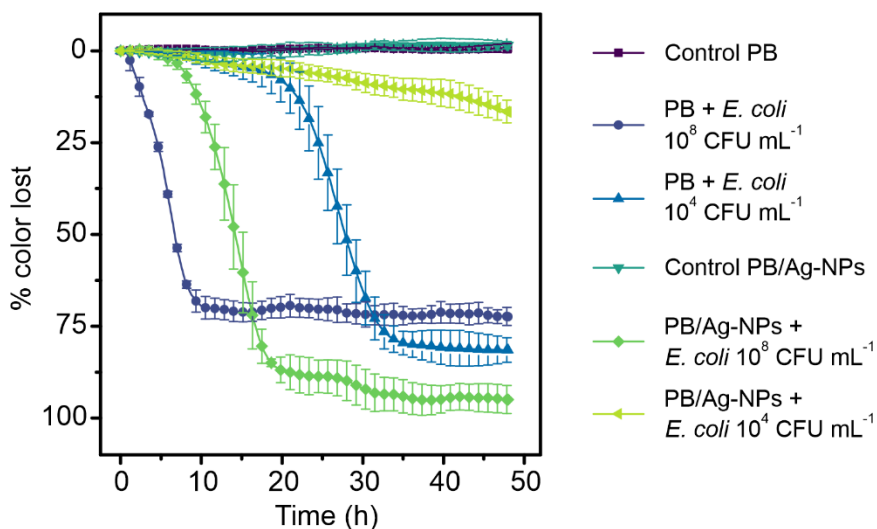

Figure 4.3.13. Bacterial-sensing response of the smart antibacterial filters. Percentage of color change obtained after filtering 10 mL of 10^8 and 10^4 CFU mL^{-1} *E. coli* suspensions through the filters modified with PB and with PB/Ag-NPs.. Filters were incubated in 2 mL of MH and the color change was recorded for 50 h. As controls, filters modified with PB and PB/Ag-NPs without bacteria were used. For all the samples, n = 3.

The electrochromic response of the filters was highly influenced by the presence of Ag-NPs, since their color change was produced in longer times due to the antimicrobial activity of the smart textiles. Thus, when samples modified with PB were filtered with 10^8 CFU mL^{-1} *E. coli* suspension, color changes were produced after 2 h, while when containing Ag-NPs, filters took almost 10 h in start the change of color. In an analogous way, when the bacterial suspension was 10^4 CFU mL^{-1},

samples delayed almost 10 h in produce the color change when comparing the PB-modified filters against PB/Ag-NPs samples. To understand the relationship of these changes between the NPs stability, ICP-OES study was realized after: (i) 2 h, when samples showed no changes; (ii) 10 h, when filters modified with PB have changed while samples with PB and Ag-NPs started changing (filtered with 10^8 CFU mL^{-1}); and (iii) 28 h, when the last situation occurred for samples filtered with 10^4 CFU mL^{-1}. Results of ICP-OES analysis are shown in Figure 4.3.14.
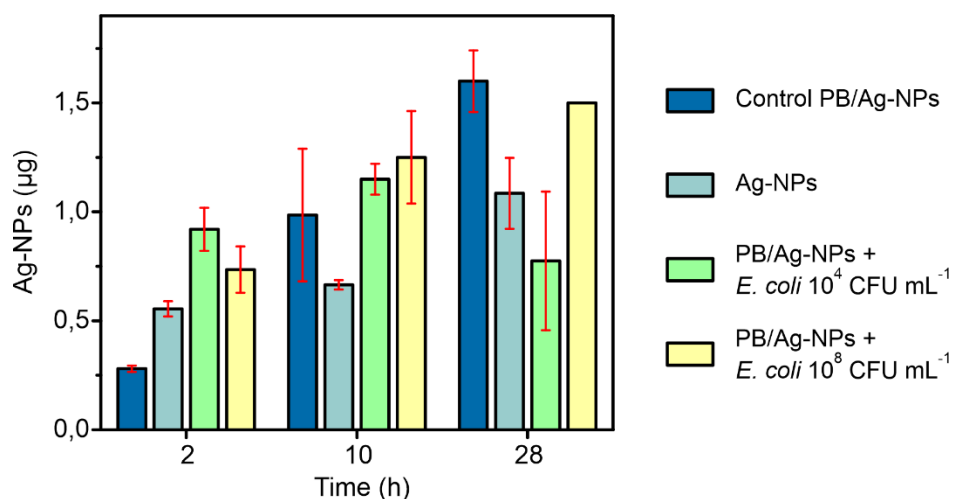

Figure 4.3.14. Ag-NPs release to the medium. Amount of Ag-NPs released to the medium after filtering 10 mL of 10^8 and 10^4 CFU mL^{-1} *E. coli* suspensions through the filters modified with PB and PB/Ag-NPs. Filters were cut in four parts and incubated in 2 mL of MH. An ICP-OES analysis was performed at 2, 10 and 28 h of the experiment. The amount of Ag was calculated in 2 mL of medium. As controls, filters modified with PB/Ag-NPs without bacteria were used. Filters modified with Ag-NPs were also analyzed for comparison. For all the samples, n = 2.

At the beginning of the experiment, samples showed similar amounts of Ag in the medium. After 10 h, samples filtrated with 10^8 CFU mL^{-1} incremented the Ag-NPs release to the medium, just before start the color change, probably because most of the NPs were in the medium and bacteria attached to the textile could remain alive, producing the color changes. After 28 h, the textile completely lost its color, and the amount of Ag-NPs was quite similar to the obtained at 10 h. The amount of Ag-NPs for samples filtered with 10^4 CFU mL^{-1} was similar to that obtained for 10^8 CFU mL^{-1} at 10 h.

4.3.9 Conclusions

In order to decrease the biofouling formation on water treatment membranes, bacterial-sensing membrane filters are developed in this chapter, allowing to measure water samples in situ and without need to use extra reagents. PB-sensing molecule was incorporated into filter membranes by cyanotype method, producing highly colored samples. NC material was chosen as the most optimal since produced the most homogeneous coating of the filters surface. Besides, pore sizes of 0.2 μm showed higher bacterial retention on the filter surface. The UV irradiation time applied during the cyanotype process was also evaluated, showing faster color changes for filters irradiated 90 s when visual inspection was conducted. However, times of response and bacterial concentrations were still high. These drawbacks were solved by developing the measurements within a sensor platform that allowed to pre-concentrate the samples (increasing the amount of bacteria on the filter surface) and to enhance the sensitivity of the method (by the use of optical fibers), which detect color changes in shorter times. In this case, 30 s of UV irradiation were chosen as the optimal conditions, since the color change started before than for 90 s. A calibration curve with *E. coli* bacteria was obtained showing good correlation with the results and bacterial concentrations of 10^4 CFU mL^{-1} could be detected in two hours. Smaller bacterial suspensions could be measured in longer times (5h). In addition, Ag-NPs were incorporated into the filters, showing good antibacterial responses. In fact, the sensing response could inform of the presence of live bacteria on the filters, being longer when the biocide NPs were present. This method has potential application for the control of biofouling formation and detection of low concentrations of bacteria in situ.

4.3.10 References

(1) Pachepsky, Y. A.; Allende, A.; Boithias, L.; Cho, K.; Jamieson, R.; Hofstra, N.; Molina, M. Microbial Water Quality: Monitoring and Modeling. *J. Environ. Qual.* **2018**, *47* (5), 931–938. https://doi.org/10.2134/jeq2018.07.0277.

(2) Hurst, C. J.; Crawford, R. L.; Garland, J. L.; Lipson, D. A.; Mills, A. L.; Stetzenbach, L. D. *Manual of Environmental Microbiology (3rd Edition)*, Third edit.; Hurst, C. J., Lipson, D. A., Garland, J. L., Stetzenbach, L. D., Mills, A. L., Crawford, R. L., Eds.; American Society of Microbiology (ASM), 2007. https://doi.org/10.1128/9781555815882.

(3) Word Health Organization (WHO). *WHO | Guidelines for Drinking-Water Quality: Fourth Edition Incroporating the First Addenum*, 4th editio.; Geneva, 2017.

(4) E. Union. Council Directive 98/83/EC of 3 November 1998 on the Quality of Water Intended for Human Consumption. *Off. J. Eur. Communities* **1998**, *330*, 32–54.

(5) ISO. ISO 9308-1. Water Quality - Detection and Enumeration of Escherichia Coli and Coliform Bacteria. Part 1: Membrane Filtration Method. **2000**, *2000*, 1–2.

(6) ISO - ISO 9308-2:2012 - Water quality — Enumeration of Escherichia coli and coliform bacteria — Part 2: Most probable number method.

(7) Kumar, S.; Nehra, M.; Mehta, J.; Dilbaghi, N.; Marrazza, G.; Kaushik, A. Point-of-Care Strategies for Detection of Waterborne Pathogens. *Sensors (Switzerland)*. MDPI AG October 2019. https://doi.org/10.3390/s19204476.

(8) Castillo-Fernandez, Ó.; Uria, N.; Muñoz, F. X.; Bratov, A. Cell Concentration Systems for Enhanced Biosensor Sensitivity. In *Biosensors - Micro and Nanoscale Applications*; InTech, 2015. https://doi.org/10.5772/61088.

(9) Dharmasiri, U.; Witek, M. A.; Adams, A. A.; Soper, S. A. Microsystems for the Capture of Low-Abundance Cells. *Annu. Rev. Anal. Chem.* **2010**, *3*, 409–431. https://doi.org/10.1146/annurev.anchem.111808.073610.

(10) K. Dwivedi, B. Potential Risk Assessment of Cyanotoxin for Water Resources. *Int. J. Curr. Microbiol. Appl. Sci.* **2018**, *7* (2), 3604–3616. https://doi.org/10.20546/ijcmas.2018.702.429.

(11) Connelly, J. T.; Baeumner, A. J. Biosensors for the Detection of Waterborne Pathogens. *Anal. Bioanal. Chem.* **2012**, *402* (1), 117–127. https://doi.org/10.1007/s00216-011-5407-3.

(12) Ezenarro, J. J.; Uria, N.; Castillo-fernández, Ó.; Párraga, N. Development of an Integrated Method of Concentration and Immunodetection of Bacteria. *Anal. Bioanal. Chem.* **2017**, *410* (1), 105–113. https://doi.org/10.1007/s00216-017-0695-x.

(13) Párraga-Niño, N.; Quero, S.; Ventós-Alfonso, A.; Uria, N.; Castillo-Fernandez, O.; Ezenarro, J. J.; Muñoz, F. X.; Garcia-Nuñez, M.; Sabrià, M. New System for the Detection of Legionella Pneumophila in Water Samples. *Talanta* **2018**, *189* (March), 324–331.

https://doi.org/10.1016/j.talanta.2018.07.013.

(14)   Ezenarro, J. J.; Párraga-Niño, N.; Sabrià, M.; Del Campo, F. J.; Muñoz-Pascual, F. X.; Mas, J.; Uria, N. Rapid Detection of Legionella Pneumophila in Drinking Water, Based on Filter Immunoassay and Chronoamperometric Measurement. *Biosensors* **2020**, *10* (9), 1–11. https://doi.org/10.3390/bios10090102.

(15)   Ezenarro, J. J.; Ackerman, T. N.; Pelissier, P.; Combot, D.; Labbé, L.; Muñoz-Berbel, X.; Mas, J.; Del Campo, F. J.; Uria, N. Integrated Photonic System for Early Warning of Cyanobacterial Blooms in Aquaponics. *Anal. Chem.* **2021**, *93* (2), 722–730. https://doi.org/10.1021/acs.analchem.0c00935.

4.4

General Discussion

The present thesis has the main objective of developing smart materials based on the use of electrochromic metabolic indicators for the control and prevention of bacterial infections. This goal has been accomplished with the utilization of Prussian blue as sensing molecule and its implementation in textiles and water membrane filters, producing highly colored and homogeneous coatings. Besides, smart materials were also endowed with antimicrobial agents and the final products were able to detect the presence of live bacteria as well as to indicate the shelf-life of the antimicrobial activity in the materials by a simple change of color detectable with the naked eye.

Regarding the strategies currently conducted in the development of smart materials that detect the presence of live bacteria, those implemented on textiles, hydrogels, wound dressings or membrane filters are summarized below.

Most of the strategies are based on the incorporation of organic dyes into textiles,[1,2] hydrogels containing cellulose[3] or polymeric layers[4]. The presence of bacteria is detected by producing a color change. However, they are sensitive to pH and temperature changes and any change in the measurement conditions may produce false positives having poor selectivity to the presence of live bacteria. Besides, in the case of the textiles, color changes were achieved in 12 and 18 hours for Gram-negative and Gram-positive bacteria, respectively. Comparing them with the methods described in this thesis, PB-modified textiles could produce a color change in 5-6 h for *E. coli* suspensions of 10^8 CFU mL^{-1} and the detection times are shorter when using textiles modified by cyanotype process, producing color changes in the same times with bacterial concentrations of 10^7 CFU mL^{-1}.

Faster sensing strategies rely in the production of hydrogels coatings modified with colorimetric or fluorescent moieties that produce the color change when are released by

interaction with bacterial enzymes. This strategy needed 1 hour to detect the presence of bacteria. Although the bacterial detection is produced in shorter times, enzymes have poor stability and their reproducibility still remains a challenge.

Other approaches rely on the use of phospholipids vesicles stabilized in lipid layers[5] or hydrogels[6] for the developing of wound dresses, which are modified with colorimetric or fluorescent indicators, being released in the presence of bacteria and producing the color changes. The detection is produced between 4 and 6 hours for high bacterial concentrations. However, vesicles present poor stability and as in the previous case, changes in the environment can produce false positives by releasing the colorimetric indicators. In opposition, PB is stably entrapped on the fibers of the textile and its stability has been proved in different media. In addition, the smart textiles presented in this thesis can achieve the bacterial detection in situ, without the need of using other reagents or layers that enhance the stabilization of the sensing molecules.

The use of Eu^{3+} in polymeric membranes and gels has been exploited for the developing of smart textiles due to their light-emitting properties, endowing the smart materials with sensing and antibacterial capacities.[7,4] However, Eu^{3+} needs to be coordinated with organic ligands to enhance its emission properties and also, it shows slight cytotoxicity, which difficulty its implementation in real samples. Besides, the described method needs the use of lamps to detect the fluorescent signals.

In opposition, Prussian blue has shown good biocompatibility and low cytotoxicity. A great advantage of the presented smart materials is that they show sensing and antibacterial capacities for itself, with no need to implement stabilizable matrix or hydrogels. Thus, the detection can be done in situ, allowing its applicability in a wide range of fields even when no equipment or laboratories are present.

In this context, cellulose derivate membranes have been modified with Metilene blue for the development of antibacterial and bacterial-sensing wound dressings.[8] The system showed color changes in presence of bacteria with an OD = 0.8, which corresponds to a bacterial concentration between 10^8 and 10^9 CFU mL^{-1}. In comparison with the current thesis, bacterial

detection could be achieved with the PB-modified filters in two hours for 10^4 CFU mL^{-1} *E. coli* suspensions, showing higher sensitivities.

In summary, the produced smart polyester-cotton textiles and nitrocellulose filters with sensing and antibacterial capacities have demonstrate high effectivity. The sensitivity and time of response have been improved along this thesis. These smart materials have shown a great potential in the control of bacterial infections, being applicable in several fields, such as hospitals, healthcare centers, schools or at home, among others.

4.4.1 References

(1)   Alisaac, A.; Alsahag, M.; Alshareef, M.; Snari, R. M.; Alhasani, M.; Abumelha, H. M.; El-metwaly, N. M. Development of Smart Cotton Fabrics Immobilized with Anthocyanin and Potassium Alum for Colorimetric Detection of Bacteria. *Inorg. Chem. Commun.* **2022**, *145*, 110023. https://doi.org/doi.org/10.1016/j.inoche.2022.110023.

(2)   Snari, R. M.; Alsahag, M.; Alisaac, A.; Bayazeed, A.; Alsoliemy, A.; Khalifa, M. E.; El-metwaly, N. M. Smart Textiles Immobilized with Hydrazone Probe for Colorimetric Recognition of Bacteria. *J. Mol. Liq.* **2022**, *366*, 120149. https://doi.org/10.1016/j.molliq.2022.120149.

(3)   Kassal, P.; Zubak, M.; Scheipl, G.; Mohr, G. J.; Steinberg, M. D. Smart Bandage with Wireless Connectivity for Optical Monitoring of PH. *Sensors Actuators B Chem.* **2017**, *246*, 455–460. https://doi.org/10.1016/j.snb.2017.02.095.

(4)   Huang, T.; Lu, H.; Ho, Y.; Lu, K.; Wang, P. A Smart and Active Film with Tunable Drug Release and Color Change Abilities for Detection and Inhibition of Bacterial Growth. *Mater. Sci. Eng. C* **2021**, *118*, 111396. https://doi.org/10.1016/j.msec.2020.111396.

(5)   Thet, N. T.; Hong, S. H.; Marshall, S.; Laabei, M.; Toby, A.; Jenkins, A. Visible, Colorimetric Discrimination between Pathogenic Strains of Staphylococcus Aureus and Pseudomonas Aeruginosa Using Fluorescent Dye Containing Lipid Vesicles. *Biosens. Bioelectron.* **2013**, *41* (1), 538–543. https://doi.org/10.1016/j.bios.2012.09.019.

(6)   Thet, N. T.; Alves, D. R.; Bean, J. E.; Booth, S.; Nzakizwanayo, J.; Young, A. E. R.; Jones, B. V.; Jenkins, A. T. A. Prototype Development of the Intelligent Hydrogel Wound Dressing and Its Efficacy in the Detection of Model Pathogenic Wound Biofilms. *ACS Appl. Mater. Interfaces* **2016**, *8* (24), 14909–14919. https://doi.org/10.1021/acsami.5b07372.

(7)   Raheem, A.; Liu, J.; Wang, J.; Wang, J.; Zhao, Y.; Wang, Y.; Wang, Y.; Wang, W.; Ul, F.; Kipper, M. J.; Tang, J. Selective Sensing of Cu2+ and Fe3+ Ions with Vis-Excitation Using Fluorescent Eu3+-Induced Aggregates of Polysaccharides (EIAP) in Mammalian Cells and Aqueous Systems. *J. Hazard. Mater.* **2020**, *399*, 122991. https://doi.org/10.1016/j.jhazmat.2020.122991.

(8)   He, M.; Ou, F.; Wu, Y.; Sun, X.; Chen, X.; Li, H.; Sun, D.; Zhang, L. Smart Multi-Layer PVA Foam/CMC Mesh Dressing with Integrated Multi-Functions for Wound Management and Infection Monitoring. *Mater. Des.* **2022**, *194*, 108913. https://doi.org/10.1016/j.matdes.2020.108913.

5

Conclusions

The main conclusions extracted from the results obtained through this PhD thesis are:

- PB is an excellent candidate for bacterial detection either in solution or after electrodeposition on transparent ITO-PET electrodes due to its suitable optical and electrochemical properties used for such purpose, and its capacity to change of color after metabolic reduction by bacteria.

- Soluble and insoluble forms of PB present differences in structure, absorption capacity and redox activity. Both forms could be metabolized by bacteria, producing a color change observable by the naked eye for each redox state. However, the soluble form presented faster metabolic reduction kinetics, which attributed to a more suitable redox potential and the presence of a single iron in its structure instead of the four required by the insoluble one.

- PB could be incorporated on polyester-cotton textiles by a single-step sonochemical coating process, only requiring 15 min. The obtained samples showed high homogeneity and color intensity. PB-NPs in the textile were not antibacterial or cytotoxic and could maintain the bacterial-sensing capacity for both, Gram-positive and Gram-negative bacteria. Regarding to the latter, a detectable color change is observed after 5-6 h of incubation with high bacterial concentrations (10^9 CFU mL^{-1}), allowing in situ bacterial detection. Textiles were able to recover the initial blue color when bacteria die through re-oxidation by environmental oxygen.

- PB was also sonochemically coated on polyester-cotton textiles already containing CuO-NPs as antibacterial agents. The NPs distribution was very homogeneous, covering more than 95 % of the textile fibers. The ICP-OES study revealed that the stability of the CuO-NPs was improved when PB was added to the samples, reducing their release to half but keeping its initial antibacterial activity. SEM images, EDX and XAS analysis confirmed that after reduction with bacteria and re-oxidation with environmental oxygen, textiles conserved the same initial structure, indicating that the antibacterial NPs did not interfere the electron exchange between bacteria and PB. The smart textiles were able to detect the lack of antibacterial activity when

bactericidal NPs were released to the medium through a simple color change, indicating the risk of infection by the presence of live bacteria on the textile surface.

- The incorporation of PB molecules to textiles though the cyanotype process improved both, the time of response and the sensitivity of the smart material. Homogeneous samples with a deep blue color were obtained in either with or without the presence of CuO-NPs. The release of the antibacterial NPs was diminished five times, even more than in the sonochemical coating case, extending the shelf-life of the smart textile. Bacterial-sensing responses were also faster than in the previous case, showing color changes observable by naked eye after 5 h of incubation with bacterial suspensions containing 10^6 CFU mL^{-1}. These responses were obtained in dry conditions, which closer to the real application. The presence of PB in the textile fibers enhanced the antibacterial activity of the smart samples, reducing the presence of bacteria a 40 % more than textiles only containing CuO-NPs in only 7 h.

- Nitrocellulose filters were modified with PB through cyanotype process for the production of bacterial-sensing water filter membranes. Modified samples showed high homogeneity in their color and in the particles distribution. NC filters with 0.2 μm of pore size were used since the bacterial retention was higher. Besides, the UV irradiation time of the samples was optimized, being 90 s the applied time when the filters color was evaluated with the naked eye. *E. coli* suspensions of 10^7 CFU mL^{-1} produced color changes in less than 9 hours. Times of response and sensitivity of the method were improved by using a pre-concentration system with optical fibers coupled. In this occasion, filters UV irradiated for 30 s were selected as the most optimal. Thus, color changes were detected in 2 h for 10^4 CFU mL^{-1} *E. coli* suspension and in less than 5 h for 10^3 CFU mL^{-1}.

- Filters were also endowed with bactericide capacity by incorporating Ag-NPs. Obtained filters showed homogeneous blue color on the samples and in the SEM images could be observed the aggregations formed by Ag-NPs attached to the fibers of the filter. The optimal concentration for Ag-NPs was found 2 mM, which showed

high antibacterial efficiency against *E. coli*. The modification of the samples with antibacterial NPs did not difficult the sensing capacity of the filters, showing color changes in 5 h for *E. coli* bacterial suspensions of 10^8 CFU mL^{-1} when filters were modified with PB, and 10 h for filters containing PB and Ag-NPs.